FINAL REPORT

PHASE I

X-RAY ASTRONOMY EXPERIMENTS
S017 & S069
APOLLO APPLICATIONS PROGRAM
AAP FLIGHT

CONTRACT NAS 9-7201

REPORT PERIOD 1 JUNE - 1 NOVEMBER 1967

PREPARED FOR

NATIONAL AERONAUTICS AND SPACE ADMINISTRATION

30 NOVEMBER 1967

GPO PRICE $ _____

CFSTI PRICE(S) $ _____

AMERICAN SCIENCE AND ENGINEERING

11 Carleton Street, Cambridge, Massachusetts 02142

Hard copy (HC) _3.00_

Microfiche (MF) _.65_

ff 653 July 65

ASE-1758

FINAL REPORT

PHASE I

X-RAY ASTRONOMY EXPERIMENTS

(S017 and S069)

APOLLO APPLICATIONS PROGRAM (AAP) FLIGHT

CONTRACT NAS 9-7201

Report Period 1 June - 1 November 1967

Prepared for

NASA Manned Spacecraft Center
Science and Applications Directorate
Spacecraft Project Engineering Office/TF3
Houston, Texas 77058

Prepared by

American Science and Engineering, Inc.
11 Carleton Street
Cambridge, Massachusetts 02142

30 November 1967

Approved:

M. Ortmann
Program Manager

FOREWORD

This is the final report for contract NAS 9-7201, Exhibit "A" Statement of Work, entitled "X-ray Astronomy Experiment (AAP S069)" as described in Article V, Paragraph B, and covers the work performed during the period from 1 June through 1 November 1967.

A preliminary Interface Control Document (ICD), which describes the interface between the S069 X-ray Astronomy "B" Experiment and the Multiple Docking Adapter (MDA) experiment carrier for the Apollo Applications Mission AAP-2, has been submitted to NASA/MSC under a separate cover (ASE-1759). Further follow-on work including a preliminary design of the scientific instrument and its interface with the experiment carrier is described in technical proposal ASE-1740-1, dated 2 October 1967. The statement of Work, Cost Estimate, and Management Plan for the Phase II effort leading to the delivery of the flight article has been submitted in document ASE-1813.

i

CONTENTS

CONTENTS (continued)

CONTENTS (continued)

iv

CONTENTS (continued)

ILLUSTRATIONS

ILLUSTRATIONS (continued)

TABLES

1.0 INTRODUCTION

1.1 Purpose

The purpose of Phase I was to define the requirements necessary to implement the X-ray Astronomy Experiment on an Apollo Applications Program (AAP) flight.

1.2 Scope

The scope of Phase I was to conduct a study, evaluation, and reappraisal of the existing S017 flight hardware for incorporation into the S069 experiment which was assigned to a new carrier on an AAP mission. In particular, the Multiple Docking Adapter (MDA) for Mission AAP-2 was given prime consideration.

The performance requirements and system concept for the S069 scientific instrument were established for a state-of-the-art equipment design. This will satisfy the scientific objectives for an experiment designed to contribute significantly to the field of X-ray astronomy. In addition, the engineering problems and reliability requirements associated with the integration of the scientific instrument into the MDA experiment carrier were evaluated and the proposed technical solutions are discussed in this report.

2.0 SCIENTIFIC BACKGROUND

2.1 Historic Development

The study of X-ray Astronomy began in 1962 when the first stellar X-ray sources were discovered by R. Giacconi, H. Gursky, F. Paolini of American Science and Engineering and B. Rossi of M.I.T.

Advances in this study were slow during the first two years, while, in fact, a significant portion of the experimental effort was directed to verifying the original observation. The first AS&E proposal for an Apollo X-ray astronomy experiment was submitted at that time (ASE-686 dated 8 September 1964; later re-issued as ASE-686-B dated 26 March 1965). This proposal was approved by NASA/HQ and became the basis for the S017 X-ray astronomy experiment.

It is instructive to examine the state of X-ray astronomy in September 1964 when S017 was proposed. There were only three X-ray sources known at that time, and consequently, there was no accurate information about the number of sources which might be found, their distribution in the Galaxy, the number of classes of objects, the lifetimes of the sources, etc. The three source locations were not known with sufficient accuracy to identify them with known stellar objects, and consequently there was little connection with other astronomical observations. The sources were the first discovered and, therefore, had to be considered atypical, as they have proved to be. The three sources included Sco X-1, the strongest X-ray source discovered to date, and the Crab Nebula, one of the three supernova known in our galaxy. The third source has since been resolved into several separate objects. The state of X-ray astronomy at that time, and the intent of the experiment, are summarized in the following quote from the proposal:

"However, the principal justification for inclusion of this experiment in the Apollo payload must lie in the explorer - scientist role of the astronaut. We know little of celestial X-ray sources except their existence. The astronaut is thus in the enviable position of the first man to look at the stars after a few preliminary breaks in the clouds. The picture of the sky in X-ray could be radically different from the usual stellar one. It is difficult to predict the course of the experiment; the sources might be concentrated, diffuse or filamentary. One need only look at ordinary photographs of the sky to realize what a variety of complex shapes, sizes, and colors occur among celestial objects. There is no reason to predict otherwise for observations in X-rays. "

The purpose and objectives of the experiment reflect the state of the field of that time. Primary emphasis was placed on exploring for new sources; positions of the three (3) known X-ray sources were to be measured to 0.1 degree; X-ray spectra of stronger sources were to be measured; certain objects of great astronomical interest were to be investigated; the galactic equator was to be scanned; the solar X-ray flux was to be measured; the diffuse X-ray background was to be measured.

The instrument proposed and approved for these measurements was, in many ways, more complex than the modern S069 experiment. The detectors were divided into 16 data channels with individual discriminators, anticoincidence circuits, and scalers. There was also a pulse height analyzer which acted on the sum of the proportional counter pulses. The field of view of each detector was $1/4^{\circ} \times 2^{\circ}$ FWHM. These fields of view were arranged in two perpendicular fans, each fan consisting of 8 detectors offset at intervals of $1/4^{\circ}$ so that the total field of view was a 2° square, divided into smaller squares like a checkerboard. Each detector actually consisted of 8 proportional counters in

parallel, so that there were a total of 128 proportional counters. This assembly was placed in a plastic scintillator well which was viewed by two photomultipliers; these signals were placed in anticoincidence to eliminate the penetrating particle background. The aspect problem was not solved but several possibilities were discussed; these included an optical camera with film and also a star camera with an image dissector or vidicon television system and electronic readout. The final aspect solution was to depend upon the properties of the Apollo vehicle. This was to be an ambitious experiment consistent with the state-of-the-art at that time and also compatible with the experimental vehicle.

The development of the actual instrument was greatly influenced by the presence of 8 large Co^{60} sources in the fuel gaging system. These sources dominated the natural background and rendered the plastic anticoincidence shield useless because of dead time problems associated with the Co^{60} background in the plastic scintillators. The final instrument had a heavy tungsten radiation shield, a smaller effective detector area, and no anticoincidence background rejection. The experiment depended on the spacecraft G&N system for aspect information, and was considerably simpler than the originally proposed experiment. The primary emphasis remained the exploration for new sources.

The experimental sensitivity was about 10^{-3} Sco X-1; sources of this intensity could be located with a statistical uncertainty of approximately $\pm 0.1^{\circ}$ during a one orbit observation. This equipment was developed and qualified. The mission subsequently was cancelled.

There has been progress in X-ray astronomy since September 1964 using sounding rockets. We now know of 30 X-ray sources and are able to draw certain conclusions about the source density in various regions of the galaxy. The source positions are illustrated in Figure 2-1. Three sources have been optically identified (two of the three as a con-
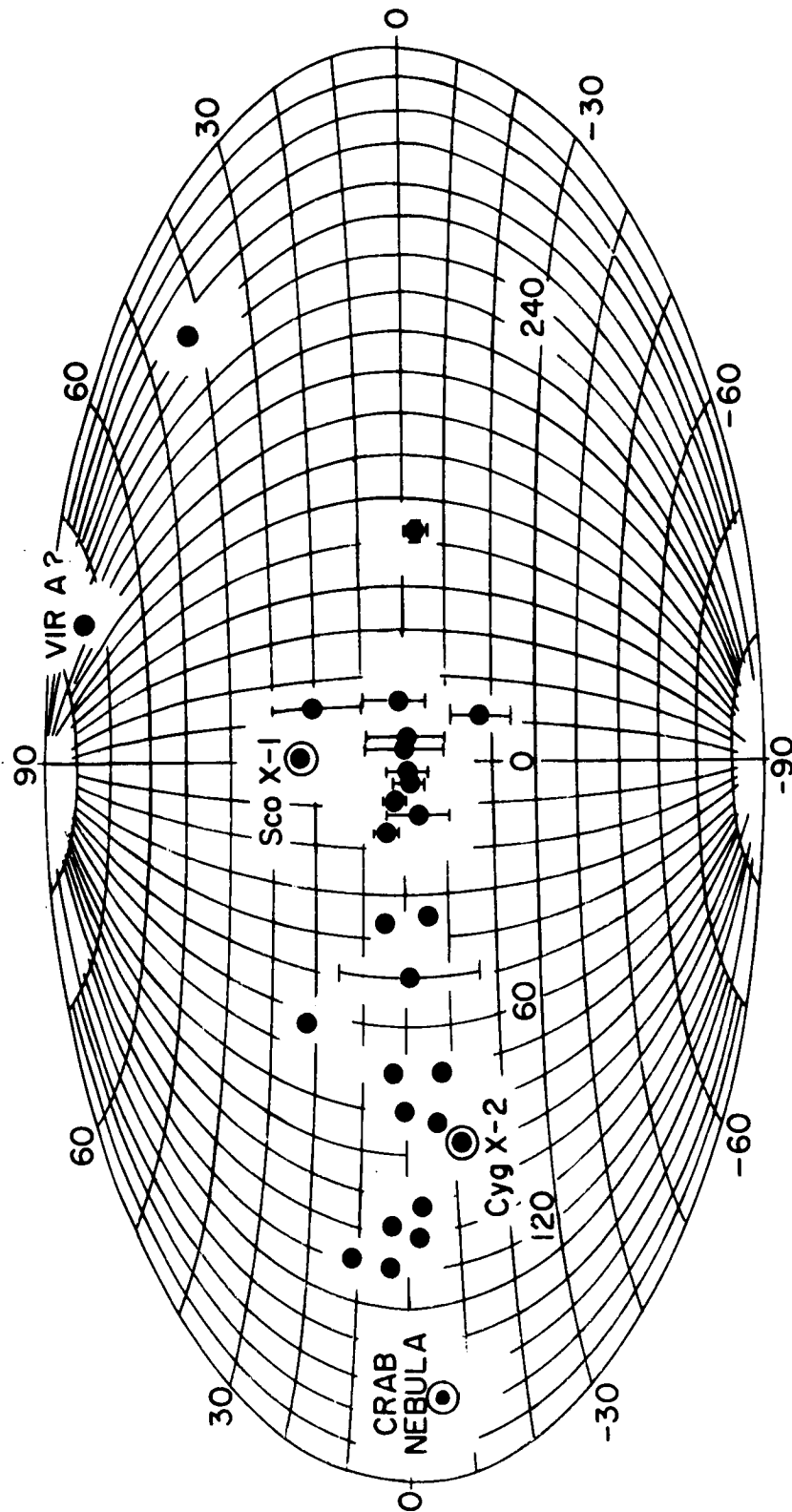
Figure 2-1. X-Ray Sky 1967.5
(The Coordinates are Galactic Longitude and Latitude)

sequence of AS&E measurements) with quite different, peculiar stellar objects. Meaningful angular size measurements exist for two sources (also AS&E measurements). There are also crude spectral measurements for the stronger sources, which indicate at least two classes of objects, and give evidence of absorption in at least one case. There is strong evidence for intensity variability in two of the sources and an indication of variability in several other sources. Finally, there is some evidence of extragalactic sources.

Progress in the U. S. can be expected to continue at this rate for several years. The limiting factor is the payload capability of the sounding rocket.

2.2 Scientific Objectives - Early 1970's

The discovery of a new source now adds one object to a list of thirty; this list will be longer by 1970, and a new source discovery will be correspondingly less important. Consequently, the emphasis in X-ray astronomy will shift from exploration to detailed study of individual sources. The following measurements will be of primary importance.

2.2.1 Source Location

There are three meaningful levels of accuracy. To identify an X-ray source unambiguously so that it is not confused with other X-ray sources requires a precision of about 1°. This is easily achieved with rockets and almost certainly will be accomplished by 1970. To make an optical or radio identification with a reasonable probability of success requires a precision of about one arc minute. This is a consequence of the density of objects in the sky - at the galactic equator

there are approximately 10^5 identifiable stars per square degree, but less than 1% of these are reasonable candidates for X-ray sources. Thus, the source candidate density is less than one per square minute except in extremely dense regions. This is illustrated in Figures 2-2 and 2-3 which show regions of the sky around two optically identified sources. In order to obtain completely unambiguous correlations, it would be necessary to have precision of the order of 5 or 10 arc seconds. The latter precision will not be possible with the pointing capability of the Apollo vehicle, but an arc minute experiment is both possible and meaningful.

The importance of accurate locations cannot be over-emphasized; astronomers have been misled many times by claims that a poorly located X-ray source corresponds to some interesting astronomical object.

2.2.2 Experimental Sensitivity

An objective for a modern experiment in 1970 is an adequate sensitivity to detect a typical source in any non-obscured region of our galaxy. Sco X-1 is a typical source of one type, and is located approximately 250 pc from the sun. The candidate source might be 25,000 pc away, and, if it is like Sco X-1, the required sensitivity would be

$$\left(\frac{250}{25,000}\right)^2 = 10^{-4} \text{ Sco X-1}$$

The Crab Nebula is a second type of source. Estimates of the distance to the Crab vary between 1100 and 1700 pc. To see the Crab at 25,000 pc would require a sensitivity of

$$\left(\frac{1100}{25,000}\right)^2 \text{ to } \left(\frac{1700}{25,000}\right)^2 = 2.10^{-3} \text{ to } 5.10^{-3} \text{ Crab}$$
$$\approx 2 \text{ to } 5.10^{-4} \text{ Sco X-1}$$

N

−15° 4301

−15° 4300

W

5'
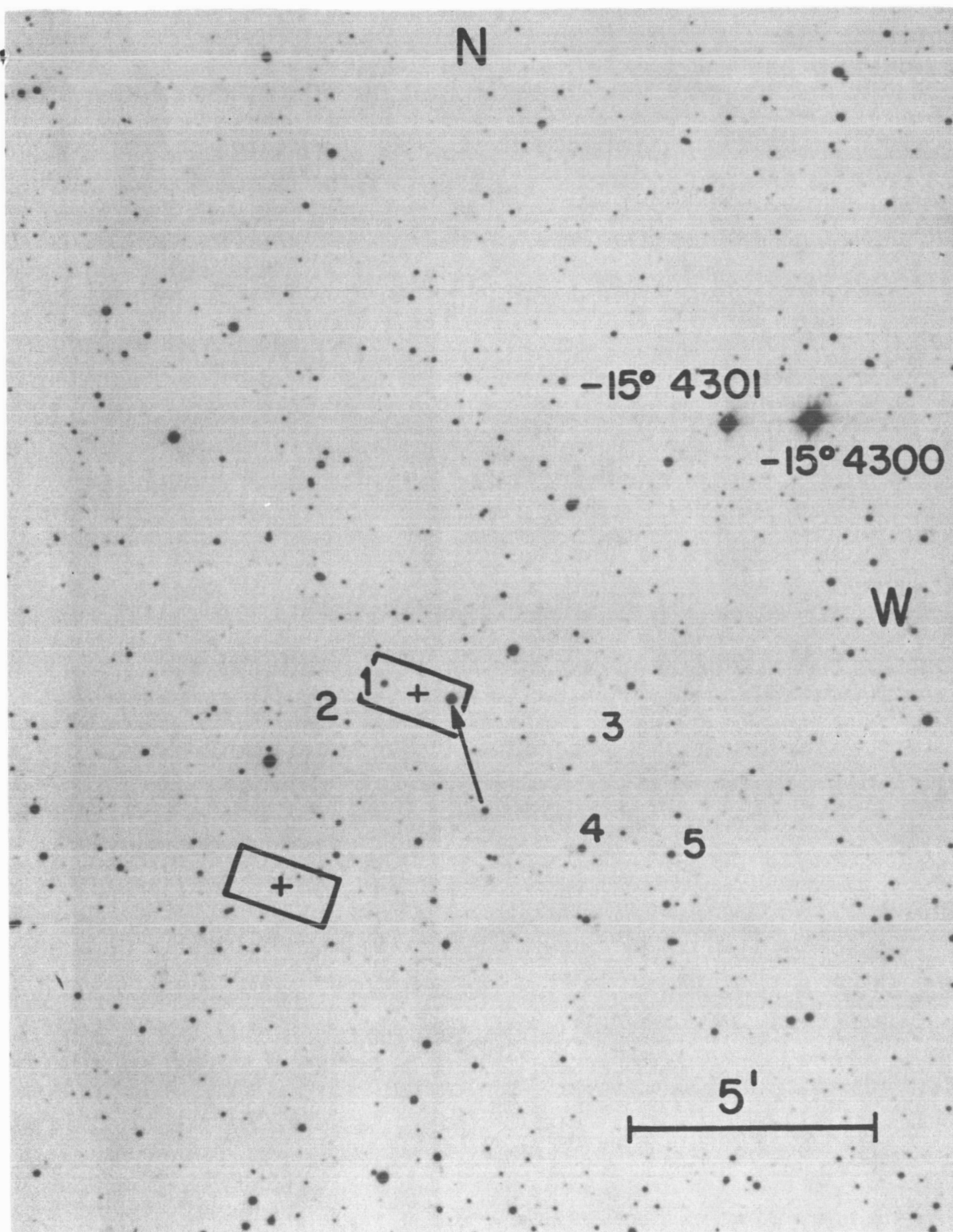
DD-082

Figure 2-2   Photograph of the region containing the X-ray position of Sco X-1 reproduced from a Palomar Sky survey print.   The two equally probable X-ray positions as determined by Gursky et al are marked by crosses surrounded by a rectangle of 1 by 2 arc minutes.   The object identified as the optical counterpart of the X-ray source is shown by the arrow.   Other marked stars were used for comparison photometry.
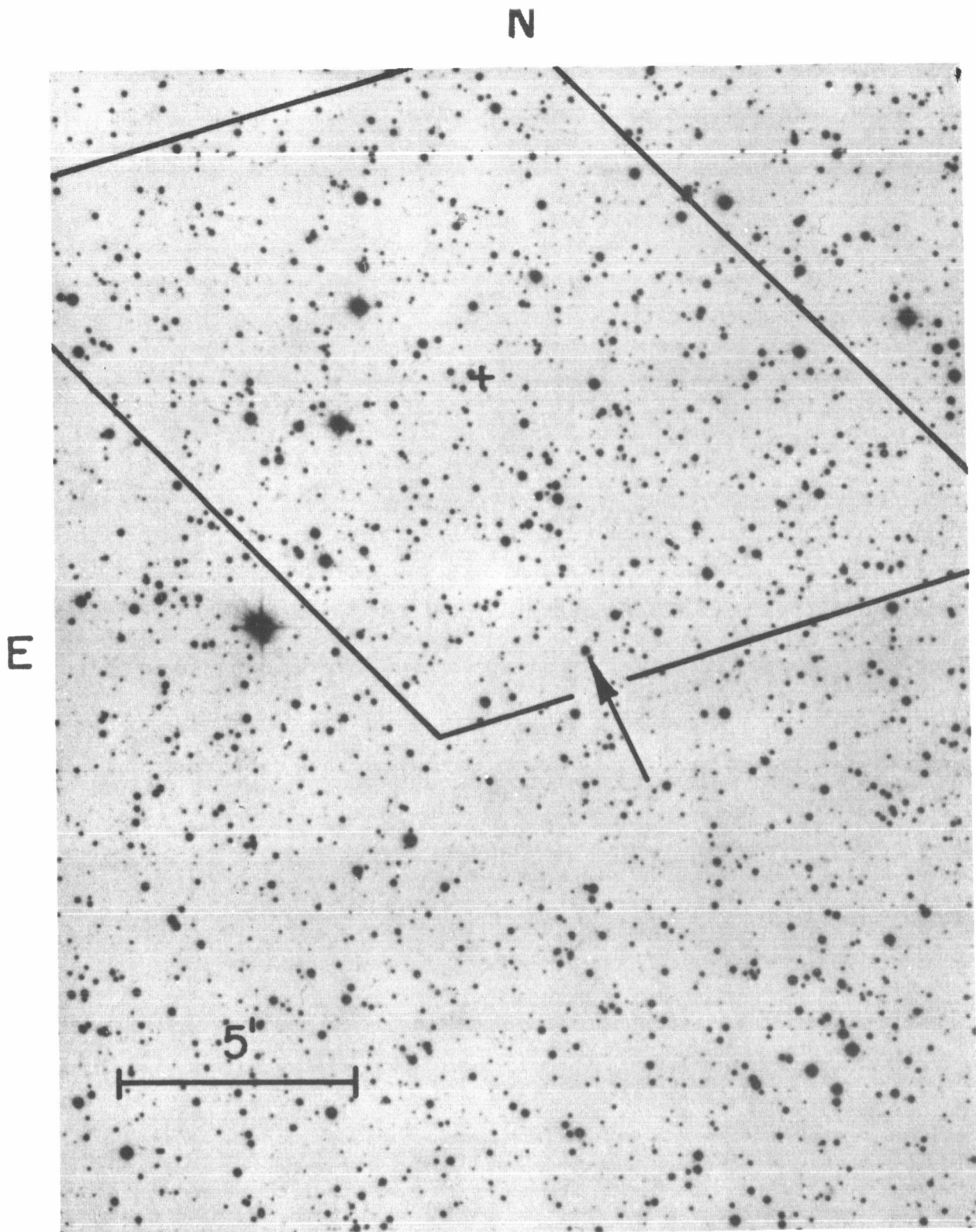
Figure 2-3. The region containing the X-ray source Cyg X-2 taken from a Palomar Sky survey print. X-ray position is marked by the cross and the area of uncertainty is the trapezoid. The optical candidate is marked by an arrow. The elongation of the optical image of the candidate object is caused by a neighboring 19th mag star and is not associated with the candidate object itself.

We see that a sensitivity of approximately 10^{-4} Sco X-1 is desirable for an adequate study of our Galaxy.

The question of extragalactic studies is uncertain. We can calculate the sensitivity required to detect a Sco X-1 type source or Crab Nebula type source in another galaxy, but in general, the required sensitivity is much greater than that required to study our own galaxy. The Magellanic clouds are an exception; a Sco X-1 source in the Magellanic clouds would have an intensity of

$$\left(\frac{250}{52,000}\right)^2 = 2.3 \cdot 10^{-5} \text{ Sco X-1}$$

Therefore, a single source study of the Magellanic clouds is possible.

It is estimated that there are 1250 X-ray sources in our galaxy. If the number of X-ray sources in an external galaxy has the same relation to the light intensity as observed in our own galaxy, then the entire galaxy might be observable as an X-ray source.

A sensitivity of 10^{-4} Sco X-1 under these assumptions, would enable us to see external galaxies brighter than magnitude 4.4; there are three such galaxies, the Magellanic clouds and Andromeda. A sensitivity of 10^{-5} Sco X-1 would enable us to see about 8 additional galaxies.

There remains the possibility of a galaxy with unusually enhanced X-ray emission.

Some recent measurements indicate that the peculiar elliptical galaxy M87 may be a source with an intensity of $5 \cdot 10^{-3}$ Sco X-1.

If verified, this would indicate that the energy emitted in X-rays by this galaxy is approximately 10 percent of the energy emitted in the optical wavelength -- a very important result. This may mean that the X-ray emission of other galaxies will be an important area of study by the flight of the S069 Experiment.

We cannot make a statistically meaningful statement about the number of such objects based on one observation. A crude guess, however, is that the density of such objects might be at least one/tenth per volume of a sphere which includes M87, or one per 1500 galaxies. We know of thirty X-ray sources in our galaxy and are beginning to have meaningful statistics; if the above crude guesses are correct, we would have to search a sphere with 300 times the volume of that extending to M87 in order to find 30 galaxies with similar emission.

The intensity from a source like M87 at the boundary of such a sphere would be

$$\left(\frac{1}{300}\right)^{2/3} \times M87 = \left(\frac{1}{44.8}\right) M87 = \left(\frac{.005}{44.8}\right) Sco\ X-1$$

$$\approx 10^{-4} Sco\ X-1.$$

This is very speculative, of course, but does indicate that a reasonable possibility of detecting extragalactic sources exists with a detector sensitivity of 10^{-4} Sco X-1.

Finally, we will calculate the sensitivity which might be required to detect an extragalactic supernova. The X-ray emission from a supernova during its maximum light output is unknown, and may be quite small. An assumption based on limited knowledge is that the ratio of X-ray flux to visible light is approximately that found in the Crab.

There are approximately .003 supernova/galaxy-year; if we are to observe the peak of a supernova during a one month observation period we must be able to observe about

$$\frac{1}{.003 \ (1/12)} \ = \ 4,000 \ \text{galaxies, approx.}$$

This requires about $(4,000/.03) = 1.5 \cdot 10^5 \ (\text{MPC})^3$ of observing volume, or a sphere of radius 31.4 MPC. A supernova of absolute magnitude $- 18$ at a distance of 31.4 MPC would have an apparent visual magnitude of 12.5 at peak and 15.5 after one month. Today, the Crab has an apparent magnitude of about 8.5; therefore the ratio of light intensities is given by

$$2.5 \ \log_{10} \ (\text{I crab/I SN}) \ = \ (15.5 - 8.5) = 7$$

$$\text{I SN} = 1.6 \cdot 10^{-3} \ \text{x Crab} \approx 1.6 \cdot 10^{-4} \ \text{Sco X-1}$$

A sensitivity of approximately 10^{-4} Sco X-1 is required for a variety of experiments; those within our galaxy are reasonably certain whereas the calculations of possible extragalactic sources are more speculative.

2.2.3 Time Variation

The visible light intensity from Sco X-1 is observed to vary erratically by a factor of about two, with small scale flicker of approximately 2% in several minutes. At several times variations of 7 to 10% have been observed in a period of 10 to 15 minutes. The intensity measurements should be accurate to at least 5% in order to test for this type of variability in the X-ray region.

2.2.4   Source Spectra

The study of spectra is a primary tool of conventional optical astronomy and will eventually be an important aspect of X-ray astronomy. The present principal X-ray detector, the proportional counter, yields only crude spectral measurements, but nevertheless, some important spectral information has been obtained. In particular, the Crab Nebula and Cyg X-1 appeared to have harder spectra than Sco X-1 and Cyg X-2. This provides some information about the differing characteristics of the X-ray sources and the important X-ray production mechanisms. The spectral information at least, can be used for partitioning the X-ray sources into different classifications. Cyg X-3 shows an unusual fall off at energies less than 2.5 keV which may be the result of absorption either at the source or in the interstellar medium. (The spectra of the Cygnus Sources are shown in Figure 3-3.) It is important to make similar measurements on sources in different parts of the galaxy, so that we can determine if this fall off at low energy is a source characteristic or a consequence of the intervening material. This will provide a technique for either studying the sources themselves or the density of interstellar material.

2.2.5   Angular Size of X-ray Mission Region

At the present time, there are accurate size measurements of only two sources, Sco X-1, which is smaller than 20 arc secs in diameter, and the Crab Nebula, which is approximately 100 arc secs in diameter in both the X-ray and optical wavelengths. The angular sizes are so different that the objects can have very little relation to one another. There are also differences in the spectra of the two objects as discussed above. The angular size of an X-ray source is, therefore, one of the important characteristics in classifying the source

and understanding the X-ray production mechanisms and the interior conditions within the source.

A modest goal for a 1970 experiment is to be able to separate Crab Nebula-like type sources from point sources anywhere in the galaxy. The Crab Nebula source is approximately 100 arc seconds in diameter and is located 1100 - 1700 pcs. A similar candidate object at a distance of 25,000 pcs would have a diameter of 4 to 7 arc seconds. Therefore, it is useful to place angular size limits of the order of 5 arc secs.

2.3 Summary

Some meaningful experimental objectives for an X-ray experiment conducted from an Apollo vehicle in 1970 are the following:

1. Experiment sensitivity 10^{-4} Sco X-1 or better.
2. Source location accuracy of 1 arc minute.
3. Source intensity accuracy of 5%.
4. Source spectrum measurements, particularly including the region below 2.5 kilovolts.
5. An angular size sensitivity of 5 arc secs.

It will be possible to accomplish the first four of these objectives with S069. It will not be possible to achieve angular size sensitivity of 5 arc seconds with the vehicle constraints of S069, but some meaningful size measurements can be made. There are, of course, other meaningful measurements such as source polarization, but these are not considered for this experiment.

3.0 SCIENTIFIC INSTRUMENT - BASIC REQUIREMENTS

The optimum design parameters of a scientific instrument can be found by a statistical analysis of error processes. Assume we have a set of measurements and a model of the expected measured values depending upon certain source parameters. The quoted experimental results are the set of source parameters which yield the maximum probability of the actual measurements. The quoted errors in the parameter values are the root mean square average of the deviations when the experiment is performed many times.

To state this more precisely, the following notation is given:

Y_i = A set of measurements (such as the number of events in the ith interval

$S_\ell^{(o)}$ = A true value of a source parameter which is to be determined by the experiment (such as the source location, its intensity, etc.)

S_ℓ = An arbitrary value of a source parameter.

$P(Y_i | S_\ell)$ = The probability of observing the experimental values Y_i if the true source parameters were S_ℓ

Then, it is shown in many treatments of statistics [1] that, given a set of measurements Y_i the most probable source parameters S_ℓ are those for which the probability function $P(Y_i S_\ell)$ is maximized. This results in the following set of equations for the quoted experimental findings.

$$\frac{\partial}{\partial S_\ell} P(Y_i | S_\ell) \bigg|_{S_\ell = \bar{S}_\ell} = 0$$

where $\bar{S}_\ell$ is the quoted experimental result.

_____

(1) See, for example Jay Orear, UCRL 8417

The distribution of the values of $\bar{S}_\ell$ obtained in this way is a measure of the experimental errors. This distribution can be described by the error matrix $E_\ell m$ where

$$\overline{\left\langle (S_\ell - S_\ell^{(o)})(S_m - S_m^{(o)}) \right\rangle} = E_{\ell m} = \text{ the average value of } \Delta S_\ell \, \Delta S_m$$

if the experiment is repeated many times. $E_{\ell m}$ will be zero if the measurements of S_ℓ and S_m are uncorrelated.

The conventional error statement, which corresponds to the standard deviation for a gaussian distribution is:

$$\sigma_{S_\ell} = \left(\overline{(\Delta_{S_\ell})^2} \right)^{1/2} = (E_\ell)^{1/2}$$

Finally, the error matrix can be calculated from:

$$E_{\ell m} = (H^{-1})_{\ell m}$$

where:

$$H_{\ell m} = \sum_{Y_i} \left\{ P(Y_i \mid S_K) \left(\frac{1}{P(Y_i \mid S_K)} \frac{\partial}{\partial S_\ell} P(Y_i \mid S_K) \right) \cdot \left(\frac{1}{P(Y_i \mid S_K)} \frac{\partial}{\partial S_m} P(Y_i \mid S_K) \right) \right\}$$

For the Poisson distribution which characterizes independent event counting experiments, this reduces to:

$$H_{\ell m} = \sum_j N_j \left(\frac{1}{N_j} \frac{\partial N_j}{\partial S_\ell} \right) \left(\frac{1}{N_j} \frac{\partial N_j}{\partial S_m} \right)$$

where N_j is the expected number of counts in the j th data interval.

This quantity has been calculated for the S069 experiment in order to optimize the design and estimate the mission time required to obtain the experimental objectives. The following assumptions were made:

a. The source is an isolated point source in a region of smoothly varying background.

b. The data are taken uniformly over a square region approximately centered at the source. This region is defined to be the locus of points traced by the central axis of the collimator and is a 2 R by 2 R square. In practice, this would be determined by the dead band of the vehicle guidance system.

In Figure 3-1, the product of the fractional intensity error and a normalizing factor is plotted as a function of collimator dimensions. The product of the position error and a normalization factor is plotted in Figure 3-2. An inspection of the graphs will show that the errors in position and intensity are decreased by a large ratio of collimator dimensions. There is an optimum narrow collimator dimension for intensity measurements at about 0.7 of the half width of the scan region. The error in the position measurement decreases with decreasing narrow collimator dimension until both collimator dimensions are smaller than the data region. The position error depends on the ratio of collimator dimensions if both are smaller than the data region, but it does not depend on a common collimator dimension factor.
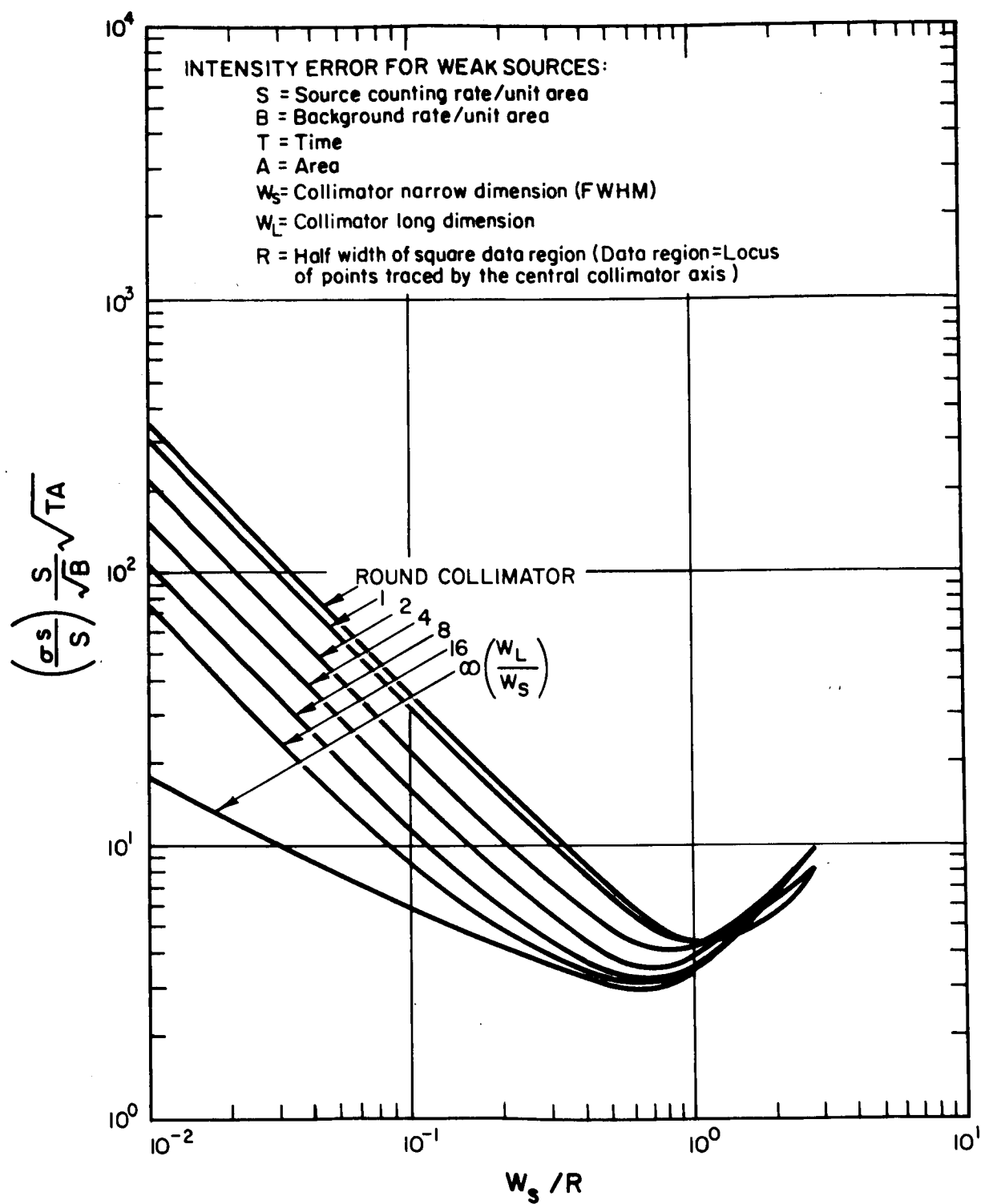
Figure 3-1 Normalized Intensity Error for Weak Sources as a
Function of Collimator and Scan Pattern Dimensions

1758
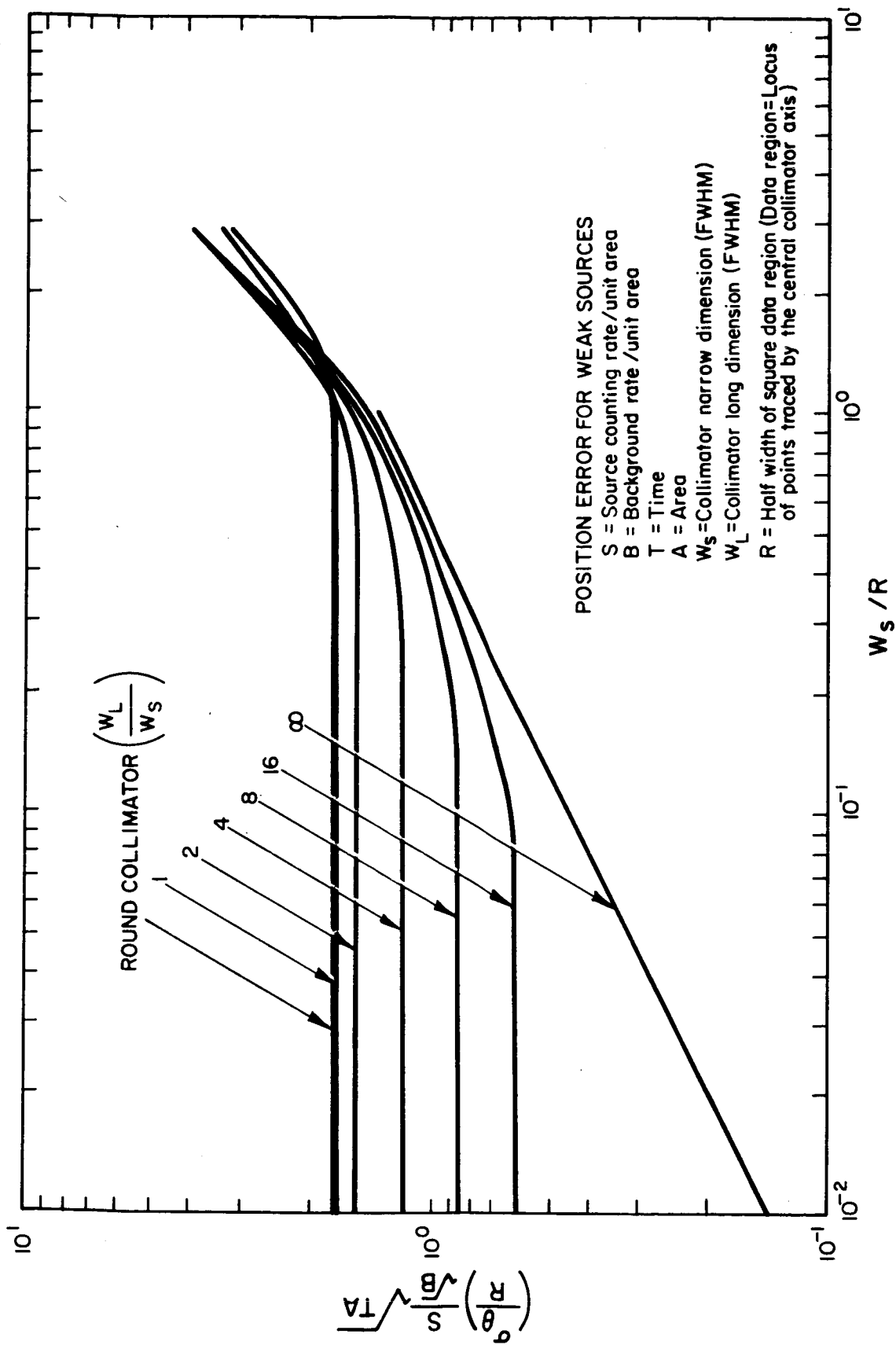
Figure 3-2 Normalized Position Error for Weak Sources as a Function of Collimator and Scan Pattern Dimensions

POSITION ERROR FOR WEAK SOURCES

S = Source counting rate/unit area
B = Background rate/unit area
T = Time
A = Area
W_S = Collimator narrow dimension (FWHM)
W_L = Collimator long dimension (FWHM)
R = Half width of square data region (Data region=Locus of points traced by the central collimator axis)

ROUND COLLIMATOR $\left(\dfrac{W_L}{W_S}\right)$

1758

3-5

In the optimum region, we have $W_L >> W_S$; $W_L >> R$; $W_S < R$.

For this case, the errors are approximately:

$$\left(\frac{\sigma_S}{S}\right) = \frac{\sqrt{3}}{\left[\frac{W_S}{R} - \frac{3}{4}\left(\frac{W_S}{R}\right)^2\right]^{1/2}} \qquad \left[\frac{1}{S} \sqrt{B} \frac{1}{\sqrt{AT}}\right]$$

$$\left(\frac{\sigma_\theta}{R}\right) = \sqrt{2}\left[\frac{W_S}{R}\right]^{1/2} \left[\frac{1}{S} \sqrt{B} \frac{1}{\sqrt{AT}}\right]$$

We also have the following expression for the background error:

$$\frac{\sigma_B}{B} = \frac{1}{\left[1 - \frac{3}{4}\left(\frac{W_S}{R}\right)\right]^{1/2}} \frac{1}{\sqrt{AT} \sqrt{B}}$$

Sometimes the criterion that the signal be three times the fluctuation of the background is used as a source requirement.

This corresponds to:

$$\left(\frac{S}{\sigma_B}\right) = S\frac{\sqrt{AT}}{B} \left[1 - \frac{3}{4}\left(\frac{W_S}{R}\right)\right]^{1/2} = 3$$

This will be shown to be a less stringent requirement than accurate position or intensity measurements.

The actual choice of collimator dimension now depends upon the relative emphasis to be placed upon position and intensity errors. In

the section on the scientific objectives, it was shown that position un-
certainties of $\pm$ 0.5 arc minutes and intensity accuracy of 5% are de-
sirable. This results in an equation for the collimator dimensions. If
we assume a G&N dead band of $\pm$ 30', we obtain

$$\frac{\left(\dfrac{\sigma_\theta}{R}\right)}{\left(\dfrac{\sigma_S}{S}\right)} = \frac{1/2}{0.05} = \frac{1}{3} = \frac{\sqrt{2}\left[W_S/R\right]^{1/2}\left[W_S/R - \frac{3}{4}\left(W_S/R\right)^2\right]^{1/2}}{\sqrt{3}}$$

or

$$\frac{W_S}{R} = 0.52.$$

The actual design has $W_S = 0.5\,R = 15'$ which is within the uncertainty
of the calculation.

The above expression also allows us to calculate the time required
for an experiment. A rearrangement of the above terms evaluated for the
case $W_S/R = 0.5$ yields the following expression for the time required
for an experiment:

$$T_I = \left(\frac{\sigma_S}{S}\right)^{-2} \frac{9.6}{S^2}\left(\frac{B}{A}\right) \qquad \text{(Intensity Limit)}$$

or

$$T_\theta = \left(\frac{\sigma_\theta}{R}\right)^{-2} \frac{1}{S^2}\left(\frac{B}{A}\right) \qquad \text{(Position Limit)}$$

The time required for a 3σ background detection of a source is:

$$T_{3\sigma} = \frac{14.4 \; B}{A} \cdot \frac{1}{S^2} \qquad (3\sigma \text{ Limit})$$

Note that the 3σ time corresponds to a fractional intensity accuracy of only ± 0.8, or a position accuracy of $\pm 0.26 \, R \approx \pm 8$ arc minutes.

These expressions indicate that for a desired accuracy and source strength, the time required for the measurement is directly proportional to the background rate and inversely proportional to the area of the detector system.

3.1 Large Area X-ray Sensor Unit

The area required depends upon the background rates and the rejection efficiency which can be obtained. Rocket flights indicate that the residual background after anticoincidence is about 0.1 events/sec-cm^2. If we assume 0.8 collimator and counter window efficiency each, then the background rate is $(0.1)/(0.8)^2 \approx 0.16$ events (effective cm^2-sec). In the laboratory we have achieved background rejection factors of 10 to 100 in the energy range of interest. If we assume an actual background rejection factor of 20 averaged over the source spectra, then we obtain a background rate of 0.008 events (effectice cm^2-sec).

The practical observation time limit is about 30 minutes, or 1800 seconds. In order to make a $\pm 1/2$ arc minute observation in 1000 seconds on a source of 10^{-4} Sco X-1, we have, approximately,

$$1800 = \left(\frac{1/2}{30}\right)^2 \frac{1}{(10^{-4} \cdot 30)^2} \left(\frac{0.008}{A}\right)$$

or

$$A = 1780 \text{ cm}^2$$

The actual design will have an effective area of about 1900 cm^2 in the position counters. This will achieve the desired sensitivity if the above background calculation describes the environment.

At high galactic latitudes, the density of objects is much less, and consequently less accurate position measurements are necessary. A position error of $\pm$ 2 arc minutes can be obtained in a 30 minutes observation time for sources as weak as $2.5 \cdot 10^{-5}$ Sco-X1.

3.2 Collimator Dimensions

As discussed above, the optimum collimator dimension is approximately $1/4^{O}$ FWHM by some long dimension. This latter dimension is not critical if it is much longer than $1/4^{O}$. In Figures 3-1 and 3-2, one observes that, for $(W_S/R) = 0.5$ there is very little improvement in performance as the ratio of collimator dimensions is increased above about 16. The actual design calls for a collimator dimension ratio of 20, or a long collimator acceptance of 5° FWHM.

The transmission of the collimator is also extremely important; the above calculations assume a net collimator and counter-window transmission of 0.64; the time required for an experiment varies inversely as this number.

3.3 Anticoincidence and Pulse Discrimination

The importance of background reduction has been emphasized above where it was shown that the time required in the experiment varies directly as background rate. There are two principal sources of background, penetrating charged particles, and non-source-associated gammas. The penetrating charged particle or cosmic ray background is about one count per cm^2. This background will be largely eliminated by placing counters behind the data counters and vetoing events which

yield pulses simultaneously in both counters. The gamma ray background, which is caused primarily by interactions of charged particles, can be distinguished from X-rays by means of the pulse shape from the proportional counter. X-rays are actually detected in proportional counter by detecting the ionization produced by the electron which is emitted when the X-ray is absorbed. This electron path is quite short with a very high specific ionization. The gamma ray is also detected because of the photoelectrically ejected electron; in this case, however, the electron velocity is high and consequently the specific ionization is less. In order to cause the same ionization as a low energy X-ray event, the path length of the gamma ray produced electron must be quite long, and consequently, the collection time for the ionization is longer than for X-ray events. This can be used to separate the gamma background from the X-ray signal. It will also result in a further rejection of charged particles events.

The important experiment parameters for the anticoincidence system are the effective thresholds necessary for the particle rejection and the relative timing accuracy enforced in the coincidence system. This is discussed in an appendix as a test report.

An extensive PSD program was conducted during this phase of the contract in order to select the optimum pulse shape criteria. The pulse parameters tested as discrimination criteria were peak pulse current, integrated charge risetime, pulse current width, and integrated charge measured with a short time constant. These tests were conducted with a variety of counter and counter voltages. The results of these tests are included as a test report in the appendix. The principal conclusion is that a significant background reduction can be obtained by using the risetime technique with an argon-CO_2 gas counter and an operating voltage of approximately 2200 volts.

3.4 Thin Window Mylar Counters

The importance of making measurements in the long wavelength X-ray region where absorption is important was emphasized in Section 2.0. An examination of Cygnus spectra as shown in Figure 3-3 indicates that absorption becomes important at energies below 2.5 keV. Unfortunately, the beryllium counter becomes inefficient at energies below 2 kilovolts. In order to improve our low energy sensitivity, we plan to include thin mylar window counters in one quadrant of the experiment. The efficiencies of thin mylar window and standard beryllium window counters are shown in Figure 3-4.

Although thin mylar window counters are operationally more efficient than standard Beryllium window counters, they do have a characteristic disadvantage in that there is some loss of its gas content while functioning in a mission. Because of this characteristic, a means to replenish the amount of gas lost is necessary in order to maintain a constant gas density. A constant gas density system has been designed; the essential element in the control system is a gas regulator counter which is exposed to a radioactive source and has a common gas system with the data counters. The control system senses the gain of the control counter and adjusts the gas pressure until a standard gain is obtained. This achieves the desired constant density system since the gain is a function of the gas density. (See Figure 5-18)

3.5 Modulation Collimator

The scientific objectives for this experiment presently include angular size measurements which can be accomplished by means of modulation collimators. The allowed depth of this experiment will allow modulation collimator resolution of about 30 arc seconds which should make angular size measurements of about 15 arc seconds possible.
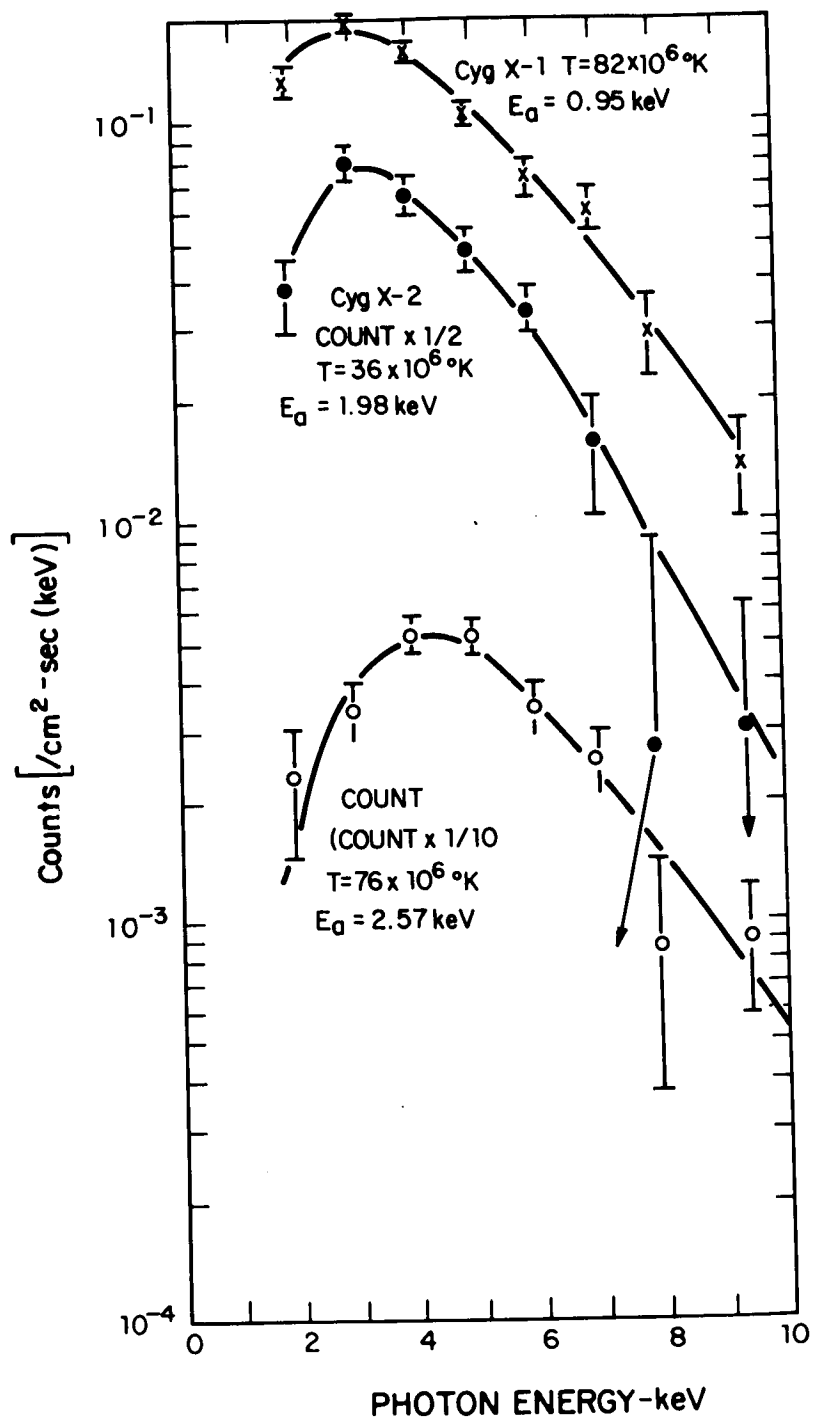
Figure 3-3 Observed X-Ray Energy Distribution

1758
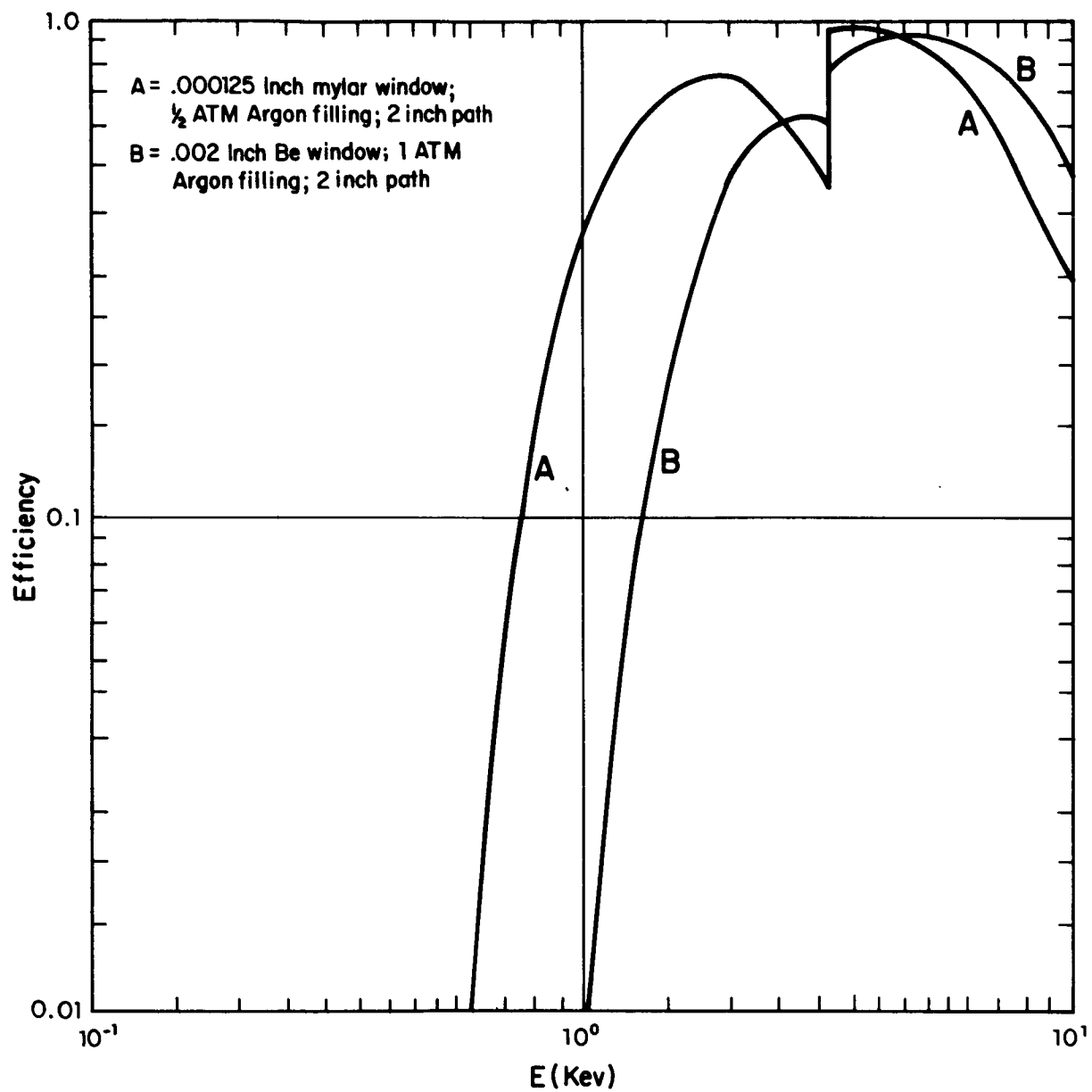
Figure 3-4 Proportional Counter Efficiency as a Function of
X-Ray Energy

1758

3-13

This will not allow us to separate Crab-like sources from point sources anywhere in the galaxy as desired, but it will be possible to make the separation for objects nearer than the galactic center. These are useful scientific results, but this function would be better performed in an experiment with a greater available collimator depth. If such a program is approved, the quadrant now planned for modulation collimators will also be used for mylar counters.

3.6 Instrument Summary

The instrument will be divided into four quadrants or detectors; these quadrants are described in Table I. All channels will have independent anti-coincidence detectors and pulse-shape discrimination circuits. There will be two 8 channel and 2 channel-pulse height analysers for recovering spectral information. Normally, the 8-channel analysers will be connected to detectors one and four. The 8-channel analysers have resolutions approximately double that expected from the counters.

The motion of the vehicle is expected to be less than 2 arc minutes/sec. The detector sampling rate will be 5 times per second for detectors without modulation collimators and 15 times per second for detectors with modulation collimators. This corresponds to 75 samples in the peak for the normal channels and 7 samples in each peak in the modulation collimator channel. It will also be necessary to measure the rates on the background reduction channels so that corrections for inefficiencies and certain types of false events can be made.

The other instrument requirements are pointing capability aspect information, and data storage and retrieval. The pointing requirement is determined by the field of view of the collimators, and must be of order $1/4^{\circ}$. It is also necessary to perform certain scan patterns

around suspected sources since it is necessary to make a local background measurement. The necessary quality of the aspect information is determined by the desired source accuracies which must be at least one arc minute. These requirements are discussed more completely in the design sections below.

Sections 4 and 5 of this final report gives a detailed coverage regarding the requirements of this instrument.

TABLE I

QUADRANT FUNCTIONS

	Detector #1.	Detector #2	Detector #3	Detector #4
Collimator Response, FWHM, X *	0.25°	5°	0.25°	0.25°
Collimator Response,* FWHM, Y	5°	0.25°	5°	5°
Modulation Collimator	none	none	3 grids 35" FWHM	none
Counter Effective Area (cm^2)	950	950	475	795
Counter Window	2 mil Be	2 mil Be	2 mil Be	.125 mil mylar
Peak X-ray Rate, Sco X-1, Counts/Sec.	28,500	28,500	14,300	39,500
Background Rate, Counts/Sec. with Anticoincidence and PSD in Favorable Parts of the Orbit	11	11	9	11

* The collimator Fields of View are shown in Figure 3-5.

POSITION COUNTERS

MODULATION COLLIMATOR

MODULATION COLLIMATOR
RESPONSE

MYLAR COUNTERS
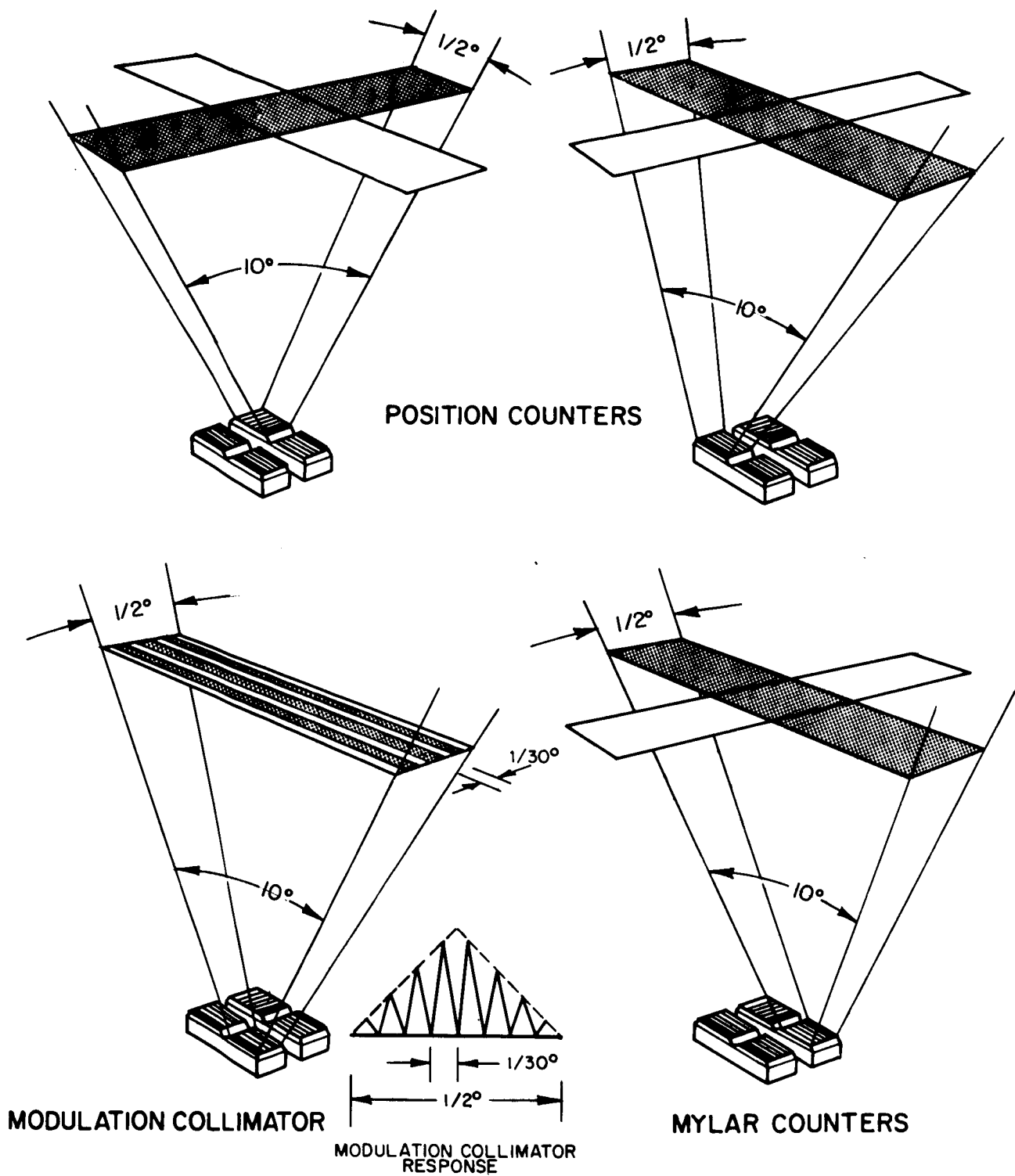
Figure 3-5 S069 SXU Collimator Fields of View

4.0   MODERN EXPERIMENT INTERFACE WITH MDA

4.1   General

During the program NASA has established an experimental location on the Multiple Docking Adapter (MDA). This has certain ramifications which affect the design of an experiment if it is to achieve the modern scientific objectives previously discussed. These ramifications include:

      a.   Systems considerations

      b.   Reliability considerations

      c.   Environmental considerations

4.2   System Considerations

An attitude sensing system must be developed referenced directly to the axes of the XSU, not the MDA. This may be in a form of optics, such as a film pack camera outboard or a camera inboard and connected to the Sensor Unit by a fiber optics "pipe". It may be a combination of optics and electronics. These and other boresighting considerations are discussed in detail in Section 5.6.4.3. Additional scientific objectives require the use of a radiation sensing instrument which can scan in various patterns. If the radiation sensor were in a fixed attitude, outboard of the MDA, this would imply using spacecraft fuel to acquire the needed motions. This is undesirable. A gimballed platform design is being considered.

4.3   Reliability Considerations

The MDA mission has a 6 months to one year storage period in space. New engineering designs reflecting the new situation are required. After this period of inactivity, the experiment plan calls for the equipment to be turned on again and comparative data taken.

4.4   Environmental Considerations

4.4.1   Thermal

The S069 experiment package may be exposed to an extreme range of thermal environments. In one orientation, it is exposed to direct sunlight with the skin on which it is mounted also exposed. On the other hand, the package may be oriented such that it receives no appreciable thermal radiation, solar or otherwise. It is doubtful that the experiment will be in operation while pointing at the sun, when the heat load would then be from solar radiation only. The heat load in a cold environment will be appreciably lower, coming only from internal power generation and any heat transfer across the interface.

The exposed area of the collimator will be about six square feet and the electrical power dissipated during operation will probably average less than twenty watts. Typical collimators essentially radiate as black bodies; this would result in an unacceptably low experiment temperature during shaded periods. The acceptable temperature range is determined by the counters which can withstand temperatures from $-40^{\circ}F$ to $90^{\circ}F$ (or higher for limited periods).

The use of insulation around the package and an aluminized Mylar film over the collimators appears to be dictated by these facts. In addition, heaters may be required, particularly if the experiment power is off during a cold exposure.

The use of aluminized Mylar is consistent with both the hot and the cold environmental extremes because the emissivity of aluminized Mylar is inherently naturally low, which is required for the cold condition. Lowering of the solar absorptivity can be accomplished by coating the sur- face of the aluminized Mylar with a layer of silicon oxide (SiO).

The information available indicates that the MDA skin temperature can vary between -130°F and +180°F. The details of this variation (length of time frequency, etc.) are not presently known, but it appears probable that a large thermal resistance between the MDA and the experiment will be required.

The major source of heating are the torque motors for the X and Y axis drives. Each motor is capable of producing about 35 watts at stall, although less than half of this wattage is dissipated under normal running conditions. The thermal path from the motors will be designed to accommodate these outputs. The drive and motor housings will be of aluminum, assuring good thermal conductivity, and the motors will be solidly mounted to their annular supports.

Thermal requirement can be further classified as follows:

(a) Internal to the MDA -- mixture of gaseous oxygen and nitrogen @ 5 psia*

     Non-operational   -40 degrees F to 140 degrees F

     Operational   -4 degrees F to 140 degrees F

(b) Internal to the MDA -- @ 1×10^{-4} mm Hg

     Non-operational   -40 degrees F to 165 degrees F

(c) External to the MDA -- @ 1×10^{-6} mm Hg

     Non-operational   -130 degrees F to 180 degrees F

     Operational   -130 degrees F to 180 degrees F

*Mixture of gaseous oxygen at partial pressure of 3.7 psia and gaseous nitrogen at partial pressure of 1.3 psia.

4.4.2 Pressure

Pressure, as well as temperature, is a design consideration for the ground operations and Spacecraft Flight missions. For the MDA, pressure shall be a design consideration in two different contexts; that is, the pressure external to the MDA and the internal pressures of the MDA.

Internal to the MDA

(a) 1×10^{-4} mm Hg   (partial pressure of gaseous oxygen 3.7 psia)

(b) 5 psia mixed gas system   (partial pressure of gaseous nitrogen 1.3 psia)

External to the MDA

(a) 1×10^{-6} mm Hg

5.0 S069 X - RAY ASTRONOMY SYSTEM CONCEPT

The S069 Experiment System, proposed by AS&E for use in an MDA, consists of three major assemblies shown in Figure 5-1 as a mock-up configuration. The nomenclature of each assembly is as follows: Display and Control Unit (DCU), Electronics Unit (EU) and X-Ray Sensor Unit (XSU). Figures 5-1a through 5-1c illustrate the various positions which the XSU can assume. Since the system, as illustrated, is strictly conceptual, the configuration of all or any of the experimental hardware is subject to change.

Figure 5-2a shows the S069 Experiment in block diagram form. The experiment equipment location diagram of Figure 5-2b includes a proposed internally mounted camera not shown in Figure 5-1. This camera, connected to an externally mounted fiber optics pipe (multi-cluster of fiber optics (is one of three aspect systems under consideration. A sketch of a fiber optics pipe and camera is shown in Figure 5-26. The second is an outboard camera called out in Figure 5-1, and the third aspect system is one involving the use of an electro-optical stellar sensing device. The description of each major assembly is given in the following paragraphs.

5.1 Display and Control Unit (DCU)

This unit explicitly defines the interfaces between the astronaut and the experiment package. Its front panel, consisting of meters, dials, lights and other displays, convey information to the astronaut regarding conditions within the experiment system. In addition, there are switches and pushbuttons which convey commands from the astronaut to the experiment package.

Figure 5-3 shows a mock-up of the conceptual front panel and the placement of panel controls and displays. The left portion of
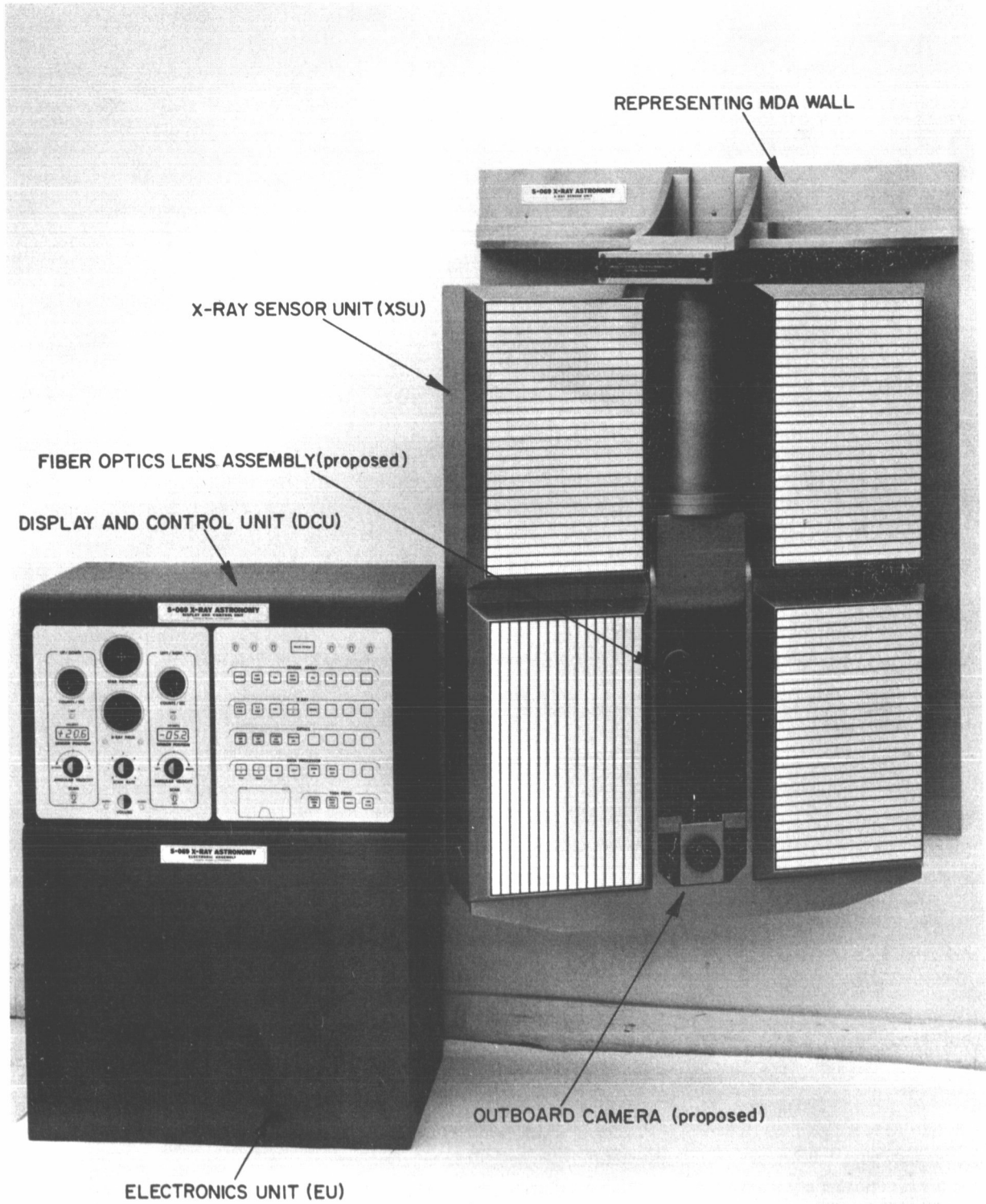
Figure 5-1   Mock-up View of S069 Major Assemblies
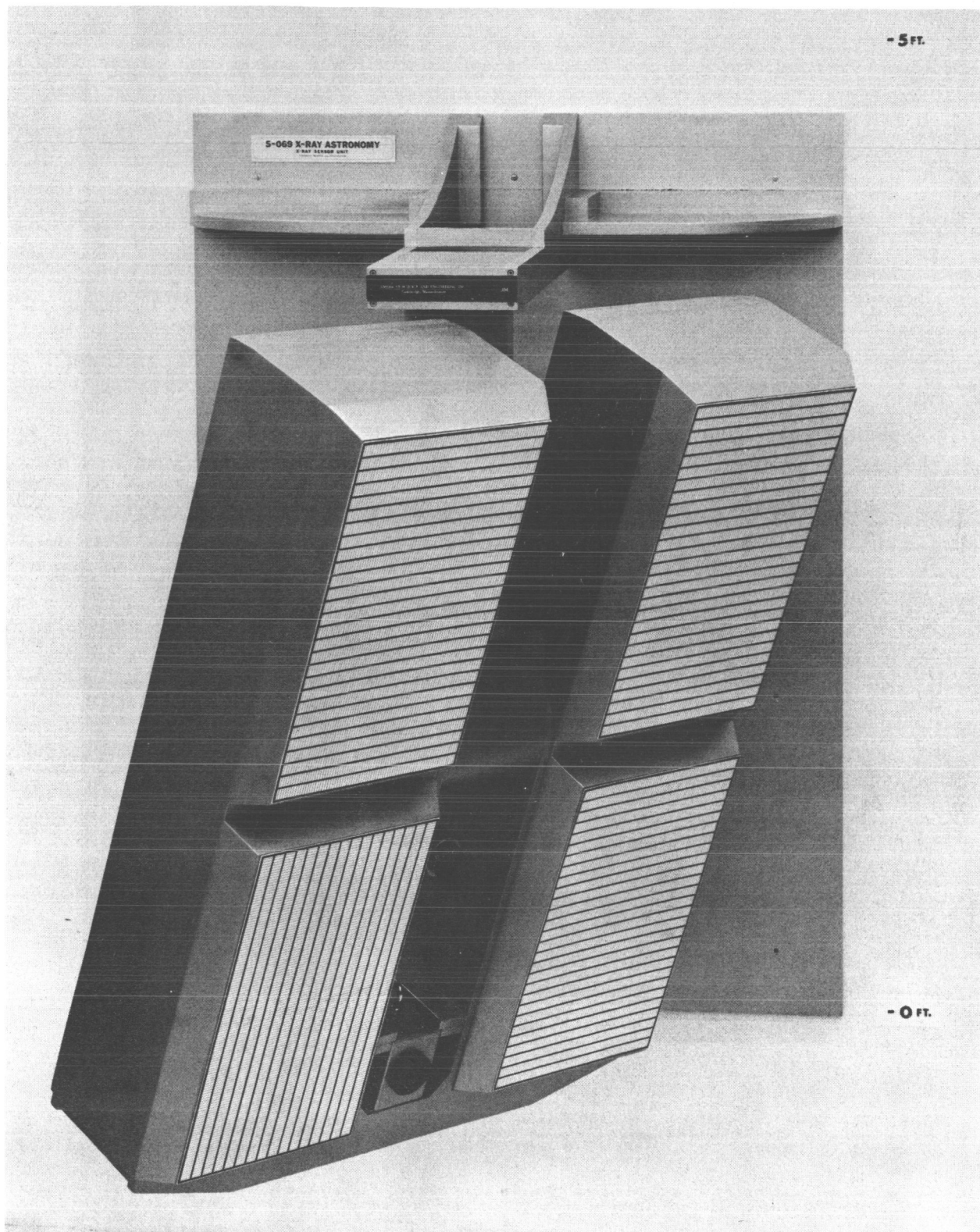
Figure 5-1a X-Ray Sensor Unit Shown Extended from MDA Wall
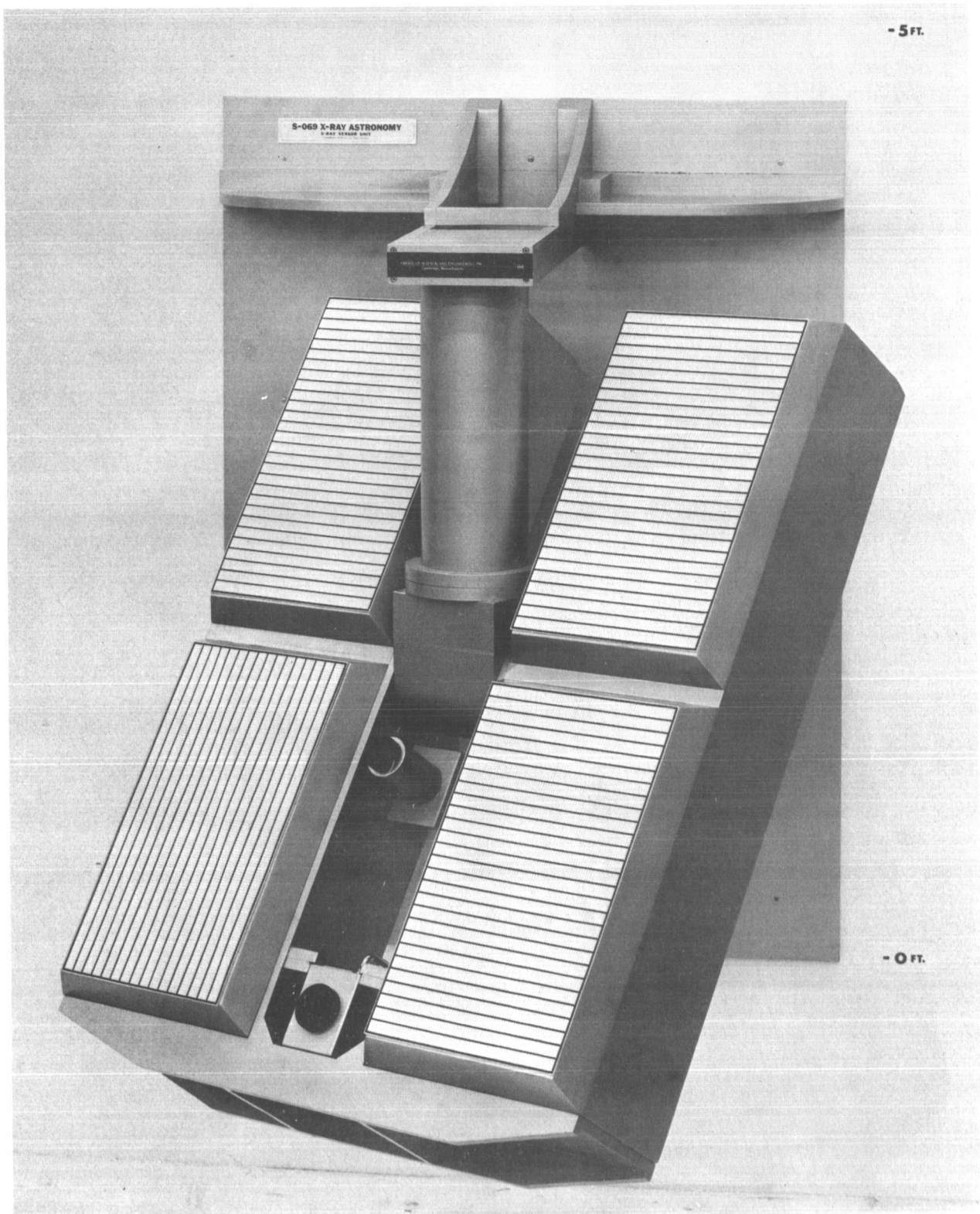
Figure 5-1b X-Ray Sensor Unit Shown Rotated to a Selected Postion

DX-004
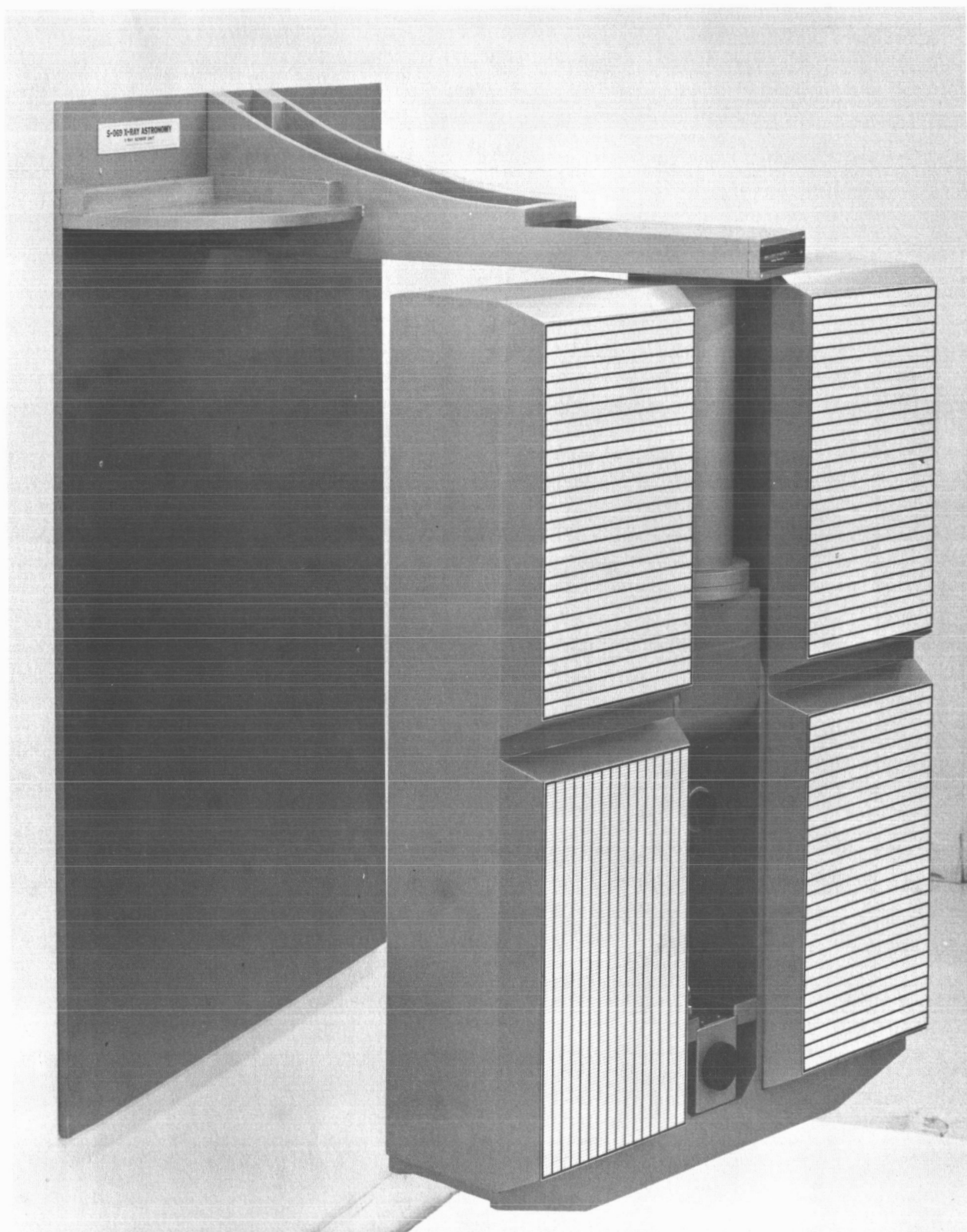
DX-005A

Figure 5-1c X-Ray Sensor Unit Shown Rotated to Another Selected
Position
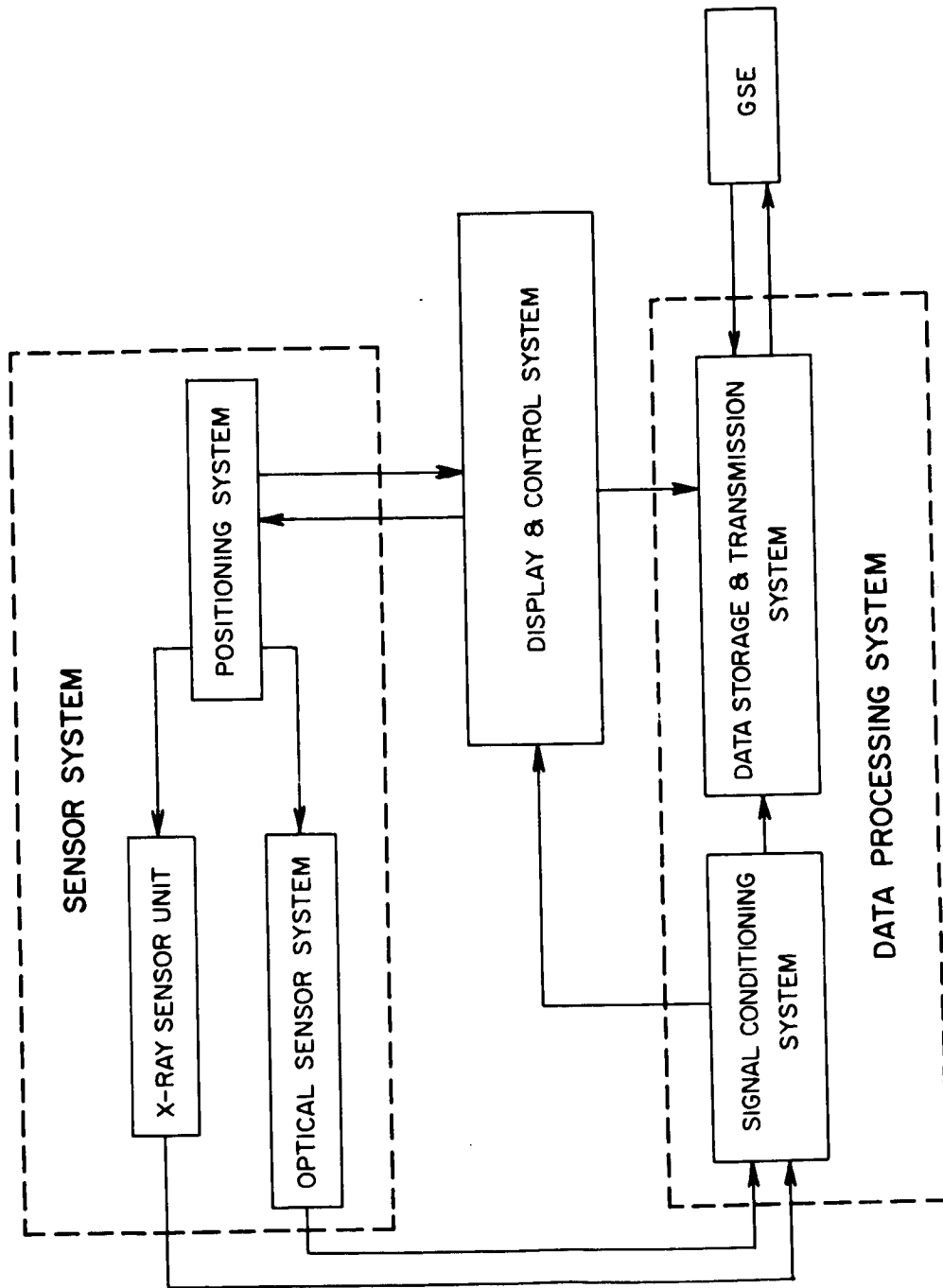
Figure 5-2a S069 Experiment Block Diagram

1758
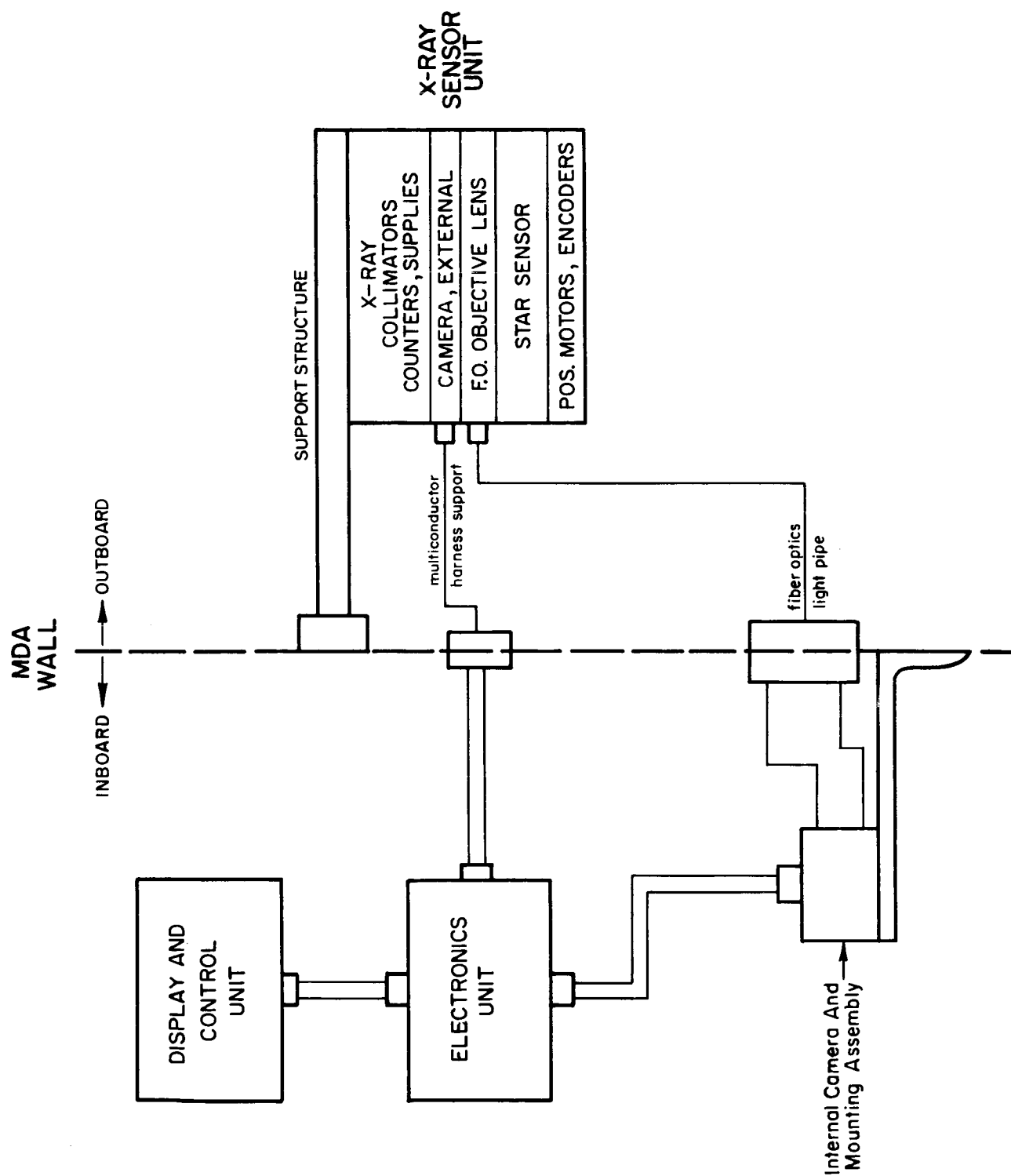
Figure 5-2b   S069 Experiment Equipment Location

X-RAY SENSOR UNIT

SUPPORT STRUCTURE

X-RAY
COLLIMATORS
COUNTERS, SUPPLIES

CAMERA, EXTERNAL

F.O. OBJECTIVE LENS

STAR SENSOR

POS. MOTORS, ENCODERS

MDA WALL

OUTBOARD

INBOARD

multiconductor
harness support

fiber optics
light pipe

DISPLAY AND
CONTROL
UNIT

ELECTRONICS
UNIT

Internal Camera And
Mounting Assembly

1758

5-7
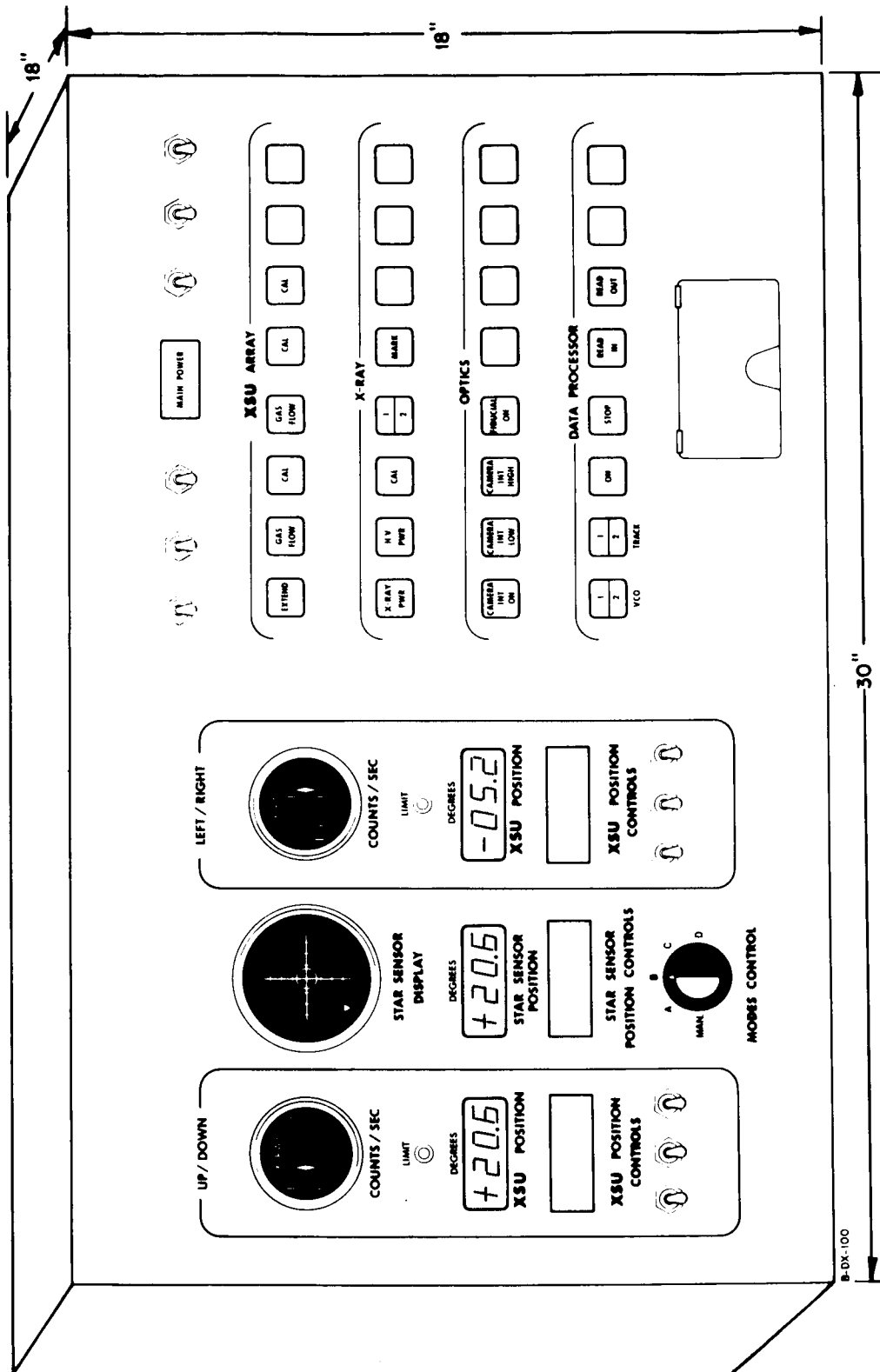
Figure 5-3 Conceptual Configuration of Display and Control Unit, Front Panel

the panel which controls the rotation of the XSU, is divided into three sections. The first section at extreme left, labeled UP/DOWN, controls the XSU movement in the up and down directions. The third section, labeled LEFT/RIGHT, controls XSU movement for left or right directions. The second or center section contains the Star Sensor Controls and indicators. Also contained in the center section is a five-position selector switch labeled MODES CONTROL which will select either manual or automatic XSU scanning sequences. The cluster of switches, to the right of the panel, are switches which provide control of the main power and the conveying of commands from the astronaut to the experiment system.

Description of the DCU controls are listed in the following subparagraphs 5.1.1 through 5.1.7.

5.1.1   Counts/Sec Indicator

Intensity of radiation from a strong X-Ray source is manifested by the frequency of pulses coming from the sensor unit. The rate, if high enough, can be integrated into a usable analog signal which will actuate this display. A maximum reading indicates that the XSU is aimed directly at the source. One indicator is provided for each axis.

5.1.2   XSU Position

This is a 3 decimal digit electroluminescent display, with an indicator for the plus or minus sign. The reading, as illustrated, shows the position of the sensor array, measured from a central zero. They also refer to "up" and "right" position. Resolution is to 0.1°.

5.1.3   Sensor Position Controls

This is a digital transducer which conveys the astronaut's

positioning command to the servo DCU positioning system. (See Figure 5-3.) The use of decimal thumb wheels marked from 0-9 are being considered at present. Other types of controls are also being investigated. There will be one control for each axis.

5.1.4 Star Sensor Display

Will be used for display of X-Ray signals detected by some type of electro-optic device of which several are being considered.

5.1.5 Star Sensor Position

Similar in function to the XSU Position display except that the Star Sensor Position is read out.

5.1.6 Star Sensor Position Controls

Function of the Star Sensor Position Control is similar to the XSU Position Control, except that it regulates the operation of a small stepping motor which moves the Sensor Unit in a stepping motion in one axis only. Compared to the Star Sensor, the XSU requires a larger drive system, such as DC torque motors to drive the XSU array in either an X or Y axis.

5.1.7 Modes Control

A five position selector switch controls the inputs to the sensor positioning system. In MAN (Manual) position, the astronaut controls the XSU directly. The four remaining positions, labeled A, B, C and D refer to preprogrammed scan sequences and allows for only one mode to be actuated at any given time.

5.2 Electronics Unit (EU)

This unit houses two separate electronic subsystems:

(a) data storage and transmission, and (b) the XSU positioning electronics as indicated in the detailed illustration of Figure 5-4. A divider, located approximately midpoint of the EU cabinet, separates the two subsystems. Connectors will be provided on the upper deck to facilitate interconnection and harnessing of all electronic modules. Overall cabinet dimensions are indicated for installation purposes to the MDA. These dimensions are preliminary and are subject to change.

5.3 X-Ray Sensor Unit (XSU)

The general mechanical design concept of the proposed XSU is shown in Figure 5-5. Mounting of this unit will be on a simple two-axis variable positioner so that its axis can be moved $\pm 45^{\circ}$ in X- and Y- directions under the control of the astronaut.

The system, in a closed position, measures approximately 3 feet wide by 4-1/2 feet high by 1 foot deep, which is a volume of 13.5 cubic feet. It will be mounted to the outside of the MDA wall and will be confined within a 7 inch envelope. After ejection of the protective shroud (SLA) the unit must be extended in order to provide clearance for making the required rotations.

At an integration and planning meeting of May 11, 1967, Huntsville, Alabama, it was suggested then that the XSU be attached to the outside wall of the MDA and centered on position II (Reference MSFC Drawing SK10-9317) having the following clearance constraints:

FWD most station   2020.069

AFT most station   1955.069

However, because of the restrictions to the field of view in Position II, MSFC has decided to mount the Variable Position XSU on the MDA outside wall, centered on Position III, with previous clearance constraints. (Ref. MSFC Drawing #SK10-7426 and letter I-S/AA-MGR of
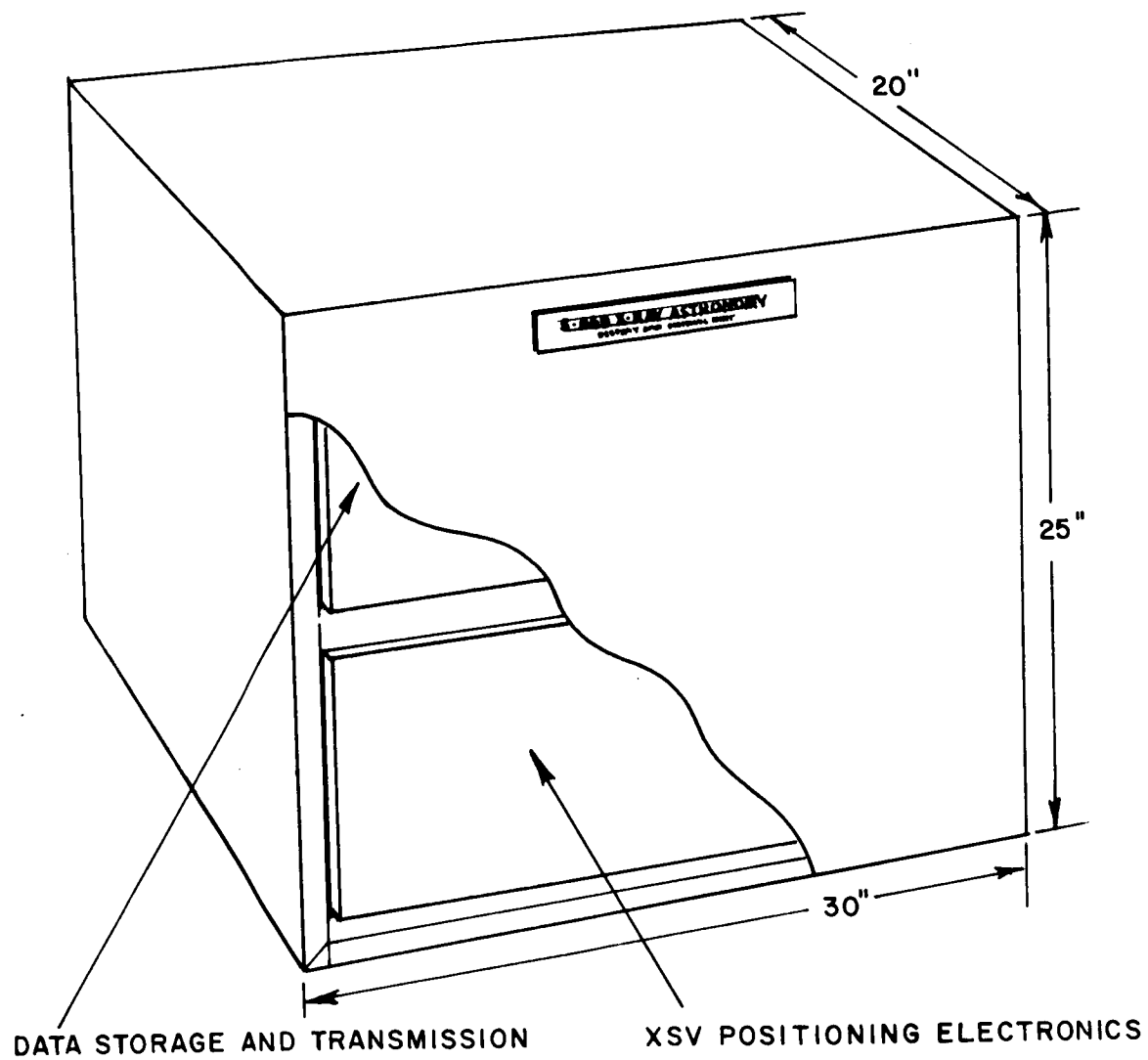
Figure 5-4 Electronics Unit Shown in Detailed Configuration

The figure shows an electronics unit box with dimensions 20", 25", and 30". Labels: DATA STORAGE AND TRANSMISSION, XSV POSITIONING ELECTRONICS.

Figure 5-5 XSU Outline Drawing
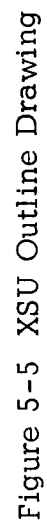
August 11, 1967).

In view of that decision no feasibility studies have been
conducted as to an available location for mounting the XSU to the
Service Module. The XSU will contain all necessary transducers to
establish the location and to study selected parameters of celestial
X-Ray sources. To properly perform this task the unit should have the
capability of directly pointing to the source independent of the space-
craft.

Two degrees of freedom (orthogonal axes) limited to plus
and minus 45° of travel is a minimum requirement for X-Ray Sensor Unit
movement. The XSU shall, in addition, contain one or more optical
systems to establish XSU attitude for precision locations and relative
sizes of the various X-ray emitters under study. Pointing and scanning
controls for the XSU shall be made available to the astronaut on the Dis-
play and Control Unit located in the MDA.

5.3.1   X-Ray Detector

X-Ray detectors will be divided into four quadrants as tabu-
lated below. Quadrants 1, 2 and 3 are similar compared to quadrant 4
which is described in paragraph 5.3.1.1.

	QUADRANT #1	QUADRANT #2	QUADRANT #3	QUADRANT #4
Fractional Area	0.25	0.25	0.25	0.25
Number of Counters	6	6	6	5 or 6
Counter Window	2 mil Be (Max)	2 mil Be (Max)	2 mil Be (Max)	Either 0.125 mil Mylar or 5 mil Be

Gas Filling	1 atm P-10	1 atm P-10	1 atm P-10	10 cm P-10 or 2 atm Xenon
Total Detector Area	1700 cm^2	1700 cm^2	1700 cm^2	1400/ 1700 cm^2
Counter Dimensions	Approx. 2" x 2" x 24".			
Anode Wires	2 mil stainless steel.			
Cathode Material	Aluminum.			
Isolation	Cathodes to be isolated from chassis.			
Construction	The pre-amplifiers will be mounted on or very close to the counter.			
Independence	The anticoincidence and PSD detector and circuitry shall be entirely separated and independent for each detector.			

5.3.1.1 Quadrant #4 - This detector will consist of a bank of counters with very thin (1/8 mil) Mylar windows operated in the flow mode. Mylar-window detectors (Quadrant 4) can sense lower energy X-Rays. As a back-up, counters with thicker windows and Xenon gas filling will be used. These are sensitive to X-Rays from 5 to 20 keV. Since it is known that these detectors can be readily obtained, maximum effort should be concentrated toward development of the thin window detectors described below.

Window Material	0.125 mil Mylar, Parylene or equivalent.
Construction	A common gas volume assembly fed by a gas flow system.
Gas Flow System	Sufficient gas to provide 3 to 5 detector fillings at operating pressure, consisting of high pressure gas

cylinder, solenoid valves, pressure reducer and regulator.

Gas Operating Pressure	Design guide - 10 cm Hg (actual value to be supplied).
Gas Density	Regulator to maintain density constant to 0. 5%.
Suggested Design	Design of a detector bank should be such that it will accommodate five counters, approximately 10 inches wide, plus an additional volume measuring 2" x 2" x 24" to contain a gas cylinder and regulation system.

5. 3. 1. 2 Collimators -- Three of the four quadrants, shown in Figure 5-5a are identical except for a 90° rotation of one quadrant's long axis with respect to the other quadrants.   The remaining quadrants have been modified to include a three-grid modulation array.

	Coll. #1	Coll. #2	Coll. #3	Coll. #4
Full X Angle	$0. 5^{\circ}$	10°	$0. 5^{\circ}$	$0. 5^{\circ}$
Full Y Angle	10°	$0. 5^{\circ}$	10°	10°
Modulation Collimator	None	None	$1' \times 10^{\circ}$	None

Based upon the resolution to be provided by three grids, in a staggered pattern, each is wound with 1 mil wire. The two outside grids are spaced 6 inches apart and the third is placed in the center. Grids are paralleled to within $\pm$ 5 arc seconds.

	Coll. #1	Coll. #2	Coll. #3	Coll. #4

Uniformity

The sections comprising each collimator should be uniform within $\pm$ 1 arc min.

Quadrant Alignment

The sections comprising each collimator (if made by building up) should be aligned to $\pm$ 1 arc min. to each other.

The four collimators should be capable of alignment with one another to an accuracy of $\pm$ 10 arc min. in the narrow direction and $\pm$ 1° in the wide direction.

Effective Area

The collimators shall be designed so that at least 85% of the face area transmits X-Rays.

5. 3. 1. 3 Pre-Amplifiers – One preamplifier will be provided for each counter. The pre-amplifiers must produce outputs at high level and low impedance to minimize noise pickup and also be suitable for both total energy measurement (pulse height) and pulse shape discrimination.

5. 3. 1. 4 Anticoincidence System – An anticoincidence will be provided which will remove the effect of penetrating cosmic radiation. This is to consist of many gas filled proportional counters totally surrounding five sides of the X-Ray detectors with only the front face being left uncovered. These detectors are to be connected in parallel and placed in anticoincidence with signals from the X-Ray detectors.

Counter Type	P-10 filled at one or two atmosphere of gas. No thin window.
Overlap	The counters must be packed together tightly to minimize dead areas in the anticoincidence shield.
Dimensions	Not critical. A thickness of 1" recommended and dimensions of 2" x 1" x 26" are suitable.

5.3.2 XSU Mounting Designs

Several configurations of the positionable sensor unit and its mounting methods have been studied.

Possible design approaches were based on the following assumptions:

(a) Physical location as per MSFC preliminary sketch.

(b) Proportional counters area min. of 6 sq. ft.

(c) Two degrees of freedom within 90° min. field of view.

(d) Approximate weight of 200-220 lbs.

The optimum physical size has been established to be 18" x 24" long by 2" square in cross section, taking into consideration:

(a) Effective counter area to dead area

(b) Manufacturing technique

(c) Weight of a counter

(d) Reliability of a counter

The configuration of the sensor unit was dictated to great extent by the available depth and by the mounting method of its

positioning system, which has the X- and Y- axes through the center of gravity of the sensor unit. This will reduce large power requirements needed during test operation and check-out in ground activities.

Possible mounting methods of the positionable sensor are:

(1) <u>Double-hinge principle, Figure 5-6</u>

Sensor unit is hinged along two vertical and two horizontal edges to achieve left and right or up and down motion.

<u>Advantages</u>

(a) Unobstructed field of view

(b) Maneuverability of $\pm 90^{\circ}$

(c) Zero or normal position close to MDA wall

<u>Disadvantages</u>

(a) Complex driving mechanism

(b) Large driving power required in ground activities due to changes in center of gravity.

(c) Complex electronics for angular readout

(2) <u>Sensor extension combined with down motion, Figure 5-7</u>

Extension and down motion is achieved by lifting the bottom edge of the sensor unit about a pivot with fixed linkages. The linkages and the lifting mechanism are mounted to the vertical trust bearing which in turn rotates $\pm 180^{\circ}$.

<u>Advantages</u>

(a) Unobstructed field of view

(b) Extension combines down motion

5-19
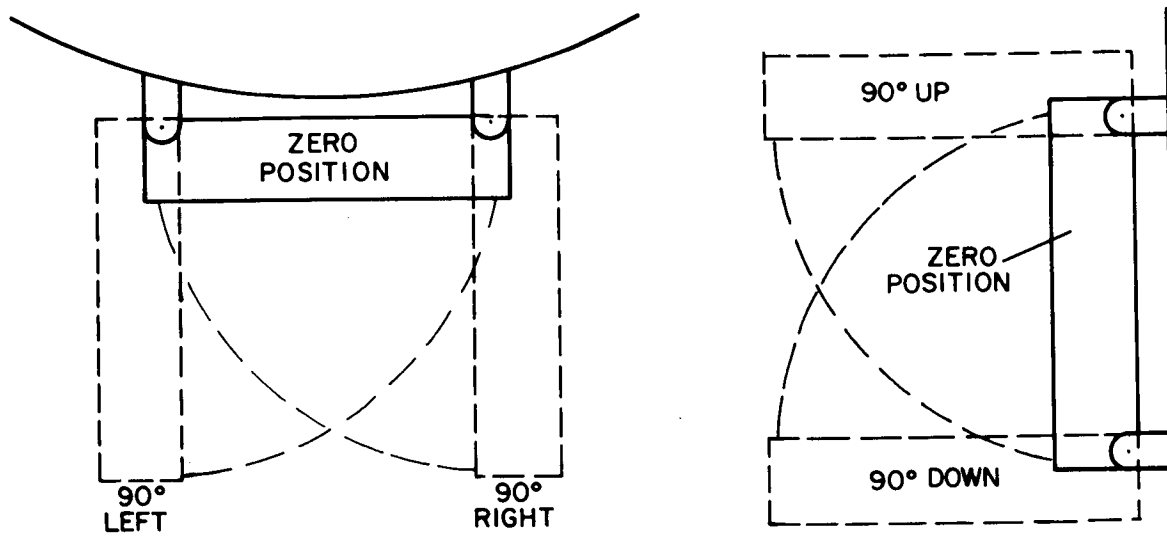
Figure 5-6 Double Hinged Principle
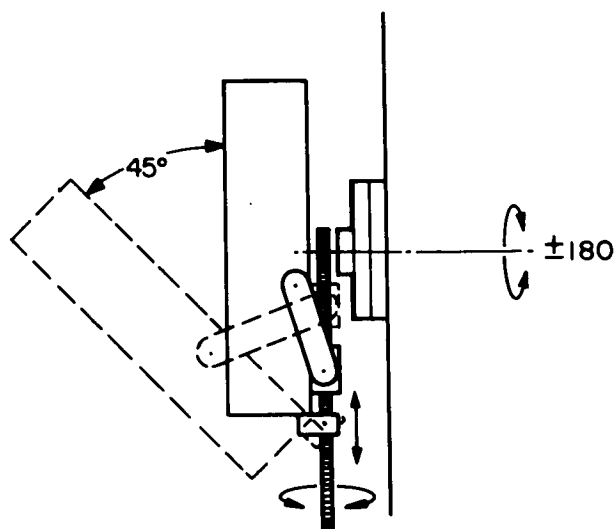
Figure 5-7 Sensor Extension Combined with Down Motion

(c) Zero or normal position close to MDA wall

Disadvantages

(a) Thrust bearing and its drive mechanism occupies large space

(b) In $\pm\,90^{\circ}$ off horizontal axis linkages support full load

(c) Complex electronics for angular readout

(3) Venetian blind principle, Figure 5-8

Sensor units modules are pivoted about center of gravity and are linked with an arm, whi ch controls the up and down motion. All modules are connected to a vertical shaft which provides left and right movement of the sensor unit.

Advantages

(a) Unchanged center of gravity

(b) Zero position close to MDA wall

(c) Straight forward angular readout

Disadvantages

(a) Large volume required in zero position

(b) Alignment difficulty of individual modules

(4) Sensor Unit extended, Figure 5-9

Sensor unit extended to the required distance which is
predetermined by the angular displacement along X- and
Y- axes.

Advantages

(a) Simple X- and Y- axis drive mechanism

(b) Unchanged center of gravity

(c) Straight forward angular readout

Disadvantages

(a) Extension has to be completed before scanning

(5) Tubular Member into MDA Wall, Figure 5-10

Sensor unit mounted at center of gravity on a cantilever
beam sliding in and out through a hole in the wall of the
MDA.

Advantages

(a) An unobstructed field of view

(b) Unchanged center of gravity

(c) Clean, uncluttered construction
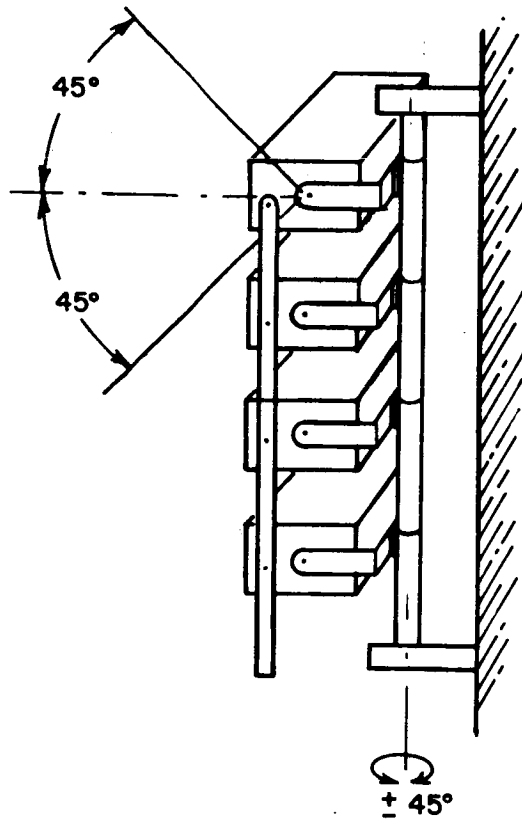
Figure 5-8 Venetian Blind Principle

Figure 5-9 Sensor Unit Extended

1758
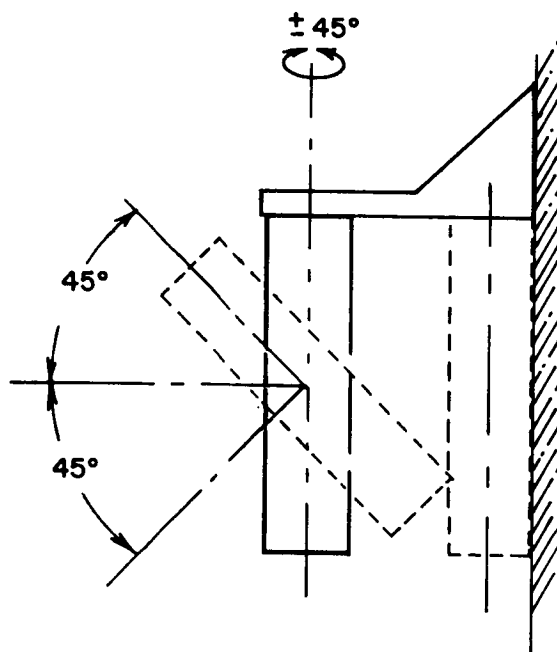
Disadvantages

(a) Hole in MDA wall approximately 10" diameter

(b) Complex electronics for angular readout

(c) Extension has to be complete before scanning

(6) 1/2 Cylindrical Well in the MDA wall, Figure 5-11

Sensor unit mounted in fixed position in respect to MDA.

1/2 cylindrical well in the MDA clears the sensor unit

in X- and Y- axis displacement.

Advantages

(a) Unchanged center of gravity

(b) Straight forward angular readout

(c) No extension of sensor unit

Disadvantages

(a) Large well in the MDA wall

(b) Complex latching mechanism for launching

Of the six XSU mounting designs described in Section 5. 3. 2,
Item 2, Figure 5-7 is considered to be the best engineering solution.

5. 3. 3   Deployment Mechanism, Figure 5-12

In the closed position, two aluminum channels are folded as
shown in Figure 5-11. Upon opening of the latching mechanism the X-Ray
Sensor will extend to the required distance from the MDA.

The main parts of the Deployment Mechanism are listed
1 through 6 below:

(1) Channel track	(4) Linkage
(2) Rack	(5) Track deployment (drive)
(3) Carriage	(6) Carriage deployment (drive)
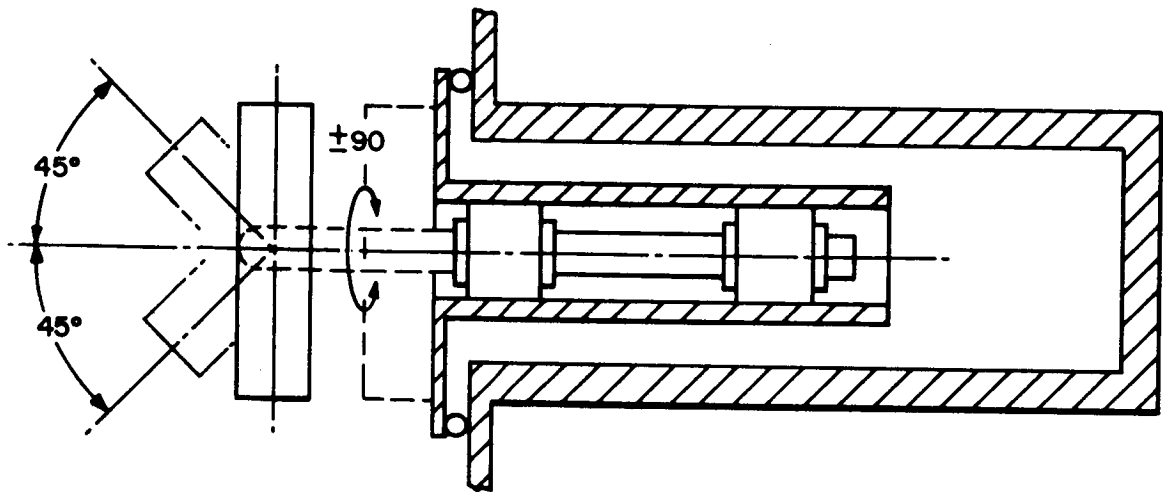
Figure 5-10   Tubular Member into MDA Wall

1758
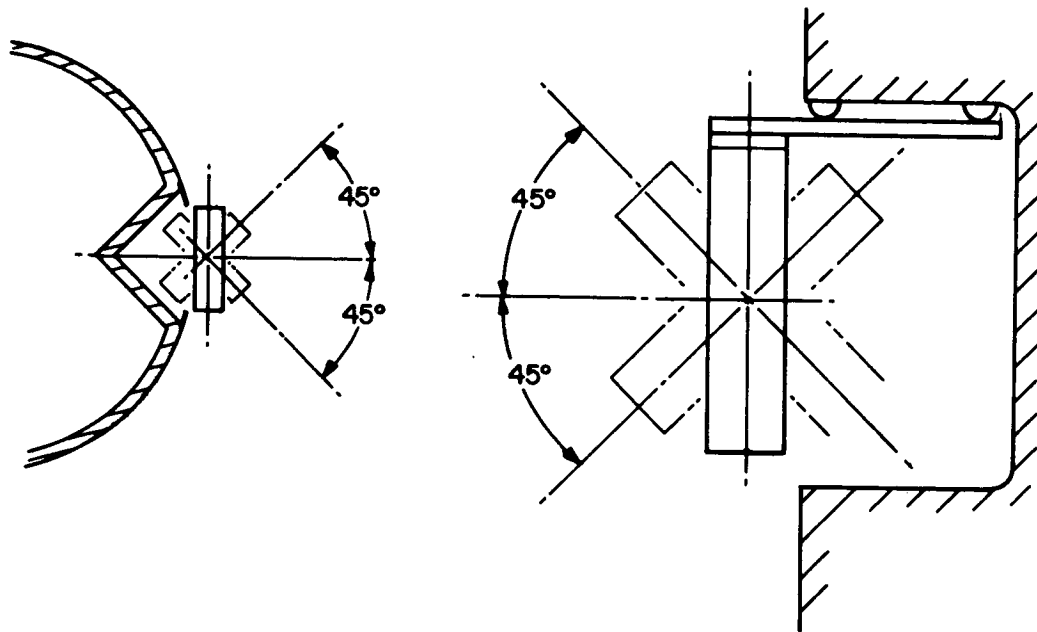
Figure 5-11   Cylindrical Well in MDA Wall

CLOSED POSITION

TRACK DEPLOYMENT SHAFT

LINKAGE

TRACK

CARRIAGE DEPLOYMENT PINION
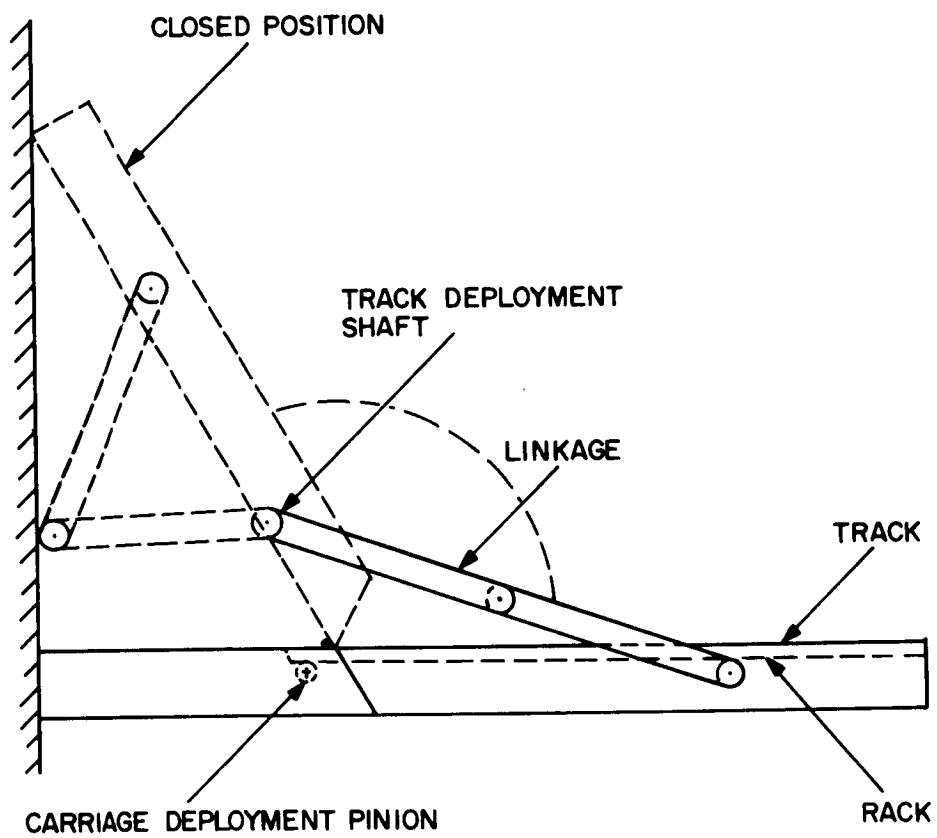
RACK

Figure 5-12 XSU Deployment Mechanism

1758

Track deployment will be driven by a spring motor, such as "Negator" type, through a pinion meshed to a nylon gear of the Track Deployment shaft. The light weight hinged section of the track assembly is estimated to weigh approximately 3.2 pounds and will permit the selection of a standard spring motor. Two spring motors are considered, both by Hunter Spring:

(1) Constant torque motor

(2) Spirator or a power spring

Constant-Torque Motor

A typical constant torque motor comprises a take-up drum and a larger output drum. These are mounted on two separate axes which are displaced from each other. The take-up drum is mounted for free rotation about its fixed axis. The spring coil is mounted on to the take-up drum and is not normally fastened to it. The outer end of the flat spring is extended and anchored to the output drum. When the output drum is rotated, the coil is progressively transferred from take-up to output drum. As this action occurs, the material is first pulled straight and then wrapped backwards counter to its relaxed curvature around the output drum. During rotation, the material already transferred to the output drum does not change stress value, and the material remaining on the take-up drum is at virtually zero stress. Only the material passing through the straight zone and undergoing a change in stress is capable of exerting any force. Release of the output drum at any degree of wind-up allows the material to revert to its natural prestressed curvature by returning to the smaller drum. This imparts rotation to the output drum and to any shaft or gear fastened thereto. The torque produced by this motor is almost perfectly constant from start to completion of the driving cycle. The torque results from two actions:

1. The pull of the extended constant force spring at the periphery of the take-up drum.

2. Release of the additional torque originally stored in backwinding the straightened section of the shape of the output drum.

The constant torque motor has a very long operating cycle which results from non-cumulative stress distribution and the large number of turns it can provide. High initial torque is maintained the entire operating cycle and energy is released at a uniform rate without any waste, and without any "droop" near the end of the cycle. High energy storage capacity is available because of higher permissible working stress. Lack of inter-coil friction eliminates any need for lubrication.

Spirator Motor

Spirator is essentially a spiral power spring in appearance and operation but its forming process derives from the development of the Negator spring. Its storage or take-up drum is mounted inside the output drum. Instead of delivering its torque by running back onto a second externally mounted drum, the backwound strip is sustained around the outer layer, and the inner end fastened to a concentric smaller drum, or arbor. Instead of being prestressed to form a reverse spiral, the Spirator spring is initially prestressed to form a tight coil. Residual stresses introduced into each increment of length are equal. Thus the outer coil is as heavily stressed as the inner coil. The residual stresses permit higher working stresses, in turn, thinner material and greater length in the same case size. The Spirator motor is a compact, single-axis mechanism. The intercoil friction, which is always present (depending upon design proportions) may cause a jerky action; therefore, a suitable lubricant is advisable.

5.3.4 X- and Y-Axis Drive, Figure 5-13

X- and Y- axis drive will provide an angular displacement of $\pm$ 45° from neutral. The large power requirements needed during operation for test and checkout in ground activities will be minimized by locating the X- and Y- axis through the center of gravity of the sensor unit. Motion will be provided by a DC torque motor for smooth low speed operation. The direct-drive DC torque motor is a servo actuator which can be directly attached to the load it drives. It has armature and a permanent-magnet field which, acting together, convert electrical currents directly into torque, to maintain desired accuracy in a positioning control system. In general, torque motors are designed for high-torque "stand-still" operation for positioning system, and for high torque at low speeds for a speed-control system. A brushless design utilizes pigtail leads for limited rotation.

The general mechanical concept of the X- and Y- axis drive is shown in Figure 5-13. The torque motor and digital encoder are mounted on a common shaft supported by a set of ball bearings, suitably lubricated to meet the space environment. The radial play to provide compensation for thermal differential will be controlled by ball bearing preload springs. Seals will be provided around joining surfaces to exclude minute particles or dirt.

To preserve the specified performance characteristics of the torque motor and to avoid any distortion of the field assembly when it is bolted in place, a strong housing of a non-magnetic material such as aluminum, magnesium or non-magnetic stainless steel will be used.

MTG FLANGE   HOUSING   ENCODER

BEARING   TORQUE MOTOR   END PLATE

|←——————— 8" ———————→|
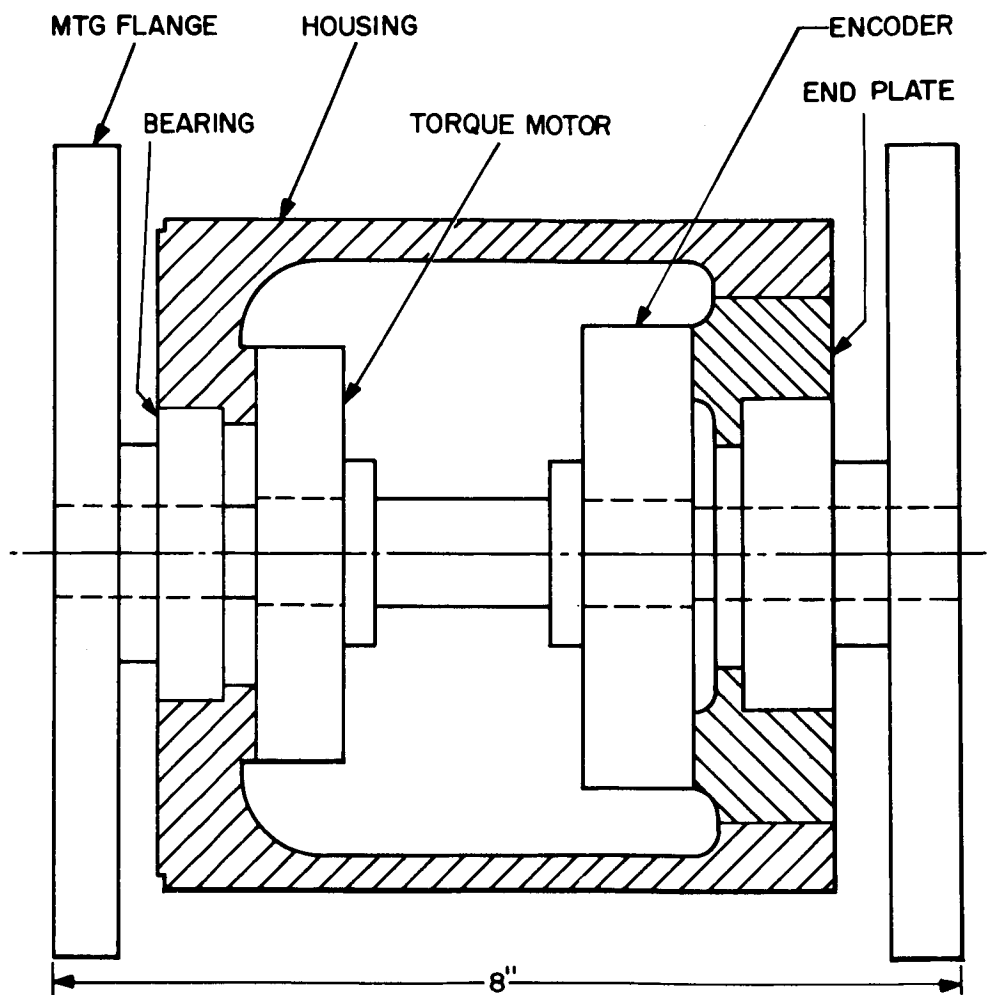
Figure 5-13 X- or Y- Axis Drive

1758

5-30

Lubricants and Bearings

(1) Lubricants - One of the major problem areas of any drive system is that of friction and wear of rubbing or sliding surfaces as encountered in the operation of gears, bearings, and electrical contacts. Lubrication is needed to reduce frictional drag and minimize the power to drive the mechanism. Excessive wear, resulting from inadequate lubrication, can be the limiting factor in the lifetime of the mechanisms, as well as that of the entire system.

Parts that are exposed to the hard vacuum of outer space will operate at pressures on the order of 10^{-6} Torr. Surface films of absorbed or chemisorbed gases that the films present on even the cleanest surfaces in the normal earth atmosphere may vanish within some time after being put into orbit.

Under these conditions, gross seizure, or cold-welding can occur between the surfaces.

Design factors that influence the choice of lubricant or self-lubricating material include:

1. Environment
   a. Vacuum
   b. Radiation
   c. Reactive Materials

2. Operating Conditions
   a. Speed
   b. Load
   c. Temperature (extended temperature range)
   d. Type of Motion

3. Parts

     a. Materials and Material Combinations

     b. Hardness

     c. Surface Finish

     d. Tolerances

4. Installation and Handling Variables

     a. Alignment

     b. Mounting Rigidity

     c. Sealing

The recommendations made on the following pages should serve as guides in determining types of lubrication that may be most suitable. They are based on limited tests and experience with satellites and space probes launched to date. Even when all of the operating conditions are known, several lubricants or self-lubricating materials may appear equally promising, the choice must be checked by service tests under the conditions of use. Equipment qualification tests should include tests to confirm the usefulness of the lubricant or self-lubricating material selected and to establish their lifetime and reliability for specific applications.

The life, or service life of solid dry film lubricants is definitely finite and difficult to predict. The only way to assure oneself of the life limit of a solid dry film lubricant is to try the lubricant on the actual mechanism or component itself.

To reduce wear life data scatter to a minimum, the following major variables need to be controlled:

    1. Identical bearing material composition and hardness

    2. Identical specimen preparation and cleanliness

3. Aligned specimen loading

4. Rigidly maintained contact areas

5. Identical lubricant thickness

6. Identical temperatures and humidity throughout all tests

7. Tests have shown that the longest lifetime with MoS_2 and other metallic sulfide films are obtained when the film is applied to molybdenum or to a molybdenum alloy; therefore a choice of substrate should be evaluated on the basis of its chemical composition.

E3C Process - (Electrolytic Chemical Conversion Coating)

The Dow Corning E3C Process is a method of forming a dry lubricant surface layer on metals. The process may be compared with surface hardening of steel by methods such as nitriding, but in the case of E3C the result is a lubricant surface rather than a hardened surface.

The Electrolytic Chemical Conversion Coating is an "in situ" process, that is, the lubricant layer is formed in place on a bearing surface and is not deposited by mechanical means. The process results in the formation of a complex molybdenum sulfide crystalline structure that incorporates the metal substrate at the treated surface.

E3C Process will exhibit:

(a) Low coefficient of friction 0.05

(b) Low evaporation rate under high vacuum

(c) Unaffected wear life after exposure to gamma radiation of $5 \times 10^{o}r$.

(d) Outstanding wear life

Molykote X-15

The Alpha-Molykote Corp. Molykote X-15 is a water-based bonded coating, which can be applied by brushing or spraying.

Molykote X-15 coating characteristics are:

    a. Temperature range from $-300^{\circ}F$ to $200^{\circ}F$

    b. Unaffected by high level gamma radiation

    c. Impact-insensitive to liquid oxygen

    d. Good lubricity properties under high vacuum (10^{-9})

    e. No corrosion protection

    f. The film will soften when subjected to water or moisture for extended periods of time

    g. Wear life not as good as resin-bonded films

Vac Kote

Ball Bros. Research Corp.'s Vac Kote vacuum lubrication process involves the use of fluid organic compounds containing metallic complexes and long chain hydrocarbon molecules or solid films consisting mainly of molybdenum disulfide. Fluid coatings are applied by vacuum processing and adhere to metallic surfaces through molecular bonding.

Solid coatings are applied by mechanical techniques.

Vac Kote was first used as an effective lubricant for rolling, sliding and other metal-to-metal contact parts associated with NASA's Orbiting Solar Observatory spacecraft. The versatility of Vac-Kote makes it effective as a conducting lubricant for motors, slip rings, potentiometers and similar hardware using wipers. The use of Vac Kote for either conducting or non-conducting applications ensures overall compatibility between components in the same system.

Versilube F-50

General Electric silicone lubricating fluid has shown excellent performance for the majority of lubricating applications.

The following are some of the important properties of Versilube F-50:

    a. Low evaporation rate under high vacuum

    b. Thermal shock resistance of $-100^{\circ}F$ to $430^{\circ}F$

    c. Non-toxic under normal industrial conditions

Lubeco 905

Lubeco 905 can best be described as a chemically-bonded, completely inorganic solid dry film lubricant. The lubricity of the Lubeco 905 lubricant is provided by a specific combination of friction-and-wear-reducing constituents of controlled particle size, such as molybdenum disulfide, graphite and several others.

Lubeco 905 will exhibit:

    a. Low evaporation rate under ultra-high vacuum

    b. Thermal shock resistance of $-325^{\circ}F$ to $+350^{\circ}F$

    c. Extremely low kinetic and static coefficient of friction

    d. Long wear life under highly loaded dynamic service conditions as well as with oscillatory motion

    e. Non-toxic characteristics, dermal and respiratory

    f. No serious changes to the composition as a result of nuclear radiation

    g. Unaffected wear life after exposure to several levels of gamma or neutron irradiation

h. Low corrosion resistance as based on the salt-spray

testing method. This corrosion promotion can be

eliminated by including necessary pretreatments.

(2) Bearings - The Barden Corp., Danbury, Conn., manu-
facturers of precision ball bearings, recently introduced experimental
ball bearings with retainers of a propriety material called BarTemp. This
material is essentially Teflon reinforced with glass fibers plus molyb-
denum disulfide.

BarTemp provides its own lubrication and can be used at
very low temperatures and at high temperatures up to $900^{O}F$, and light
loads. Since both Teflon and MoS_2 are effective lubricants in vacuum,
BarTemp also appears suitable for vacuum applications. BarTemp
bearings are produced with radial play to provide compensation for thermal
differentials that may be encountered in high or low temperature operation.
For quieter operations, bearings may be mounted opposed and axially
preloaded with springs to remove unwanted looseness.

Bearings lubricated with grease and oil should be double
shielded, both to reduce lubricant evaporationand to minimize contamina-
tion.

Bearings lubricated with bonded films of MoS_2 should be
carefully spun-in and blown free of loosened debris before operation.

Large low-speed support bearings for space application are
difficult or impractical to enclose or hermetically seal. The conven-
tional bearings can be used in most cases.

Materials used for bearings should be made of corrosion-

resistant materials or protected by suitable films of oils, greases, or other coatings. Seals should be provided around joining surfaces or couplings to exclude minute particles or dirt. These precautions are particularly important for parts mounted on the exterior of a vehicle since they are most subject to weathering.

5.3.5 Encoder

The S069 experiment requires 16 bit encoders. A shaft position encoder has been selected which makes one revolution for 360° readout. Because the XSU will only be positioned $\pm45^\circ$ in both the X and Y axes, the encoder need only cover 90°; however, any value of coverage beyond the 90° spread, up to 360°, will suffice.

A choice between incremental, absolute or a combination of the two still had to be made. An incremental encoder would be ideal for a digital servo loop, but it did not inherently carry with it a simple means of zeroing and/or updating its position.

An absolute readout encoder had precise position information, but required more electronics because of the need for V-scan or U-scan operation. Parallel readout meant that many more conductors would be needed in the cable between the XSU and the MDA. Ultimately, we look to the least hardware and maximum probability of success as the criterion of design.

It appeared wiser to use a combination of the two methods. The following style has been chosen: an incremental encoder with two incremental phase shifted tracks (for direction sensing) and three absolute tracks. The incremental track shall be a 16 bit track with resolution to 19.78 seconds. The three absolute tracks shall give precise measurements at 0°, $\pm 15^\circ$, $+ 30^\circ$ and $+ 45^\circ$. The encoder tracks shall cover 120° on the encoder disc. The choice of three absolute tracks allows for seven positions (2-1) for updating. The seven

positions 1 through 7 in binary will be converted to read the absolute angle within the DCU.

Further discussions on encoder selection criteria are covered in Section 5.2.1.2, Control Systems.

Axial Moment of Inertia of XSU

For the purpose of simplification consider the XSU as a rectangular parallelepiped where:
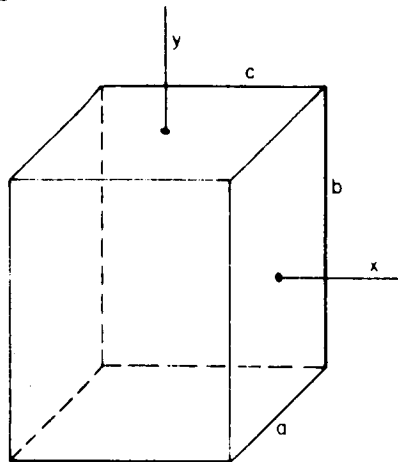
a = 10 inches

b = 45 inches

c = 36 inches

W_x = 185 lbs.

W_y = 195 lbs.

g = 386 in/sec^2

$$I_x = \frac{W_x}{g} \cdot \frac{(a^2 + b^2)}{12}; \qquad I_y = \frac{W_y}{g} \cdot \frac{(a^2 + c^2)}{12};$$

$$I_x = \frac{185}{386} \cdot \frac{(10^2 + 46^2)}{12} = \frac{185}{386} \cdot \frac{2216}{12} = 88.5 \ \text{lbs-in-sec}^2$$

$$I_y = \frac{195}{386} \cdot \frac{(10^2 \times 36^2)}{12} = \frac{195}{386} \cdot \frac{1396}{12} = 58.7 \ \text{lbs-in-sec}^2$$

Friction Torque

Coefficient of friction is low, since oils or greases will not be employed. The drag effect of lubricants on conventional ball bearings, increasingly noticeable as speed increases and temperature declines, is absent in dry film lubricant.

X-Axis

$$T_x = \frac{\mu\ P\ d}{2}$$

P = 185 lbs.

d = 1 inch

μ = 0.005

$$T_x = \frac{185 \times 1 \times 0.005}{2} = .46\ \text{in.-lb.}$$

Y-Axis

$$T_y = \frac{\mu\ P\ d}{2}$$

P = 195 lbs.

d = 7 inches

μ = 0.005

$$T_y = \frac{195 \times 7 \times 0.005}{2} = 3.41\ \text{in.-lb.}$$

Angular Velocity of X- or Y- axis assume 1/8 RPM or

ω = 0.013 rad/sec

Angular Acceleration

$$\alpha = \frac{\omega}{\tau}$$

ω = 0.013 rad/sec

τ = 0.5 sec

$$\alpha = \frac{0.013}{0.5} = 0.0065\ \text{rad/sec}^2$$

Torque Required

X-Axis

$$T_x = I_x \cdot \alpha = (88.5) \times (0.0065) = .575 \text{ in.-lb.}$$

$$T_{total} = .575 + .46 = 1.035 \text{ in.-lb.} = 16.5 \text{ in.-oz.}$$

Y-Axis

$$T_y = I_y \cdot \alpha = (58.7) \times (0.0065) = 0.38 \text{ in.-lb.}$$

$$T_{total} = .38 + 3.41 + 3.79 \text{ in.-lb.} = 60.6 \text{ in.-oz.}$$

5.3.6   X-Ray Proportional Counters

The X-Ray counter design for the S069 program originated
with the counter design used on the S017 and rocket experiments. The
S017 design had a mismatch in coefficients of thermal expansion
between the aluminum body and the beryllium windows which was mitigated
by the use of a monel faceplate. The monel, having approximately the
same coefficient of expansion as beryllium, enabled the resulting
stresses to be concentrated at the aluminum monel joint away from the
fragile window area. The use of monel generated a second problem,
however, excessive weight. A search for a design which was both
lightweight and did not have a thermal coefficient mismatch resulted
in the selection of an all-beryllium counter. The present configuration
is shown in Figure 5-14. The counter is composed of a beryllium cathode,
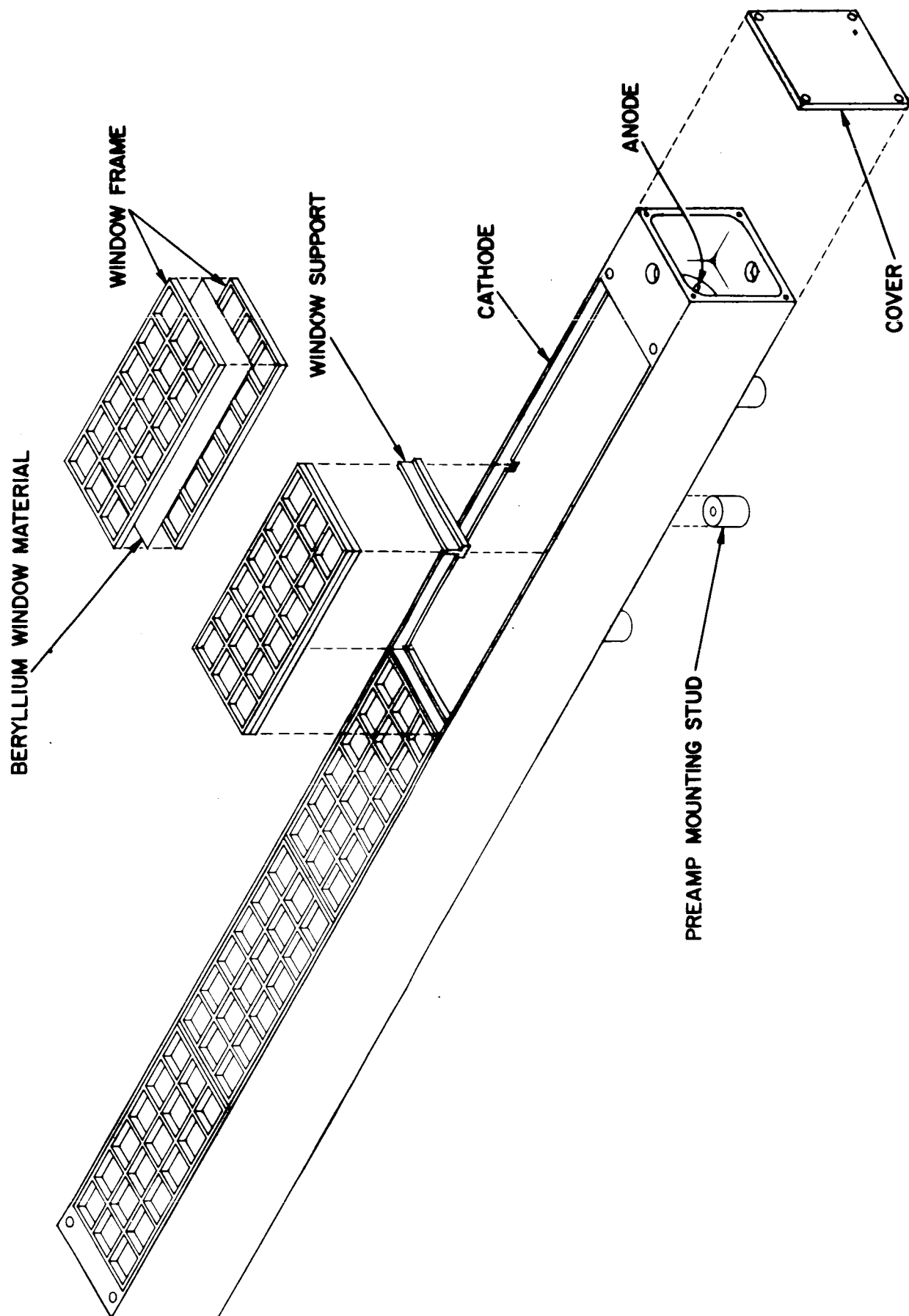
Figure 5-14 X-Ray Proportional Counter

WINDOW FRAME

WINDOW SUPPORT

BERYLLIUM WINDOW MATERIAL

CATHODE

ANODE

COVER

PREAMP MOUNTING STUD

four T-shaped window supports, and five window sections. Each window section is composed of two window frames with a thin beryllium sheet sandwiched in between. The use of five window sections as opposed to one long section was selected for two reasons. First, the beryllium sheet for our specifications is not readily available in lengths greater than six inches, and secondly, in the event of a window failure, one short section can be removed and replaced at considerably less expense than one long section. A detailed specification covering design, performance, quality assurance and testing requirements for the counter has been prepared. It has been sent to several counter manufacturers for review, and upon receipt of their comments, final changes will be made. LND, Inc. has indicated they can produce a lightweight counter that can withstand a wide temperature range by utilizing a magnesium cathode.

Reuter-Stokes, on the other hand, claim that their counter made of aluminum can also withstand a wide temperature range.

Harshaw Chemical has suggested a counter with an all-welded construction to avoid gas contamination from epoxy outgassing. This concept will be investigated and sample counters may be purchased for evaluation.

5.3.7 Background Proportional Counters

Background proportional counters are similar to the X-ray counters except that they do not have an X-ray window. One method of fabrication already used is to weld together two extruded aluminum rectangular tubes. This concept is shown in Figure 5-15. Two gas volumes, instead of a single large one, are maintained in this

PINCH-OFF

CATHODE

ANODE
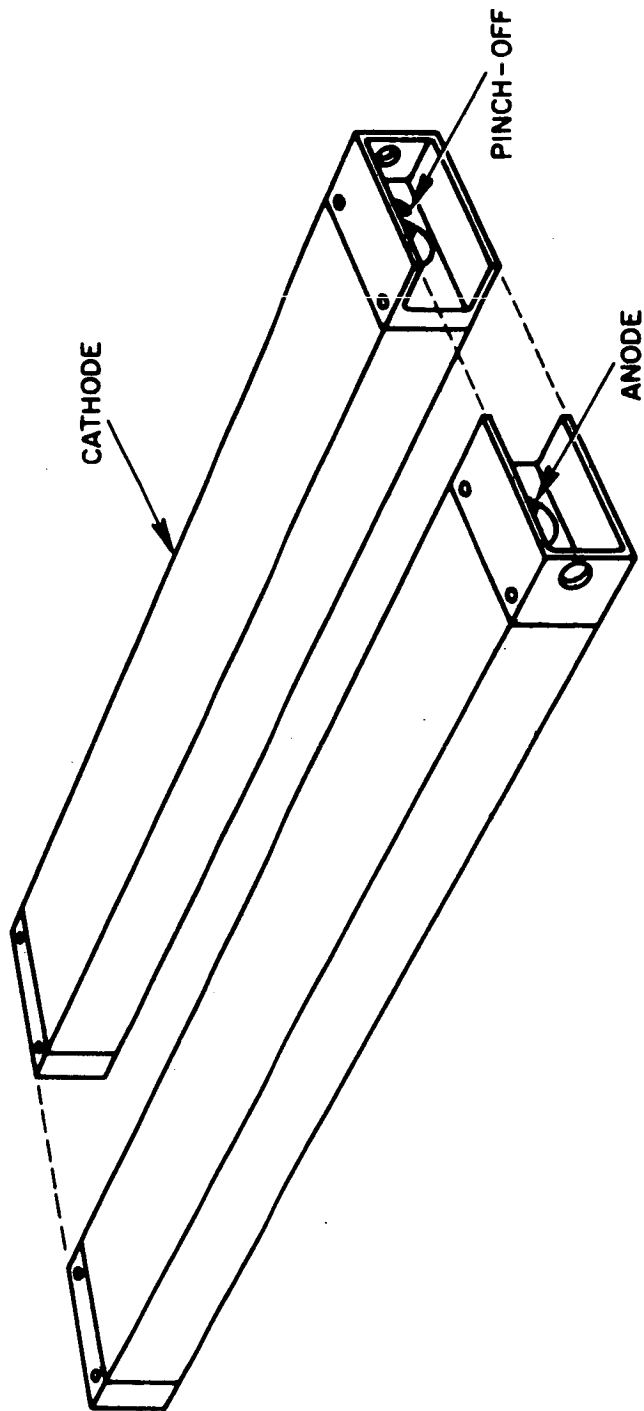
Figure 5-15 Background Proportional Counter

method in order to increase the potential reliability. The two gas volumes are sealed off from each other so that if one fails, operation of the other will not be affected.

5.3.8 Collimator Fabrication Technique

The collimators are mounted to a very rigid structure in front of the proportional counters. Several different fields of view were considered and many techniques of fabrication were investigated. Four of these were selected as the most promising for further study and evaluation. Investigation of manufacturing techniques was based on the following assumptions:

(a) field of view will be rectangular, $1/2^\circ$ x 10° full width

(b) 85% transmissibility

(c) wall thickness (from cell to cell) minimum .001 in. x
.020 in.

(d) material: aluminum

(e) depth: 3 in. to 5 in.

The four manufacturing techniques are as follows:

(1) Chemical milling
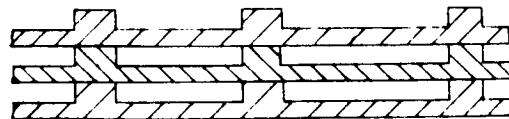
Etched, to required depth and width, aluminum sheets are stacked, one on top of the other, maintaining alignment for optimum structural stability, and optical accuracy.

(2) Rectangular tubes
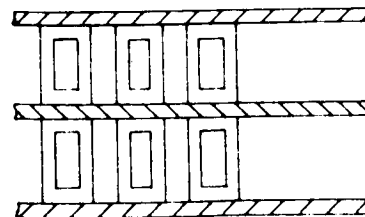
Here, the tubes are of uniform thickness of .001 inch, spaced from each other vertically by a .020 inch separator, and horizontally by a gap equalled to the inside width of a tube.

(3) Sandwich technique
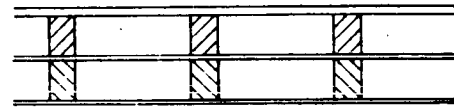
.003 inch thick aluminum sheets are separated by .020 inch square aluminum spacers epoxy bonded in place.

(4) Honeycomb
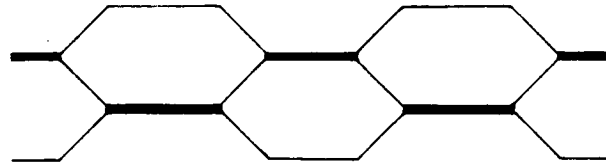
Material in web or roll form is fed into high-precision machines where continuous ribbons of structural adhesives are applied. Sheets are cut and stacked layer upon layer on HOBE form. HOBE slices are then expanded to honeycomb panels.

The estimated weight in pounds per square foot of frontal area and transmission in percent is shown in Figures 5-16 and 5-17 respectively.

5.3.9 Gas Replenishment System

The Gas Replenishment System, as shown in Figure 5-18, will be required to perform the following operations during the various phases of the mission:

5.3.9.1 Pre-Launch - Capable of maintaining a slight pressure over atmospheric to prevent contamination.

5.3.9.2 Launch - Capable of venting the counters to avoid bursting of the windows.

5-45

CHEMICAL MILLING AND
SANDWICH TECHNIQUE

HONEYCOMB

RECTANGULAR TUBES

POUNDS PER SQUARE FOOT

LENGTH (INCHES)
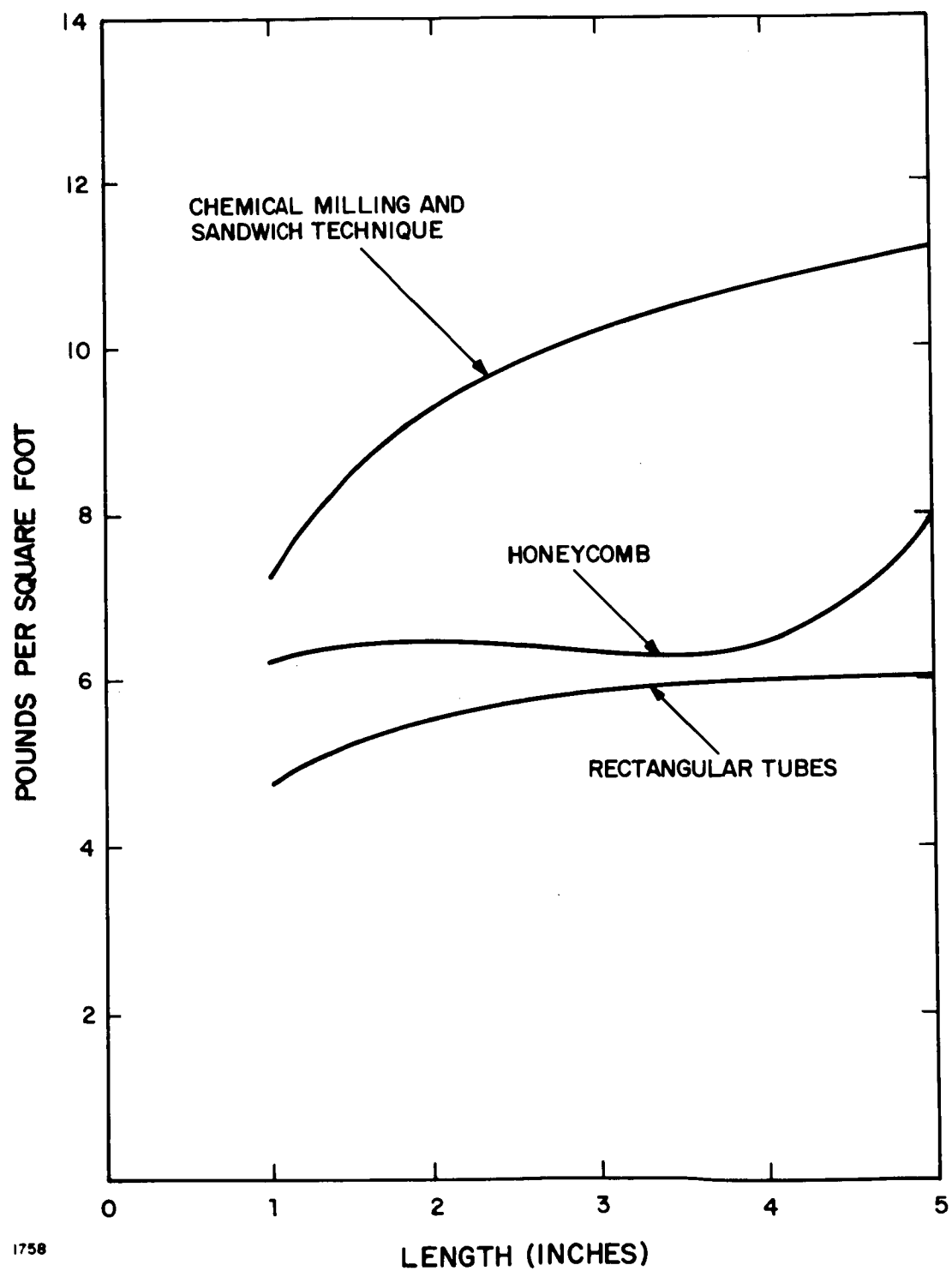
1758

Figure 5-16   Weight Comparisons of Various Fabrication Techniques
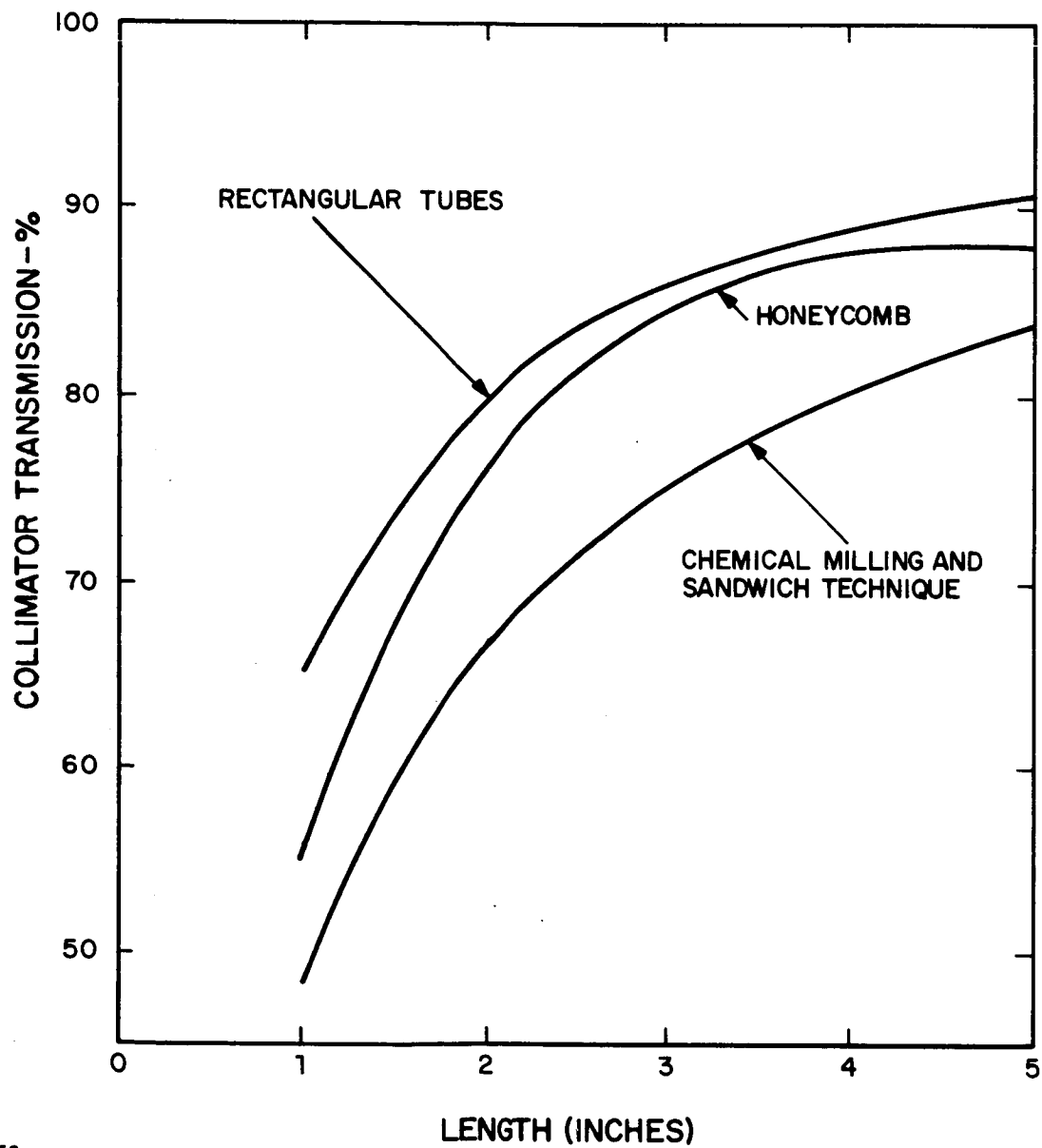
Figure 5-17 Estimated Transmission of Collimators in %

1758

Excess Pressure Vent (One Way Device)

Gas Resevoir A — R_1 (P_1) → Vent

V_2 V_3 → Vent

Data Counters V_1 → Gas Regulator Counter, Initial Gas Filling, and Internal Radioactive Source

V_4

Gas Increment Volume

Gas Resevoir B — $R_{2(B)}$ V_5

Note:

Counter Should be Slightly Less Than One System Filling
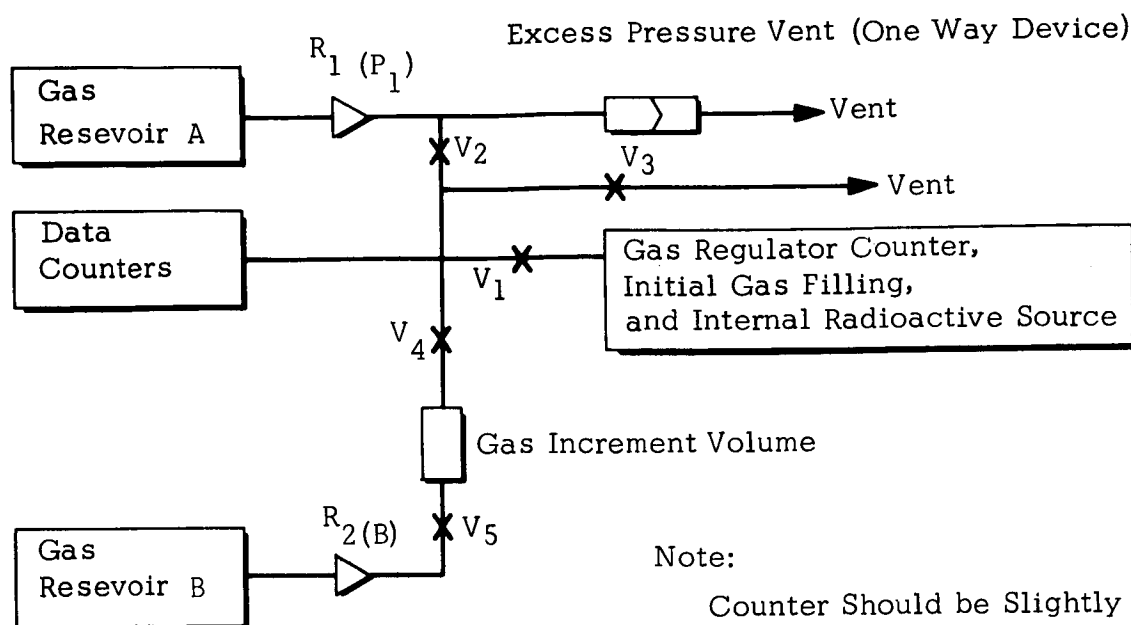
R_1, R_2 = Pressure Regulators
P_1 = Ambient Pressure + 10 cm Hg
Vent Pressure $\simeq$ 15 cm Hg
P_2 = Several Times Operating Pressure

Phase	V_1	V_2	V_3	V_4
Prelaunch	C	O	C	C
Launch	C	O	C	C
Early Orbits	C	C	O	C
Data Period	O	C	C	*

* During the Data Period V_4 Is Normally Closed and V_5 Open. When Gas Increments Are Necessary, V_5 Is Closed, V_4 Opens Momentarily and Closes, Then V_5 Opens.

Possible Electronics

Input Gas Regulator Counter → PHA (2 Channel PHA) → CRM / CRM (Count Rate Meters with Appropriate Time Constants) → Diff Amp (Differential Amp) → Disc → ...

Close V_5 Open V_4

Inhibit Input → Disc → Gate Generator

Delays (Monostables with Trailing Edge Timing)

Close V_4

Open V_5
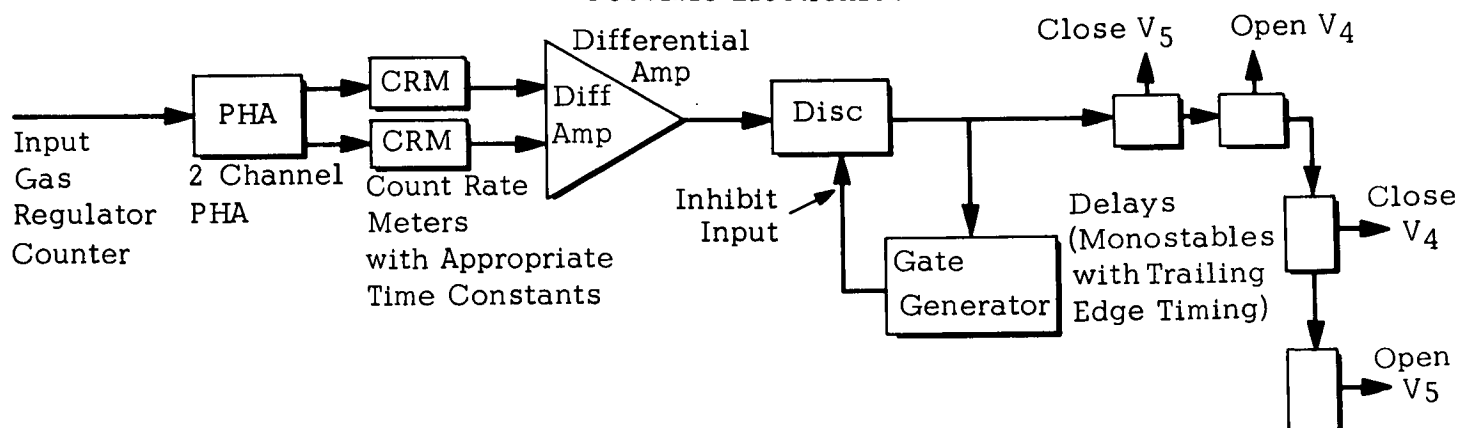
1758

Figure 5-18 Block Diagram of Constant Gas Density System

5.3.9.3   Orbit – Continual venting of the counters in order to remove contaminants which could be introduced during launch.

5.3.9.4   Data Period – Capable of maintaining a constant density gas.

5.3.9.5   Constant Gas Density – This requirement will be achieved by including a radioactive source and a control counter sharing the gas system of the data counters. The control counter would be connected to a two channel Pulse Height Analyzer (PHA). Hence, the source line would be evenly divided between the two channels during operation. A gas density change would change the ratio of counts in the two PHA channels. This ratio change would be used to correct the gas density. The correction could be either a small gas dump or an analog control.

5.4 Internal Camera Assembly

An absolute aspect measurement will be made by photographing the star field. A camera mounted inside the MDA will be capable of providing the aspect information. A camera suitable for this application, a 16 mm cine sequential with detachable magazine, is manufactured by J. A. Maurer, Inc.

The camera will be mounted to a fixed position relay lens system, and will be focused on an image coming from a flexible, coherent fiber optics light pipe. The outboard end of the fiber optics pipe terminates at an objective lens system mounted on the X-ray sensor unit.

The camera mechanism consists basically of a solenoid, a solenoid actuated clutch, a micro-motor and associated gearing. The number of frames exposed per second is determined by the rate at which the solenoid is pulsed. The motor and clutch are controlled by an

*Mixture of gaseous oxygen at partial pressure of 3.7 psia and gaseous nitrogen at partial pressure of 1.3 psia.

internal, solid-state transistorized circuitry. Film loss never occurs in any mode of operation, because the transistorized circuit automatically causes the clutch to disengage after each exposure and prevents it from re-engaging the micro-motor until the solenoid is pulsed again.

5.5 Systems

As shown in Figure 5-19, the System Function Block Diagram, the Apollo S069 Experiment may be considered as composed of the following major functional groupings:

1. Positioning System

2. Data Storage and Transmission System

3. Signal Conditioning System

    a. Amplifiers

    b. Pulse Shape Discriminator

    c. Logic and Timing Networks

    d. PCM Encoder

4. Aspect Sensing System

    a. Cameras, F.O.

    b. Start Tracker

    c. TV or other

5.5.1 XSU Positioning System

The Analog Positioning System enables the Sensor Array to be pointed to any location that is within $\pm$ 45 degrees in either the horizontal or vertical direction as illustrated in Figure 5-5. Motion in two orthogonal directions is supplied. The Sensor Positioning System shall be a firm, rigid, non-slip type which maintains the set angles throughout

X-RAY SENSOR UNIT

DISPLAY & CONTROL UNIT

MAIN TOWER 28V

MOTOR X AXIS Y AXIS

CAMERA

STAR SENSOR

±45° LIM. CKTS

FIBER OPTICS

SUN SENSOR

ENCODERS X AXIS Y AXIS

SENSOR MOTOR

SERVO ELEC.

CONTROLS

STAR SENSOR DISPLAY

HOUSE KEEP CONTROLS

X-AXIS Y-AXIS COUNT RATE DISPLAY

SENSOR MOTOR CONTROL DISPLAY

NUMERIC DISPLAY AND ELECTRONICS

X-AXIS Y-AXIS SENSOR POS. DISPLAY

LIGHT PIPE

SUB-COMM.

A/D

TO SW. ON DCU

HIGH VOLTAGE SUPPLIES, 4 PER QUAD.

PRI. PWR.

REFERENCE VOLTS

BACKGND DET.   OTHER DET.

TO DCU

AMPLIFIER SUPPLIES, 2/QUAD.

X-RAY CALIBRATE

FRAME FORMATTER

GAIN ADJ.

BACKGROUND DET. / PREAMPS 9 PER QUAD.   9

SUM AMP 1/QUAD.

THRESH. DET.

ANALOG COUNT RATE

PHA-

ACR

AMPLIFIERS GROUP 1

PULSE SHAPE DISC.

PULSE HEIGHT DISC.

INH.

INH.

NOR

AND

OR

PSDR

SRI

NRI

TRI

QUAD. A

BE. WINDOW DETECTORS & PREAMPS

SUM AMP

QUAD. B

BE. WINDOW DET. / PREAMPS USING MODULATION COLLIMATION

SUM AMP

AMPLIFIERS - GROUP 2

8 BIT SCALERS

QUAD. C

BE. WINDOW DETECTORS & PREAMPS (6)

SUM AMP

AMPLIFIERS - GROUP 3

PHA 2 2 LEVEL

QUAD. D

MYLAR WINDOW DETECTORS & PREAMPS

SUM AMP

AMPLIFIERS - GROUP 4

PHA 3 2 LEVEL

PHA 4 8 LEVEL

GAS SYSTEM

DET. SELECT SWITCH MATRIX

PHA SELECT SWITCH MATRIX

ANALOG CIRCUIT POW. SUP.

DIGITAL CIRCUIT POW. SUP.

X-RAY DATA ANALYZER

5-51-A

Figure 5-19 Functional Block Diagram

orbital conditions. The detectors, aspect cameras, etc., shall be supported in a rigid fashion. What follows is a listing of performance criteria, then a brief discussion of Control Systems.

5.5.1.1   Design and Performance Criterion - The XSU Positioning System shall meet the following design and performance criteria:

Limits of Motion - The Sensor Positioning System shall be capable of pointing the X-ray Sensor Array a minimum of $\pm$ 45 degrees about two orthogonal axes.

Sensor Positioning Controls - The Sensor position controls shall be located on the Display and Control Unit and will be operated by the astronaut.

Pointing Accuracy - The Sensor Positioning System shall have a $\pm$ 0.1 degree pointing accuracy to the desired deviation angle from the null position on the XSU.

Angular Drift - With no command input, the angular drift of each axis shall be less than 0.1°/Orbit.

Smoothness - During periods of constant angular velocity motion, the angular accelerations shall be less than 0.1 arc min/sec^2.

Angular Readout Resolution - The resolution of angular read-out to telemetry shall be $\pm$ 20 arc seconds, maximum.

Scanning - Scanning is defined as a regular motion about a fixed orientation in space of the Sensor Array central axis. The scanning is required in order to:

(a)   Discover unknown sources of X-rays.

(b)   Pinpoint the location of known but weak sources.

(c)   Point the array at known X-ray sources. The astronaut will position the Sensor Array approximately on target and then go into a scan pattern. By observing the real time displays, he will then fix on the target.

(d)   Determine the outlines and intensity distribution of a large source. This is accomplished in conjuntion with a one-way scan on one axis and the output of the modulation collimators.

Modes of Operation - The Sensor Position System shall provide two modes of operation:

Manual Mode

Scan Mode

(a)   Manual Mode - When the "Scan Mode Control" is set in "Manual" position, the astronaut can then manually position the XSU. He does this by dialing the attitude he wishes the XSU to assume. Thumb wheels, each wheel graduated in decimal steps, are provided. The maximum slew rate will be 1 degree/second.

(b)   Scan Mode - In this mode, the Sensor Array is set automatically in a scan pattern on a fixed point in space by the astronaut with the appropriate setting on the scan mode control. Two scan rates with stepped increments between each rate will be provided:

Fast.............................5 arc min/sec.

Slow.............................1 arc min/sec.

Both axes may be operated independently or simultaneously.

Typical scan patterns being considered are:

a. Back and forth motion about a small region in space.

b. Long zig-zag motion along an arc of a great circle.

Parameters, such as range of scan, velocity of scan, and uniformity of motion are to be determined.

Scan Pattern - The scan pattern has not been defined as yet. However, it is desirable to have a type of pattern which utilizes the least power, and will generate the required data most efficiently. The final scan pattern adopted will have a minimum number of instantaneous reversals per field.

Scan Rate - Scanning must be accomplished at a slow rate. Hence, the maximum scan rate that will be used is 0.10 degrees/second.

Motor Cogging - Less than 20 seconds of arc.

Duty Cycle - The estimated duty cycle is 50 percent. Typical servo operation: start, stop, and reversals.

5.5.1.2   Control Systems - There are two broad classes of control configurations, open and closed loop, Figure 5-20. The open loop system is familiar: a command signal is generated. This is amplified to power a motor which in turn, moves the load, in this case the XSU. Closed loop does this too, but with an added feature: it generates a signal at the output as well (at the XSU) indicative of the load motion. This signal is compared with the command signal, by feeding it back, and the difference between the two is used as a corrective signal (error signal). The error
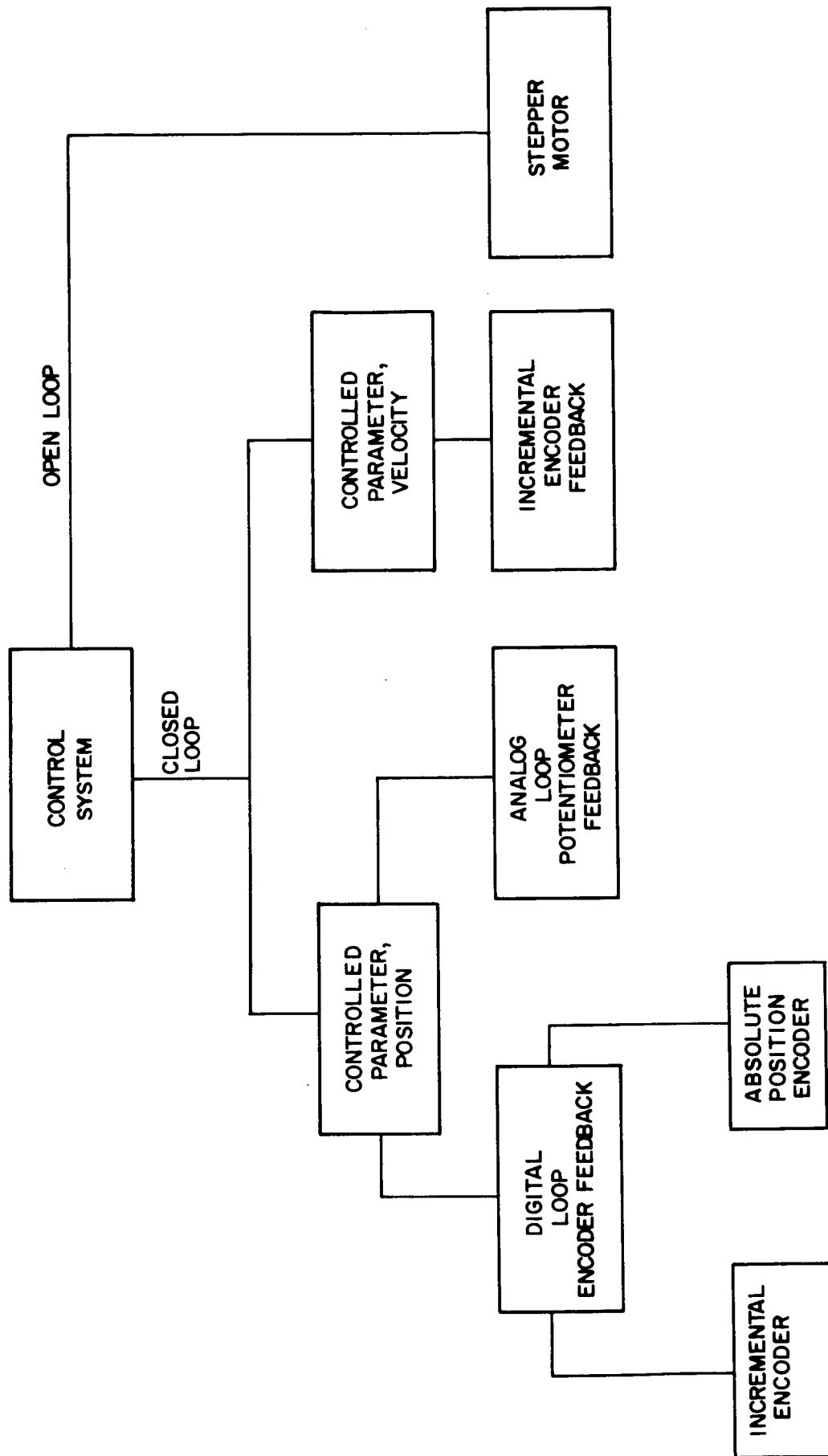
Figure 5-20 Position System Concepts, Logic Diagram

1758

signal forces the output to go where the command signal directs. When it does so, the error goes to zero and the motor stops.

A stepper motor was contemplated as the XSU prime mover in an open loop. This motor goes in incremental steps in response to pulsed signals, each step being detented so it cannot move unless activated. It is attractive because conceptually it is simple. In practice, stepper motors come in approximately 15° steps. To attain a resolution of 20 seconds requires a gear train ratio of 15 x 60 x 60/20 = 2700 : 1. Gear train ratios of this size with its attendant backlash, mounting and friction problems, together with wear problems in digital motors, make the successful realization of this approach unlikely. A closed loop system appeared better.

Again, with reference to Figure 5-20 two choices are provided for controlling the velocity of the XSU or its position. A major drawback to a velocity loop is its susceptibility to drift. The S069 requirement is 0.1°/orbit $= \dfrac{.1 \times 60 \times 60}{90 \text{ min}} = 4$ arc-secs/minute maximum. This is very difficult to satisfy.

The choice between a digital or analog position loop is not a clear cut one. Each can be built to satisfy the performance criterion. Figure 5-21 shows the analog approach, and Figure 5-22 the digital. Identical power amplifiers, torque motors, and readout encoders are common to both. The bulk of the cost is contained in these items, making each system's cost roughly equal. It will be noted that the analog system contains an inverter at its input circuits. This is brought in to make the command circuits less vulnerable to drift. An inverter with its extra weight and possible RF interference effects is a liability, yet this is balanced by the greater complexity involved in the digital error register.
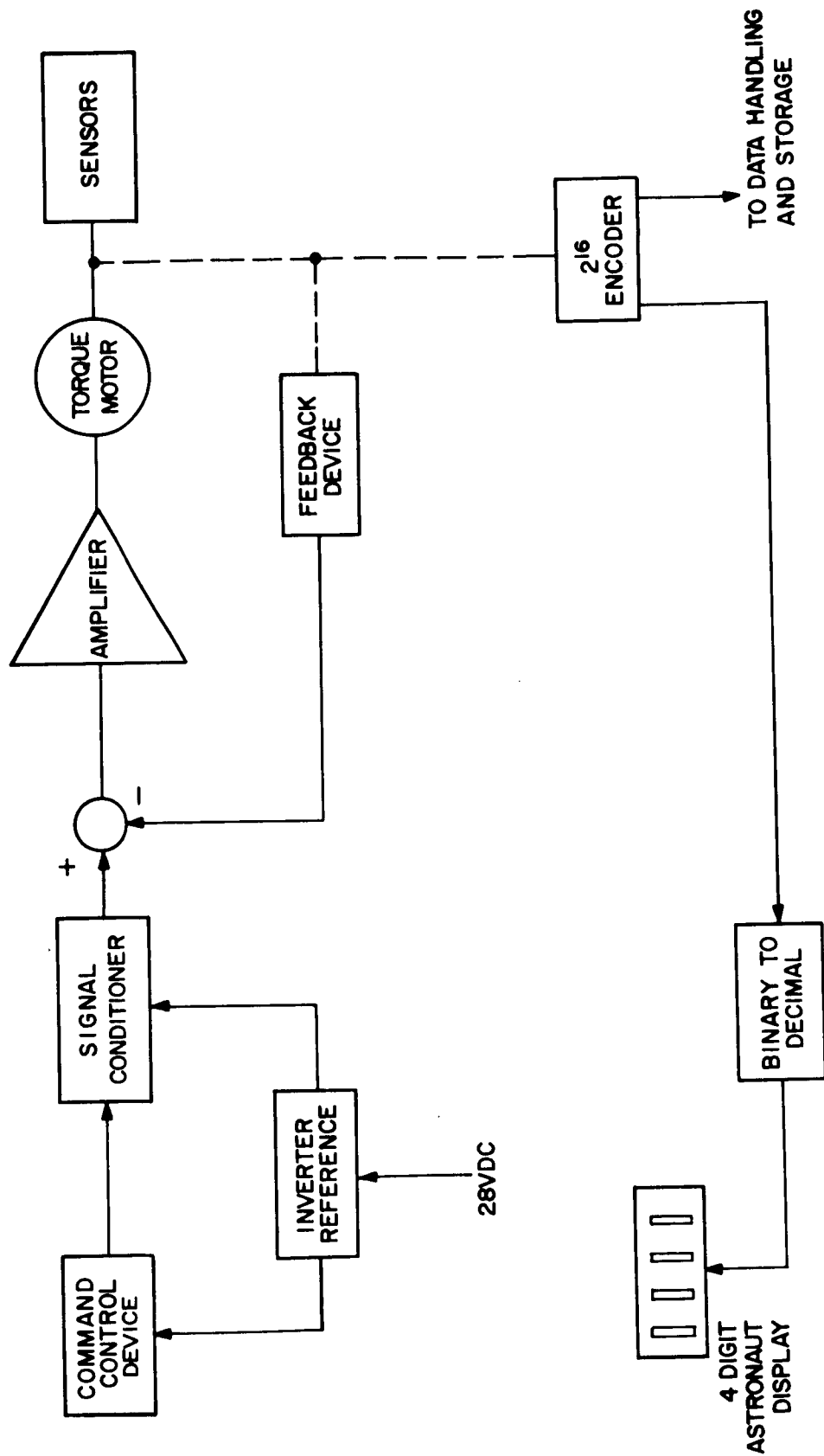
Figure 5-21 Analog Positioning System

1758
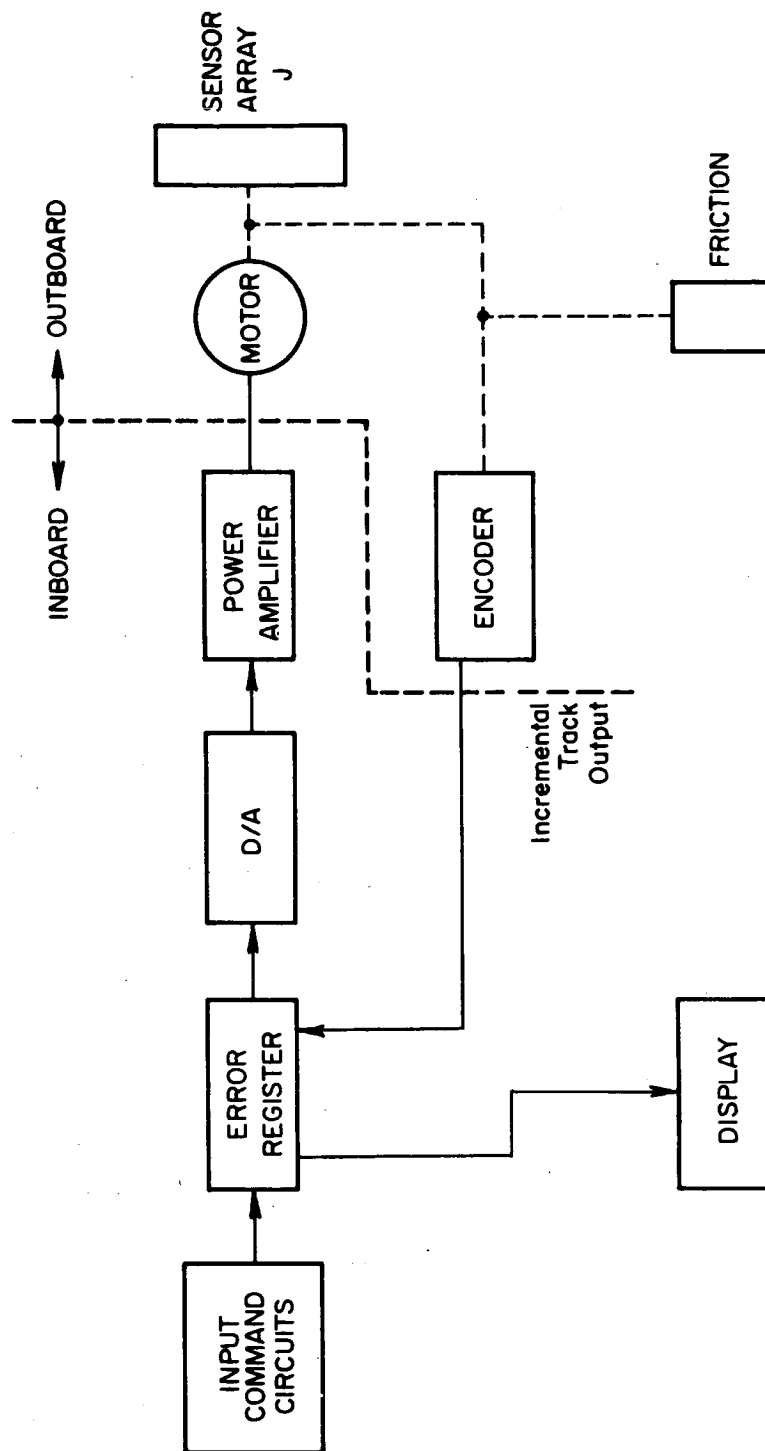
Figure 5-22 XSU Positioning System

The selected position control, Figure 5-22, uses digital techniques, and an incremental encoder.

The error register duplicates the function of the comparator (or summing point) of the analog servo loop.

The error register is actually comprised of two registers: one to store the input command, and another to store the position of the XSU.

The input command is a natural binary number, and the XSU position also is encoded as a natural binary number. Digital subtraction is performed on these two numbers continually. The result, with a sign, plus or minus, is converted to an analog voltage. This voltage represents the difference between the desired position of the XSU and the actual, hence the term "error". Ideally, if any error voltage exists, it will drive the torque motor of the XSU in a direction to reduce this error (and error voltage) to zero. Since the motor responds only to error voltage magnitude, it stops automatically.

The input command is obtained from the thumbwheel control in the DCU panel, as set in by the astronaut. It contains a sign, and three decimal numbers, for example, $\pm 20.6^{\circ}$. These numbers are converted to natural binary internally. The XSU, at reference position, is considered to be at zero degrees. Since it can go plus or minus about this reference, sign must always accompany the number. The binary number is then set into register "A", of the error register, replacing the number already there.

A 16-bit incremental encoder on the drive axis generates one pulse (or bit) for every 19.77 seconds of arc movement of the XSU. The present position of the XSU is encoded in the "B" register of the error register. It is the B register which counts or accumulates the pulses from

the encoder, thus keeping track of the XSU position.

A new command set into the X register will not agree numerically with the present position number in the B register. It is then that an error results, and the position control acts.

Two general classes of shaft angle encoders exist, incremental and absolute. As stated, the incremental generates a train of pulses, each pulse spaced one from another at a small angular "increment". The absolute position encoder has imprinted upon its disk a unique pattern which can be translated into signals. A separate pattern exists every 19.77 secs of arc over the total excursion of 90° ($\pm 45^{\circ}$). A separate accumulator, needed for the incremental is not required for the absolute. If the imprinted angular numbers (absolute) are in Gray code, 16 conductors plus a return (exclusive of power, heaters, etc.) are required, whereas the incremental requires a total of 2. A total of 34 conductors is required for the two absolute encoders, compared to 4 conductors if incremental encoders are used. These conductors must be brought into the MDA via a sealed connector in the spacecraft wall. The reliability of a connector goes down with every increase in the number of pins, going down in an exponential way. (MIL Handbook 217-A). Clearly, it is a great advantage to keep the number of conductors down.

Gray code is superior to natural binary in that it avoids the possibility of an ambiguous readout. Natural binary encoders can be modified to avoid ambiguity by using V scan techniques. When this is done, the conductor quantity per encoder rises to 32 plus a return. (This can be reduced to 17 by using logic networks within the encoder).

To Summarize: With an absolute encoder, to avoid ambiguity in angular number presentation, one must use: a non-natural binary code

(Gray), accept 17 conductors, and then convert to natural binary within the E. U. for position control operation.

With an incremental encoder, 2 conductors are needed. There is no possibility of ambiguity, and an accumulator within the E. U. is needed to store the count.

In the practical engineering model, it is proposed to use some absolute position numbers on the same disk as the incremental to update the stored count periodically, as it is possible that a stray noise pulse would upset the number in the accumulator.

5.5.2 Data Storage and Transmission System

The Data Storage System - Signals will be in PCM only, or PCM-FM format.

Voltage Controlled Oscillators (VCO) - If a PCM-FM system is used, voltage controlled oscillators will be redundant and will have an input common mode rejection of 100 db minimum, 40 db minimum at 1000 Hz and decrease linearly to 35 db at 2000 Hz for the common mode voltages up to 50 V. The power ground, input signal return, and chassis ground shall be mutually isolated from each other.

The VCO output frequency shall change no more than 1% of design bandwidth when the signal source impedance is varied within the nominal range.

The output at center frequency shall be adjustable from zero volts to at least 1.5 volts, peak to peak across its load.

AM of the output waveform measured across the bandwidth shall not exceed 10 percent.

Relative to the DC response, the frequency response shall not vary more than 2 percent out to a cut-off frequency corresponding to a MI of 2.

Voice - Provisions for getting voice data either Real Time or Recorded, shall be made. The audio data shall be mixed directly with the VCO outputs and shall appear directly on the transmitter baseband.

Transmitter - The RF link shall be implemented by a frequency modulated TBD watts transmitter operating on a center frequency to be determined; it shall feed the spacecraft VHF antenna system. The transmitter shall be deviated in accordance with IRIG Standards.

(a) RF Carrier Power Output - A minimum of 5 watts, terminated in 50 ohms for all input voltages and anticipated environmental conditions.

(b) Carrier Deviation - The deviation of the carrier frequency shall be ± 125 kc.

(c) Isolation - Isolation impedance between the modulation input, output, and 28 VDC power input shall meet or exceed the limits specified.

Recorder - Recorder operation is straightforward. The data system shall afford either real time data transmission or data recording, whichever the operational situation may call for. Signal switching shall be accomplished in a way that minimizes variations of signal circuit loading and that will maintian high reliability. Real time operation may be implemented by merely by-passing the tape recorder.

(a) Recorder characteristics will be:

Configuration	Reel to tape transport using concentric shafts
Record Time	44 minutes
Playback Time	4 minutes
Playback Tape Speed	40 ips

To make possible overall airborne and ground support recorder wow and flutter compensation, a 32 Hz reference oscillator shall be mixed with the VCO outputs of the airborne data system.

Data Readout and Sampling Rates – Listed as follows are typical data channels required to be returned on telemetry and the frequency and precision of each one. Only those that apply to the experiment directly have been included. There are additional engineering requirements. The sampling rates may be used as a guide and may be negotiated in the interests of compiling a reasonable telemetry system.

(a) Digital Data

Channel Designation	Precision	Sampling Rate
Channel X1	12 bits	8 words each 5 per second
Channel X2	12 bits	2 words each 5 per second
Channel X3	12 bits	2 words each 15 per second
Channel X4	12 bits	8 words each 5 per second
Camera #1	30 bits	once every 8 seconds
Camera #2	30 bits	once every 2 seconds
Shaft Encoder X	16 bits	once every second
Shaft Encoder Y	16 bits	once every second

Data from Quadrant 1 and Quadrant 4 may be in serial form provided that the time interval between the end of the data accumulation period of the first and last of the 8 channels does not exceed 20% of the interval between readout cycles, (i.e. 40 msec for 5 samples/sec). Data from Quadrant 2 and Quadrant 3 should be coincident.

In addition to these data the following five counting rates are defined and may be monitored as listed below:

Total Rate (TR) – This is the rate from the detectors without anticoincidence, PSD or any energy discrimination.

AC Rate (ACR) – This is the rate of inhibit pulses from the anticoincidence logic to the signal rate.

PSD Rate (PSDR) – This is the rate of inhibit pulses from the PSD logic to the signal gate.

Sum Rate (SR) – This is the logical sum (Not arithmetic sum) rate of AC rate and PSD rate. If a pulse occurs in both AC and PSD outputs simultaneously, it is only counted once.

Net Rate (NR) – This is the signal rate after energy discrimination, AC and PSD inhibit. It is identical to the main scaler outputs.

Monitor Circuit – The monitor circuit will be a standard 8-bit scaler preceded by a window energy discriminator. All circuits in this

5-65

monitor should be fed from an isolated power supply since it must be possible to turn off the digital supply and maintain normal operation.

5.5.3   Signal Conditioning System

The Signal Condition System accepts the signal from the proportional counters and processes it into a digital signal for storage on the tape recorder. The functional block diagram is shown in Figure 5-19.

5.5.3.1   Amplifiers – It is difficult to divorce the amplifier design from the system design since a drastically different performance can be required depending on the physical location of the PSD module. The four solutions to the amplifier-PSD problem that were considered are: (a) PSD Gating inside MDA, slow risetime preamp for total energy measurement, in parallel with a fast preamp for PSD both on the XSU; (b) PSD gating inside MDA, common fast preamp for both PSD and total energy measurement, then split the two into separate paths inside the MDA; (c) PSD gating on the sensor array outside the MDA, parallel amplifiers as in solution (a) and (d) and total energy measurement on the sensor array outside the MDA.

Solution (a) requires two preamps per quadrant out on the array and implies diverting some of the signal charge to the PSD channel thereby degrading the signal to noise ratio of the total energy channel. This also requires exposing more circuitry to the temperature extremes of the XSU and two coaxial cables per detector quadrant being brought through the MDA wall. The only advantage is the reduction of bandwidth required on the total energy channel. This will allow the use of more feedback (for the same amplifier) to stabilize the gain thereby increasing the accuracy of the total energy measurement. The PSD amplifier stability need not be as high as the total energy amplifier since the PSD threshold

is not as critical as the total energy measurement.

Solution (b) requires a bandwidth for the common amplifiers of about 70 MHz with a gain of about 7. Since the total energy channel uses the preamp it must be gain stabilized over the temperature extremes found on the XSU. The wide bandwidth required for PSD will degrade the signal to noise ratio but as long as the preamp does not overload on noise the ratio can be improved by filtering after the PSD is split off inside the MDA. Only one coaxial cable per detector quadrant needs to be brought through the MDA wall.

For solution (c) to be more effective than (a) the PSD gating must be done on the array which implies the use of a linear gate. The linearity and temperature performance typically found in high speed linear gates precludes their use in this application. The design effort required to develop an acceptable linear gate is disproportionate with the alternative solutions.

Solution (d) requires exposing a major portion of the total energy electronics to the array temperatures, as well as bringing many digital signal wires through the MDA wall. Both of these are undesirable as the temperature extremes will tend to degrade measurement accuracy while the digital wires will require buffer amplifiers to drive the shunt capacity of the excess wire length.

The best compromise appears to be solution (b) as it uses the fewest components, places the least number of elements on the array and has the minimum number of wires brought through the MDA wall.

Two prime factors determine the number of preamps that will be required for each detector array: reliability and system alignment.

Each array will consist of 6 proportional counters tubes which are delivered from the manufacturers with a ±20% gain variation. Some method of gain equalization must be provided in the system to allow an accurate measurement of total energy. This can be accomplished by (a) varying the accelerating potential of each tube, (b) attenuating the inputs to the preamp, or by (c) varying the preamp gain. The first method requires either separate supplies (6 per array) or high voltage resistive dividers. Separate supplies are obviously not feasible and resistive dividers are undesirable due to the instabilities associated with high voltage resistors as well as the difficulties encountered in trimming a divider network with 2,000 volts impressed on it. Method (b) does not permit the use of low imput impedance preamps, which is quite desirable as the tubes are charge sources, since the attenuation networks will have to consist of extremely small resistors. This method is also undesirable as it shunts some signal away from the amplifier, and therefore must degrade the signal to noise ratio. These two methods have the advantage of permitting the use of a signal preamp for each detector array, not considering system reliability.

The last method allows the use of a common high voltage supply for all the tubes in an array (or all the arrays), has a better signal to noise ratio than method (b) but requires a separate preamp for each tube. A reliability analysis was performed to show the difference between using method (b) with 2 tubes per preamp and method (c). The results showed method (c) to be an order of magnitude more reliable.

Based on these considerations the decision was made to use method (c). The anticoincidence tubes do not need to have their gains equalized as no total energy measurement is performed on their output.

The next item to be considered in the system configuration is the quantity and physical location of the amplifier which sums the outputs of all the tubes in a single array. Locating this amplifier inside the MDA wall requires 6 coaxial cables be brought through wall for each array. It also requires that each preamp have capability to drive about 20 feet of coaxial cable shunt capacity. The other choice is locating the summing amplifier near the preamps on the array, thereby reducing the number of coaxial cables to be brought through the MDA wall. A reliability analysis was performed to show the difference between using 3 summing amplifiers, each being fed by 2 preamps, and using a single summing amplifier. The single amplifier approach was shown to be more reliable since a secondary summing amplifier must be used with the 3 primary summing amplifiers, thereby inserting another failure mechanism into the system. Thus, the decision was made to use a single summing amplifier. This will require only 1 signal coaxial cable per array be brought through the MDA wall. The anticoincidence tubes for each array will also be summed in a single amplifier and will require a second co-axial cable for each array.

The remaining amplifier is the integrating amplifier for the total energy measurement and is located in the electronics box inside the MDA since that is the most practical location for it.

Preliminary analysis has shown it to be feasible to use a basic building block approach for the amplifier design to increase design flexibility. From a black box approach, the functional differences between the three amplifier types that have been discussed (preamp, summing amp and integrating amp) are determined by the input and feedback networks. Thus, the basic building block should have high open-loop

gain, wide bandwidth, and the capability to drive at least 20 feet of co-axial cable without running into oscillation. Further analysis and design will be required in this area.

5.5.3.2 Threshold Detectors – This decision making element compares the analog signals with a preset threshold and converts the output into digital signals that are compatible with the logic building blocks. Analysis has shown that a Fairchild μA710 integrated circuit comparator can be used in the three functional modules requiring a threshold detector: the anticoincidence detector, the PSD and the PHA. Since it is an integrated circuit it can be used as a basic building block thereby reducing design, fabrication, and test time. The μA710 has been qualified on other programs and has the speed and offset stability needed for this type of instrumentation.

The anticoincidence and PSD channels may require some pulse stretching to utilize the μA710 but this is a fairly standard procedure.

5.5.3.3 PHA – The PHA is nothing more than an Analog to Digital Converter with a set of parallel accumulators counting the number of occurrences of each level. If the accumulators are considered as separate memories the A/D output can be considered as the memory address. Each X-Ray particle in the energy range of 1 to 10 kev will cause an output from the A/D thereby addressing one of the accumulators which has its contents indexed by 1 count. The accumulators are read out to the Data Storage and Transmission System at prescribed intervals.

A simple constant resistive ladder A/D is not suitable since the energy range to be digitized may not be separated into geometrically related bands. An n-bit weighted resistor network may be used, which

will require 2^n-1 decoding gates, semiconductor switches and resistors, n binaries, and a single threshold detector. The A/D will have to take maximum of 2^n-1 steps to complete a conversion; the time to complete the conversion cycle is relatively long.

Another form of A/D conversion that might be used incorporates 2^n-1 parallel threshold comparators each referenced to switch at a separate level. 2^n decoding gates and n binaries will be needed but the conversion time is exceedingly small. The stability aspects of each method and component costs still have to be analyzed before a decision can be made, however, either method appears to be practical.

The anticoincidence/PSD inhibit input is used as a common input to the transfer gates separating the A/D from the accumulator memories. In the absence of an inhibit signal the accumulators are indexed in the normal manner. However, with the inhibit signal present the indexing action is blocked.

5.5.3.4   Monitors - Five secondary signals are to be monitored and developed from the functional modules previously described. The anticoincidence (ACR) and PSD rates are derived from their respective threshold detectors, the Sum Rate (SR) is derived from the inhibit driver, the Total Rate (TR) from the lowest level of the PHA output, and the Net Rate from the input to the lowest level PHA accumulator memory (after inhibiting). These signals are digital in form and are monitored on a subcommutated basis as prescribed in the Scientific Specification.

5.5.3.5   Accumulators - The maximum number of counts which each accumulator will have to store is determined by the peak count rate at the detector array and the sample time between readouts. These quantities, listed in Table I, cluster between 960 and 5,740 counts per

TABLE II

PEAK COUNT RATES

Item	PHA	Monitor				
		Net Rate	Total Rate	A/C Rate	PSD Rate	Sum Rate
Quadrant #1 (counts/sec)	28,700	28,700	32,000	5,100	6,300	9,700
#PHA channels	8					
Counts/channel/sec	14,350	28,700	32,000	5,100	6,300	9,700
sample time (sec)	1/5	1/6	1/6	1/6	1/6	1/6
counts/sample	2,870	4,783	5,333*	850	1,050	1,617
Quadrant #2 (counts/sec)	28,700	28,700	32,000	5,100	6,300	9,700
#PHA channels	2					
counts/channel/sec	28,700	28,700	32,000	5,100	6,300	9,700
sample time (sec)	1/5	1/6	1/6	1/6	1/6	1/6
counts/sample	5,740	4,783	5,333*	850	1,050	1,617
Quadrant #3 (counts/sec)	14,400	14,400	17,000	5,100	4,800	8,200
#PHA channels	2					
counts/channel/sec	14,400	14,400	17,700	5,100	4,800	8,200
sample time (sec)	1/5	no sample	N.S.	N.S.	N.S.	1/5
counts/sample	960					1,640*
Quadrant #4 (counts/sec)	39,600	39,600	42,300	4,200	7,000	9,800
#PHA channels	8					
counts/channel/sec	19,800	39,600	42,300	4,200	7,000	9,800
sample time (sec)	1/5	N.S.	N.S.	N.S.	N.S.	1/2
counts/sample	3,960					4,900*

sample. Since each monitor uses a single accumulator for the 5 rate signals, the accumulator's size is determined by the rate signal with the largest counts per sample. These controlling quantities, marked by an asterisk, cluster between 1640 and 5333 counts per second. Except for detector array #3 which only uses 2 PHA and 1 monitor accumulator, the remaining accumulators must all be designed for count rates between 2870 and 5740 counts per sample. Design fabrication and testing time can be saved by using a single design for all the accumulators. These cost savings should more than offset the hardware cost of a few extra binaries.

An analysis of various accumulator types are performed to develop the design trade-offs between readout bit rate and hardware complexity with data accuracy as the design variable.

Three types of accumulators were considered: straight binary, S-T mode and un-normalized logarithmic.

Straight binary will require 13 binaries with no provision for overflow. As the incoming data is asynchronous to the sampling clock, the accuracy will be $\pm$ 1/2 count.

An S-T mode counter counts input pulses until the most significant bit is 1 (S mode) and then counts clock pulses until readout occurs. (T mode) as shown in Figure 5-23. During S mode operation the counter acts like a straight binary counter with an accuracy of $\pm$-1/2 count. For a counter b binaries long the equation for perfect operation in the T mode is:

$$R = \frac{2^{b-1}}{T - \frac{n_T}{f}} \qquad (1)$$

where   R = counting rate in pulses per second

T = accumulation time between readouts (sample time)

n_T = count in the first b-1 bits of the accumulator in the T mode

f = clock frequency in pulses per second.

5-73
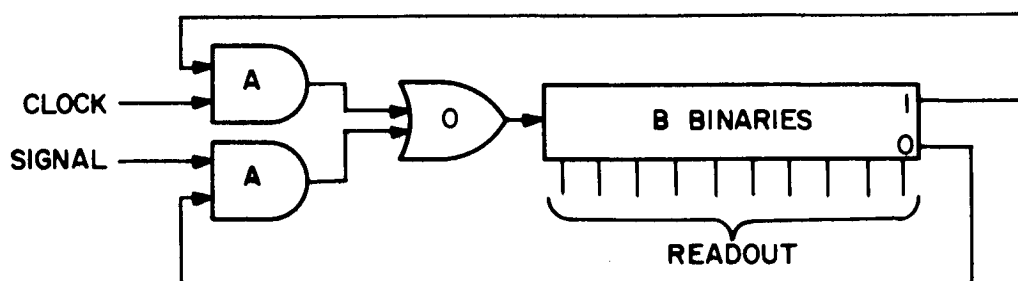
Figure 5-23 S-T Mode Counter

1758
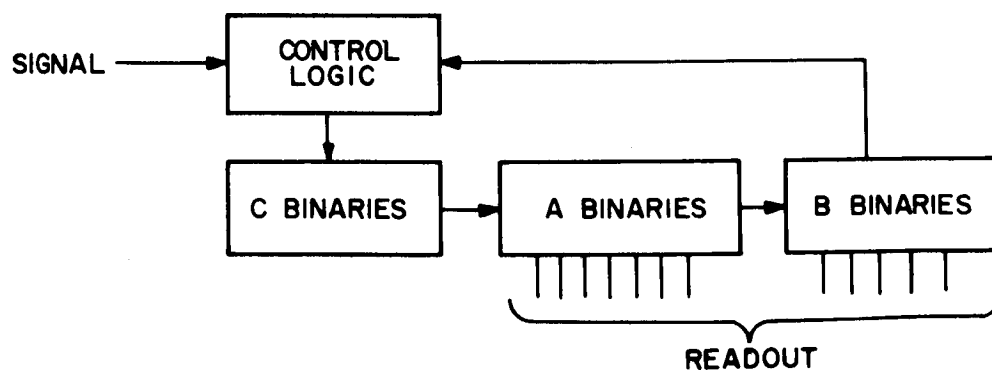
Figure 5-24 Unnormalized Logarithmic Counter

It can be shown that the maximum percentage error in the T mode is related to the input count rate, sample time and counter length by the following expression:

$$\frac{\Delta R}{R}/max = \pm \frac{RT}{2^{2(b-1)}} \times 100 \qquad (2)$$

Note that RT is the quantity listed in Table I as counts per sample. The scientific specification permits an accumulator error of no more than $\pm 1/2\,\sigma$ where σ is the standard deviation of the input count. For one sample period the standard deviation is

$$\sigma = N^{-0.5} = (RT)^{-0.5} \qquad (3)$$

The length of the S-T mode counter needed to provide this accuracy is found by substituting equation (9) in equation (2) with the following result:

$$b = 1.5 + \log_2 (RT)^{0.75} \qquad (4)$$

From Table I the maximum RT is equal to 5740 so that b equals 10.85 . Since a fractional binary does not exist, 11 binaries and 2 gates will be needed and the readout word is 11 bits long.

The un-normalized logarithmic counter shown in Figure 5-24 consists of three parts, the mantissa counter which is a binaries in length, the exponent counter which is $\underline{b}$ binaries long and the pre-scaler which is $\underline{c}$ binaries long. The pre-scaler feeds register $\underline{a}$. The a and b registers contain the numbers $\underline{m}$ and $\underline{n}$, respectively, where m and n are functions of the number of input pulses $\underline{n}$ that have been applied to the register.

The ranges of m and n are

$$0 \le m \le 2^a - 1$$
$$0 \le n \le 2^b - 1$$

$$0 \le N \le N_{max} - 1 \qquad (5)$$

where N_{max} is the number of input pulses which cause the counter to overflow and $N_{max} - 1$ is the storage capacity of the system. The value of N_{max} is increased by the use of the pre-scaling counter that is inserted in groups of P binaries, the input source, and the a register, after a predetermined count is reached, beginning with n=1 and continuing for the interval $1 \le n \le c$. For the interval $\underline{n} > \underline{c}$ no further prescalers are inserted and accumulation is linear with N. The readout word consists of the counts in the a and b registers and is b bits in length.

In summary, it has been shown that a straight binary counter will require 13 binaries and a readout word of 13 bits, the S-T mode counter will require 11 binaries and 2 gates, and a readout word of 11 bits, while the un-normalized logarithmic counter will require 15 binaries and 6 gates and a readout word of 9 bits.

Since the S-T mode counter requires the same hardware as a straight binary counter and fewer readout bits, while providing for overflow it is the obvious choice between these two types. It also has fewer components than the un-normalized logarithmic counter and is much easier to decode and check-out. However, the S-T mode counter does require 2 more readout bits. The S-T mode counter should, therefore, be used as the standard accumulator unless the S069 experiment is found to require too high a bit rate. At that point the problem should be reassessed keeping in mind the extra hardware required to reduce the readout word length by 2 bits.

5.5.3.6   Telemetry Bit Rate and Format – It has been shown that 11 bit S-T mode accumulators will provide the necessary accuracy. However, 11 bit words are not desirable for telemetry usage as they are long, and cannot be split into groups smaller segments for data that does not require such high accuracy. If the data storage and transmission system uses a NRZ recording technique it is very desirable to have a level transition about every 12 bits to facilitate bit synchronization during data handling on the ground.

Using a parity check bit every 11 data bits will produce a 12 bit readout word with the desired level transition. This is an acceptable word length that can be split into two 6-bit words or three 4-bit words for maximum telemetry usage.

Table III shows the data that must be recorded and the number of bits per second required. The readout bit rate to record and transmit this data is 1952 bits per second not including status flags and housekeeping information. Neither 4 nor 6-bit words appear to have a decided advantage so a final decision will be made after the housekeeping information is available and the data storage and transmission system is firmed up.

A preliminary format, based on 4 bit words is shown in Figure 5-25 . The gray areas are unassigned at this time and are available for frame counting, housekeeping or expansion of data recording requirements.

5.5.4   Aspect Systems

5.5.4.1   General – The purpose of the aspect system is to enable the experimenter to determine the pointing direction of the X-ray sensor unit at any instant of time. This direction must directly or indirectly be expressed in an inertial system of coordinates. An overall pre-

TABLE III

DATA HANDLING REQUIREMENTS

Item	bits/ sample	sample/ sec	bits/ sec	Item	bits/ sample	sample sec	bit/ sec
PHA 1-1	12	5	60	Shaft 1	16	1	16
PHA 1-2	12	5	60	Shaft 2	16	1	16
PHA 1-3	12	5	60				
PHA 1-4	12	5	60	Camera 1	30	1/8	3.75
PHA 1-5	12	5	60	Camera 2	30	1/2	15
PHA 1-6	12	5	60				
PHA 1-7	12	5	60	Star Sensor			
PHA 1-8	12	5	60	Magnitude	4	30	120
TR1	12	2	24	Position	6	1/60	0.1
SR1	12	2	24				
NR1	12	1/2	6	Time	30	1	30
ACR1	12	1/2	6				
PSDR1	12	1/2	6	Sync	12	8	96
PHA 2-1	12	5	60	Housekeeping			
PHA 2-2	12	5	60				
TR2	12	2	24				
SR2	12	2	24				
NR2	12	1/2	6				
ACR2	12	1/2	6				
PSDR2	12	1/2	6				
PHA 3-1	12	15	180				
PHA 3-2	12	15	180				
SR 3	12	5	60				
PHA 4-1	12	5	60				
PHA 4-2	12	5	60				
PHA 4-3	12	5	60				
PHA 4-4	12	5	60				
PHA 4-5	12	5	60				
PHA 4-6	12	5	60				
PHA 4-7	12	5	60				
PHA 4-8	12	5	60				
SR4	12	2	24				
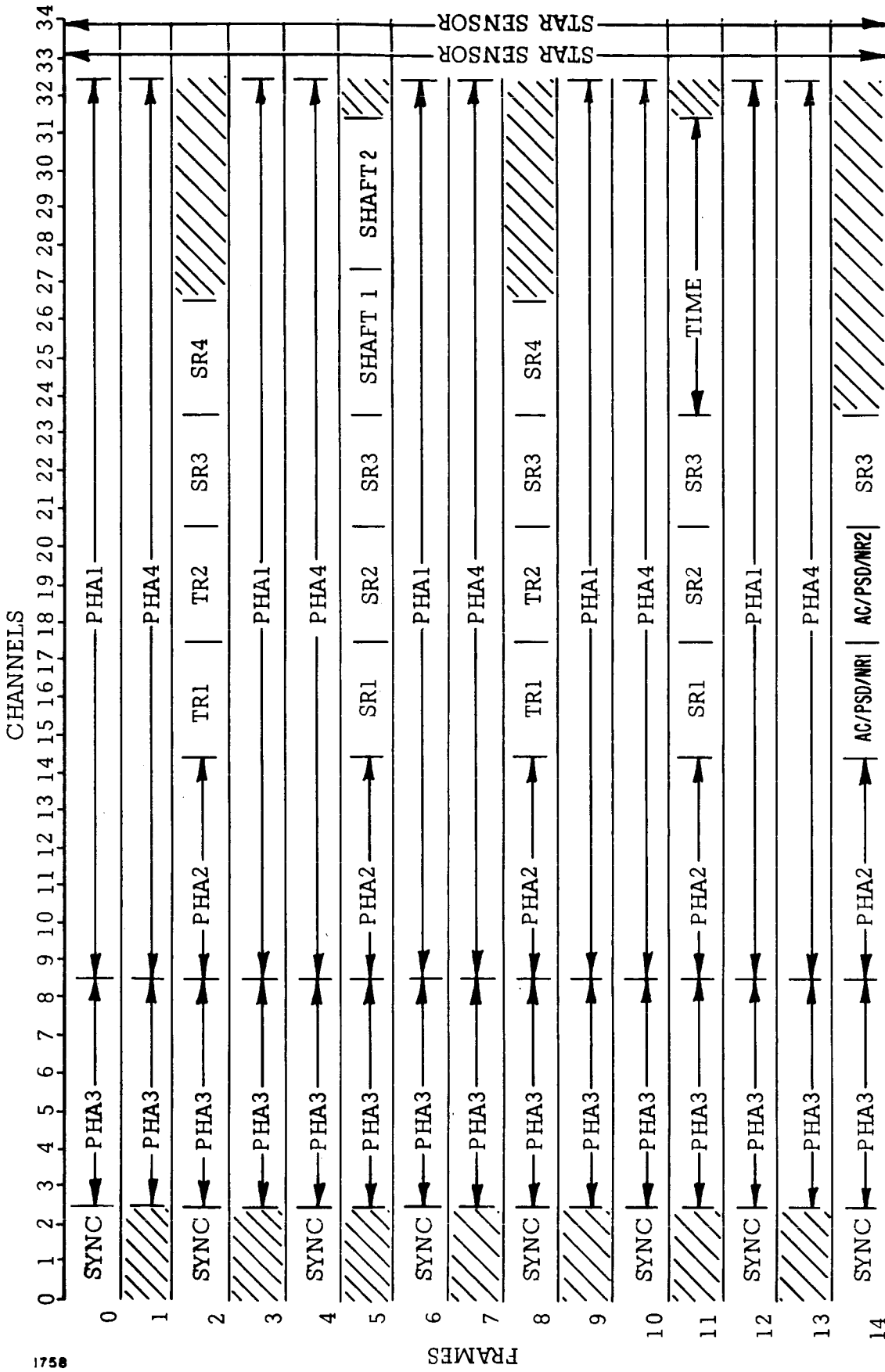
Figure 5-25 Preliminary PCM Word Format for Telemetry

1758

cision of $\pm$ 1 arc minute is desirable.

Below are listed some approaches to this problem; each are discussed in turn:

(a) Star camera attached to the XSU.

(b) Star camera/fiber optics of system.

(c) Shaft angle encoders or sensor positioning system.

(d) Electro-optical star pattern sensing using scanning techniques.

5.5.4.2 Star Camera – Of the four systems, a photograph of the star field of interest represents the simplest approach in conception. The camera marker system, previously boresighted with the line of "sight" (LOS) of the radiation detectors, will yield the position of the LOS directly in absolute coordinates. Exposed film must be obtained by EVA. A system is provided for sequence coding the frames and simultaneously marking the telemetry record so that positive identification can be made of each exposed film frame. X-ray data is thus matched to a specific spatial attitude. Film packs exposed to outer space have disadvantages. There are reports of electrostatic streaking of the image, and long term drying out effects of the film. The second system attempts to overcome these defects.

5.5.4.3 Star Camera/Fiber Optics System, Figure 5-26

General – The star field as sensed on the XSU can be "piped" into the MDA via a fiber optics bundle. A camera, mounted inboard is focused on the image coming from the pipe. This avoids an EVA for film retreival. In addition, the film is in a more suitable environment.

Resolution – Resolution and positional accuracy of star images transmitted through a fibre optics relay system are limited
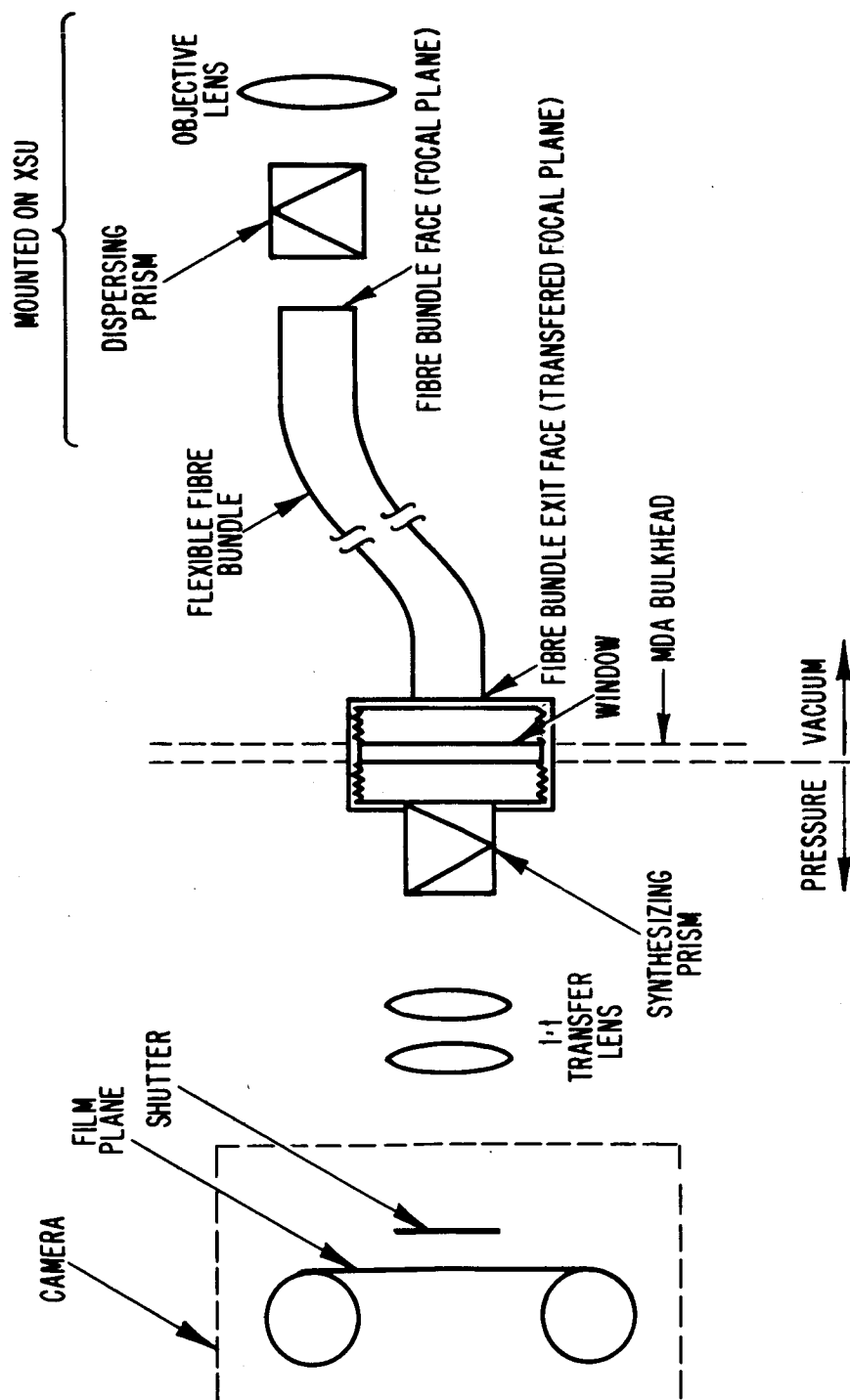
Figure 5-26 Fiber Optics Transmission System

MOUNTED ON XSU

OBJECTIVE LENS

DISPERSING PRISM

FIBRE BUNDLE FACE (FOCAL PLANE)

FLEXIBLE FIBRE BUNDLE

FIBRE BUNDLE EXIT FACE (TRANSFERED FOCAL PLANE)

FIBRE BUNDLE EXIT FACE

WINDOW

MDA BULKHEAD

VACUUM

PRESSURE

SYNTHESIZING PRISM

1:1 TRANSFER LENS

SHUTTER

FILM PLANE

CAMERA

1758

5-81

by the discreteness property of the fibres. Moreover, the modern fabrication technique of combining 36 individual filaments into a single multifibre before assembly into the coherent array introduces another level of quantizing noise into the system. The image enhancer developed by the American Optical Company is an attempt to reduce discreteness noise by taking each image point and dispersing it into a spectrum of itself, transmitting the spectrum through the fibre bundles and recombining the light into a conjugate image point. Thus the information contained in a single image point is transmitted by many fibres and, barring systematic errors in the fabrication of the system, quantization noise is reduced. American Optical claims that the image enhancer will nearly double the resolution of their best coherent image guide. The S069 design requirement at present is 0.5 minute of arc resolution.

Sensitivity – In order to identify a star field unambiguously with only approximately initial aspect information, three star images are needed. But the density of stars varies systematically with galactic latitude so that a system capable of operating anywhere in the sky must be capable of producing three star images in those regions of the sky where the star density is lowest; i.e. at the galactic poles.

Moreover, statistical fluctuations in the local stellar densities must be considered before establishing the angular field and limiting magnitude requirements of the system. Near the galactic poles, we may assume a Poisson distribution to be valid, since open clusters and associations are found mostly at low galactic latitudes.

Definitions:

$P(n)$ = probability of finding n stars in one square degree

μ = mean number of stars per square degree

$\underset{\sim}{a}$ = angular field in square degrees

$P(n, a) = \dfrac{e^{-a\mu}(a\mu)^n}{n!}$ = Probability of finding n stars in a square degrees

$P(n) = \dfrac{e^{-\mu}\, \mu^n}{n!}$

If we desire a confidence level of, say, 90% for finding three (3) or more stars, the condition is $= n = \infty$

$$\sum_{n=3}^{} P(n, a) = 0.9$$

yielding a μ = 5.25

an 80% confidence level yields aμ = 4.3.

The field of view of our camera is fixed by the film frame size (10mm x 12.5mm) and the effective focal length. The focal length is, in turn, chosen so that one resolution element in the focal plane corresponds to 0.5' of arc. In the following analysis, we assume that it is the fibre optics transfer system that limits resolution, and that lenses and emulsion will not notably limit resolution performance.

The American Optical Company has devised a system that offers .005mm. resolution in the film plane. If we say .005mm = (system focal length) x 0.5' of arc. then the system focal length is 33.5mm. Assuming 1 : 1 imaging from the output end of the light pipe to the film plane, this figure would be the focal length of the objective lens. A shorter focal length would not provide the angular resolution we require, while a longer focal length increases angular resolution at the expense of angular field. We will see that a smaller angular field means that fainter stars must be photographed to fulfill our three stars with 90% confidence requirement. Since there is tradeoff between the light gathering power and resolving power of our objective it remains to be seen whether we can tolerate a longer focal length. Even if this is tolerable, one might well choose to

increase aspect accuracy with the better statistics of image counts in excess of three, than with a larger film plane scale.

A suitable emulsion for our purposes is Kodak 2496 RAR on a 4 mil Estar base. (An Estar base provides the dimensional stability necessary for accurate positional measurements.) This film will resolve 200 lines/mm. with proper processing, and requires .01 erg/cm^2 to produce a density of 0.1 above mean fog level. The band width of the system is limited at the blue end by the fibre optics with a strong cutoff at 4000 $\overset{o}{A}$, and at the red end by the film, which cuts off sharply at 7000 $\overset{o}{A}$. Film and optical transmission characteristics are relatively flat between these limits. We will assume an insertion loss of 50% for the entire system and attenuation of 10%/foot in the light pipe (from published data). Mechanical considerations seem to dictate a length of 4 feet 8 inches for the light pipe. This yields a total system loss of 70% in intensity.

$$\left(\frac{\text{Intensity out}}{\text{Intensity in}}\right) \text{system} = 0.3$$

We know that our "typical" star the sun, has a color temperature of 6700°K. Using the black body approximation to spectral energy distribution, we find 0.4 of the sun's energy output between 4000 and 7000 $\overset{o}{A}$. A star of visual magnitude 5.1 of similar spectral type provides 1.1×10^{-7} ergs/cm^2 -sec. in the relevant spectral range. The exposure time is taken as drift rate of the vehicle divided by the angular resolution. If the drift rate is as high as 6'/sec, a resolution of .5' yields as exposure time of .0835 seconds. (The shutter may open for a much longer period but the figure is appropriate to light gathering capability calculations.) We then have $.92 \times 10^{-8}$ ergs/cm^2 available, but system losses (above) reduce this figure to an effective value of $.275 \times 10^{-8}$ ergs/cm^2. We require .01 ergs/cm^2 in the film plane. The objective lens will intensify as the

square of its diameter divided by the square of the diameter of the image
size. The required lens diameter is then given by:

$$\frac{D^2}{(.005)^2} = \frac{.01}{.275 \times 10^{-8}} = 4.35 \times 10^6$$

$$D^2 = .25 \times 10^{-4} \times 4.35 \times 10^6 = 1.09 \times 10^2$$

$$D = 10 \text{ mm}$$

$$f = \frac{f\ell}{D} = 3.35$$

We would of course prefer to exceed light gathering require-
ments with a faster lens if this can be achieved without loss of resolution.
The numerical aperture of the fibre optics allows an objective lens as fast
as f 1.0.

5.5.4.4 Problem Areas –

(a) Camera jitter in the film advance mechanism.

Four (or more) fiducial marks may be placed at the periphery
of the field by cementing individual light pipe fibres to the image bundle.
These would communicate with a small electric lamp producing the record-
ing spots. The center of this fiducial grid defines the aspect of the system
and it is this center that must be boresighted with the collimators. Jitter
is then irrelevant to data reduction, and not a problem.

(b) Mechanical Stability.

The projected light resolution of the system would be seriously
degraded by defocusing due to vibration or thermal stress. This might be
a critical design problem.

(c) Dirt and the Sun

The objective lens must be protected from both. The fiber optics

bundle (light pipe) has very serious dynamic and environmental limitations. It must withstand the motions of the XSU (bending, some torsion). A jacketing and harnessing arrangement may alleviate this. Temperature extremes and vacuum effects will have to be accounted for. A fiber optics bundle has been successfully used in space by the Boeing Company. However, the Boeing arrangement was fixed mounted, whereas our system will be connected to a gimbal platform, resulting in some flexibility in the optics pipe.

5.5.4.5 Shaft Angle Encoders - Two 16 bit binary shaft angle encoders are provided, one for each axis of the XSU. They measure XSU angular position relative to the drive axes. These do give spatial attitude information when used with the G & N data in the CM, subject to the following errors (unknown angular displacements):

1. Encoder error. This is the error of the encoder itself. This figure is usually less than the quantizing error, and so is of no consequence.

2. Error between mechanical boresight axis and the radiation boresight axis (L.O.S.). This will be reduced by calibration and alignment procedures prior to flight.

3. Errors in the deployment mechanism. The drive axes coordinates will differ from that of the MDA in unknown ways. Fabrication, Thermal and other strain effects create this.

4. Finally the MDA reference axes to the command module axes. This is the docking misalignment.

5.5.4.6 Star Pattern Sensing - This method is basically the electronic analogue of a photograph. A picture essentially displays the angular distances between stars and if some of these stars are known,

then attitude is uniquely determined. Electronic sensing and scanning can be made to generate pulses representing star positions versus scan time thus yielding angular distances. If the spacecraft were nearly still in space, scanning speeds would be kept slow, and the frequency of the pulse train coming from the sensing head on the DSU would be low enough to be recorded on the tape, then eventually to be telemetered to the ground. Star patterns are recognized on the ground by resorting to previously sorted star positions within a computer. Published data indicates that only a few thousand star patterns need be stored to cover the entire sky. The search can be speeded up by the knowledge of the XSU's approximate whereabouts given by the G & N computer aboard the spacecraft. Almost immediately, with an appropriate computer in a ground station, the attitude may be known within one or two orbits.

5. 5. 5   Ground Support Equipment

5.5.5.1   Mission – The Ground Support Equipment for Experiment S069 discussed herein refers to that portion of the special test equipment required to support proper operation of the experiment during alignment and calibration, qualification testing and checks of the experiment at MSFC and KSC during flight qualification and pre-launch test activities. Figure 5-27 shows in flow chart form a preliminary test plan which is typical of the Apollo Applications Program and which it is expected the X-ray Astronomy Experiment will probably follow. The Ground Support Equipment will be expected to provide support through-out this program from the beginning of Prototype system tests through launch of the Flight Unit. Table IV lists the primary Ground Support Equipment Requirements in support of this program.

5.5.5.2   Test Configurations – There are three basic test

```
┌──────────────┐        ┌──────────────┐                                    ┌──────────────┐
│ PROTOTYPE    │        │ FLIGHT       │                                    │ FLIGHT UNIT  │
│ INTEGRATION  │        │ BACKUP       │                                    │              │
│ UNIT (PIU)   │        │ UNIT         │                                    │              │
└──────┬───────┘        └──────┬───────┘                                    └──────┬───────┘
       │                       │                                                   │
       ▼                       │          ┌──────────────┐                         │
┌──────────────┐               └─────────▶│ SYSTEM TESTS │◀────────────────────────┘
│ INSTRUMENT   │                          └──────┬───────┘
│ AND          │
│ CALIBRATE    │                                 ▼
└──────┬───────┘                          ┌──────────────┐
       │                                  │ ALIGNMENT    │
       ▼                                  │ AND          │
┌──────────────┐                          │ CALIBRATION  │
│ SHIP TO MSFC │                          └──────┬───────┘
└──────┬───────┘                                 ▼
       │                                  ┌──────────────┐      ┌──────────────┐
       ▼                                  │ QUALIFICATION│      │ QUALIFICATION│
┌──────────────┐                          │ TESTS        │◀────▶│ TESTS        │
│ INTEGRATE    │                          │ IN-HOUSE     │      │ OUT-OF-HOUSE │
│ WITH         │                          └──────┬───────┘      └──────────────┘
│ MDA          │                                 ▼
└──────┬───────┘                          ┌──────────────┐
       ▼                                  │ SHIP TO MSFC │                    (A)
┌──────────────┐                          └──────┬───────┘                     │
│ EVALUATION   │                                 │                             ▼
│ STUDIES      │                                 ▼                      ┌──────────────┐
└──────┬───────┘                          ┌──────────────┐              │ INCOMING     │
       ▼                                  │ BENCH CHECK  │              │ CHECKS       │
┌──────────────┐                          └──────┬───────┘              └──────┬───────┘
│ STORE        │                                 ▼                             ▼
│ PIU          │                          ┌──────────────┐              ┌──────────────┐
└──────────────┘                          │ INTEGRATE    │              │ VEHICLE      │
                                          │ WITH MDA     │              │ INTEGRATION  │
                                          └──────┬───────┘              └──────┬───────┘
                                                 ▼                             ▼
                                          ┌──────────────┐              ┌──────────────┐
                                          │ INTEGRATION  │              │ INTEGRATION  │
                                          │ AND ALIGNMENT│              │ SYSTEM TESTS │
                                          │ TESTS        │              └──────┬───────┘
                                          └──────┬───────┘                     ▼
                                                 ▼                      ┌──────────────┐
                                          ┌──────────────┐              │ SIMULATED    │
                                          │ SHOCK AND    │              │ MISSION      │
                                          │ VIBRATION AND│              │ TESTS        │
                                          │ ALIGNMENT    │              └──────┬───────┘
                                          │ TESTS        │                     ▼
                                          └──────┬───────┘              ┌──────────────┐
                                                 ▼                      │ VEHICLE      │
                                          ┌──────────────┐              │ ASSEMBLY     │
                                          │ THERMAL      │              │ ON PAD       │
                                          │ VACUUM AND   │              └──────┬───────┘
                                          │ ALIGNMENTS   │                     ▼
                                          │ TESTS        │              ┌──────────────┐
                                          └──────┬───────┘              │ PRELAUNCH    │
                                                 ▼                      │ CHECKS       │
                                          ┌──────────────┐              └──────┬───────┘
                                          │ OTHER TESTS  │                     ▼
                                          └──────┬───────┘              ┌──────────────┐
                                                 ▼                      │ LAUNCH       │
                                          ┌──────────────┐              │ VEHICLE      │
                                          │ SHIP TO KSC  │              └──────────────┘
                                          └──────┬───────┘
                                                (A)
```

1758

Figure 5-27 X-Ray Astronomy Experiment Test Flow Chart

configurations involved which the GSE must support. First and most complex is the in-house alignment and test configuration. During this phase the GSE must supply a spacecraft interface to permit the experiment to operate correctly as a functional entity while the instrument is calibrated and aligned by means of in-house laboratory equipment and while it is being subjected to the in-house evolution and qualification test program. Spacecraft power, commands, telemetry decommutation, recording, display, and other test functions must be supplied by the GSE. A major function is involved in collecting data, testing limits and data reduction during this phase. Calibration with radioactive test sources involve the collection of statistically valid samples and the derivation of statistical performance characteristics of the instruments. This involves the exercise of as many as 14 external and internal test sources, command of the instrument into as many as twenty test configurations and the monitoring of over 100 housekeeping values for both absolute and go-no go limit values. It involves the accumulation of over 20 types of digital data for periods over 3 minutes in duration. It involves the reduction of this data into a form which can be readily evaluated and used. There are other functions such as telemetry format and timing signal generation, calibration tests, control of test sequences etc. which must also be performed. During environmental testing, performance data must be continually recorded and evaluated as the environmental parameters are varied. During the remainder of the program, somewhat simpler versions of these tests must be performed. However, the output monitoring requirements remain essentially constant throughout the program. When the experiment is shipped to MSFC for integration with the MDA, the GSE will be required to support incoming inspection tests to insure that it is operating properly prior to integration.

During and after experiment integration with the MDA, the basic function of the GSE becomes somewhat different. The MDA is then able to supply the spacecraft power, telemetry interface and command system. It is expected that the MDA will be interfacing with the MSFC checkout system including the Digital Data Acquisition System (DDAS) facility. Primary system checks will be performed using the command and telemetry channels. The GSE will continue to monitor operation via the GSE connector interface in basically a backup mode of operation. In the event of a random failure, the GSE will provide a fault isolation and repair function to minimize experiment down time. In accordance with the test plans of other Apollo applications it is assured that this type of test configuration will remain constant throughout the remainder of the test program until the flight vehicle is assembled on the launch pad. During the pre-launch test period most of the confidence checks of the Experiment will be made via the command and telemetry links and by means of a carry near portable test set. During this period, almost complete reliance on the Launch Control Center facilities will be made to insure adequate monitoring of the Experiment. It is doubtful that these facilities would be completely adequate without possible utilization of some features of the GSE requiring real time monitoring of either the GSE connector interface or of the video output of the telemetry ground station. Much remains to be unsolved in this area dependent upon: 1. MSFC support equipment provisions; 2. Final definition of experiment test requirements; 3. MDA equipment provisions; 4. MSFC test plans.

5.5.5.3 Basic Requirements – The basic requirements referred to in Table IV are influenced quite strongly by the field support requirements defined by fundamental test configurations and by test facility provisions for GSE. The AS & E GSE hardware configuration is also influenced to the extent that in all cases it cannot be co-located

TABLE IV

X-RAY ASTRONOMY EXPERIMENT GSE REQUIREMENTS

1. Support in-house alignment and calibration tests.

2. Support in-house qualification tests.

3. Support incoming inspection tests at MSFC.

4. Implement a simulated spacecraft interface test program prior to
    MDA integration.

5. Provide a minimal field repair facility.

6. Provide a fault isolation capability between the experiment. space-
    craft and telemetry systems.

7. Provide a fault isolation capability at major replaceable assembly
    level within the experiment.

8. Provide for monitoring and checkout of the experiment during flight
    qualification and pre-launch checkout of the vehicle.

9. Provide a source of accurate calibrated test inputs during alignment
    and calibration.

10. Provide telemetry decommutation, readout, recording and display
    facility.

11. Provide spacecraft power, simulated commands and interconnection
    test points.

12. Provide line drivers between the experiment GSE connector and GSE
    in certain test configurations.

with the Experiment. Therefore, compromises in function and performance must be made. From the above requirements, it is evident that a rather complex configuration is needed as a basic facility throughout most of the program. Furthermore, due to minimal access provided at the launch facility, the use of additional limited capability carry-near equipment may be required for fault isolation. If the Prototype and Flight Models are under test simultaneously in different locations, two sets of GSE will be required. Portability is a requirement for the GSE because of the various locations involved. The environmental requirements of carry-near equipment are severe because of the exposed conditions encountered in the Service Structure.

Depending on test configurations the GSE may be located up to 100 feet from the Experiment. Typical of this problem is that of properly instrumenting the MDA during thermal vacuum testing at MSFC.

The use of external calibration and test sources throughout the test program is almost mandatory if comprehensive testing is to be performed. These sources require periodic activation during a test sequence. Although sufficient internal calibration provisions are made in the Experiment to provide pre-launch and in-orbit confidence checks, they are not sufficient to detect subtle degradations during flight qualification testing and must be augmented by other provisions. Quick look telemetry provisions are essential throughout the program up through pre-launch checks. These factors are presently under consideration in GSE concepts.

5.5.6 Checkout Procedures

5.5.6.1 Test unit requirements studies indicate the need for two sets of GSE, for supporting the Prototype Unit test program and the Flight Unit Test Program. Each set would contain one carry-near portable test

set (for limited Experiment confidence testing and fault isolation), and a portable rack mounted test set (for supporting alignment and calibration of the Experiment, fault isolation and repair at replacable subassembly level). Also included are spacecraft electrical interface simulators, reception, detection, format stripping, testing and recording of telemetry data, provision of test sources and controls. Provision should be made for testing distances up to 100 feet, as well as compatibility with other test conditions at MSFC.

5.5.6.2 Increased Complexity - The complexity of the instrumentation in Experiment S069 and the necessity for monitoring large numbers of variables indicates a need for automatic test equipment. This permits testing and recording of data in a minimum of time. Small, rugged stored program central processors, economically priced, are available and ideally suited for the task.

5.5.6.3 Use of S017 GSE - It is not practical to use the custom designed components of the Experiment S017 GSE, however components of the telemetry ground station which are standard functional units may be used.

5.5.6.4 Self Test Features - The inclusion of self test features in the design of S069 are necessary for orbital in-flight testing and simplify pre-launch checkout.

5.5.6.5 Test Connector - A GSE connector with selected inputs and outputs is necessary on the Experiment and will be used during all phases of the test program.

5.5.6.6 GSE Function - The role of the AS & E supplied GSE at MSFC and KSC is dependent on the functions performed by the spacecraft checkout equipment, particularly the spacecraft command and tele-

metry quick-look facilities. The enivironmental, documentation, configuration control and operational constraints are in need of clarification by MSFC to permit early definition of requirements.

5.5.6.7 Functional Description - Figure 5-19 is a functional block diagram of the recommended GSE configuration.

In the absence of an MDA, spacecraft power, clock and external command functions are supplied to the Experiment via the spacecraft interface connectors under control of the central processor.

Data from the Experiment is monitored via the telemetry ground station and the GSE interface connectors. Special test signals and commands are supplied via the GSE connector. External test sources for testing the radiation and optical sensors are controlled via a command buffer switch. The central processor is programmed to provide the following controlled conditions for each test: data acquisition, data accumulation and storage, test data against pre-determined limits, formatting and to record data and test results. Manual control is available to permit selective testing of the Experiment.

Limited access confidence checks and fault isolation is provided in the carry-near test set.

The central processor recommended for this application is one of the economically priced small computers designed especially for instrumentation applications with provisions for internal buffering and control.

5.5.6.8 X-Ray Astronomy Experiment Calibration and Checkout Provisions -

1. Internal precision digital test source to provide for digital logic and telemetry checks.

2. Internal precision analog test source to provide for analog telemetry checks.

3. Internal ramp modulated pulse train source for PHA calibration tests.

4. Internal radioactive test source for proportional counter and PHA analog spectral calibrations.

5. Selected external command system controls to permit remote evaluation and check-out of the experiment.

6. Selected digital, discrete and analog housekeeping telemetry outputs for system monitoring.

7. Ground support equipment connector provisions for the insertion of and monitoring of selected signals.

COMMANDS (KEYBOARD)

1. Analog PWR supply on

2. Digital PWR supply on

3. Quad A HVPS on

4. Quad B HVPS on

5. Quad C HVPS on

6. Quad D HYPS on

7. Servo PWR on

8. Sub commutator on

9. Command RCVR on

10. Telemetry trans on

11. Camera #1 on

12. Camera #2 on

13-16. Detector select switch

17-20. PHA select switch

21. Int. Cal #1 Digital

22. Int. Cal #2 PHA

23. Int. Cal #3 FE^{55}

24. Inhibit background Quad A

25. Inhibit background Quad B

26. Inhibit background Quad C

27. Inhibit background Quad D

28. Inhibit PSD Quad A

29. Inhibit PSD Quad B

30. Inhibit PSD Quad C

31. Inhibit PSD Quad D

32. Int. Cal #4 Servo

33. Picture sequences auto/man

HOUSEKEEPING MONITOR POINTS (ANALOG)

1. Temperature HVPS #1 Quad A
2.   "   " #2 "   "
3.   "   " #3 "   "
4.   "   " #4 "   "
5.   "   " #1 " B
6.   "   " #2 "   "
7.   "   " #3 "   "
8.   "   " #4 "   "
9.   "   " #1 " C
10.   "   " #2 "   "
11.   "   " #3 "   "
12.   "   " #4 "   "
13.   "   " #1 " D
14.   "   " #2 "   "
15.   "   " #3 "   "
16.   "   " #4 "   "
17. Voltage   " #1 " A
18.   "   " #2 "   "
19.   "   " #3 "   "
20.   "   " #4 "   "
21.   "   " #1 " B
22.   "   " #2 "   "
23.   "   " #3 "   "
24.   "   " #4 "   "
25.   "   " #1 " C
26.   "   " #2 "   "
27.   "   " #3 "   "

28. Voltage HVPS #4 Quad C

29.   "   "   #1 "   D

30.   "   "   #2 "   "

31.   "   "   #3 "   "

32.   "   "   #4 "   "

33. Temperature analog CRT PWR supply

34.   "   digital CRT PWR supply

35. Voltage Pos. Analog

36. Voltage Neg. Analog

37. Voltage Pos. Digital

38. Sun Sensor Bias

39. Star Sensor Bias

40. Star Sensor Ref. Voltage

41. Star Sensor Comparator Voltage

42. + Cal

43. 0 Cal

44. - Cal

45. Analog count rate #1

46. Analog count rate #2

47. Analog count rate #3

48. Analog count rate #4

49. Temperature monitor background cntr

50.   "   "   Quad A   "

51.   "   "   Quad B   "

52.   "   "   Quad C   "

53.   "   "   Quad D   "

54. PSD rejection level PHA #1

55.   "   "   "   PHA #2

56. PSD rejection level PHA #3

57. " " " PHA #4

58. Amplitude rejection level PHA #1

59. " " " PHA #2

60. " " " PHA #3

61. " " " PHA #4

62. Sensor X Axis Pos.

63. Sensor Y Axis Pos.

64. Tell Tales & Discretes.

TELL TALES

1-33. All commands

34. Door Open

35. Shutter #1 open confirm

36. Shutter #2 open confirm

37. $+45^{\circ}$ LIM SW X

38. -45° LIM SW X

39. $+45^{\circ}$ LIM SW Y

40. -45° LIM SW Y

41. Film advance #1 confirm

42. Film advance #2 confirm

43. Int. Cal. #1 on

44. Int. Cal. #2 on

45. Int. Cal. #3 on

46. Int. Cal. #4 on

47. Servo Error Threshold X

48. Servo Error Threshold Y

CALIBRATION TEST SOURCES

1. Background counter pulse train input

2. Quadrant A staircase pulse train input

3. Quadrant B staircase pulse train input

4. Quadrant C staircase pulse train input

5. Quadrant D staircase pulse train input

6. Quadrant A Fe^{55} test source

7. Quadrant B Fe^{55} test source

8. Quadrant C Fe^{55} test source

9. Quadrant D Fe^{55} test source

10. External Co^{60} test source

11. External Simulated Star Source

12. External Simulated Sun Source

13. External Collimated resolution reticle for Camera #1

14. External Collimated resolution reticle for Camera #2

6.0 S017 COMPATIBILITY

In previous paragraphs, the conceptual design of a modern X-ray Astronomy scientific instrument is described for the S069 Experiment. The new instrument reflects the state-of-the-art scientific objectives for the AAP-2 mission scheduled for the early 1970's. If existing S017 experiment hardware is to be utilized for this mission on the MDA, S017 must be changed for three basic reasons:

1. Scientific tasks to be performed exceed the capability of the present equipment.

2. The experiment will be carried in a different vehicle (MDA, not CSM Block I).

3. Advanced circuit techniques and more reliable components must be incorporated.

The S017 hardware must be changed because the original equipment was designed solely to perform specific tasks within a unique set of vehicle restraints. Hence S017, designed to other specifications, may not simply be incorporated into the new flight system of a different spacecraft.

6.1   Science Requirement

6.1.1   Description of Existing S017 XSU and Processing Circuits

The S017 detector system consists of eight proportional counters each having an effective collection area of about 18 cm^2. Four tubes are coupled with wide angle collimators and designated as "Guard" counters. The collimator axes are arranged in an offset orthogonal

pattern to view the "X and Y" directions. Each of the Guard counters drives an analog Linear Count Rate Meter (LCRM) coupled to the telemetry as back-up data and to the Display and Control Unit (DCU) to aid in source location and boresighting. The remaining four tubes are coupled, in pairs, to orthogonal, narrow angle collimators and designated "Xo" and "Yo" Position counters. The "Xo" channel electronics includes a LCRM for back-up and DCU usage, a digital 9-bit, S-T mode accumulator to provide primary count rate information and an 8 channel Pulse Height Analyzer (PHA) to provide energy spectrum data. Each PHA channel has a 9-bit, S-T mode accumulator to record the occurance rate in each channel. The Yo channel electronics is identical to the Xo channel with one exception; there is no PHA.

6.1.2 Analog Circuit Compatibility Problems

The S017 preamplifiers and video amplifiers were designed for total energy measurements exclusively, and have a risetime of 200 nonoseconds. The S069 experiment uses Pulse Shape Discrimination (PSD) to increase measurement effectiveness, and theoretical analysis and preliminary data from PSD experiments indicate a need for an overall (preamp input to PSD input) risetime of no greater than 10 nanoseconds and possibly as low as 3 nanoseconds. The design of the S017 preamps and video amplifiers is such that a simple change of components will not produce the required risetime.

6.1.3 Digital Circuit Compatibility Problems

The threshold detectors and steering circuits of the PHA were designed for the low count rates expected with the S017 proportional counters, and have operational dead-times on the order of 10 microseconds, which will introduce substantial dead-times for the peak counting

rates expected with S069. The threshold detectors and steering circuits also have no provision for a PSD or anticoincidence input. The modifications to reduce the operational dead-time and provide the "inhibit" input, are basically a new design.

The S017 accumulators used in the PHA, and Xo and Yo channels, are a single design, 9-bit ripple-thru binary counter with feedback arranged for S-T mode operation. The peak counting rates for S069 will require S-T mode accumulators of at least 11 bits to achieve the desired accuracy. The S017 accumulators were designed in 4-bit modules, with the ninth-bit part of the steering circuit. By adding a 2-bit module to each accumulator, the S017 equipment can be made compatible with S069. However, the repackaging modifications are extensive and can produce other problems, such as excessive propagation delay and increased noise pickup.

Using S-T mode accumulators to achieve the desired accuracy requires the readout gating, buffer storage and output shift registers to be expanded to 11 bits, and the formatting in other portions of the experiment to be changed. (The first bit of the S017 accumulators was used as a prescaler and not read out.) These modifications are extensive both electrically and mechanically.

6.1.4 Packaging

The S069 experiment incorporates new functions, such as PSD and anti-coincidence, and these functions require faster switching times than the present S017 will allow.

The overall circuit requirements of the S069 experiment are at least four times those of the S017 experiment. Using the present packaging philosophy as a guide, it will take between 30 and 40 boards to meet the S069 design requirements. On the S017 experiment, there are only 25 board positions available. By rearranging the internal layout of the S017 electronics unit, room can be made for 36 to 40 boards. This estimate is based on tighter spacings which can yield marginal performance due to noise pickup and thermal problems.

6.1.5 S017 X-Ray Sensor Unit

The S017 sensor area must be larger in order to obtain the required experimental sensitivity. This results in a new package problem with larger counters and more high voltage supplies required. In addition, a Mylar-window type of counter is being considered to measure lower energy X-rays. This requires the incorporation of a gas replenishment system.

Following the first 30-day planned orbital flight, the X-Ray Astronomy Experiment carried on the MDA should be capable of operation after six months of orbital storage. This requires a more demanding Quality Assurance (QA) program than was appropriate for the original S017 mission. This is discussed in detail in Appendix B.

6.2 New Interfaces

The placement of the experiment on the multiple Docking Adaptor generated new specifications:

a. The first and most apparent was that G & N data would no longer be available to the experiment. S017 logic, designed to extract guidance information from the CM computer would now not be needed. In its place, installed on the XSU, would be a camera. A backup camera, installed within the MDA and optically connected to the XSU by a fiber optics pipe, would be added for necessary reliability. The electronics must be modified to include the camera film coding, film advance signals, etc.

b. To search for an X-ray source and pin-point its location, scanning must be used. The astronaut accomplished this with the fixed S017 by controlling the movements of the CM. This is impractical with an entire CM/MDA cluster. A moving platform evolved for this purpose. Though not strictly a modification, a positioning control system implied a new design for the S017 Display and Control Unit. Controls and position displays have to be added. Servo electronics must be incorporated.

c. With S017 signal conditioning circuits expanded in scope and complexity, with servo electronics added, and G & N extraction logic circuits removed, with larger housekeeping circuits needed, a new encoder for the PCM pulse train must be designed or procured. A new frame format must be established.

d.   The frog otolith experiment, included with the S017 experiment, is not required for S069.   This will modify the DCU panel, and modify the data storage design.

6.3   Components

It is not considered strictly necessary to modify existing equipment by substituting improved types of components.   Manufacturers of aerospace hardware are continuously improving their standards, yet it would be unwise not to take advantage of a superior product, especially when it results in savings in size, weight and power dissipations.   This is particularly true of the tape recorder.   For these reasons, and only where it is feasible, some portions of S017 may be updated.

6.4   Ground Support Equipment

The possibility of adapting the S017 GSE for use with Experiment S069 has been considered.   The equipment involved includes a portable telemetry ground station, a portable checkout unit, a portable fault isolation unit, a portable test set, and an in-house test console as illustrated in Figure 6-1.

The majority of this equipment is special purpose with the exception of standard units of the telemetry ground station.

Three possibilities exist: 1. Modify the existing system by adding equipment where necessary; 2. Utilize existing standard equipment and design new special purpose equipment where required; 3. Develop an entirely new set of Ground Support Equipment.
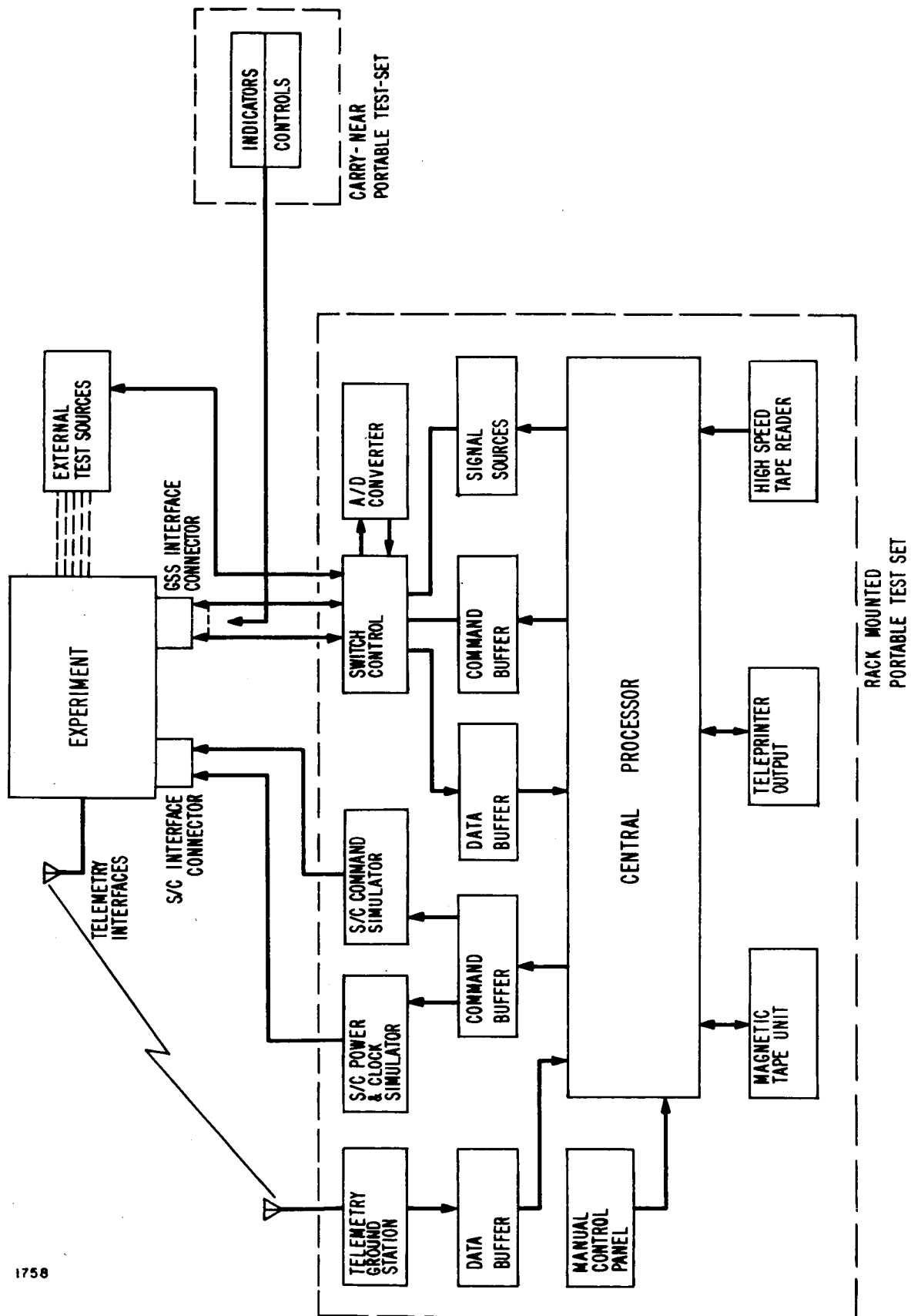
Figure 6-1 Ground Support Equipment Block Diagram

1758

Factors to be considered are as follows:

1. Differences between S017 and S069 experiments.

2. Functional capability of existing GSE.

3. Experience gained with S017 GSE.

4. Reliability considerations.

5. Costs involved.

6.4.1 Differences Between S017 and S069

The primary reason for the system changes incorporated in S069 has been to improve the experiment to obtain improved scientific data. From the GSE viewpoint, this change has made testing more complex. The detailed changes are:

	S017	S069
Pulse Height Analyzers	2	4
Background Cancellation	No	Yes
Pulse Shape Discrimination	No	Yes
Sun Sensor	No	Yes
Variable Gas Detector	No	Yes
Detector Selection Switching	No	Yes
PHA Selection Switching	No	Yes
Command Receiver	Yes	No
Frog Otolith Circuitry	Yes	No (?)
Camera	0	2
Positioning	No	Yes

There are other more subtle changes involved in the system modifications listed above which affect telemetry, interfaces, circuitry, type and number of units to be tested.

6.4.2 Functional Capability of Existing GSE vs Requirements for Support of Experiment S069.

With the exception of standard units within the portable telemetry ground station, all other pieces of GSE are custom built to support the specific requirements of Experiment S017. The GSE is a manual checkout system with special test switches, interface wiring, indicators, signal generators, etc., designed to test the circuitry and components of S017. A new equipment configuration would require reworking the GSE to provide for the changes in testing. At present, there is a capability to calibrate and test only one PHA at a time. Simultaneous checkout of PHA's should be provided. The most sophisticated tests involved in check-out of the S069 excluding optical alignment procedures are concerned with determining the proper operation of the pulse shape discriminator and background cancellation system efficiencies. These involve the use of both radioactive sources and special pulse trains, as well as the measurement of timing intervals and the accumulation of performance data. These tests cannot be accomplished with the present GSE. S017 GSE has no provision for testing the added systems such as the second camera, the positioning servo and the larger number of input sensors.

6.4.3 Experience Gained with Experiment S017 GSE

Since the S069 is considerably more sophisticated than the S017, testing it will require a longer period of time. Test times and data recording problems indicate a more automatic approach would be desirable because data recording becomes a major portion of the testing time. Repeatability of test conditions and test data have also been a

problem, and from this it is recognized that improvements are needed in this area.

6.4.4 Reliability Considerations

Conversion and modification of the S017 GSE for use with the S069 poses reliability problems. These are in the areas of circuit board alterations, changes in connectors, switches, etc., without damage to the components.

6.4.5 Cost Implications

When considering the extent of the modifications required, design effort involved, documentation changes, replacement of components damaged during disassembly, etc., any cost savings accomplished by utilizing the S017 GSE for the S069 system may not be appreciable. However, the major purchased items incorporated in the portable ground support can be used where applicable.

Therefore, it is concluded that the major purchased items of the S017 ground station should be used and that custom built GSE for S017 should not be used. Further, the GSE for S069 should contain provisions for more rapid testing and data gathering than was previously provided.

APPENDIX A

PRELIMINARY RELIABILITY ANALYSIS OF S069 CONCEPTUAL DESIGN

1.0 INTRODUCTION

This reliability analysis was performed on the proposed S069 Experiment configuration as defined by the Function Block Diagram in Figure 5-18, Section . The purpose of the analysis was to: (1) determine the range of achievable reliability as a function of various redundancy configurations and required operating time (mission time); (2) perform redundancy studies on S069 subsystems to serve as a basis for future design trade-offs involving cost, weight, volume, power, maintainability, etc. ; (3) perform preliminary reliability analyses on those areas of the design where reductions in failure rate will produce a significant improvement in system reliability.

It should be emphasized that in this analysis, conservative component reliability estimates were used in order to identify those subsystems which particularly require careful component selection during the detailed design phase. Consequently, the final equipment design is expected to exhibit an appreciably higher overall reliability than is indicated in this preliminary analysis.

2.0 SUMMARY OF RESULTS

2.1 S069 System Reliability

The analysis indicates a probability of .86 that the S069 Experiment will perform without failure during a 100-hour mission. Considering the conservative assumptions discussed in Section 3.0 of this analysis, and our intent to (1) select reliable, qualified parts and materials; (2) conduct 100% screening and burn-in of electronic parts; (3) employ adequate derating; and (4) eliminate or improve high failure rate items, it is our judgment that a reliability of greater than .90 can be achieved in the final experiment design.

	t = 40 hours	t = 100 hours
Best Case Configuration	.95	.86
Worst Case Configuration	.93	.80

The S069 operating requirements of 40 and 100 hours were chosen to reflect an expected range of operating conditions as tabulated below:

40 hours	100 hours
Two 20-hour data-taking periods	Two 20-hour data-taking periods. 30 hours during pre-launch 30 hours stand-by in orbit

Although several areas seem to offer the potential for significant reliability improvement, the largest gains can be made in the areas of the X-ray sensor unit and the positioning system. Presently, less than 66% capability in the X-ray detector area is considered unacceptable and constitutes a failure of the experiment.

The addition of a switching matrix between the sensing unit and the signal conditioning circuits would provide a variety of cross-switching and could possibly bypass failed components to the extent that acceptable data could be obtained during the life of the experiment.

In view of the limited flexibility of the positioning system configuration, improving its reliability will consist primarily of ensuring that the most reliable and qualified parts and materials available are incorporated into the design.

3.0 ASSUMPTIONS

a. With the exception of those components shown explicitly in re-
dundant configuration, each part of the experiment is con-
sidered to be series-connected and failure of any piece-part
constitutes a failure of the experiment.

b. Where series reliability dependency is indicated, the sum-
mation of individual part failure rates is performed under the
assumption that the exponential failure distribution applies.
The predicted failure rates, therefore, apply only to random
failures and presume that no parts are influenced by wear-
out characteristics during the useful life of the experiment.

c. Maximum expected ambient operating temperature is 125°C.
No part exceeds its maximum rated level in the expected
operating environment.

d. Average piece-part failure rates were estimated using the
maximum-minimum methods of MIL-HDBK-217A, Section 4.6,
assuming that each part was properly applied. These failure
rates are conservative, since they do not reflect the reduc-
tion in failure rates resulting from AS&E 100% screening
and burn-in, and part procurements based on vendor Hi-
Rel programs. (Actual piece-part stresses will be determined
during the design phase of the program.) Where component
parts lists were not available, such as high voltage power
supply, subcommutator, A/D converter, and VCO, failure
rates were estimated based on similar items in other programs.

4.0 DESCRIPTION OF ANALYSIS

The S069 Experiment was divided into six functional subsystems as follows:

R_{oss}	Optical Sensing System
$R_{xrsu/sc}$	X-ray Sensor Unit/Signal Conditioner
R_{dst}	Data Storage and Transmission
R_{dcs}	Display and Control System
R_{ps}	Positioning System
R_{m}	Multiplex

A reliability analysis was performed on each subsystem for estimated operating times of 40 and 100 hours. In the case of $R_{xrsu/sc}$ and R_{dst} further redundancy studies were performed to determine the best and worst case reliability for various power supply and data transmission configurations. The S069 system reliability was then computed as shown in Paragraph 4.1, utilizing the appropriate best or worst case configuration subsystem reliabilities.

4.1 System Reliability

Optical Sensing System	X-ray Sensor Unit	Signal Conditioner	Data Storage & Transmission	Display and Control System	Positioning System	Multiplex
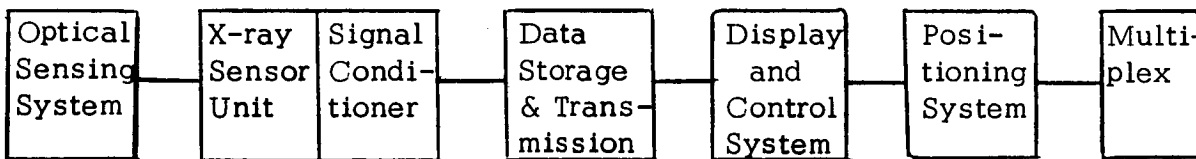
where $R_{S069} = R_{oss} R_{xrsu/sc} R_{dst} R_{dcs} R_{ps} R_{m}.$

Utilizing the subsystem reliability values shown in Table I, R_{S069} was computed for best and worst case configurations as follows:

R_{S069} (Best Case):

    t = 40 R = (.99955) (.98784) (.99573) (.99045) (.97844) (.99059) = .95060

    t = 100 R = (.99870) (.96977) (.98936) (.97629) (.94696) (.97680) = .85788

R_{S069} (Worst Case):

    t = 40 R = (.99955) (.96930) (.99251) (.99045) (.97844) (.99059) = .92884

    t = 100 R = (.99870) (.92432) (.98132) (.97629) (.94696) (.97680) = .80439

TABLE I SUBSYSTEM RELIABILITY MATRIX					
Subsystem	Case	Configuration	Para.	t = 40	t = 100
R_{oss}	Nominal		4.2.1	.99955	.99870
$R_{xrsu/sc}$	Best Worst	Configuration #1 Configuration #3	4.2.2.1 4.2.2.3	.98784 .96930	.96977 .92432
R_{dst}	Best Worst	Direct or Tape Tape Required	4.2.3 4.2.3	.99573 .99251	.98936 .98132
R_{dcs}	Nominal		4.2.4	.99045	.97629
R_{ps}	Nominal		4.2.5	.97844	.94696
R_m	Nominal		4.2.6	.99059	.97680

4.2 Subsystem Reliability

4.2.1 Optical Sensing System (R_{oss})

R_1
| Fiber Optics & Receiving System/Camera |

R_3
| Sun Sensor & Electronics |

R_4
| Star Sensor & Electronics |

R_2
| Main Camera & Electronics |
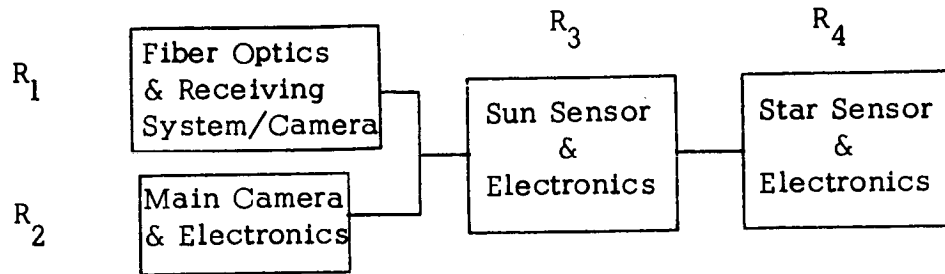
$$R_{oss} = (R_1 + R_2 - R_1 R_2)R_3 R_4$$

$$= (2R_1 - R_1^2)R_3^2 \quad \text{Assuming}$$

$$\lambda_1 = \lambda_2 = 175 \times 10^{-6}$$

$$R_1 = R_2 \qquad \lambda_3 = \lambda_4 = 50 \times 10^{-6}$$

$$R_3 = R_4$$

t	R_{oss}
40 hrs.	.99955
100 hrs.	.99870

4.2.2 X-Ray Sensing Unit/Signal Conditioner

4.2.2.1 Power Supply Configuration #1 – Redundant pair of low voltage power supplies for each section.
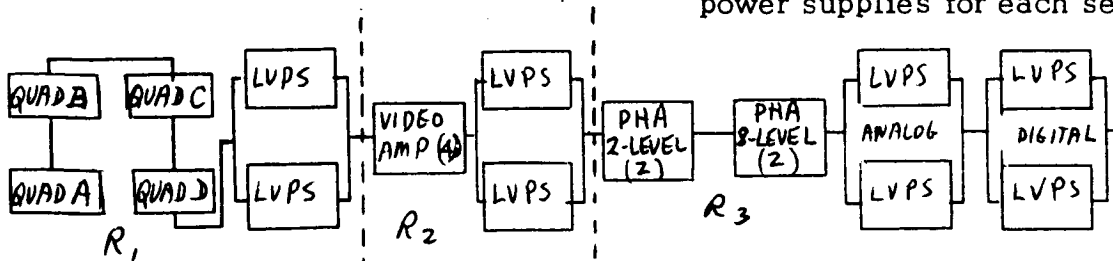
$$R_{xrsu/sc} = R_1 R_2 R_3 \quad \text{where units of } R_1 R_2 R_3 \text{ are as shown in Table II.}$$

$R_{xrsu/sc}$ (using best and worst reliability values from Table II)

	t = 40	t = 100
Best Case	.98784	.96977
Worst Case	.96953	.92543

TABLE II $R_{xrsu/sc}$ RELIABILITY MATRIX			
Unit	Con-figuration	t = 40	t = 100
High Voltage Power Supply* (Para. A1)	a b c	.99533 .99998 .99999	.98836 .99985 .99992
Quad A, B, C, D Background Detector* (Para. A3)	1 2 3	.99999 .99999 .99999	.99999 .99999 .99998
Quad A, B, C X-Ray Detector* (Para. A4)	1 2	.99999 .99999	.99999 .99996
Quad D X-Ray Detector* (Para. A5)	1 2	.99997 .99994	.99996 .99980
Low Voltage Power Supply* (Para. A2)	a b ** c	.99629 .99997 .99999	.99077 .99990 .99995
PHA 2-Level* PHA 8-Level* (Para. A6)		.99830 .99750	.99590 .99380
Video Amplifier		.99910	.99770
Quad A, B, C, D Summing Amp.		.99910	.99770
Quad A, B, C, D Amplifier PS		.99997	.99990

*See Supplement A_1 for redundancy analysis.
**Used for $R_{xrsu/sc}$ analysis.

A-8

4.2.2.2 <u>Power Supply Configuration #2</u> - Redundant low voltage power supply for each pair of Quads (A & B)(C & D) sections 1 through 3.

SECTION 1
$R_1 = R_A^3 R_B R_C^2$

SECTION 2
$R_2 = R_A^2 R_B^2$

SECTION 3
$R_3 = R_A^2 R_B^2 R_C^2 R_D^2$
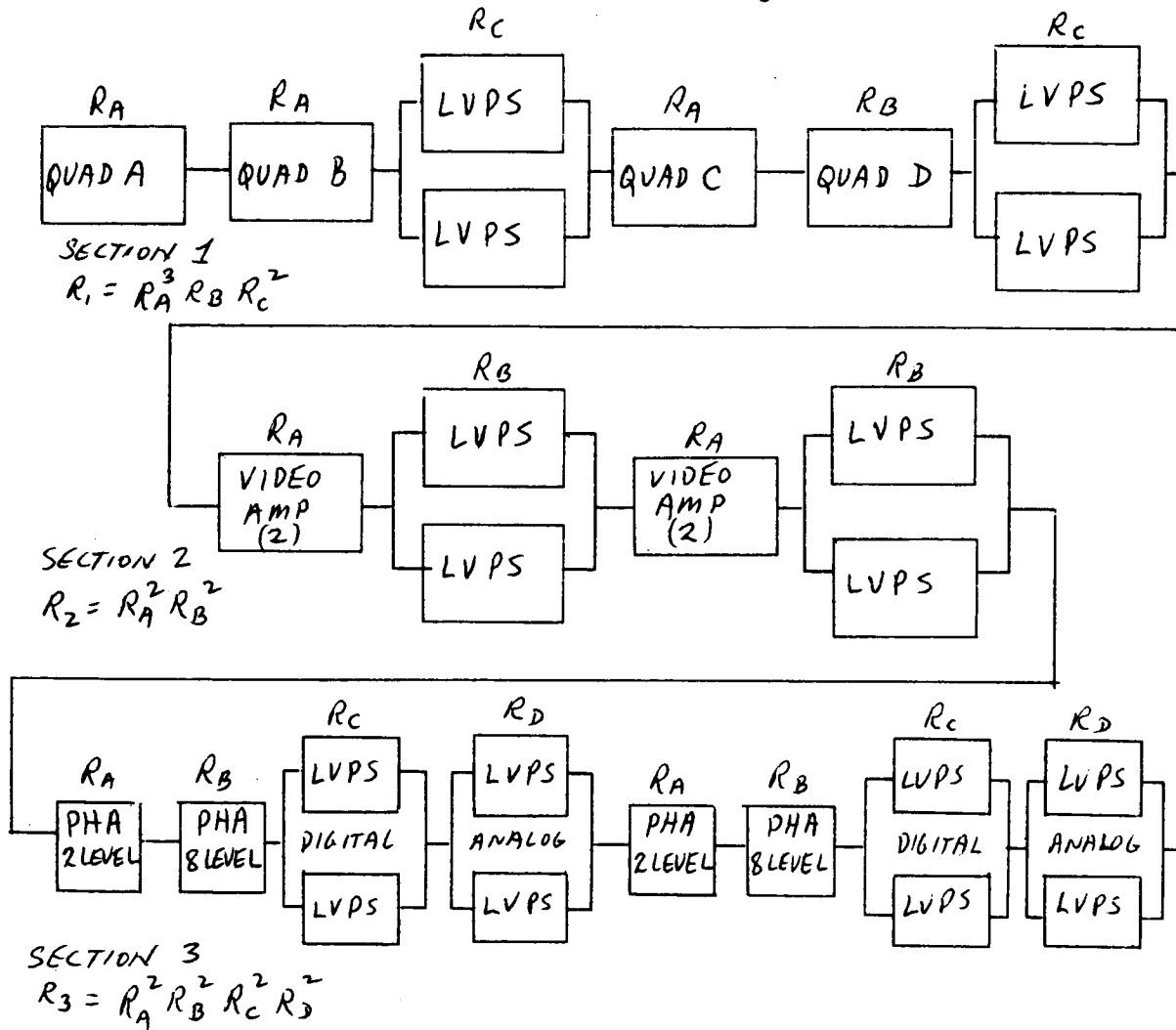
$R_T = R_1 R_2 R_3$ (Using best and worst reliability values from Table II)

R_T	t = 40	t = 100
Best Case	.98776	.96938
Worst Case	.96945	.92506

4.2.2.3 Power Supply Configuration #3 – Redundant low voltage power supply for each Quad.

SINGLE QUAD CHAIN
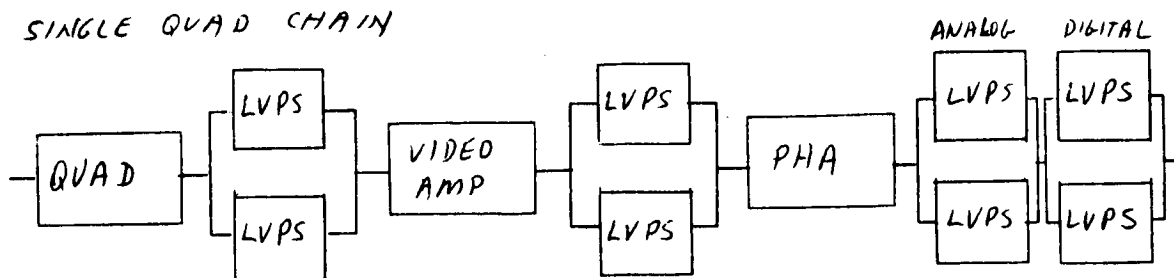
R_1 = Quad A chain

R_2 = Quad B chain

R_3 = Quad C chain

R_4 = Quad D chain

$R_T = R_1 R_2 R_3 R_4$ (Using best and worst reliability values from Table II)

Best Case:

t	R_T
40 hrs.	.98760
100 hrs.	.96861

Worst Case:

t	R_T
40 hrs.	.96930
100 hrs.	.92432

A-10

4.2.3 Data Storage and Transmission (R_{dst})
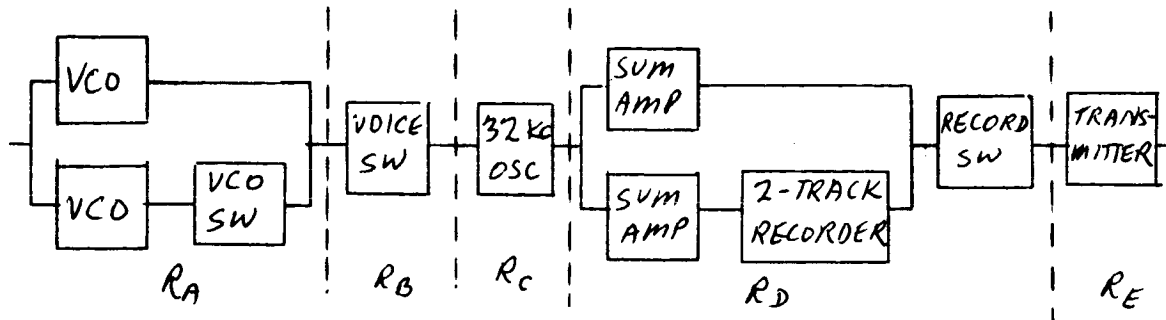
$$R_{dst} = R_A R_B R_C R_D R_E$$

VCO Switch   – 1 cycle – one time operation in the event of VCO failure

Voice Switch   – assuming 2 cycles/hours operation

Recorder Switch – assuming 1 cycle/hours operation.

Section R_A

$$R_A = e^{-\lambda t} + R_{sw} e^{-\lambda t}(\lambda t) \qquad \lambda = 13 \times 10^{-6}$$

$$R_{sw} = .99999$$

$t = 40$ hours	$R = .99949$
$t = 100$ hours	$R = .99871$

Section R_D – Assuming direct transmission 50% and recorder transmission 50% of total operating time.

$$\lambda_1 = \lambda_2 = 22.98 \times 10^{-6}$$

$K_1 = 33\%$ duty cycle

$K_2 = 67\%$ duty cycle

$\lambda_3 = 110.886 \times 10^{-6}$

$\lambda_4 = .25 \times 10^{-6}$

(Recorder energized during direct transmission)

$$R_D = R_1 + R_2R_3 - R_1R_2R_3$$

$$R_D = \left[e^{-K_1(\lambda_1 t)} + e^{-K_2(\lambda_2 + \lambda_3)t} - (e^{-K_1\lambda_1 t})(e^{-K_2(\lambda_2 + \lambda_3)t}) \right] e^{-\lambda_4 t}$$

$$R'_D \text{(Tape Recorder required)} = e^{-(\lambda_2 + \lambda_3)t}$$

t = 40 hours

R_D = .99998

R'_D = .99674

t = 100 hours

R_D = .99997

R'_D = .99184

R_{dst}:

	t = 40	t = 100
Best Case (Direct redundant to tape)	.99573	.98936
Worst Case (Tape required)	.99251	.98132

where

$\lambda_B = .5 \times 10^{-6}$

$\lambda_C = 13 \times 10^{-6}$

$\lambda_E = 80 \times 10^{-6}$

A-12

4.2.4 Display and Control System (R_{dcs})

Servo Electronics $\left.\begin{array}{l}x\\y\end{array}\right\}$ Axis	Encoder Electronics $\left.\begin{array}{l}x\\y\end{array}\right\}$ Axis
R_1	R_2
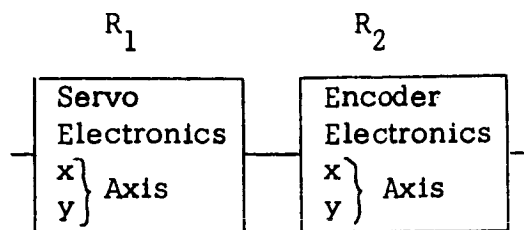
$R_1 = R_2$

$R_1 = R_x R_y$

$R_x = R_y$

$\lambda_x = 60 \times 10^{-6}$

$$R_{dcs} = R_1 R_2 = R_x^4 = e^{-4\lambda_x t}$$

t	R_{dcs}
40 hrs.	.99045
100 hrs.	.97629

4.2.5 Positioning System (R_{ps})

Motor/Tach $\left.\begin{array}{l}x\\y\end{array}\right\}$ Axis	Position Encoder $\left.\begin{array}{l}x\\y\end{array}\right\}$ Axis
R_1	R_2
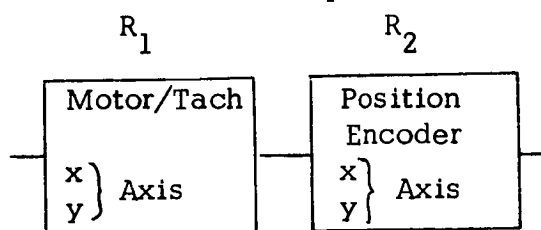
$R_1 = e^{-(\lambda_x + \lambda_y)t}$

where $\lambda_x = \lambda_y = 22.32 \times 10^{-6}$

$R_2 = e^{-(\lambda_x + \lambda_y)t}$

where $\lambda_x = \lambda_y = 250 \times 10^{-6}$

(assuming 10 cycles/hr. operation)

$$R_{ps} = R_1 R_2$$

t	R_{ps}
40 hrs.	.97844
100 hrs.	.94696

4.2.6 Multiplex (R_m)

Sub-Commutator	A/D	System Clock	Timing Gate	Multiplex
R_1	R_2	R_3	R_4	R_5
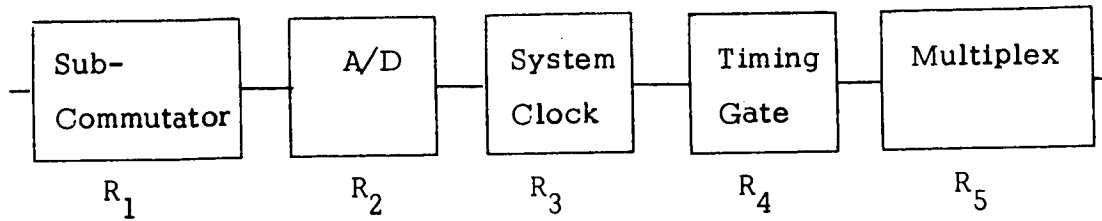
$$R_m = R_1 R_2 R_3 R_4 R_5$$

$$= e^{-(\lambda_1 + \lambda_2 + \lambda_3 + \lambda_4 + \lambda_5)t}$$

where $\lambda_1 = 3.8 \times 10^{-6}$

$\lambda_2 = 25.6 \times 10^{-6}$

$\lambda_3 = 53.0 \times 10^{-6}$

$\lambda_4 = 1.8 \times 10^{-6}$

$\lambda_5 = 151 \times 10^{-6}$

t	R_m
40 hrs.	.99059
100 hrs.	.97680

A-14

SUPPLEMENT A₁ – REDUNDANCY STUDIES

A 1. **High Voltage Power Supply**

$\lambda = 117 \times 10^{-6}$

a. **Single Power Supply**

$R = e^{-\lambda t}$

t = 40	R = .99533
t = 100	R = .98836

b. **Redundant** – with both units operating simultaneously

$R = 2R - R^2$

$R = 2e^{-\lambda t} - e^{-2\lambda t}$
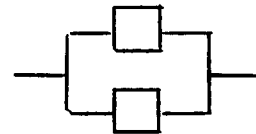
t = 40	R = .99998
t = 100	R = .99985

c. **Redundant** – standby with switch for one time switchover operation

$R = e^{-\lambda t} + R_s e^{-\lambda t}(\lambda t)$
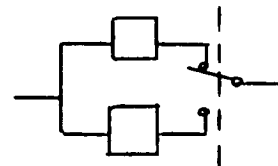
t = 40	R = .99999
t = 100	R = .99992

A-15

A 2. <u>Low Voltage Power Supply</u>

$\lambda = 92.66 \times 10^{-6}$

a. <u>Single Power Supply</u>

$R = e^{-\lambda t}$

t = 40	R = .99629
t = 100	R = .99077

b. <u>Redundant</u> - with both units operating simultaneously

$R = 2R - R^2$

$R = 2e^{-\lambda t} - e^{-2\lambda t}$
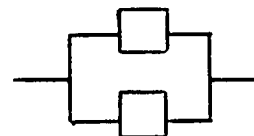
t = 40	R = .99998
t = 100	R = .99990

c. <u>Redundant</u> - standby with switch for one time switchover operation

$R = e^{-\lambda t} + R_s e^{-\lambda t}(\lambda t)$
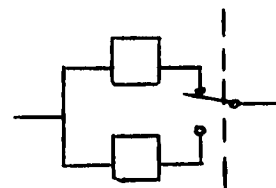
t = 40	R = .99999
t = 100	R = .99995

A 3. <u>Quad A, B, C, D Background/Anti-Coincidence Detectors</u>

9 Detectors/Quad $\lambda = 30 \times 10^{-6}$

a. <u>Configuration #1</u> - Detectors mechanically isolated, electrically redundant without pre-amps.
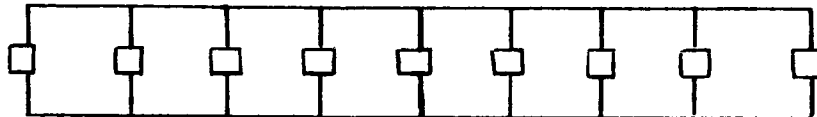
$R_{Det} = (R + Q)^9$

Allowing 3 failures out of 9 for 66.7% minimum operating efficiency

$R_{Det} = R^9 + 9R^8Q + 36R^7Q^2 + 84R^6Q^3$ where;

$$Q^n = (1-R)^n$$

$R_{Det} = -56e^{-9\lambda t} + 189e^{-8\lambda t} - 216e^{-7\lambda t} + 84e^{-6\lambda t}$

t = 40 hours   R = .99999

t = 100 hours   R = .99999

b. <u>Configuration #2</u> - Detectors mechanically isolated, electrically redundant with one pre-amp in series with each detector.

Detectors

Pre-amps

λ_1 (Detector) = 30×10^{-6} λ_2 (Pre-amp) = 23.18×10^{-6}

$\lambda = \lambda_1 + \lambda_2 = 53.18 \times 10^{-6}$

Allowing 3 failures out of 9 for 66.7% minimum operating efficiency

$$R = -56e^{-9\lambda t} + 189e^{-8\lambda t} - 216e^{-7\lambda t} + 84e^{-6\lambda t}$$

t = 40 hours	R = .99999
t = 100 hours	R = .99999

c. <u>Configuration #3</u> – Mechanically isolated, electrically redundant as shown with one pre-amp for each set of 3 detectors.
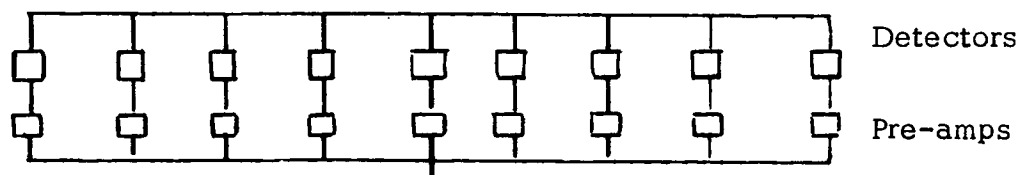
$$\lambda_1 \text{(Detector)} = 30 \times 10^{-6}$$

$$\lambda_2 \text{(Pre-amp)} = 23.18 \times 10^{-6}$$
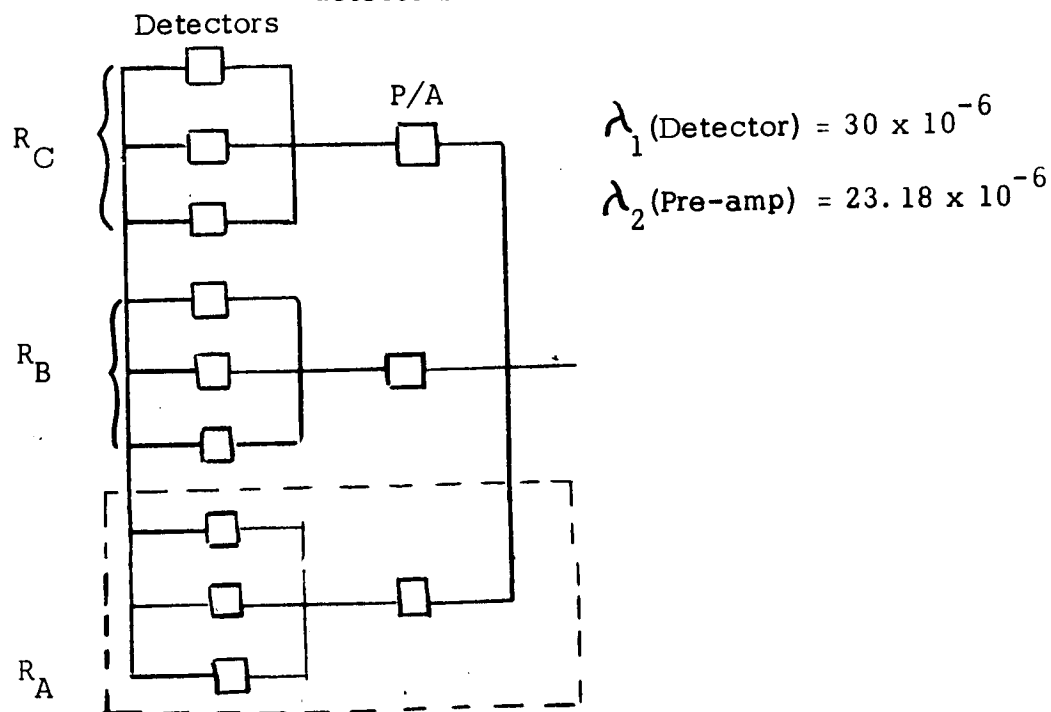
Allowing any three detector failures or any one pre-amp failure for 66.7% minimum operating efficiency,

$$R_A = e^{-\lambda_2 t} (3e^{-2\lambda_1 t} - 2e^{-3\lambda_1 t})$$

t = 40 hours   R = .99999

t = 100 hours   R = .99768

$$R_A = R_B = R_C$$

For the probability of survival of two out of three sets,

$$R_T = (3R_A^2 - 2R_A^3)$$

t = 40 hours   R = .99999

t = 100 hours   R = .99998

A 4. Quad A, B, C X-Ray Detectors

6 Detectors/Quad

a. Configuration #1 – Detectors mechanically isolated, electrically redundant with one pre-amp in series with each detector.

Detectors $\lambda_1 = 30 \times 10^{-6}$

Pre-amps $\lambda_2 = 23.18 \times 10^{-6}$
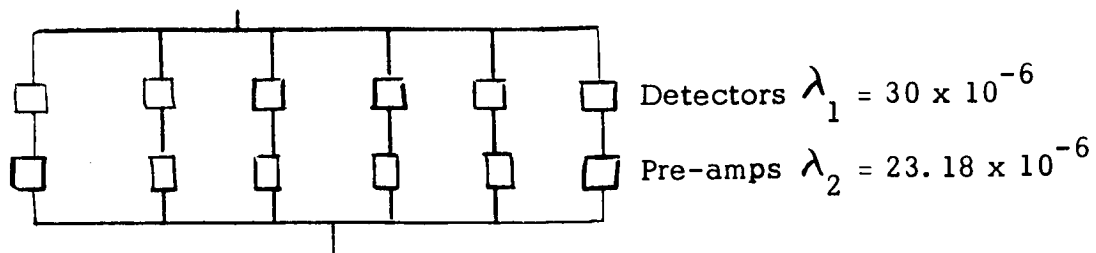
$$\lambda = \lambda_1 + \lambda_2 = 53.18 \times 10^{-6}$$

Allowing 2 failures out of 6 for 66.7% minimum operating efficiency

$$R = 15e^{-4\lambda t} - 24e^{-5\lambda t} + 10e^{-6\lambda t}$$

t = 40 hours   R = .99999

t = 100 hours   R = .99999

b. Configuration #2 – Mechanically isolated, electrically redundant with one pre-amp for each parallel pair of detectors.
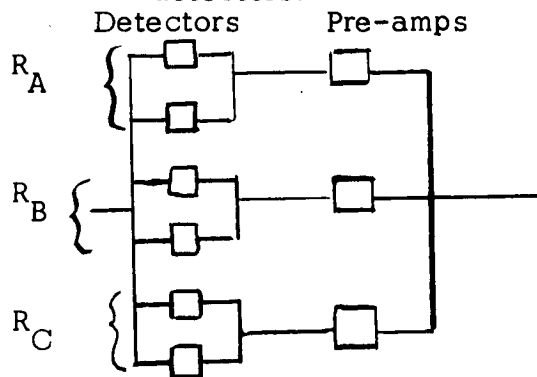
$$\lambda_1 \text{ (Detectors) } = 30 \times 10^{-6}$$
$$\lambda_2 \text{ (Pre-amps) } = 23.18 \times 10^{-6}$$

For 2 sets where one detector failure each is permitted $R_A = R_B$, and one set where no detector failure is permitted (R_C) for a total of 2 detector failures out of 6 resulting in a 66.7% minimum operating efficiency,

$$R_A = R_B = e^{-\lambda_2 t}(2e^{-\lambda_1 t} - e^{-2\lambda_1 t})$$

t = 40 hours	R = .99999
t = 100 hours	R = .99769

$$R_C = e^{-(\lambda_2 + 2\lambda_1)t}$$

t = 40 hours	R = .99999
t = 100 hours	R = .99173

Allowing any one set to fail out of 3;

$$R_T = R_A^2 + 2R_A R_C - 2R_A^2 R_C$$

t = 40 hours	R = .99999
t = 100 hours	R = .99996

A 5. Quad D X-Ray Detector

6 Detectors/Quad

Because the gas system has been provided as backup to gas losses within the Quad D detectors, the following assumptions and considerations are included in this section of this analysis:

1) λ_1 (detectors) $= 50 \times 10^{-6}$ estimated failure rate, for thin mylar window detector. Since the gas system is utilized to reduce the effects of gas leakage, it is assumed that there is a 50% reduction in the failure rate due to this major failure mode. Therefore, the estimated failure rate of the detectors used in this analysis is λ_1 (detectors) $= 25 \times 10^{-6}$.

2) A weighting factor of $K_1 = .75$ represents the expected proportion of mechanical failures out of all failures.

3) A weighting factor of $K_2 = .25$ represents the expected proportion of electrical failures out of all failures.

4) The total gas system failure rate is estimated as 105.93×10^{-6} hrs.

   a. Configuration #1 - Detectors mechanically serial dependent, electrically redundant, with one pre-amp in series with each detector.

λ_1 (Detector) $= 25 \times 10^{-6}$

λ_2 (Preamp) $= 23.18 \times 10^{-6}$

λ_3 (Gas System) $= 105.93 \times 10^{-6}$

$K_1 = .75$

$K_2 = .25$
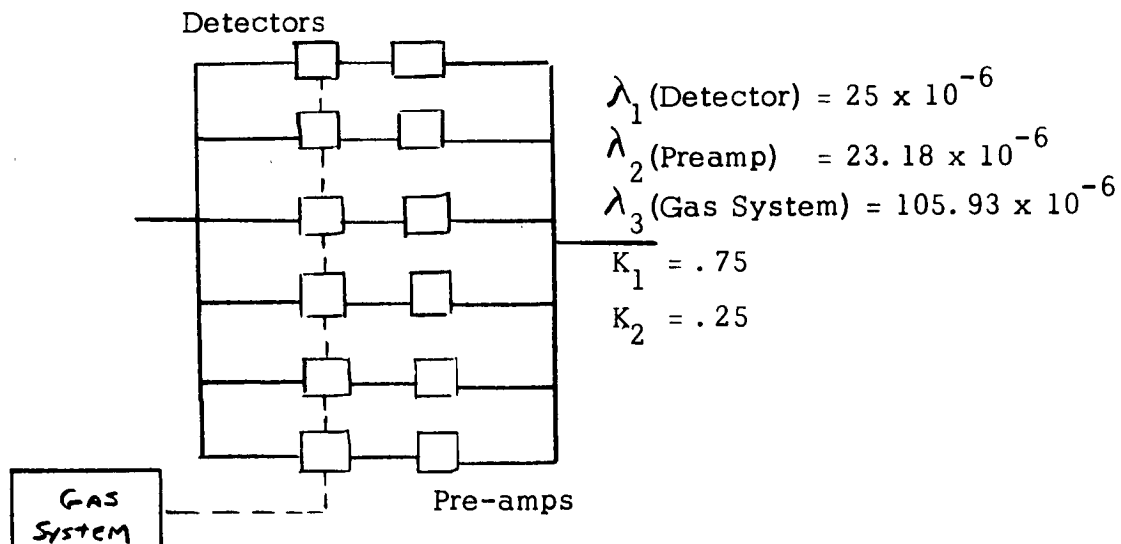
Allowing only 2 failures out of 6 for a 66. 7% minimum operating efficiency,

$$R_T = (R_2 R_3 + Q)^n (R_{1,4}(t)) \qquad \text{where } R_{1,4}(t) = \int_t^\infty f(t)dt$$

(for the gas system in a standby redundant mode of operation)

where; $R_1 = e^{-K_1 \lambda_1 t}$ (mechanical reliability of detector)

$R_2 = e^{-K_2 \lambda_1 t}$ (electrical reliability of detector)

$R_3 = e^{-\lambda_2 t}$ (reliability of pre-amp)

$R_4 = e^{-\lambda_3 t}$ (reliability of gas system)

$$R_T = \left[15e^{-4(K_2 \lambda_1 + \lambda_2)t} - 24e^{-5(K_2 \lambda_1 + \lambda_2)t} + 10e^{-6(K_2 \lambda_1 + \lambda_2)t} \right]$$

$$\left[e^{-6K_1 \lambda_1 t} + \frac{6K_1 \lambda_1}{\lambda_3 - 6K_1 \lambda_1} \left(e^{-6K_1 \lambda_1 t} - e^{-\lambda_3 t} \right) \right]$$

t = 40 hours	R = . 99997
t = 100 hours	R = . 99996

b. <u>Configuration #2</u> - Detectors mechanically serial dependent, electrically redundant with one pre-amp for each parallel pair of detectors.

Detectors   Pre-amps

λ_1 (Detector) = 25×10^{-6}

λ_2 (Pre-amp) = 23.18×10^{-6}

λ_3 (Gas System) = 105.93×10^{-6}

$K_1 = .75$

$K_2 = .25$
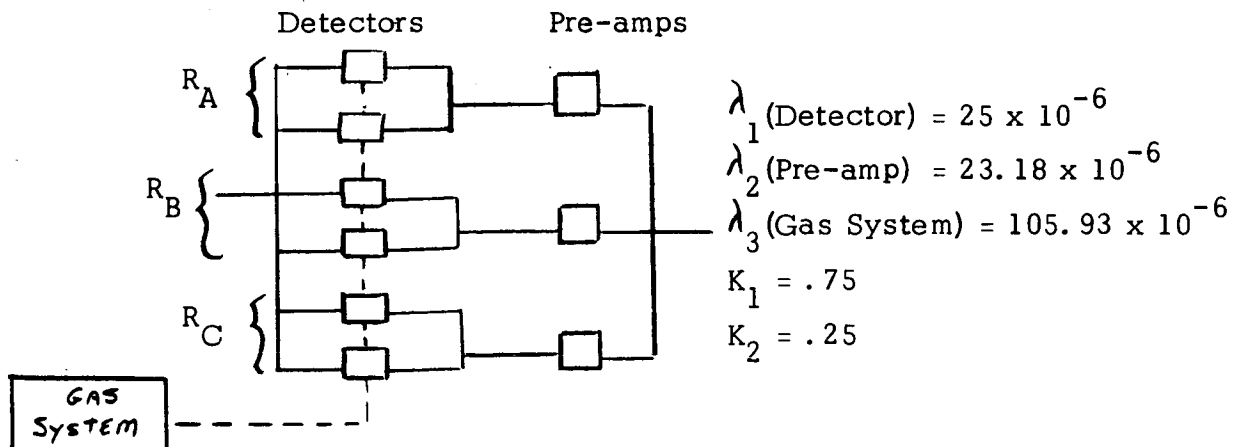
For two sets where one detector failure each is permitted $R_A = R_B$; and one set where no detector failure is permitted (R_C) for a total of 2 detector failures out of 6 resulting in a 66.7% minimum operating efficiency,

$$R_A = R_B = e^{-\lambda_2 t}(2e^{-K_2 \lambda_1 t} - e^{-2K_2 \lambda_1 t})$$

t = 40 hours	R = .99907
t = 100 hours	R = .99769

$$R_C = e^{-(\lambda_2 + 2K_2 \lambda_1)t}$$

t = 40 hours	R = .99857
t = 100 hours	R = .99643

Allowing any one set to fail out of 3; and the function $R_{1,4}(t)$ is the same as configuration #1

$$R_T = (R_A^2 + 2R_A R_C - 2R_A^2 R_C)(R_{1,4}(t))$$

$$= (R_A^2 + 2R_A R_C - 2R_A^2 R_C)\left[e^{-6K_1 \lambda_1 t} + \frac{6K_1 \lambda_1}{\lambda_3 - 6K_1 \lambda_1}(e^{-6K_1 \lambda_1 t} - e^{-\lambda_3 t})\right]$$

t = 40 hours	R = .99994
t = 100 hours	R = .99980

SUPPLEMENT A_1 - cont.

A6I. **PHA Electronics**

a. **PHA - 2 Level**

λ_1 (PHA) $= 3.88 \times 10^{-6}$

λ_2 (PSD) $= 30.56 \times 10^{-6}$

λ_3 (Threshold Det.) $= 3.48 \times 10^{-6}$

λ_4 (Scaler) $= 9.08 \times 10^{-6}$

λ_5 (Scaler Timing Block) $= 5.08 \times 10^{-6}$

λ_6 (Scanner) $= 2.8 \times 10^{-6}$
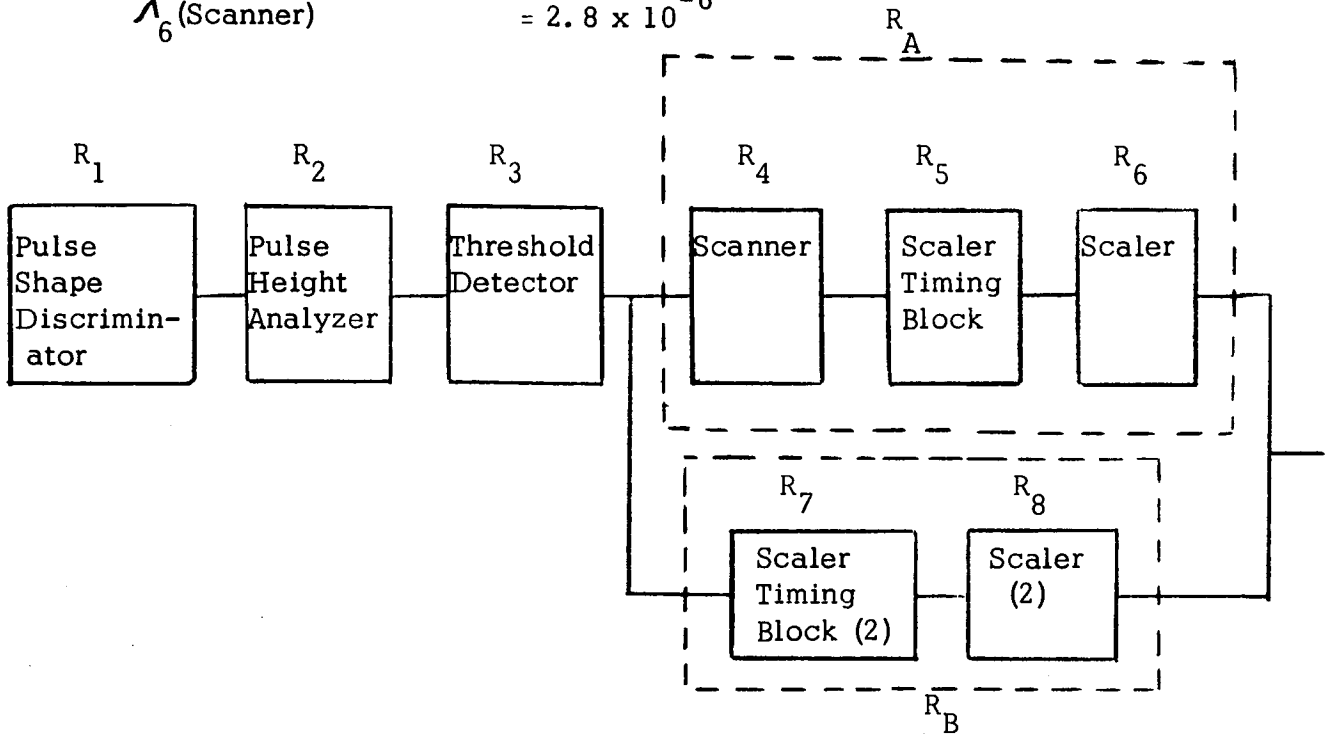
$$R_T = R_1 R_2 R_3 (R_A + R_B - R_A R_B)$$

$$R_T = e^{-(\lambda_2 + \lambda_1 + 2\lambda_3)t} (e^{-(\lambda_6 + \lambda_4 + \lambda_5)t} + e^{-(2\lambda_5 + 2\lambda_4)t} - e^{-(3\lambda_4 + 3\lambda_5 + \lambda_6)t}$$

$$R_A = R_4 R_5 R_6$$

$$R_B = R_7 R_8$$

$t = 40$ hours $R = .99830$

$t = 100$ hours $R = .99590$

b. <u>PHA - 8 Level</u>

Same configuration as 2-Level except for 8 sections instead of 2.

$$R_T = e^{-(\lambda_2 + \lambda_1 + 8\lambda_3)t} (e^{-(\lambda_6 + \lambda_4 + \lambda_5)t} - e^{-(9\lambda_4 + 9\lambda_5 + \lambda_6)t})$$

$t = 40$ hours $R = .99750$

$t = 100$ hours $R = .99380$

SUPPLEMENT B₁ – COMPONENT FAILURE RATES

		Failures per 10^6 hrs.	No. of Parts	Total Failure Rate
B 1.	**Pre-Amplifier**			
	Transistor	3.0	5	15.0
	Diode	1.0	3	3.0
	Resistor	0.3	13	3.9
	Capacitor	0.1	6	0.6
	Inductor	0.34	2	0.68
				23.18
B 2.	**Summing Amplifier**			
	Transistor	3.0	5	15.0
	Diode	1.0	3	3.0
	Resistor	0.3	13	3.9
	Capacitor	0.1	4	0.4
	Inductor	0.34	2	0.68
				22.98
B 3.	**Video Amplifier**			
	Transistor	3.0	5	15.0
	Diode	1.0	3	3.0
	Resistor	0.3	13	3.9
	Capacitor	0.1	4	0.4
	Inductor	0.34	2	0.68
				22.98

		Failures per 10^6 hrs.	No. of Parts	Total Failure Rate
B 4.	Scalers			
	Resistor	0. 3	2	0. 6
	Capacitor	0. 1	2	0. 2
	Inductor	0. 34	2	0. 68
	Integrated Circuit	0. 4	19	7. 6
				9. 08
B 5.	Scaler Timing Block (one for each scaler)			
	Resistor	0. 3	2	0. 6
	Capacitor	0. 1	6	0. 6
	Inductor	0. 34	2	0. 68
	Integrated Circuit	0. 4	8	3. 2
				5. 08
B 6.	Count Rate Meter			
	Transistor	3. 0	2	6. 0
	Resistor	0. 3	5	1. 5
	Capacitor	0. 1	4	0. 4
	Inductor	0. 34	2	0. 68
	Integrated Circuit	0. 4	1	0. 4
				8. 98
B 7.	Scanner			
	Integrated Circuit	0. 4	7	2. 8

	Failures per 10^6 hrs.	No. of Parts	Total Failure Rate
B 8. **Pulse Shape Discriminator**			
Transistor	3. 0	4	12. 0
Diode	1. 0	13	13. 0
Resistor	0. 3	12	3. 6
Capacitor	0. 1	8	0. 8
Inductor	0. 34	4	1. 36
Integrated Circuit	0. 4	2	0. 8
			31. 56
B 9. **Threshold Detector**			
Diode	1. 0	1	1. 0
Resistor	0. 3	2	0. 6
Capacitor	0. 1	4	0. 4
Inductor	0. 34	2	0. 68
Integrated Circuit	0. 4	2	0. 8
			3. 48

B 10. **Pulse Height Analyzer**

	Failures per 10^6 hrs.	8-Channel	2-Channel	8-Channel	2-Channel
Diode	1. 0	1	1	1. 0	1. 0
Resistor	0. 3	2	2	0. 6	0. 6
Capacitor	0. 1	4	4	0. 4	0. 4
Inductor	0. 34	2	2	0. 68	0. 68
Integrated Circuit	0. 4	9	3	3. 6	1. 2
				6. 28	3. 88

		Failures per 10^6 hrs.	No. of Parts	Total Failure Rate
B 11.	**Low Voltage Power Supply**			
	Transistor	3. 0	16	48. 0
	Dual Transistor	6. 0	1	6. 0
	Diode	1. 0	20	20. 0
	Resistor	0. 3	47	14. 1
	Capacitor	0. 1	18	1. 8
	Inductor	0. 34	2	0. 68
	Transformer	0. 34	6	2. 08
				92. 66
B 12.	**Gas System**			
	Gas System Electronics			
	PHA	3. 88	1	3. 88
	Count Rate Meters	8. 98	2	17. 96
	Differential Amplifier	12. 0	1	12. 0
	Discriminator	15. 0	1	15. 0
	Gate Generator	7. 52	1	7. 52
	Delay Circuits	5. 0	4	20. 0
				76. 36
	Gas System Mechanical			
	Regulators	. 56	2	1. 12
	Valves	. 56	5	2. 80
	Solenoids	. 06c (.30 x 10^{-6} cycles @ 2 operations/hr.)	5	. 65
	Gas Regulator Counter	25. 0	1	25. 0
				29. 57
	Total Gas System Failure Rate			105. 93

B 13. **Additional Estimated Failure Rates**

	Failures per 10^6 hrs., cycles
Hi-Voltage Power Supply	117. 0
Multiplex	151. 0
Subcommutator	3. 8
Analog/Digital Converter	25. 6
Timing Gate	1. 8
System Clock (electronic time code generator)	53. 0
$\pm\ 45^{\circ}$ Limiting Circuits	1. 5
Star Sensor and Electronics	50. 0
X-ray Counter per Detector (except Quad D detectors)	30. 0
Motor/Tach	22. 32
Servo-electronics	60. 0
Voltage Control Oscillator	13. 0
Transmitter	80. 0
32 kc Reference Oscillator	13. 0
Calibrator	8. 0
Tape Recorder	111. 0
Position Encoder	25. 0 c
2 Pole Commutator	3. 8
Relay	0. 48 c
Switch	0. 25 c
Camera & Electronics	175. 0

APPENDIX B

RELIABILITY EVALUATION OF S017 PARTS AND MATERIALS

The original S017 Experiment parts and materials were selected to give a reasonable assurance of performing successfully during a 20-hour mission and were satisfactory for this purpose. In comparison, the S069 Experiment must operate for a considerably longer mission time initially, shut down for 6 to 8 months, and then repeat the mission. A review of the existing S017 hardware is necessary to determine whether it can meet the new mission requirements. A listing of the S017 parts and materials, along with appropriate comments as to their acceptability, is included in this document.

In general, the minimum criterion for determining the acceptability of a part or material is evidence of qualification to a military standard with environmental test requirements equivalent to its intended space application. Parts or materials not thus qualified could be considered acceptable based on past usage history or NASA acceptance in known applications. Furthermore, items which are designated acceptable now should be superceded by more reliable replacements as they become available. For example, the Department of Defense is planning to replace the RC07 and RC20 resistors with "established reliability" versions. Similarly, RL07 resistors should be replaced with RLR07 or ultimately RNR types.

Where a part has been designated acceptable, it should be procured to a specification which requires the next highest reliability requirement. For example, where the military version of transistors satisfies the environmental requirements and is acceptable to some minimal reliability level, it should be procured as a JAN-TX device.

B-1

Burn-in testing and additional screening requirements imposed at proper points in a manufacturer's processing cycle, will provide the following:

a.   Early detection, analysis, and elimination of failure causes and modes thereby weeding out infant mortality failures and reducing the long-term random failure rate.

b.   A greater probability of reliable performance during the life of the experiment.

Parts and materials designated unacceptable are those items as determined from available information to be commercial parts (unpredictable reliability), low reliability MIL designated parts, or materials having undesirable or unknown characteristics which may degrade the probability of mission success.

It should be pointed out that the use of military specifications and standards, as a prime objective, assures that parts have satisfactorily met their performance requirements under a specified environmental range as demonstrated through part level qualification performed on a sample basis. This normally infers some inherent degree of reliability. The actual reliability of the device can only be determined through life testing and documented use history.

In military equipment applications (aircraft, shipboard and ground equipment), a part which meets the required environmental range (without immediate failure) may have a relatively low reliability which can be remedied by major redundancy and a generous supply of spares. This type of trade-off, however, is not available for the present S017 equipment. Constraints such as volume, weight, power, and no repair dictate the need for high reliability parts.

In determining acceptance, each part type must be reviewed on its individual qualifications and history. Where adequate supporting data or documentation is lacking, satisfactory substitutions or additional specification of requirements must be provided. For example, filter 1200-027, listed herein, is designated unacceptable, "purchased commercial". Presently, there is no QPL (Qualified Parts List) for MIL-F-15733; however, this part can be purchased under an acceptable manufacturer's "high reliability" counterpart.

The following list is a summary of the parts listed herein showing percentage of parts by generic type which have adequate reliability for the extended orbital operating and storage periods.

	TOTAL	Acceptable	% Acceptable
Capacitors	175	0	0
Diodes	130	97	73.8
Transistors	54	35	65
Transformers & Coils	27	0	0
Resistors	517	481	93.4
Relays	8	0	0
Micro circuits	93	0	0

Acceptance within the materials list is more difficult to establish since a detailed engineering design review of the application of questionable items is required.

Capacitors

QTY	PART NUMBER	DESCRIPTION	STATUS Accept	STATUS Not Accept	REMARKS
77	CS13	Solid Electrolytic		X	MIL-C-26655/2
2	CL65	Nonsolid Electrolytic		X	MIL-C-3965/4
4	CTM	Plastic		X	MIL-C-27287
3	CM05	Mica		X	MIL-C-5/18
5	2D2E1-104E	Metalized Mylar		X	Purchased Commercial
4	2D2E1-223E	Metalized Mylar		X	Purchased Commercial
1	2D2E1-683	Metalized Mylar		X	Purchased Commercial
1	EPC04X223-K	Ceramic		X	Purchased Commercial
2	EPC04X821-K	Ceramic		X	Purchased Commercial
41	MC70	Ceramic		X	Purchased Commercial
1	MC80	Cerafil		X	Purchased Commercial
3	DD30	Ceramic Disk			Purchased Commercial
1	CD7	Mica		X	Purchased Commercial
5	TRW601-PE	Mylar Epoxy Dipped		X	Purchased Commercial
2	109D	Tantalum		X	Purchased Commercial
1	TAM	Tantalum		X	Purchased Commercial
11	TY06	Glass		X	Purchased Commercial
8	TY07	Glass		X	Purchased Commercial
3	TY08	Glass		X	Purchased Commercial

Diodes

QTY	PART NUMBER	DESCRIPTION	STATUS		REMARKS
			Accept	Not Accept	
86	1N914	Medium Speed Switching	X		MIL-S 19500/116
2	1N752A	5.6V Zener Diode	X		MIL-S 19500/127
1	1N3713	Tunnel Diode		X	Purchased Commercial
16	UT262	Controlled Avalance Rectifier		X	Purchased Commercial
12	1N3981	Rectifier		X	Purchased Commercial
5	1N645	General Purpose	X		MIL-S 19500/240
2	1N4574A	Temperature Compensated Reference		X	Purchased Commercial
3	FD700	High Speed Switch		X	Purchased Commercial
1	1N751A	Reference	X		MIL-S 19500/127
2	1N3600	Switching	X		MIL-S 19500/231
		Filters			
3	Erie 1200-027	L Section EMI Broad band 10 Amps.		X	Purchased Commercial
		Coils			
18	Delevan 1537-76	100 Millihenry 5%		X	Purchased Commercial
3	Miller 9350-14	180 Millihenry 10%		X	Purchased Commercial

Transistors

QTY	PART NUMBER	DESCRIPTION	STATUS Accept	STATUS Not Accept	REMARKS
8	2N708	NPN Si. Switch		X	
9	2N3251	PNP Si. Low Power Switch	X		MIL-S 19500/323
9	2N2222	NPN Si. Low Power	X		MIL-S 19500/255
6	2N2219	NPN Si. Low Power	X		MIL-S 19500/251
10	2N930	NPN Si. General Purpose - Low Noise	X		MIL-S 19500/253
1	2N2484	NPN Si. Low Level, Low Noise		X	Purchased Commercial
1	2N915	NPN Si. Low Power RFA		X	Purchased Commercial
9	2N2221	NPN Si. High Speed Switch & VHF Amp.		X	Purchased Commercial
1	2N1131	PNP Si. Medium Current Switch	X		MIL-S 19500/117
		Transformers			
1	D1-T240 (UTC)	Interstage, Output & Wide Pulse			Purchased Commercial
2	D1-T278	Interstage or Driver			Purchased Commercial
3	2100-5	-------	--	--	AS&E

Resistors

QTY	PART NUMBER	DESCRIPTION	STATUS		REMARKS
			Accept	Not Accept	
49	RN55C	Metal Film	X		MIL-R-10509/7
18	RN55D	Metal Film		X	MIL-R-10509/7 MSFC-PPD-600
11	RN60C	Metal Film	X		MIL-R-10509/1
2	RN60D	Metal Film		X	MIL-R-10509/1 MSFC-PPD-600
4	RN65C	Metal Film	X		MIL-R-10509/2
259	RC07	Carbon Composition	X		MIL-R-11/8
31	RC20	Carbon Composition	X		MIL-R-11/3
1	RC32	Carbon Composition	X		MIL-R-11/6
114	RL07	Metal Film	X		MIL-R-22684/1
12	RL20	Metal Film	X		MIL-R-22684/2
1	MV608	Varnished High Voltage Comp. Film		X	Purchased Commercial
2	3280P-1-502	Trimpot		X	Purchased Commercial
4	3011P-1-105	Trimpot		X	Purchased Commercial
4	3012P-1-504	Trimpot		X	Purchased Commercial
1	224P-500-202	Trimpot		X	Purchased Commercial
2	50-2-1-103	Trimpot		X	Purchased Commercial
2	TM 1/8 (T/I)	Sensistor		X	Purchased Commercial

Relays

QTY	PART NUMBER	DESCRIPTION	STATUS Accept	Not Accept	REMARKS
4	Sigma 32RJPD	Dual Coil Latching DPDT		X	Purchased Commercial
1	Bourns 3101L-000-1251A	Sub-Miniature DPDT 1.0 Ampere		X	Purchased Commercial
1	Bourns 3101L-000-0650A	Sub-Miniature DPDT 1.0 Ampere		X	Purchased Commercial
2	Bourns 3900L-1-000	Time Delay DPDT 1.0 Ampere		X	Purchased Commercial
		Miscellaneous			
AR		Outer Space Wire	X		MIL-W-81044/4-24-9
AR		Wire	X		MS21985-229
AR		Wire	X		MS21985-24
AR	44/0411-24-29	Wire		X	Purchased Commercial
AR	Series 24	Wire		X	Purchased Commercial
11	6040-37P	Connector		X	Purchased Commercial
1	6040-23P	Connector		X	Purchased Commercial
1	6040-23S	Connector		X	Purchased Commercial
1	346-10-19PW	Connector		X	Purchased Commercial
1	100316-008	Time Delay Unit	--	--	Parko Electronics

Microcircuits

QTY	PART NUMBER	DESCRIPTION	STATUS Accept	Not Accept	REMARKS
21	DT𝄞 L951	Monostable Multivibrator		X	Purchased Commercial
28	F 𝄞 C13151	Clocked Flip Flop		X	Purchased Commercial
38	F 𝄞 C12151	Dual Gate		X	Purchased Commercial
6	FSC9194651	Quad two – input gate		X	Purchased Commercial

MATERIALS	MANUFACTURERS P/N OR MIL NUMBER	REMARKS
Slotted Terminal	CTC 2089-2-05	Acceptable - Silver Finish is questionable
Slotted Terminal	CTC 1785-2-05	Acceptable - Silver Finish is questionable
Slotted Terminal	CTC 1018-2-05	Acceptable - Silver Finish is questionable
Slotted Terminal	A 2089-1-05	Not identifiable
Locking Terminal Lug	H.H.Smith 1468	Acceptable
Turret Terminal	CTC 2085-2-05	Acceptable - Silver Finish is questionable
Shake Proof Terminal	2106-04-00	Not identifiable
Hex Nut (6-32)	ESNA 22NM107-62	Not acceptable Cadmium Plated.
Hex Nut (4-40)	ESNA 681660-40	Brass & Cadmium Plating. Not acceptable. Accept Alum.
Miniature Hex Nut (2-56)	ESNA 79LH1660-26	Carbon Steel is not acceptable Accept Stainless Steel.
Hex Nut (4-40)	NAS 671C-4	Acceptable
Self Locking Nut (4-40)	MS 21043-04	Acceptable - Prefer Nickel Plating instead of Silver.
Nylon Hex Nut (2-56)	UNC-2B	Questionable
Self Locking Nut (2-56)	UNC-3B (NAS 1291C02M)	
Hex Nut	MS35649-24	Acceptable without Cadmium Plating or Black Oxide Finish
Hex Nut	MS35649-44	Acceptable without Cadmium Plating or Black Oxide Finish
Hex Nut	Crescent AN 335	Not Acceptable
Button Head Screw	Crescent 6-32 x 3/8	Not Identifiable
Flat Head Screw	Crescent 4-40 x 5/16	Not Identifiable
Flat Head Machine Screw	MS 35249-24	Acceptable - Superseded by MS 51959

MATERIALS	MANUFACTURERS P/N OR MIL NUMBER	REMARKS
Nylon Button Head Screw (2-56)	UNC-2A-.25 Long.	Questionable
Panel Head Screw (2-56)	MS 35233-3 Crescent UNC-2A-.25 Long.	Acceptable without Cadmium Plating or Blk. Oxide Finish
Panel Head Screw	MS-35233-2	Acceptable Superseded by MS 51957
Panel Head Screw	MS-35233-14	Acceptable Superseded by MS 51957
Bracket	4688-21-10	Acceptable
Bracket	4688-21-8	Acceptable
Bracket	4688-21-7	Acceptable
Bus Wire	AWG # 22, 24, 26	Acceptable if QQ-W-343
Outer Space Wire	MIL-W-81044/4-9-24	Acceptable
Wire	MS 21985-22-9	Acceptable
Wire	MS 21985-24	Acceptable
Single Conductor Wire AWG # 24	Raychem 44/0411-24-9	Acceptable
Teflon Wire	MIL-W-16878	Acceptable
Hook-up Wire	Raychem Series 44	Acceptable
Flat Washer (#4)	AN 960C-4	Acceptable without Cadmium Plating or Blk. Oxide Finish
Nylon Washer (.02" thick)		Questionable
Washer	MS 35333-69	Acceptable without Cadmium Plating
Washer	MS 35333-70	Acceptable without Cadmium Plating.
Loctite Sealer	Loctite Co.	Outgasses
Conformal Coating	2105-5	Not identifiable
Polyurethane Coating	PR-1538	Outgasses
Epoxy	Armstrong C7	

MATERIALS	MANUFACTURERS P/N OR MIL NUMBER	REMARKS
Epoxy	Armstrong X-81	
Band Clamp	Wechesser WL-725	Nylon is Questionable
Cable-tite Clamp & Keeper	Dakota 2C1-25-9	Acceptable
Spacer	A S & E 104-700-246	Questionable - Flammable Material
Spacer	CTC 1300-9	Not Acceptable - Cadmium Plated
Subminiature Teflon Stand-off	Selectro ST-SM-7L2	Acceptable
Stand-off	Amaton 9537B-SS-0440-7	Acceptable
Stud	NCS-2-0-10	
Transipad	Milton Ross 10042	Acceptable
Transipad	Milton Ross 10058	Acceptable
Sleeving, Clear Teflon	MIL-I-22129	Acceptable
Solder SN60 WRAP 2	QQ-S-571	Acceptable
Mounting Tab	Weckesser A-30-167	Nylon is Questionable
Mounting Plate	A S & E 104-700-243	Acceptable - Print has Errors
Capacitor Mount	Milton Ross 10120	Acceptable
Unwaxed Clear Lacing	MIL-T-713	Nylon and Acetate Twine are Questionable
High Voltage Preamp Cable	A S & E 104-610-103	Specification Control Drawings not adequate.
Right Angle Connector	Cannon Precision 6040-37P	
Connector	Deustch 346-10-19PW	
Mylar Tape	Mystik 7355	

Drawings To Be Reviewed

104-507-301

104-515-301

104-605-201   Black Oxide Finish not acceptable

104-613-201

104-619-001

104-619-302

104-700-244

104-700-701

104-701-701

104-707-701

104-708-701

104-710-701

APPENDIX C

COUNTER LIFE TIME TESTS

Tests were conducted to determine life expentancy and probable counter failure modes. The principal series of tests was conducted on the original S-017 proportional counters. These counters were filled with 90% xenon and 10% methane. The counters were divided into seven groups. Each group was made up of four to five counters and subjected to different environmental test procedures, the results are summarized below:

1. Five units were subjected to vacuum cycling. Cycling consisted of (1) evacuation to a pressure of about 1×10^{-3} mm Hg (Torr) in a period of five minutes, (2) remaining at this pressure for a period of 2 to 3 minutes; and (3) a 2-minute return to atmospheric pressure.

    The five units were subjected to 50 vacuum cycles. The test has been discontinued as no unit had suffered visible damage or any significant deterioration in performance. We conclude from this that vacuum cycling is not a significant failure mode in modern proportional counters.

2. Four units were subjected to $160^{\circ}F$ temperature at ambient pressure for a period of 32 consecutive days. The temperature was then dropped to room temperature which is $77^{\circ}F$. There is general qualitative agreement for all units in the following respect:

a. There is initially a rapid decrease in gain followed by a gradual decrease. The loss in gain appears to be roughly exponential in character and the period for the gain to be decreased to half of its original value about 30 days.

b. The resolution of the counters gradually deteriorated. There is no apparent initial effect similar to the rapid initial variation in gain.

c. The units were then returned to 77°F. Three of the four units stabilized at the performance level observed at the end of the high temperature period. One exception showed a sharp drop and vacillated over a broad range for 10 days before finally settling at a higher level than was measured at the end of the high temperature period.

3. Five counters were kept in a vacuum environment (2×10^{-5} mm Hg) for a period of 77 days. Ambient temperature varied within the range from 92°F to 95°F.

None of these five counters suffered any significant loss in resolution. Two showed gradual gain decreases, and dropped to about 80 percent of their original values by the end of the 77-day test period.

Three of the five counters exhibited only a small initial drop in gain which leveled off at the 93-94 percent region and remained at this level for the remainder of the test period.

4. Five units were kept in a vacuum of 2×10^{-5} mm Hg at a temperature of 160°F for a period of 77 days, at the end of which time all units were brought up to atmospheric pressure and room temperature of 80°F. Comparison of these results with those of Group 3 shows immediately that gain and resolution vary with temperature and not with ambient pressure.

    Comparison with the results for Group 2, sustained high temperature, indicates similar overall responses to temperature for both groups. Upon being brought down to room temperature, the gain of all units increased slightly with improved resolution.

5. When temperature was determined to be a cause of counter failure, 4 units were placed in a 130°F environment for 48 days in order to determine the effects of intermediate temperatures. Their behavior was substantially the same as the failure pattern noted at 160°F, but took place on a slower time scale. The time required for these counters to drop to 1/2 of the original gain was approximately 38 days.

6. Four counters were subjected to a high counting rate environment. Two counters were exposed to flux which resulted in about 3×10^{3} counts per second for a period of 180 days or about 5×10^{10} total counts. These counters have shown a very slow decrease in gain. One now has approximately 0.86 of its original gain and the other 0.77. Two of the counters were subjected to a flux 10^{4} counts per second for a period of 180 days or about 1.6×10^{11} total counts. These counters have experienced a substantial loss in gain and also deterioration in resolution. In one case, the gain is .42 of its original value and the other case .30.

7. All of the above tests were performed on the original S-017 proportional counters which were filled with 90% xenon and 10% methane. The principal result is the rate of failure at elevated temperatures. The times required for these counters to reach half of their original gain was 38 days at 130°F and 30 days at 160°F. An extrapolation of the performance at 92°F indicates that these counters would loose 1/2 of their original gain after 250 days.

Excessive accumulation of counts has also been shown to be a cause of counter failure. The number of counts required to cause significant performance degradation exceeds that expected in an Apollo flight.

These results show the performance under extreme conditions. The purpose of these tests was to see if such degradation would occur and if so, to determine its causes.

In addition to the above group of counters, a control group was also tested with the same equipment and found to have no performance variations.

As a consequence of the above tests, certain other tests were initiated which are described below:

8. In order to further investigate the effects of counting rate on counter life, a count rate life test was conducted with 2 small counters.

The counters were exposed to about 50,000 counts per second with a 500,000 count/sec exposure for 6 minutes every hour.

After 10^{10} counts, the argon-methane counter had deteriorated to a point where it was no longer acceptable. The argon CO_2 counter had acceptable performance after 10^{10} counts. However, by 2.4×10^{11} counts, its gain had decreased to .87 of its original value and its resolution had deteriorated to 33%.

We conclude that CO_2 quench gas is significantly better than methane in counting rate life expectancy. This is consistent with the findings of other laboratories which have reported that, after an extensive counting history, a greasy substance is sometimes found on the counter anode wire. Methane fragments can polymerize and form such a greasy substance, and this is not likely in the case of CO_2.

9. The gas contents of two counters were analyzed. One was a control counter and the other had been subjected to a 160°F environment for 40 days.

    The chamical analysis indicated some water and ethylene in both counters. The only obvious difference was that the ethylene contents of the counter which had been subjected to 160°F for 40 days was four times as great as the ethylene content of the control counter. It would be necessary to test for the effects of ethylene on counter performance in order to determine the significance of the differing ethylene contents.

10. One of the counters, Serial #SN3622, which had been subjected to a temperature of 160^OF for 40 days, was evacuated and re-filled with argon and CO_2 quench gas. This counter then was tested and found to have a double peaked pulse height response. The counter was again evacuated and filled with argon and methane quench gas, and again found to have the double peaked response. The counter was disassembled and the anode wire was found to have a gray deposit and some white crystals at the end of the counter opposite the connector. The double peaked response function was caused by different counter gain in the region of the deposit. This double peaked distribution was also observed in counter #SN3627 which had undergone a 92° environment for 77 days. In this case one of the peaks disappeared when the end of the counter opposite the connector was shielded from the X-ray source.

We conclude from the above that, at high temperatures and a moderate radiation environment, the methane quench gas counters formed crystals and deposits on the anode. In the case of the particular counters tested, these deposits were formed preferentially at one end of the counter. This is possibly the result of high inherent gain at that end due to poorly compensated counter geometry.

11. The small Argon-Methane counter, which was used for the counting rate life expectancy test was also disassembled. No crystals were discovered on the anode. The anode wire, however, was pitted, particularly in the region exposed to the X-ray flux.

This counter also had a double peaked pulse height response; however, our earlier conclusion, that the counting life and high temperature failure modes are similar, is doubtful. An examination of the history of the counters shows that the second peak resulting from excessive counts develops on the low gain side of the original peak, whereas in the case of a high temperature failure the second peak develops on the high gain side of the original peak.

12. The results of series of the counter lifetime tests and recommendations for future studies are summarized below:

   a. Counter failures have been observed at high temperatures. This may be a consequence of the methane quench or epoxy outgassing. The failure mechanism involves a deposit on the anode wire and does not necessarily contaminate the gas.

   b. Counters are also observed to fail after a large number of accumulated counts. CO_2 quench gas counters have an accumulated count life expectancy at least 25 times as great as methane quench gas counters.

   c. Additional investigation into these failure modes should be performed. In particular, the deposits on the anode wires should be chemically analyzed. The gas contents of the failed counters should also be more accurately analyzed.

d. The CO_2 quench gas counters should be tested in a sustained high temperature environment. This may determine whether the failure mode is associated with the gas filling or with some of the counter construction materials.

APPENDIX D

PULSE SHAPE DISCRIMINATION STUDY

Part I - Theory

An extensive pulse shape discrimination study has been performed in order to develop rejection techniques for background events, particularly gamma ray events which are not usually eliminated by the anticoincidence technique.

An X-ray is absorbed in a X-ray counter as the result of the photoelectric effect; this usually ejects an electron from the tightest bound level the X-ray is capable of exciting. There are typically two or more electrons emitted from this first atom – the initial photoelectron and also Auger electrons produced when the atom de-excites.

The ranges of these electrons are quite small; the range of an electron in argon is approximately:

$$R \approx \left(\frac{E}{10\text{keV}} \right)^2 \text{ x } 0.132 \text{ cm} \quad \text{(Valid for E} \lesssim 100 \text{ keV)} \quad (1)$$

Thus, even a 10 KeV X-ray, which is near the top of our effective energy range, results in track lengths of less than 0.132 cm. An X-ray event in a proportional counter therefore starts with a small region of high ionization.

The electrons then drift towards the center wire, and the positive ions drift towards the cathode, but at a much slower rate. The cloud of electrons drifts reasonably coherently, but some diffusion occurs. When the electrons are quite close to the wire the field gradients become high enough so that the electrons acquire sufficient energy to ionize other atoms, and consequently electron multiplication occurs. The secondary electrons produce more secondary electrons, etc., and charge builds up rapidly near the wire. Most of the ions are actually formed quite near the wire; this is easily seen, for the mean free path of the electrons is only about $3 \cdot 10^{-4}$ cm, and the number of electrons is approximately doubling every mean free path near the wire. Thus, 1/2 of the electrons-ion pairs are formed with $3 \cdot 10^{-4}$ cm of the wire, 3/4 within $6 \cdot 10^{-4}$ cm of the wire, etc. (A more accurate calculation will be performed below.)

One might think that 1/2 of the charge associated with an event is collected when the electrons reach the anode wire. This is false because the positive ions are still near the wire and result in a surface charge on the anode; this surface charge is almost equal to the charge of electrons which have been collected. As the positive ions drift towards the cathode the surface charge on the anode is reduced and the charge is collected by the external circuitry.

The actual current which results from an ion pair can be calculated from the work done on the ion pair by the bias field of the counter. If the

counter voltage remains fixed, which is approximately true in practice, then we have the following equation for the current due to one pair:

$$VI = -\ell \left(\vec{E} + \cdot \frac{\vec{dr}_+}{dt} - E \cdot \frac{\vec{dr}_-}{dt} \right) \tag{2}$$

Where I is the current, V is the counter voltage, E + and E - are fields at r + and r -, which are the positions of the positive ion and electron respectively. The different sign, of course, refers to the differing charges of the ion and electron.

The total charge can be obtained by integrating the above expression; let us assume that the initial ionization occurs at r_o, and r_a and r_b are the positions where the electron and ion strike the anode and cathode respectively

$$q = \int I \, dt = \frac{-e}{V} \left[\int \vec{E}_+ \frac{dr_+}{dt} \, dt - \int \vec{E}_- \cdot \frac{\vec{dr}_-}{dt} \, dt \right] \tag{3}$$

$$q = \quad = \frac{-e}{V} \left[\int_{\vec{r}_o}^{\vec{r}_b} \vec{E} \cdot \vec{dx} - \int_{\vec{r}_o}^{\vec{r}_a} \vec{E} \cdot \vec{dx} \right] \tag{4}$$

$$q = \quad = \frac{-e}{V}\left[\left(V(\vec{r}_o) - V(\vec{r}_b)\right) + \left(V(\vec{r}_a) - V(r_o)\right)\right] \qquad (5)$$

$$q = \quad = \frac{-e}{V}\left[V(\vec{r}_a) - V(\vec{r}_b)\right] = -e \qquad (6)$$

Thus, we see that the total charge eventually collected is -e for each ion pair regardless of where it is originally formed. In addition, the fraction collected as a result of the motion of the electron is

$$q_{el} \qquad \frac{V(\vec{r}_a) - V(\vec{r}_o)}{V} \qquad (7)$$

Since the pairs are usually formed near the anode, we have $V(\vec{r}_o) \approx V(\vec{r}_a)$ and the charge contribution due to electron motion is small.

We will now consider a typical counter in greater detail. We will assume a cylindrical counter for theoretical convenience, but the size of the counter and other important parameters are similar to those of the Apollo experiment.

Let r_1 = a = anode radius = 0.001 inches = 0.00254 cm

r_2 = b = cathode radius = 1.0 inches = 2.54 cm

V = 2300 volts

P = Gas Pressure = 760 mm Hg at room temperature

E = Electric field gradient

Then

$$E = \frac{V/r}{\log_e (r_2/r_1)} = \frac{333}{r} \text{ volts/cm} \tag{8}$$

$$(E/p) = (0.438/r) \text{ volts/cm} - \text{mm Hg} \tag{9}$$

$$0.1725 \leq (E/p) \leq 172.5 \text{ volts/cm} - \text{mm Hg}$$

We can now calculate the size of the multiplication region; if α is the probability that an electron will ionize another atom in moving a unit distance, and $n(x)$ is the number of electrons when the electron cloud drifts past the position x, we obtain the following equation:

$$\frac{dn}{dx} = \alpha n \tag{10}$$

or

$$\log_e \frac{n(a)}{n(x)} = \int_x^a dx \, \alpha(x) \tag{11}$$

We can now calculate the size of the region in which 90 percent of the pairs are formed:

$$\log_e \left(\frac{r(a)}{0.1 n(a)} \right) = \log_e (10) = 2.302 = \int_x^a dx \, \alpha(x) \tag{12}$$

D-5

An approximate expression for α in argon is

$$\alpha \approx A_{p\ell}^{\,-B/(E/p)} \tag{13}$$

where

A ≈ 14 and B $\approx 18^{\circ}$ for argon. In our case,

$$\alpha \approx (1.064) \cdot 10^4 \, \ell^{\,-r} \tag{14}$$

and

$$\int_x^a dx^1 \, \alpha(x^1) = \frac{(1.064)(10^4)}{411} \left(\ell^{-(411)a} - \ell^{-(411)x} \right) \tag{15}$$

When this is set equal to 2.302, we obtain X = 0.00325 cm, or 90 percent

of the ion pairs are formed within between 0.00325 cm and the anode

radius of 0.00254 cm, a distance of $7.1 \cdot 10^{-4}$ cm, or 0.279 anode radii.

A similar calculation shows that 99 percent of the ions are formed

within 0.674 wire radii of the anode.

Evaluation of equation (7) shows that, for 90 percent of the electron-

ion pairs, less than 3.8 percent of the collected charge results from the

motion of the electron.

We can now estimate the time required for the electrons to traverse

the multiplication region. Accurate measurements of electron drift

velocities for the field gradients existing near the anode do not exist, and the concept of a drift velocity is probably invalid for these gradients. The estimated time, however, is so short that even relatively large errors are not important.

In the region where 90 percent of the ion pairs are formed we have $134.9 \leq (E/p) \leq 172.5$ (volts/cm – mm Hg). The drift velocity in a gas mixture of 90 percent argon and 10 percent CO_2 is 4 cm/μsec at $(E/p) = 0.6$ and increasing with (E/p). In a gas mixture of 90 percent argon and 10 percent CH_4 the drift velocity between $(E/p = 0.3$ and 0.6 is decreasing approximately as $(E/p)^{-1/4}$). If this behavior is extrapolated to $(E/p) = 172.5$, which is extremely conservative, the drift velocity would be 1.04 cm/μsec. Therefore, for either gas, the time required for the electrons to traverse the region where 90 percent of the multiplication occurs is less than $7.1 \cdot 10^{-4}/1.04 \cdot 10^6 = 6.8 \cdot 10^{-10}$ seconds. This time is negligible in terms of typical amplifier risetime, etc.

The drift velocities of positive ions is well approximated by

$$V = \mu (E/p) \tag{16}$$

and, for argon $\mu \approx 1,040$ (cm/sec) volt/cm – mHg)$^{-1}$. Therefore, in our case the positive ion drift velocities in the multiplication region are greater than

$$(1,040)(134.9) = 1.40 \cdot 10^5 \text{ cm/sec}$$

The transit time through the multiplication region is therefore less than

$$(7.1 \cdot 10^{-4}/1.4 \cdot 10^{5}) = 5 \cdot 10^{-9} \text{ seconds.}$$

Therefore, except for times of the order of 5 nanoseconds, which are small compared to typical amplifier response times, it is a good approximation to consider the current from an original ion pair to start when the electron reaches the anode, and to have the same shape as that produced by a positive ion starting from the anode at the time of arrival of the electron.

We can now calculate the current resulting from an electron which arrives at the anode as time t_o:

$$VI = - \vec{E} \cdot \vec{V}$$

and, using equation (16) and equations (8) and (9)

$$VI = \frac{-\ell}{\log_\ell (r_2/r_1)} \quad \frac{V}{r} \cdot \mu \cdot \frac{V}{r \log (r_2/r_1)p}$$

or,

$$I = \frac{-\ell \, V \, \mu}{r^2 \left[\log (r_2/r_1) \right]^2 p} \tag{18}$$

and, solving for r;

$$\frac{dr}{dt} = V = \mu \, (E/p) = \frac{\mu \, V}{p \log_\ell (r_2/r_1) \, r} \tag{19}$$

or

$$r^2 = r_1^2 + \frac{2\mu V (t - t_o)}{p \, \log_\ell \, (r_2/r_1)}$$ (20)

and, we obtain the current as:

$$I(t) = \frac{- e \, V \, \mu}{p \left[\log \, (r_2/r_1) \right]^2 \left[r_o^2 + \frac{2\mu V \, (t - t_o)}{p \log_\ell \, (r_2/r_1)} \right]}$$

or, simplifying

$$I = \frac{q_o}{(t - t_o) + T_1}$$ (21)

where

$$q_o = \frac{-e}{2 \, \log_\ell \, (r_2/r_1)}$$ (22)

$$T_1 = \frac{r_1^2 \, p \, \log_\ell \, (r_2/r_1)}{2 \, \mu \, V}$$ (23)

This is valid until the positive ion reaches the cathode. This occurs when $r^2 = r_2^2$, or, from equation 20, when

$$(t - t_o) = T_2 = \frac{(r_2^2 - r_1^2) \, P \, \log_\ell \, (r_2/r_1)}{2 \, \mu \, V}$$ (24)

In summary, we have the following expression for the current resulting from an electron which reaches the wire at to

$$I = 0 \quad \text{for } (t-to) < 0 \tag{25a}$$

$$I = \frac{q_o}{(t-to) + T_1} \quad \text{for } 0 \leq (t-to) < T_2 \tag{25b}$$

$$I = 0 \quad \text{for } (t-to) \geq T_2 \tag{25c}$$

and, q_o T, and T_2 are defined in equations 22, 23 and 24 respectively.

In the case we are considering, $r_1 = 2.54 \cdot 10^{-3}$ cm, $r_2 = 2.54$ cm, P = 760 mm Hg, $\mu = 1.04 \cdot 10^3$, and V6 = $2.3 \cdot 10^3$. This results in the following values:

$$T_1 = 7.08 \cdot 10^{-9} \text{ seconds} \tag{26}$$

$$T_2 = 7.08 \cdot 10^{-3} \text{ seconds} \tag{27}$$

A finite track length can be approximated by distributing the above current over a finite time of arrival. If the initial charge is spread out over a time $T\ell$, and the first electron arrives at $t_o = 0$, we obtain the following expression for the current:

$t < 0 : I(t) = 0$

$0 < t < T$

$$I_\ell(t) = \int_o^t \frac{(q_o/T_\ell) \, dt^1}{(t - t^1) + T_1} = \left(\frac{q_o}{Te}\right) \log_\ell \left(1 + \frac{t}{T_1}\right) \tag{27a}$$

$T_\ell < t < T_2$:

$$I_\ell (t) = \int_0^{T_\ell} \frac{(q_o/T_\ell)\, dt^1}{(t-t^1 0 + T_1} = \left(\frac{q_o}{T_\ell}\right) \log_\ell 1 + \left[\frac{T_\ell}{(t-T) + T_1}\right] \qquad (27b)$$

The times after the total collection time T_2 are not interesting in practice because the amplifier clipping time constants are much less than $T_2 \approx 7$ milliseconds.

The preamplifiers used with proportional counters are usually charge sensitive devices. The charge collected as a function of time can be obtained by integrating the above expressions (equations 26 and 27).

The following results are obtained:

T_ℓ = initial track length in time = 0.

$$q(t) = 0 \qquad\qquad\qquad t < 0 \qquad\qquad (28a)$$

$$q(t) = q_o \log_\ell \left(1 + \frac{t}{T_1}\right) \qquad 0 < t < T_2 \qquad (28b)$$

In the case where $T_\ell = 0$, we obtain, after integrating equation 27,

$$q(t) = 0 \qquad\qquad\qquad t < 0 \qquad\qquad (29a)$$

$$q(t) = \frac{q_o}{T_\ell} \left\{(t + T_1) \log \left(1 + \frac{t}{T_1}\right)\right\} \qquad 0 < t < T \qquad (29b)$$

$$q(t) = \frac{q_o}{T} \left\{ (t + T_1) \log \left(1 + \frac{T_\ell}{(t-T_\ell) + T_1} \right) \right.$$

$$\left. + T_\ell \log \left(1 + \frac{(t-T_\ell)}{T_1} - T_\ell \right\} \right. \qquad T_\ell < t < T_2$$

(29c)

The current and charge wave forms predicted by the above equations are plotted in Figures 1 and 2 for various track times. The track times chosen correspond to the following track lengths:

Time, T_ℓ	Track Length, Argon-CH_4	Track Length, Argon-CO_2 at r = 2 cm
$0 \cdot 10^{-9}$	0 cm	0
$53 \cdot 10^{-9}$	1/4	.053 cm
$106 \cdot 10^{-9}$	1/2	.106 cm
$212 \cdot 10^{-9}$	1	.212 cm
$424 \cdot 10^{-9}$	2	.424 cm

The curves represent events in which the total charge is the same but the pulse shapes are different because of different distributions of the initial ionization. An examination of Figures 1 and 2 show the following significant features of pulse shape which can be used to differentiate between X-ray and background events:
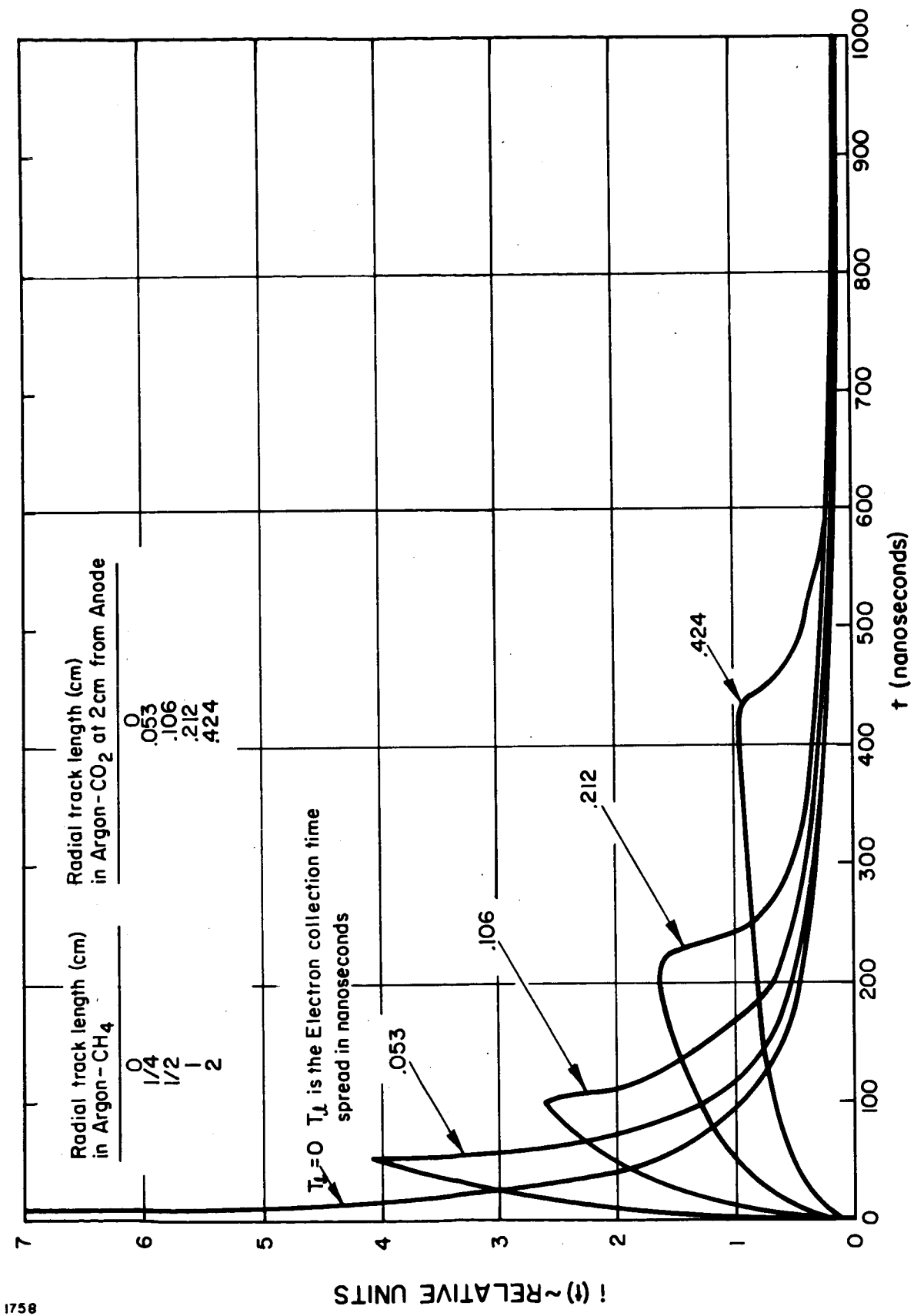
Figure 1   I (t) For Various Radial Track Lengths. Total Charge Is The Same For All Curves.

1758
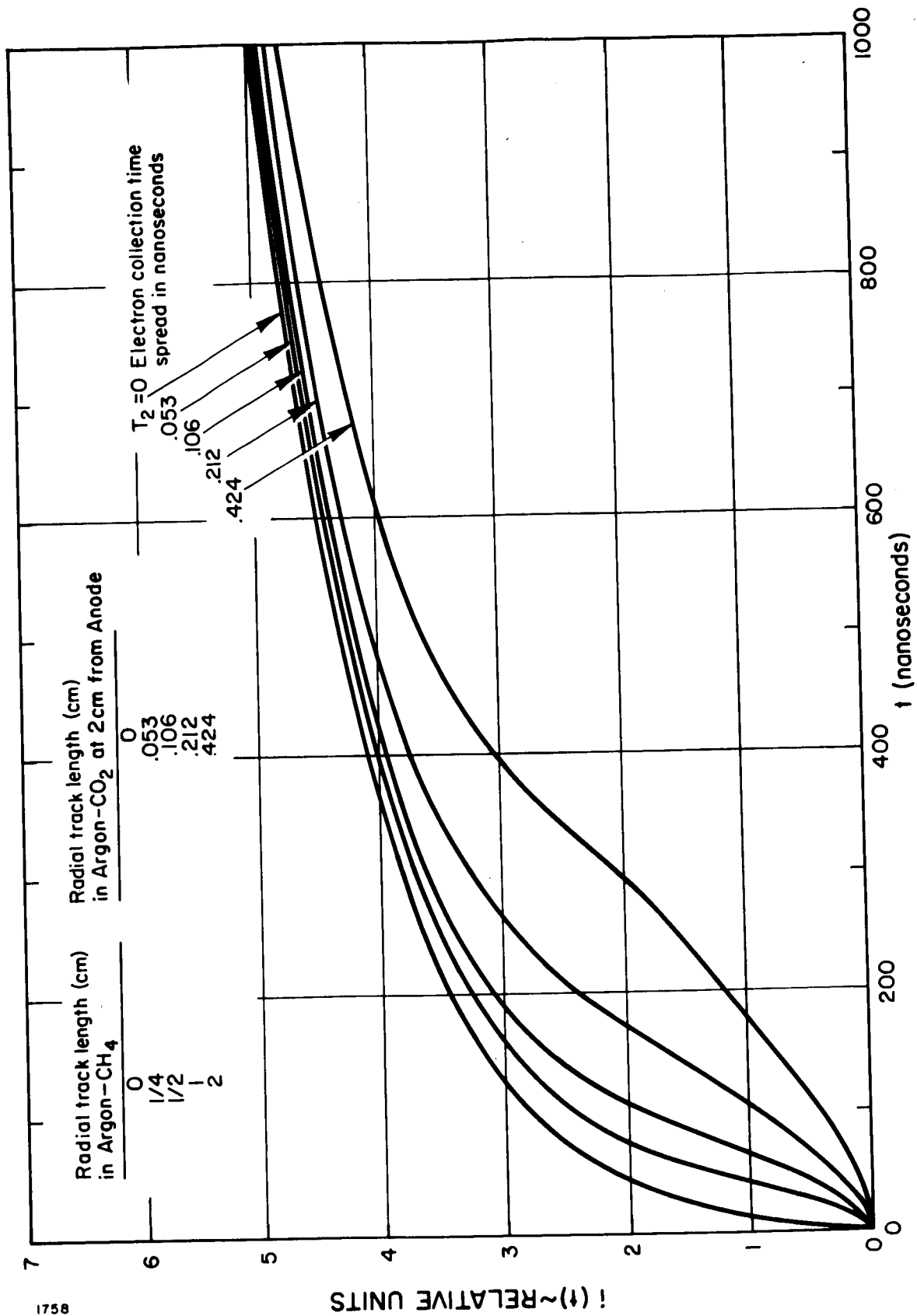
Figure 2   Integrated Charge ($Q(t)$) For Various Radial Lengths.
Total Charge is the Same for All Curves.

1758

1. The peak current amplitude of the X-ray events is greater than that of events with an extended radial distribution.

2. The width of the current pulse for X-ray events is narrower than that of the background events.

3. The charge risetime of X-ray events is shorter than the risetime of background events.

4. The charge which would be collected during a short integration time constant would be greater for X-ray events than for the background events.

A test program was conducted to determine the optimum background rejection technique. Results of this study are discussed in the next section.

EXPERIMENTAL RESULTS

Part II

The experimental program consisted of measuring the X-ray acceptance
and background acceptance for different X-ray energies as functions of
pulse shape criteria. Three counter gases were investigated. These
were P-10, which is 90 percent argon and 10 percent methane, a 90 per-
cent xenon and 10 percent methane mixture, and a 90 percent argon,
10 percent carbon dioxide mixture. These gases are common proportional
counter fillings. The tests were conducted at a variety of counter voltages
in order to determine the effect of counter voltage on the rejection
efficiency. As discussed above, four criteria were investigated:
integrated charge risetime, peak current, current width, and short time
constant charge integration. The circuit techniques used for the measure-
ment are discussed in Section 3 of the appendix. Most of the work was
done with the argon CH_4 mixture because it has a very quick charge
collection time, a useful property in the pulse height analysis and anti-
coincidence electronics. At the end of the program the argon-CO_2
mixture was tested and found to be greater superior. However, there was
not time to optimize the rejection techniques when using this gas.

1. ### Test Results for the Integrated Charge Risetime Technique with Argon CH_4 Mixture Gas

The results for this case are tabulated in Table I. The important
information is contained in the column labeled background acceptance

Table I

Counter Gas: 90% Argon; 10% CH_4

Pulse Shape Technique: Integrated Charge Risetime

(Note – Some data are shown more than once).

Line	X-ray Run No.	Background Run No.	Background Source	Differentiation Time Constant (μ sec)	X-ray Energy (keV)*	Counter Voltage	Background Acceptance at 90% X-ray Level (%)	Remarks (**Background not subtracted)
1	12	13	Na22	0.1	5.9	2300	13.5	**
2	17	16	→	0.2	→	→	4.0	**
3	10	11	→	0.5	→		8.3	**
4	3	5	Na22	0.8DL	5.9	2300	10.0	**
5	20	21	Na22	0.2	5.9	2100	36.5	**
6	17	16	→	→		2300	4.0	**
7	127	129	→	→		2300	6.3	
8	22	23	Na22	0.2	5.9	2400	12.0	**
9	72	73	Co60	0.2	5.9	2250	12.7	
10	76	77	→	→	→	2300	9.7	
11	127	129	→	→	→	2300	5.2	
12	74	75	Co60	0.2	5.9	2350	14.6	
13	130	131A	Na22	0.2	1.45	2300	38.5	
14	126	128A			2.9		25.7	
15	127	129A	→	→	5.9	→	6.3	
16	17	16	Na22	0.2	5.9	2300	4.0	**
17	130	131	Co60	0.2	1.45	2300	38.3	
18	126	128	→	→	2.9	→	25.7	

*1.45 keV = Al source: 2.9 keV = Fe55 escape peak; 5.9 keV = Fe55; 10 keV = Au195; 22 keV = Cd109;

+ D.L. = Delay Line

Table I (Continued)

Counter Gas: 90% Argon; 10% CH$_4$

Pulse Shape Technique:

(Note – Some data are shown more than once).

Line	X-ray Run No.	Back-ground Run No.	Back-ground Source	Differen-tiation Time Constant (μ sec)	X-ray Energy (keV)*	Counter Voltage	Background Acceptance at 90% X-ray Level (%)	Remarks (**Background not subtracted)
19	127	129			5.9		5.2	
20	76	77			5.9		9.7	
21	84	85	Co^{66}	0.2	10.0	2300	8.25	**
22	6	5	Na^{22}	0.8DL	1.45	2300	55.5	**
23	3	5			5.9		10.0	**
24	7	5			10.0		29.2	**
25	4	5	Na^{22}	0.8DL	22.0	2300	18.0	**

*1.45 keV = Al source: 2.9 keV = Fe^{55} source; 5.9 keV = Fe^{55} escape peak; 5.9 keV = Fe^{55}; 10 keV = Au^{195}; 22 keV = Cd^{109};

+ D. L. = Delay Line

at 90 percent X-ray acceptance level. Several conclusions can be drawn

from the data in Table I. First, from lines 1 to 4, we observe an optimum

performance with a differentiation time constant of approximately 0.2

microseconds. Second, from lines 5 to 8 or lines 9 to 12, we find that

the optimum performance occurs at a counter bias voltage of approxi-

mately 2300 volts. Lines 6 and 7 are equivalent measurements as are

lines 10 and 11. The spread in values obtained is an indication of the

accuracy of the measurements. A comparision of lines 6, 7, 10 and 11

also indicates that a slightly superior performance is achieved in

rejecting Na^{22} background compared to CO^{60} background. Na^{22} is a

positron emitter, and one detects both the positrons and the 510 keV

anilation gamma rays. CO^{60} emits gamma rays of approximately 1.2 MeV

energy. The difference in the background rejection may indicate that

the technique rejects charged particle events more efficiently than gamma

rays. Tests were then conducted at these optimum voltages and differen-

tiation time constants for a variety of X-ray energies. These results are

tabulated in lines 13 to 21. The performance is quite acceptable for

energies above 5.9 KeV and presumably is acceptable for energies above

approximately the argon K edge at 3.2 KeV.

The data of runs 16 and 17 are plotted in Figure 3. An anti-discrimina-

tion setting of 19.6 would result in acceptance of 90 percent of the X-ray

events and only 4 percent of the background. It should be noted, however,
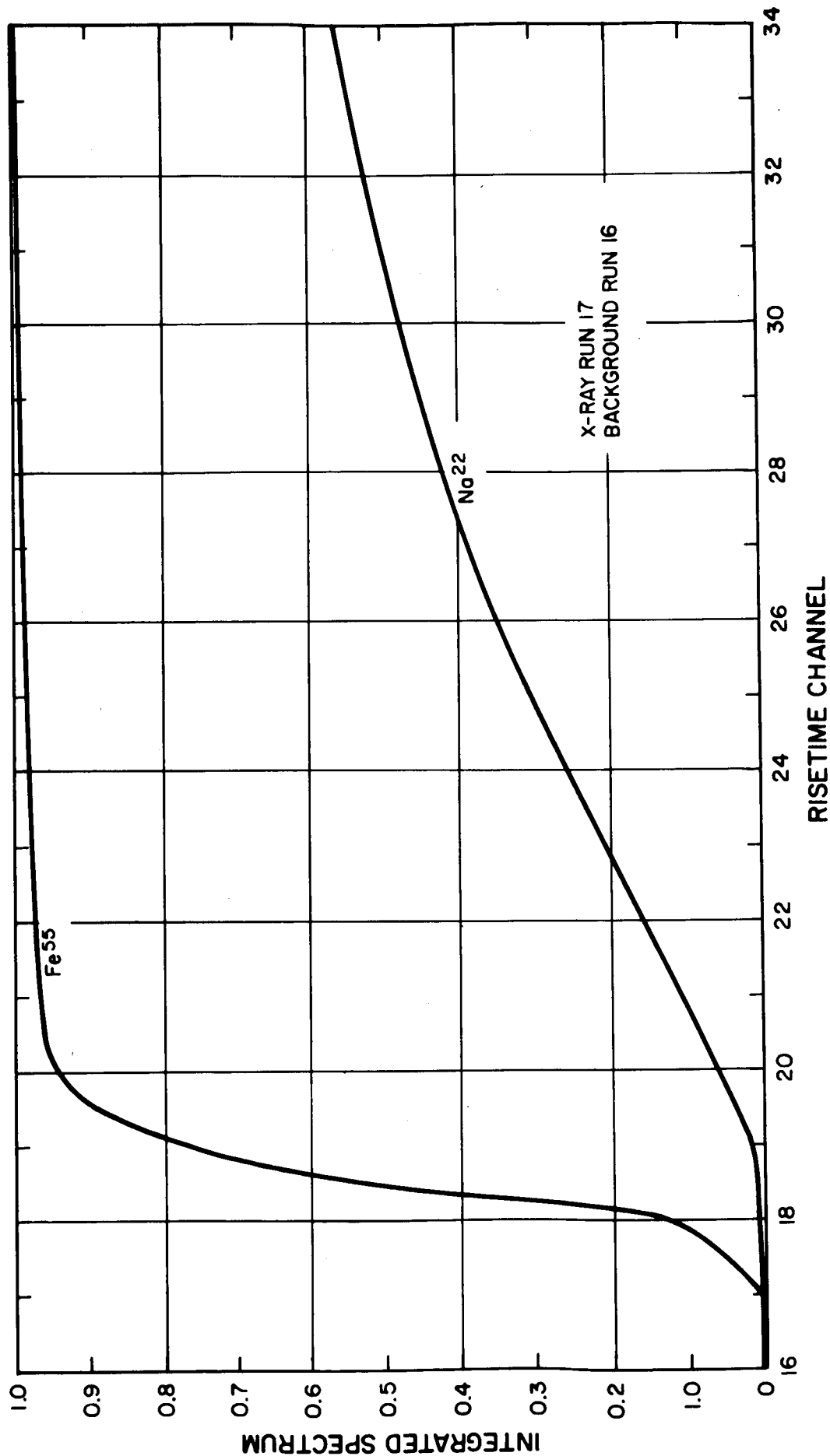
Figure 3   Integrated Rise Time Spectrum
Double RC Differentiation, $Z = 2.0$ μsec.
90% Argon and 10% CH4 Quench Gas
HV = 2300V

1758

that operation at this point results in a severe dependence on discrimination threshold stability. A more feasible operating point is approximately channel 21 with 96 percent acceptance of Fe^{55} and 11 percent background acceptance.

2. Test Results for the Peak Current with Argon
CH_4 Gas

The data used in this technique are tabulated in Table II. The data of lines 1 through 5 indicate an optimum performance region between 2300 and 2330 volts. The data of lines 6 to 12 is taken in this optimum operating region. The results are essentially equivalent to those obtained with the integrating charge risetime technique. The data of X-ray run 34 are plotted in Figure 4. A discrimination setting of 20.6 would result in 90 percent acceptance of 5.9 keV X-rays and only 7.6 percent of background events at that energy. The slope of the acceptance curve at that point is quite acceptable. This technique, however, requires a wide bandwidth electronic system.

3. Test Results for the Integrated Charged Risetime Technique with Current Pulse Width

The results of this technique are tabulated in Table III. Either this technique or the circuitry used for the measurement or both were very susceptible to noise, and the results are very erratic. This technique also requires more sophisticated circuitry than any of the other techniques tested and does not have any significant performance advantages. The

Table II

Counter Gas: 90% Argon; 10% CH$_4$

Pulse Shape Technique: Peak Current

(Note – Some data are shown more than once).

Line	X-ray Run No.	Background Run No.	Background Source	Differentiation Time Constant (μ sec)	X-ray Energy (keV)*	Counter Voltage	Background Acceptance at 90% X-ray Level (%)	Remarks (**Background not subtracted)
1	38	39	Na^{22}		5.9	2100	85.0	
2	34	35	→^{22}		→	2300	6.7	
3	40	41	Na^{60}		5.9	2400	11.9	
4	134	137	Co^{60}		5.9	2330	7.2	
5	58	69	Co^{60}		5.9	2350	13.7	
6	34	35	Na^{22}		5.9	2300	6.7	
7	37	35	Na^{22}		10.0	→	6.4	
8	36	35			22.0	2300	22.0	
9	132	135	Co^{60}		1.45	2330	33.7	
10	133	136	→Co^{60}		2.9	→	25.3	
11	134	137			5.9	→	7.2	
12	138	139	Co^{60}		22.0	2330	7.7	

*1.45 keV = Al source; 2.9 keV = Fe^{55} escape peak; 5.9 keV = Fe^{55}; 10 keV = Au^{195}; 22 keV = Cd^{109};
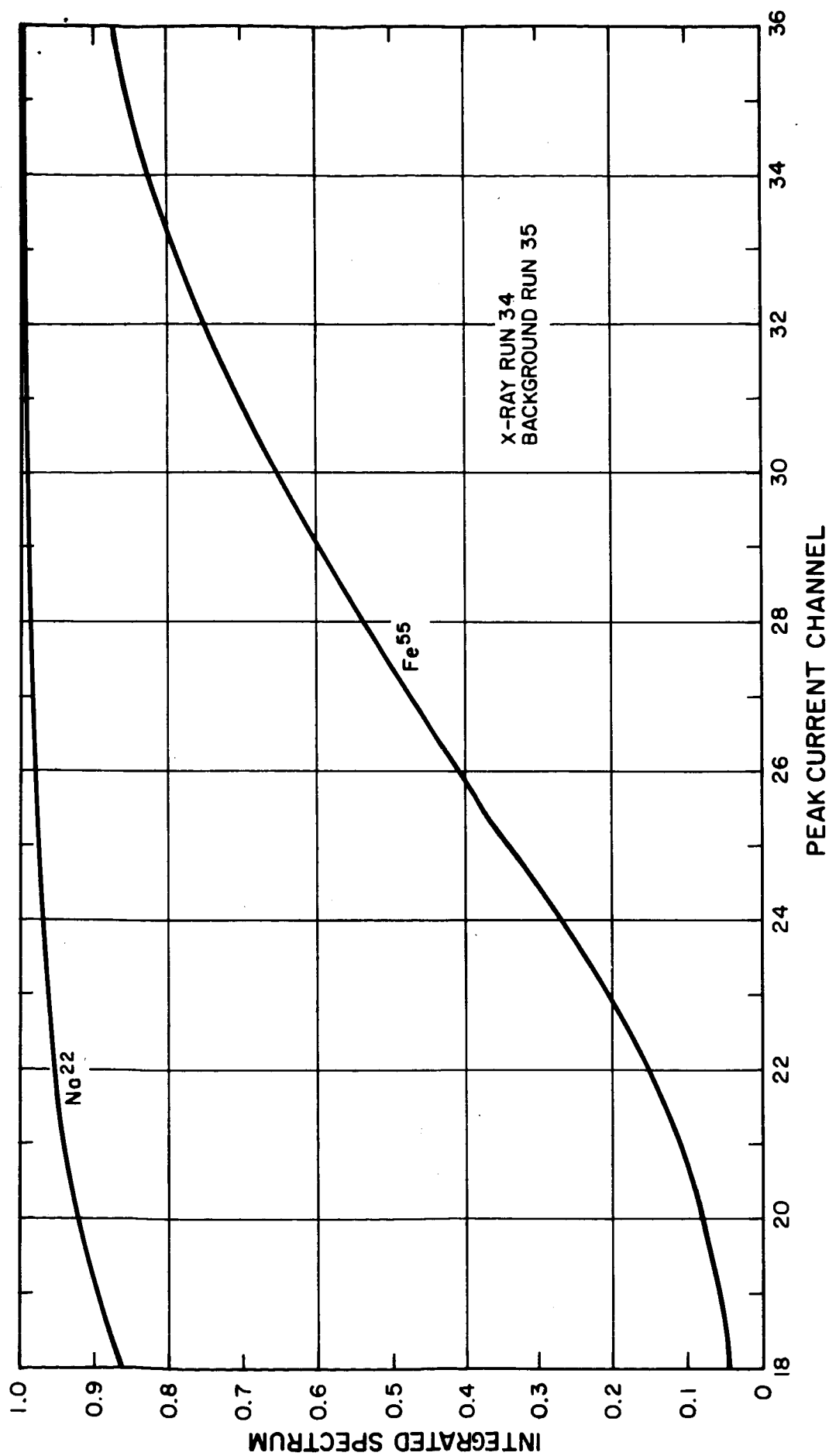
+ D.L. = Delay Line

Figure 4   Integrated Peak Current Spectrum
90% Argon and 10% CH4 Quench Gas
HV = 2300V

1758

Table III

Counter Gas: 90% Argon; 10% CH$_4$

Pulse Shape Technique: Current Pulse Width

(Note – Some data are shown more than once).

Line	X-ray Run No.	Background Run No.	Background Source	Differentiation Time Constant (μ sec)	X-ray Energy (keV)*	Counter Voltage	Background Acceptance at 90% X-ray Level (%)	Remarks (**Background not subtracted)
1	49	50	Na^{22}		5.9	2200	38.2	
2	42	43	→ Na^{22}		→	2300	11.7	
3	47	48	Na^{22}		5.9	2400	6.0	
4	112	115	Co^{60}		5.9	2400	16.0	
5	64	65	→		→	2450	17.4	
6	66	67	→			2500	11.0	
7	120	123	Co^{60}		5.9	2500	23.7	
8	42	43	Na^{22}		5.9	2300	11.7	
9	45	43	→ Na^{22}		10.0	→ 2300	11.9	
10	44	43	Na^{22}		22.0	2300	27.4	
11	110	113	Co^{60}		1.45	2400	81.0	
12	111	114	→		2.9	→	35.2	
13	112	115	→		5.9	→ 2400	16.0	
14	116	117	Co^{60}		10.0	2400	13.8	
15	118	121	Co^{60}		1.45	2500	48.4	
16	120	123	→		5.9	→	23.7	
17	66	67	→		5.9	→ 2500	11.0	
18	124	125	Co^{60}		10.0	2500	21.0	

*1.45 keV = Al source: 2.9 keV = Fe^{55} escape peak; 5.9 keV = Fe^{55} escape peak; 10 keV = Fe^{55}; 22 keV = Au^{195}; 22 keV = Cd^{109};

+ D.L. = Delay Line

optimum operating voltage appears to be somewhat higher than observed in the other tests; operation at the higher voltage results in a poorer pulse height resolution. This technique should, therefore, be eliminated from future considerations.

The data of X-ray run 47 are shown in Figure 5. An anti-discrimination setting of 20.4 would result in 90 percent X-ray acceptance and only 6 percent background acceptance. The slope of the X-ray acceptance curve is useful at that point.

4. Short Time Constant Integration

The results of data taken with a short time constant are given in Table IV. This technique yields the same results as the peak current method would yield in a low bandwidth system. A comparison indicates that the peak current method is superior in the energy region of primary interest.

5. Tests with Xenon-Methane Mixture Counter

The results of test with the xenon counter are given in Table V and indicate that this technique is not useful with xenon-methane counter.

6. Test Results with a 90 percent Argon - 10 Percent CO_2 Counter

Some tests were performed with this mixture and excellent results were obtained. These tests are summarized in Table VI. Unfortunately, these tests were conducted late in the program, and results are incomplete.
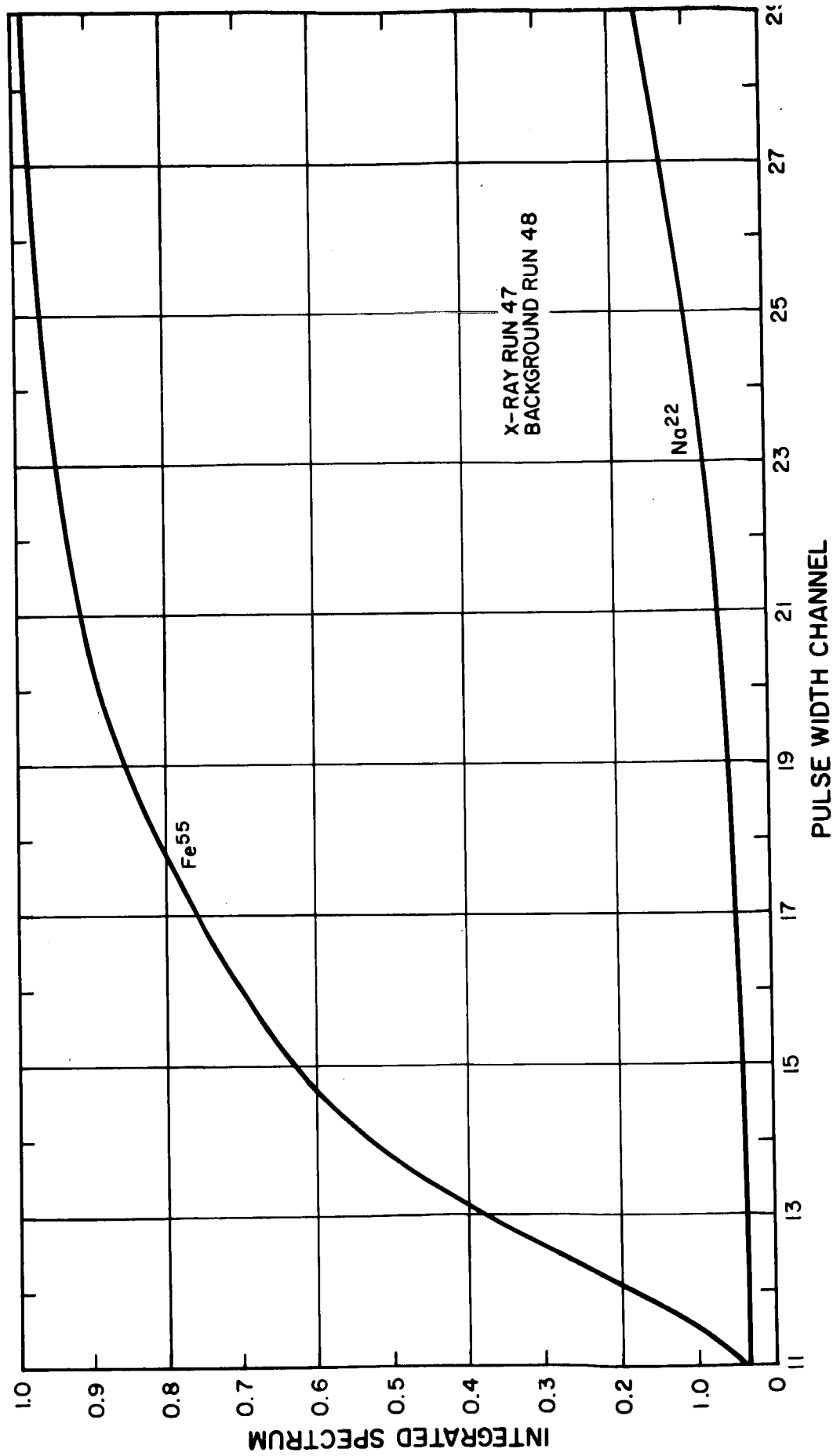
Figure 5   Integrated Pulse Width Spectrum
Argon Counter SN 4546, HV = 2400 V.
10% CH4 Quench Gas

1758

Table IV

Counter Gas: 90% Argon; 10% CH_4

Pulse Shape Technique: Short Time Constant Integration

(Note – Some data are shown more than once).

Line	X-ray Run No.	Back-ground Run No.	Back-ground Source	Differen-tiation Time Constant (μ sec)	X-ray Energy (keV)*	Counter Voltage	Background Acceptance at 90% X-ray Level (%)	Remarks (**Background not subtracted)
1	57	58	Na^{22}		5.9	2300	16.5	
2	59	58	Na^{22}		22	2300	18.7	
3	60	61	Co^{60}		5.9	2400	49	
4	62	63	Co^{60}		5.9	2500	71.5	

*1.45 keV = Al source: 2.9 keV = Fe^{55} escape peak; 5.9 keV = Fe^{55}; 10 keV = Au^{195}; 22 keV = Cd^{109};

+ D.L. = Delay Line

D-27

Table V

Counter Gas: 90% Argon; 10% CH$_4$

Pulse Shape Technique: Integrated Charge Risetime

(Note – Some data are shown more than once).

Line	X-ray Run No.	Background Run No.	Background Source	Differentiation Time Constant (μ sec)	X-ray Energy (keV)*	Counter Voltage	Background Acceptance at 90% X-ray Level (%)	Remarks (**Background not subtracted)
1	24	25	Na^{22}	0.8DL	5.9	2500	49.7	
2	28	29	→	→	→	2700	49.2	
3	26	27	Na^{22}	0.8DL	5.9	2900	70.2	
4	30	31	Na^{22}	0.5	5.9	2700	41.7	
5	32	33	Na^{22}	2.0	5.9	2700	35.8	
6	70	71	Co^{60}	NA	5.9	2900	42	Peak current tech.

*1.45 keV = Al source: 2.9 keV = Fe^{55} escape peak; 5.9 keV = Fe^{55}; 10 keV = Au^{195}; 22 keV = Cd^{109};

+ D.L. = Delay Line

Counter Gas: 90% Argon; 10% CH$_4$

Table VI

(Note – Some data are shown more than once).

Line	X-ray Run No.	Background Run No.	Background Source	Differentiation Time Constant (μ sec)	X-ray Energy (keV)*	Counter Voltage	Background Acceptance at 90% X-ray Level (%)	Circuit Technique
1	140	143	Co^{60}	0.8DL	1.45	2000	4.7	Integrated Charge
2	141	144			2.9		7.7	Rise Time
3	142	145			5.9		1.0	
4	146	147			10	2000	3.6	
5	148	151			1.45	2100	10.2	
6	149	152			2.9		3.0	
7	150	153			5.9		0.8	
8	154	155			10	2100	4.9	
9	156	159			1.45	2200	7.8	
10	157	160	Co^{60}		2.9		5.0	Integrated Charge
11	158	161		0.8DL	5.9	2200	1.0	Rise Time
12	165	167		NA	5.9	2300	12	Peak Current
13	168	169		NA	10	2300	28	Peak Current

*1.45 keV = Al source: 2.9 keV = Fe^{55} escape peak; 5.9 keV = Fe^{55};·10 keV = Au^{195}, 22 keV = Cd^{109};

+ D.L. = Delay Line

D-29

The test parameters presented in Table VI were chosen after a quick examination of some very sketchy data and may not be optimum. The tests results indicate that performance improves for higher counter voltages in the case of low X-ray energies, and for lower counter voltages in the case of higher X-ray energies. The result obtained with the rise-time technique and counter voltage of 2200 volts are shown in Figure 6. The separation between X-ray acceptance threshold and background acceptance threshold is much greater than was observed with the argon methane counter. At the 90 percent X-ray acceptance level the back-ground acceptance is only 1 percent for 5.9 keV events.

It would also be feasible to choose a single pulse shape discrimination level for all three energies. This results in a considerable electronic simplification.

The peak current technique was also investigated with the argon CO_2 counter. The peak current tests are not conclusive, for in the case of argon CO_2 counters the signal is much lower and our system was limited by amplifier noise. The results, however, are not as good as those obtained with the charge risetime technique.
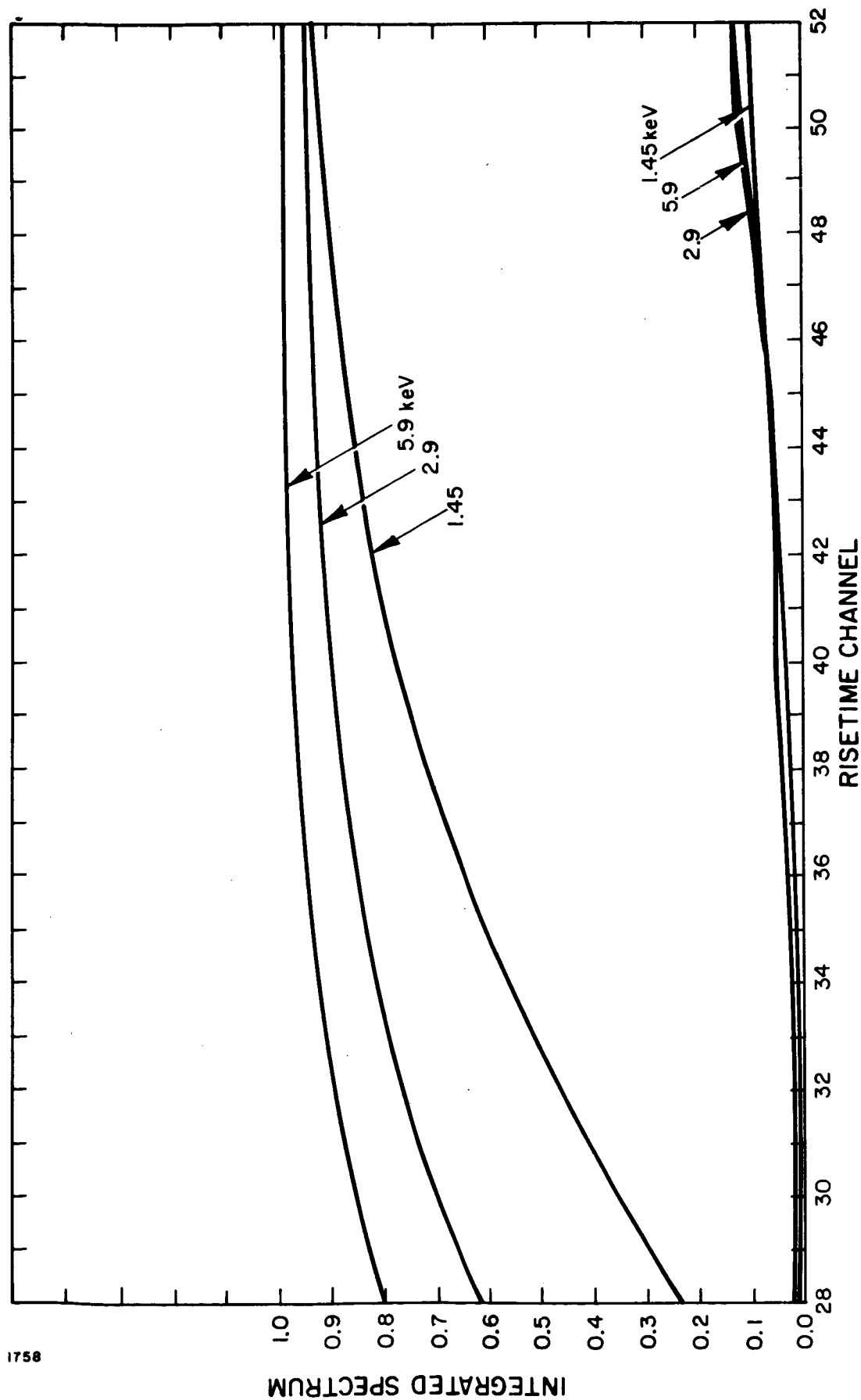
Figure 6   Integrated Rise time Spectrum
Double Delay Line Differentiation, $\tau = 0.8\ \mu\text{sec}$.
Argon Counter, HV = 2200 V
10% CO_2 Quench Gas

1758

Experimental Conclusions

1. A substantial background reduction is achieved with an argon CO_2 counter and the integrated charge risetime criteria. Rejection ratios of 11:1 to 90:1 in the X-ray energy range 1.45 keV to 5.9 keV have been obtained.

2. The xenon-methane mixture does not yield useful results for this technique background rejection.

3. The methods suitable for an argon - CH_4 counter can be divided into a low bandwidth (integrated charge risetime) and high bandwidth (peak current, pulse width) techniques.

   a. The low bandwidth technique requires more stable discriminators, yields slightly better results at lower X-ray energies, and slightly worse results at higher energies.

   b. The high bandwidth techniques require superior amplifiers, but have less stringent discriminator threshold stability requirements. The peak current method is somewhat simpler to implement than the pulse width method.

4. An optimum counter voltage is approximately 2300 volts for argon-methane counters; the optimum voltage for the argon CO_2 counter is probably about 2200 volts, but further tests must be performed.

EXPERIMENTAL PROCEDURES FOR PULSE SHAPE DISCRIMINATION MEASUREMENTS

PART III

1. Integrated Charge Risetime Measurements

A block diagram of the electronics used for the risetime measurements is shown in Figure 7.

The pulse amplitude signal in all tests is obtained from an Ortec 109 charge sensitive amplifier with a 50 microsecond time constant.

The risetime quantity measured is the time interval between a low threshold discrimination pulse, which therefore occurs near the beginning of the pulse, and the zero-crossing time after the pulse is doubly differentiated. The latter quantity depends only upon pulse shape, and principally upon the risetime of the pulse.

2. Peak Current Measurements

The electronics used for the peak current measurements are block diagrammed in Figure 8.

The input impedance of the original fast amplifier is 50 ohms. The original proportional counter output is divided between the fast amplifier channel and the charged sensitive amplifier. The pulse splitting assumes that the input impedance of the pre-amplifier is quite small; it is necessary to add the 2000 pf capacitor to achieve a low impedance at high frequency; this degrades the pulse height resolution by about 10 percent. This pulse splitting technique was used in all of the studies which require a current shape response as well as a charge shape response.
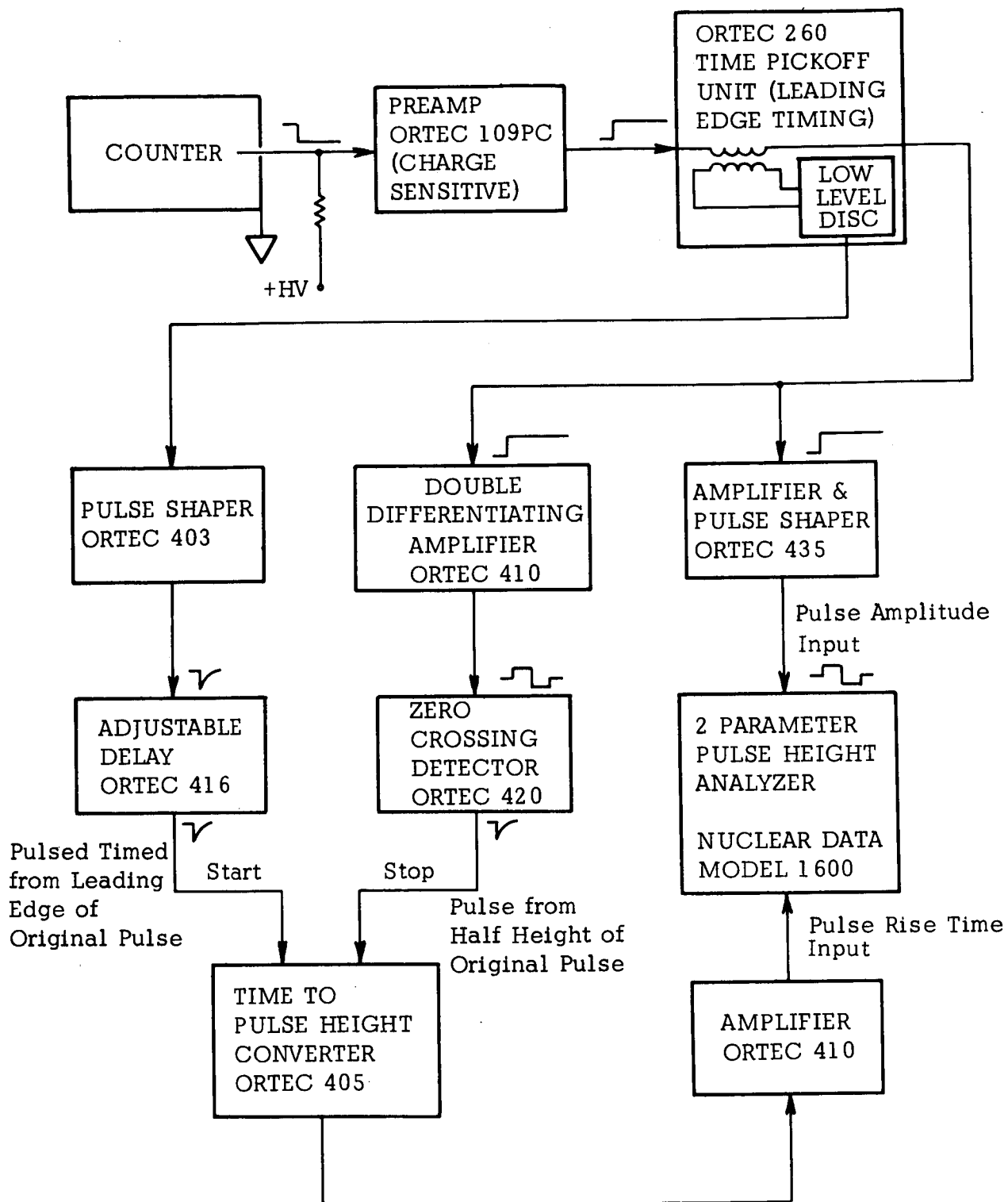
Figure 7 Block Diagram, Rise Time Measurements in Pulse Shape Discrimination Study

COUNTER

.005μf

+HV

2000pf

50

100K

FAST
AMPLIFIER*

PREAMP
(CHARGE SENSITIVE)
ORTEC 109PC

PEAK SENSING
CIRCUIT
ASE-SK127-3000

AMPLIFIER &
PULSE SHAPER
ORTEC 410

AMPLIFIER &
PULSE SHAPER
ORTEC 410

Amplitude Input

Peak Current Input

2 PAREMETER
ANALYZER

NUCLEAR DATA

MODEL 1600

*Amplifier = Lecroy 133
+ EG&G AN101

Total Gain Adjustable
up to X1600

1758

Figure 8 Block Diagram, Peak Current Measurements in Pulse Shape Discrimination Study

The current pulse is amplified by the fast amplifier and acted upon peak sensing circuit. The peak sensing circuit yields a slow decaying pulse with an amplitude equal to one-half of the original input amplitude. This long pulse is further amplified, shaped and presented to the pulse height analysis.

The peak sensitive circuit is shown in Figure 9. Q1 and Q2 act as a differential amplifier and conduct approximately equally during quiescent periods. Q4 and Q5 are also a differential amplifier with Q5 normally conducting most of the current -- Q4 conducts only the bias current of Q2 and Q8. A negative signal causes Q1 and Q4 to conduct more strongly until the voltage on capacitor C18 is equal to the input voltage. When the input signal falls below its peak value, Q1 and Q4 turn off, which results in the peak voltage being stored on C18. The decay of this voltage depends upon the leakage current of Q2 and Q8. This process is repeated by transistors Q6 through Q11. This results in a voltage equal to the peak of the input current being stored across C22. This voltage decays with a 50 microsecond time constant determined by C22 and R53. The emitter-follower Q13 acts as an output buffer; the output impedance is about 51 ohms. The input impedance of the following device is also 50 ohm in this series of tests; consequently the output signal is a long pulse with an amplitude equal to one-half of the input peak amplitude.
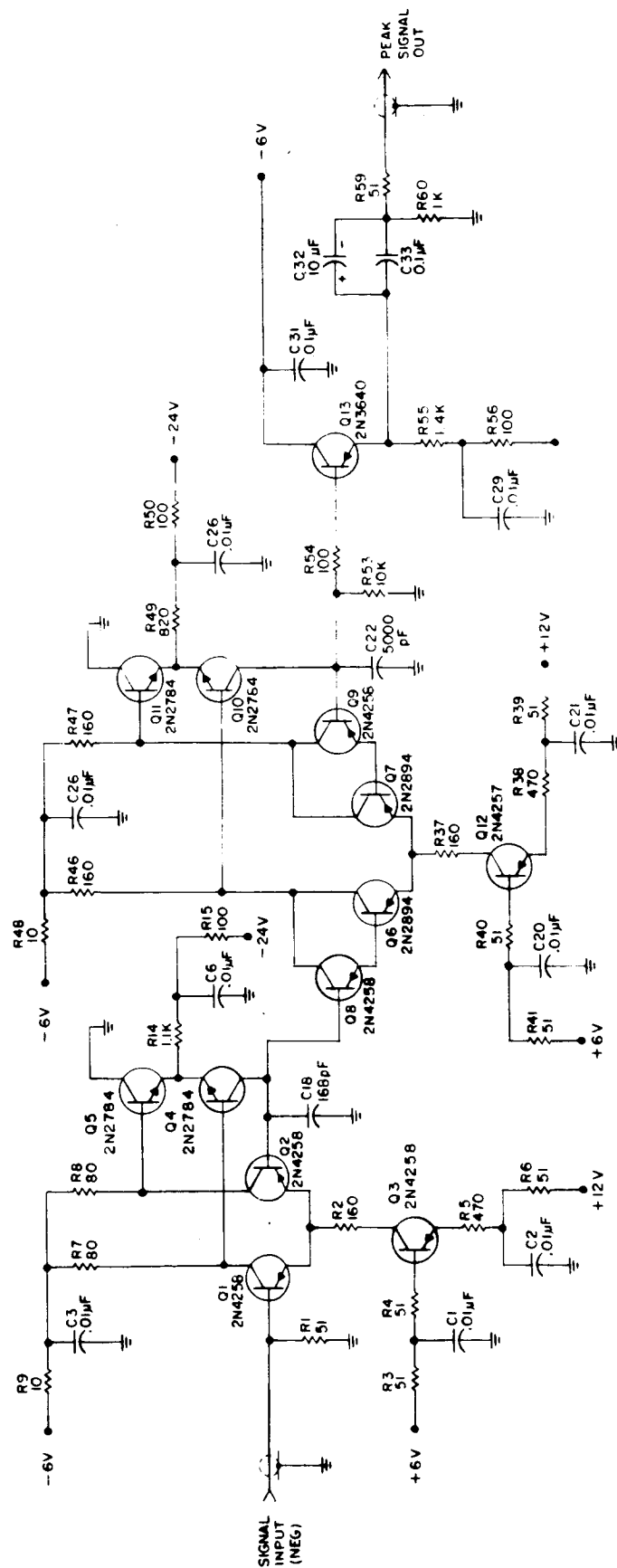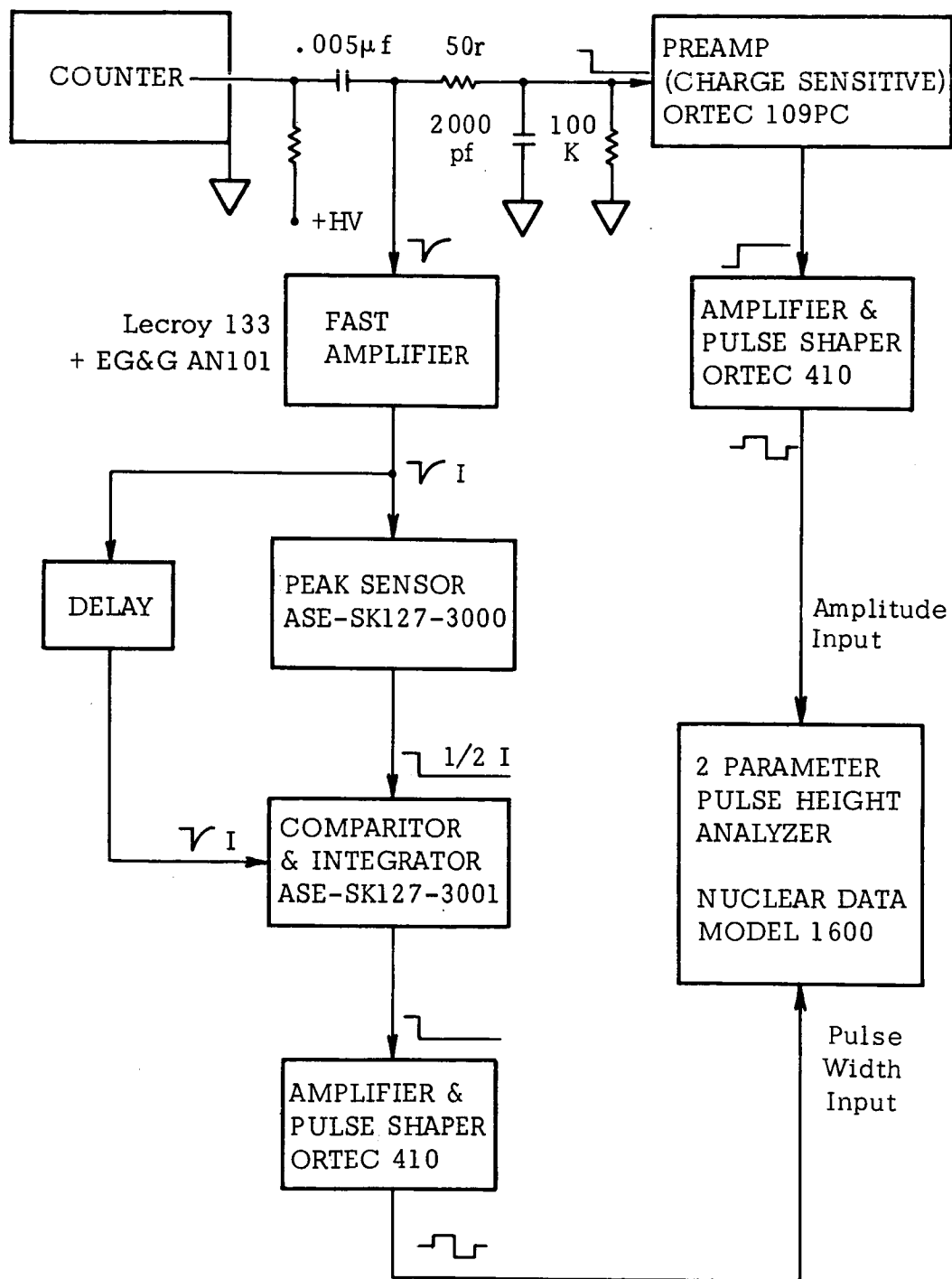
Figure 9   Peak Current Sensitive Circuit for Pulse Shape Discrimination Studies

1758

3. Current Pulse Width Measurements

A block diagram of the electronics used for the current pulse width measurement is shown in Figure 10. The charge pulse is obtained in the manner discussed in the preceding section. The fast current pulse is acted upon by the peak sensor which yields a slowly decaying pulse with an amplitude of one-half the original current pulse. This decay is so slow that the pulse can be considered as a level for this discussion. This level is then compared with the original pulse which has been delayed so that the peak sensing circuit has had an adequate time to function. The comparator-integrater circuit integrates a constant current which lasts as long as the original input pulse is more negative than one-half of its peak value. The amplitude of the output pulse of the capacitor circuit, therefore, is proportional to the time interval between the 1/2-height points of the original pulse. The comparator circuit is shown in Figure 11. Q1, Q2 and Q3 form a biased differential amplifier; Q1 conducts only when the input current is more negative than both the threshold voltage present at the base of Q2 and the 1/2-peak level voltage which is present at the base of Q3. Q5 only conducts when Q1 is conducting; therefore the total charge delivered to C20 is proportional to the time interval between the 1/2-points of the original pulse. The emitter-follower Q7 is used as an output buffer.

Figure 10   Block Diagram, Current Pulse Width Measurements,
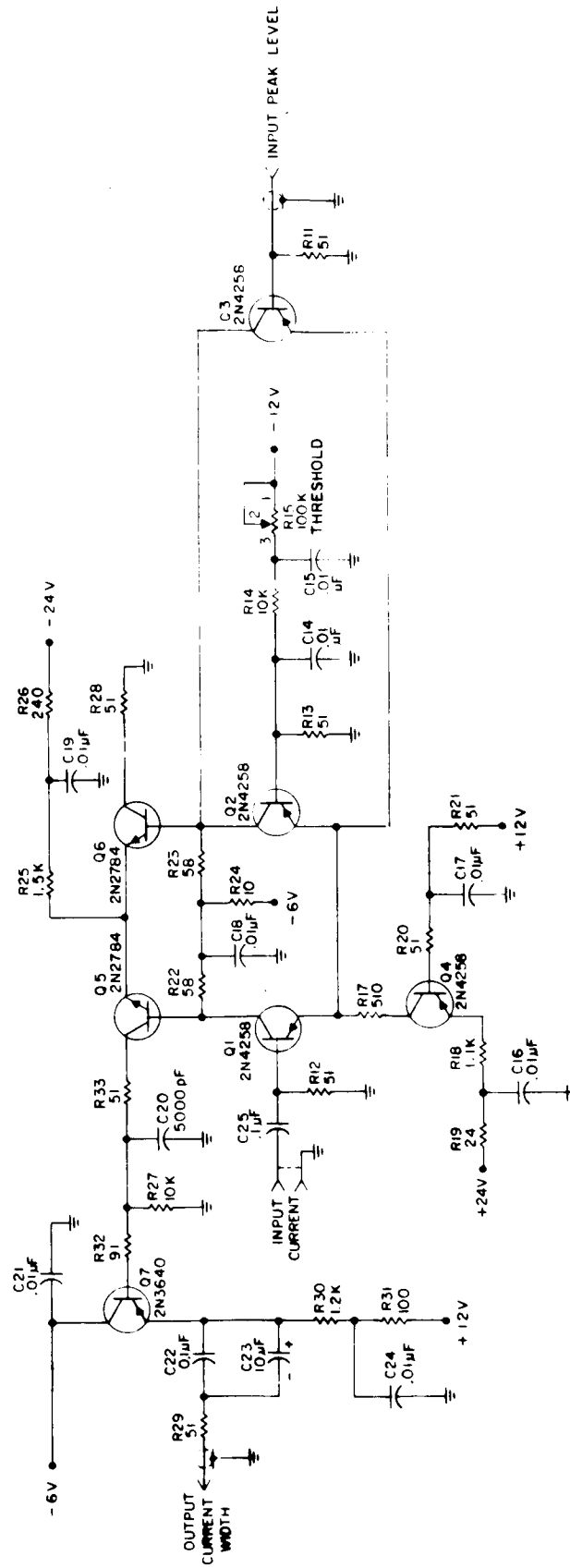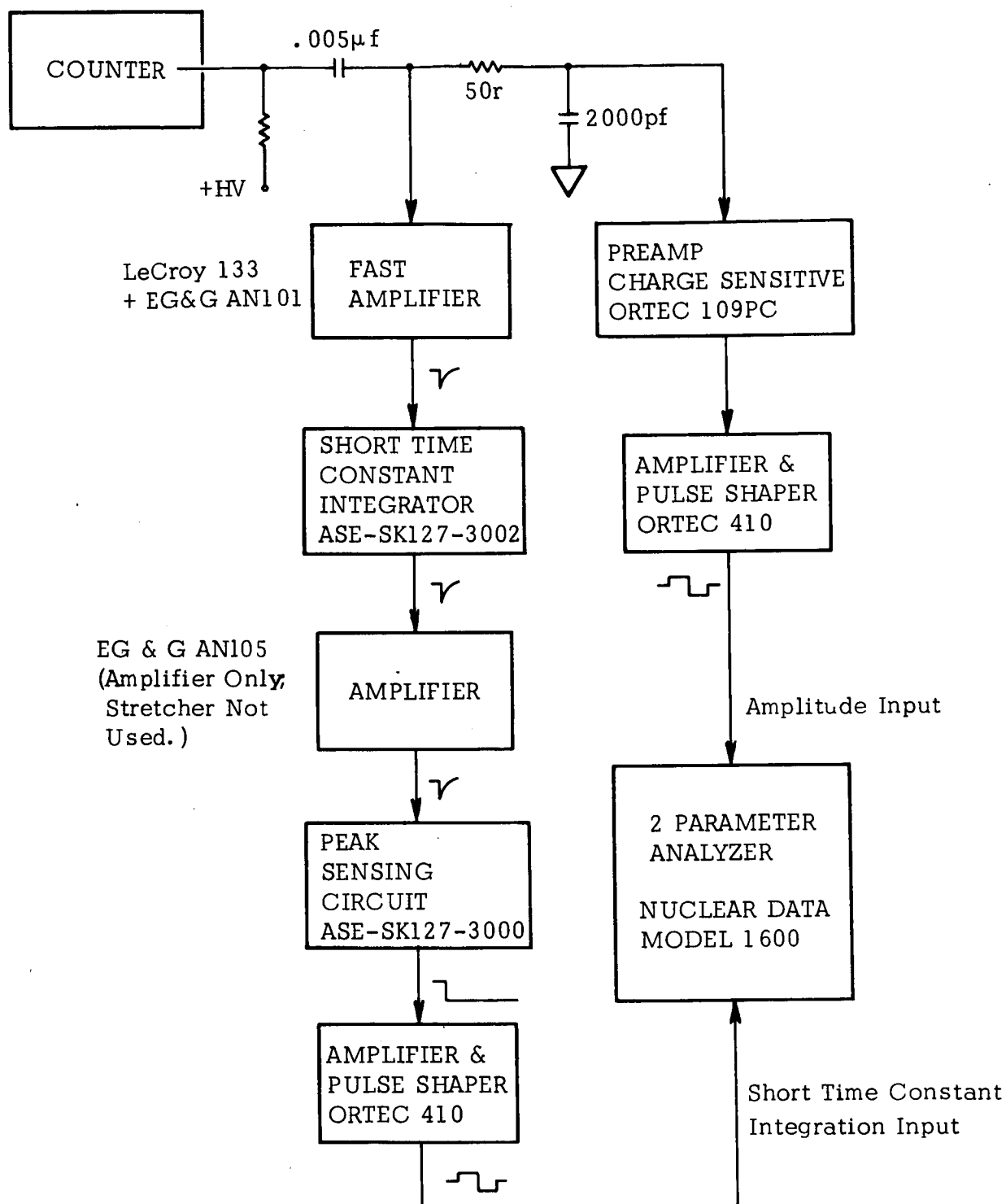Pulse vs Shape Discrimination Study

Figure 11   Current Comparator Circuit for Pulse Shape Discrimination Current Width Measurements

4. Short Time Constant Integration

The electronics used for the short time constant integration measurements are block diagrammed in Figure 12. The short time constant integrator essentially averages the pulse over its integration time. Its output is acted upon by the peak sensing circuit described earlier. This signal, therefore, corresponds to the maximum value of the input pulse current averaged over a time approximately equal to the pulse integrator integration time constant.

The pulse integrator circuit is shown in Figure 13. Q1 and its associated circuitry correctly terminate the 50-ohm input cable and provide a high impedance source for the integration network consisting of C8, R6 and RV.

The integration time is C8 (R6 + RV). The emitter-follower Q2 is used as an output buffer.

Figure 12 Block Diagram, Short Time Constant Integration Measurements,
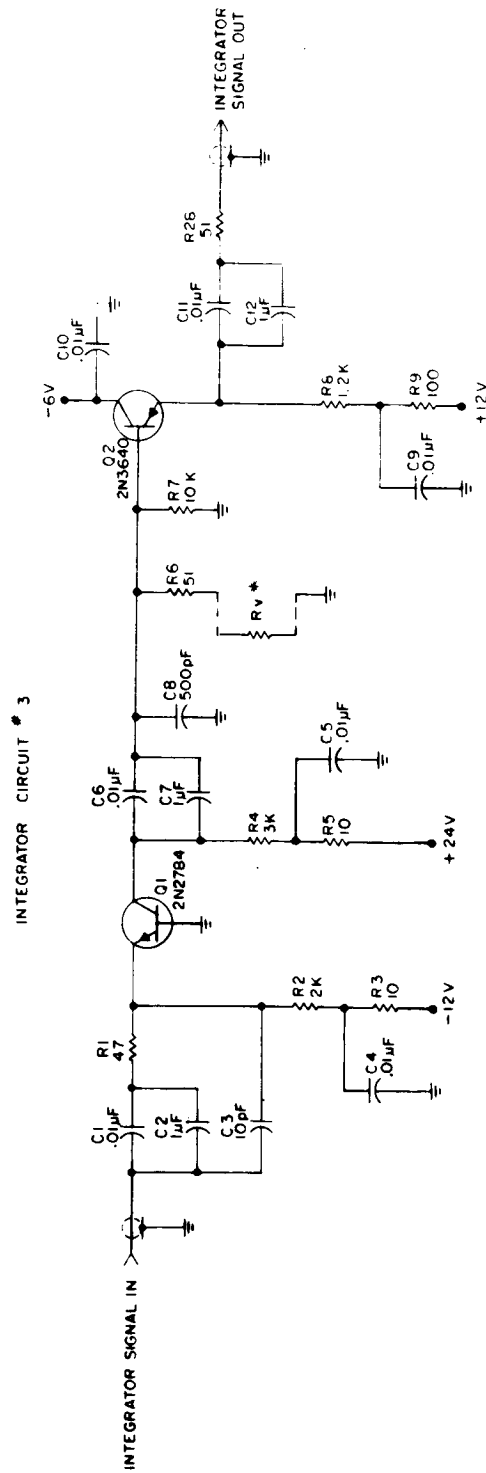Pulse Shape Discrimination Study

Figure 13   Pulse Integrator for Pulse Shape Discrimination Short Time Constant
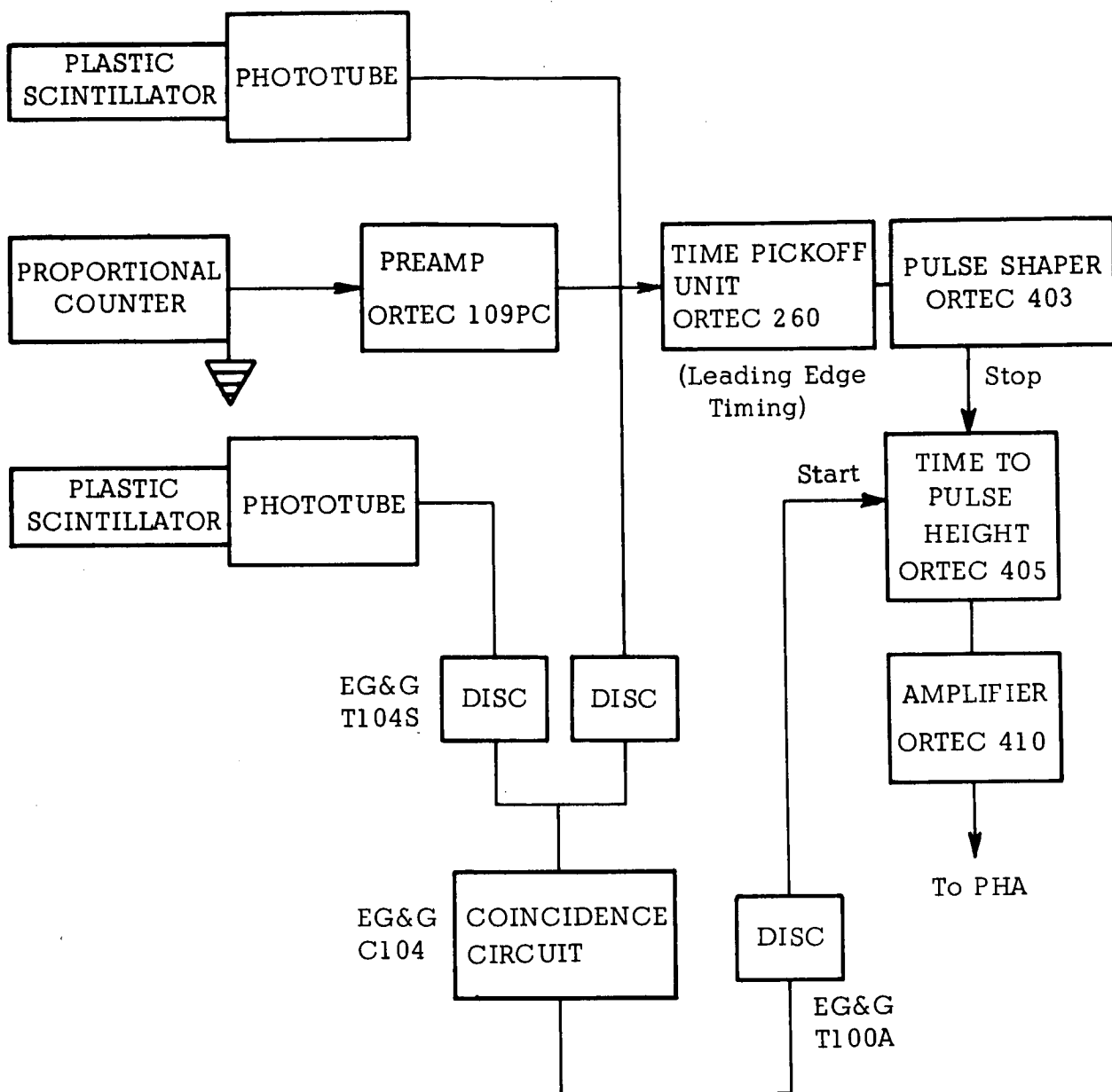Integration Measurements

APPENDIX E

PROPORTIONAL COUNTER PULSE DELAY MEASUREMENTS

Proportional counter pulse delay measurements were made for both the argon CH_4 counter and the argon CO_2 counters in order to establish anti-coincidence requirements. The pulse delay time is a consequence of the time required for the electrons, which are produced where the X-ray is absorbed, to drift into the multiplication region.

The information consists of the measurement of the time delay between the passage of a cosmic ray particle through a scintillation counter telescope and the detection of the event by the proportional counter. A block diagram of the experimental apparatus is shown in Figure 1. The electronic delays and the delays in the scintillator system are negligible compared to the inherent delay in the proportional counter.

The results for the argon CH_4 and argon CO_2 counter are shown in Figures 2 and 3 respectively. From these measurements the time allowed for the anti-coincidence gate must be at least 0.9 microseconds if argon CH_4 counters are used and 2.5 microseconds if argon CO_2 counters are used. This time interval is actually the delay time between the event and the leading edge of the pulse. The actual anti-coincidence gate may have to be longer depending upon the particular electronics, pulse shaping circuit, etc.

The cause of the different time delay distribution in the two types of counters is not completely understood.

PLASTIC SCINTILLATOR — PHOTOTUBE

PROPORTIONAL COUNTER → PREAMP ORTEC 109PC → TIME PICKOFF UNIT ORTEC 260 — PULSE SHAPER ORTEC 403

(Leading Edge Timing)

Stop

PLASTIC SCINTILLATOR — PHOTOTUBE

Start

TIME TO PULSE HEIGHT ORTEC 405

EG&G T104S   DISC   DISC

AMPLIFIER ORTEC 410

To PHA

EG&G C104   COINCIDENCE CIRCUIT

DISC

EG&G T100A

1758

Figure 1   Block Diagram of Experimental Apparatus for Proportional Counter Cosmic Ray Pulse Delay Distribution Measurements
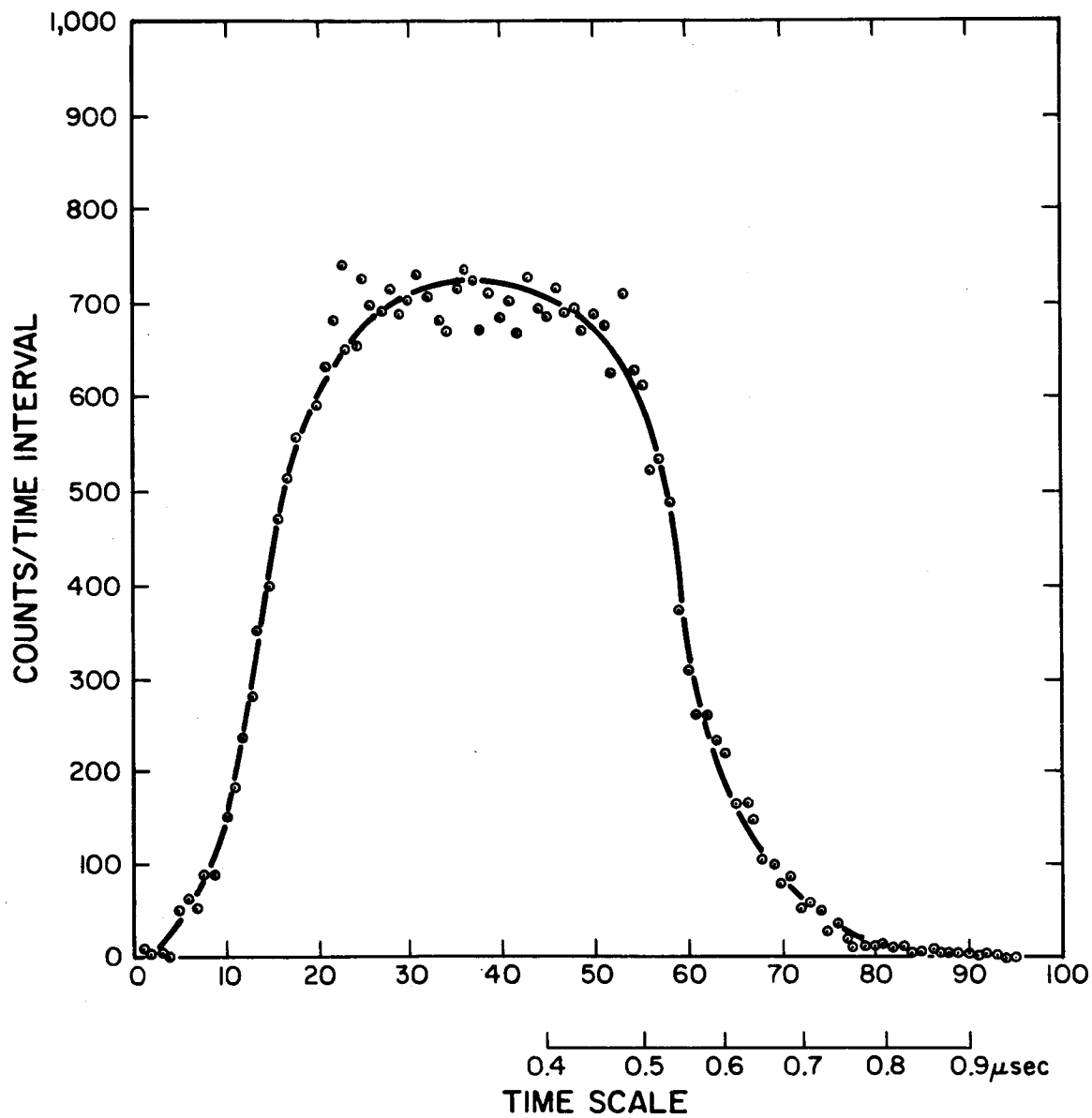
Figure 2   Delay Distribution, 90% Argon, 10% CH4 Counter, 2300 Volt.
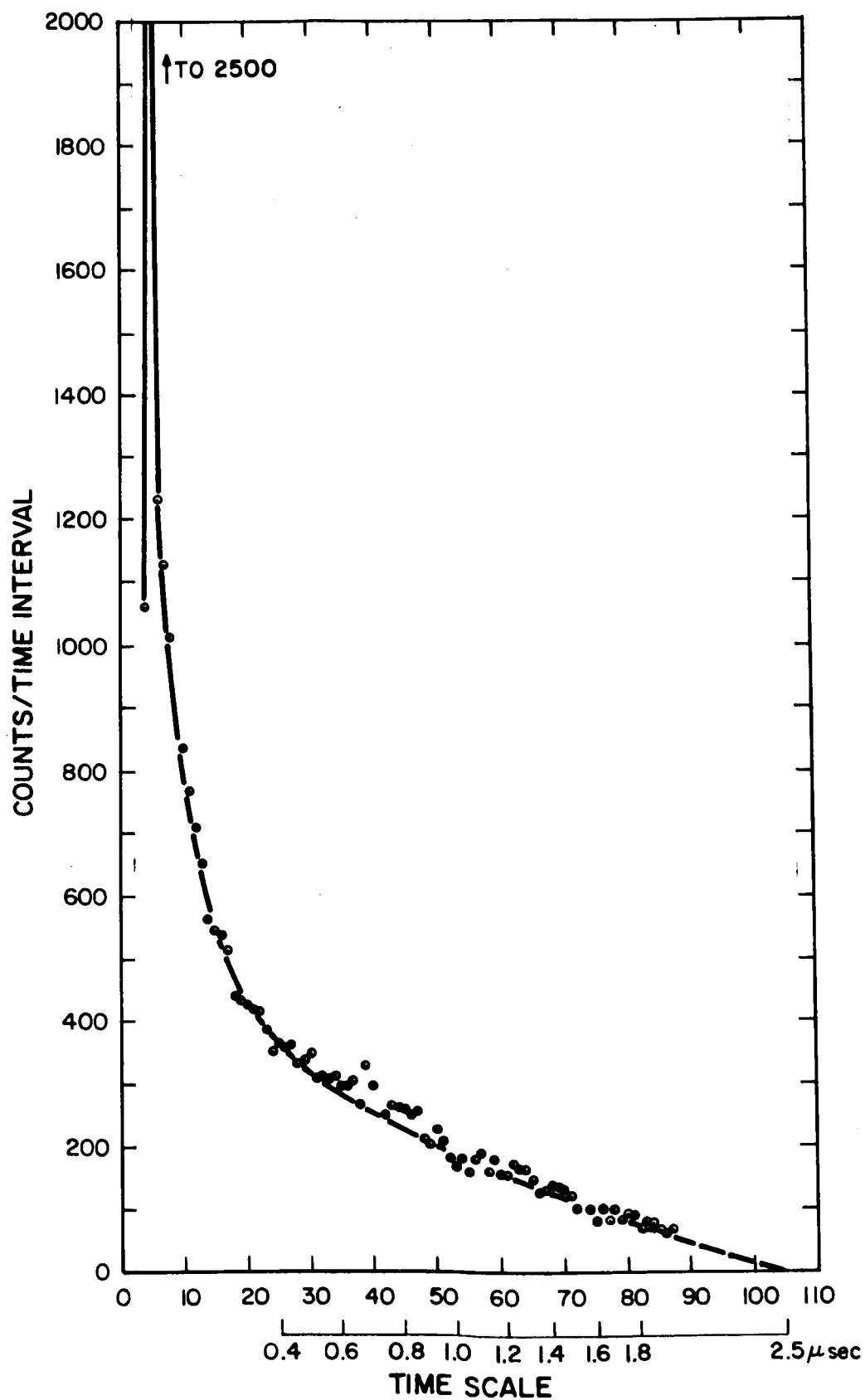
1758

Figure 3   Delay Time Distribution, 90% Argon, 10% CO_2 Counter, 2200 V.